INTRACAVITY TERAHERTZ OPTICAL PARAMETRIC OSCILLATORS

David A. Walsh

A Thesis Submitted for the Degree of PhD
at the
University of St. Andrews

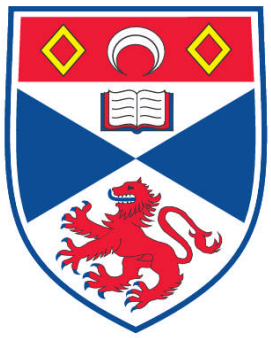

2011

Full metadata for this item is available in
Research@StAndrews:FullText
at:
https://research-repository.st-andrews.ac.uk/

Please use this identifier to cite or link to this item:
http://hdl.handle.net/10023/1713

This item is protected by original copyright

Intracavity Terahertz Optical Parametric Oscillators

David A Walsh

Thesis submitted for the degree of

Doctor of Philosophy

20th August 2010

Candidate's declarations

I, David Alan Walsh, hereby certify that this thesis, which is approximately 45,000 words in length, has been written by me, that it is the record of work carried out by me and that it has not been submitted in any previous application for a higher degree.

I was admitted as a research student in April, 2005 and as a candidate for the degree of Doctor of Philosophy in April, 2005; the higher study for which this is a record was carried out in the University of St Andrews between 2005 and 2009.

Date …….. signature of candidate …….……

2. Supervisor's declaration:

I hereby certify that the candidate has fulfilled the conditions of the Resolution and Regulations appropriate for the degree of Doctor of Philosophy in the University of St Andrews and that the candidate is qualified to submit this thesis in application for that degree.

Date …… signature of supervisor …….

3. Permission for electronic publication:

In submitting this thesis to the University of St Andrews I understand that I am giving permission for it to be made available for use in accordance with the regulations of the University Library for the time being in force, subject to any copyright vested in the work not being affected thereby. I also understand that the title and the abstract will be published, and that a copy of the work may be made and supplied to any bona fide library or research worker, that my thesis will be electronically accessible for personal or research use unless exempt by award of an embargo as requested below, and that the library has the right to migrate my thesis into new electronic forms as required to ensure continued access to the thesis. I have obtained any third-party copyright permissions that may be required in order to allow such access and migration, or have requested the appropriate embargo below.

The following is an agreed request by candidate and supervisor regarding the electronic publication of this thesis:

Access to printed copy and electronic publication of thesis through the University of St Andrews.

Date …….……..…. signature of candidate ……..……

signature of supervisor ……

Acknowledgements

First of all I have to express my gratitude to my academic supervisor, Professor Malcolm Dunn. Not only for offering me the opportunity to undertake a PhD, but also for the support and guidance given, and the unwavering and infectious enthusiasm for the research even when things didn't seem to be working. I couldn't have hoped for better.

Throughout my PhD studies I have been most fortunate in having the support of many friends and colleagues. My sincerest thanks must go to Dr David Stothard and Dr Tom Edwards, without whose guidance and assistance my research would have been vastly more difficult (and far less fun). A big thanks must also go to Dr Peter Browne, whose yearly visits to the group were both greatly enjoyable and productive. I must also thank Dr Cameron Rae for many helpful technical discussions and for unending willingness to repeatedly loan lab equipment. Outside of the optics lab I have to thank Shona Matthew, Caroline Thompson and Peter Thomas for creating a great work environment with plenty of laughter and productive scientific conversation in equal measures – particular thanks have to go to Shona for keeping my IT skills honed, and to Peter for the camaraderie during the time that we were both intensively writing up.

I must also thank my good friends David Miller, Maarten Verbraeken, Michael Summers, and also Christopher Reardon for their friendship (and limitless banter) throughout my time in St Andrews, and with whom many memories were formed that are sure to last a lifetime.

A special thanks must go to Willemijn, whose presence in my life has both enriched the good times and softened to lows, and who has continually supported me in many ways. Finally, another sincere thank you must go out to my parents, who have believed in me and supported me in all my endeavours, and without whom I would not be where I am today.

This work was partially funded by the Engineering and Physical Sciences Research Council, the Royal Society's Paul Instrument Fund and a Scottish Enterprise Proof of Concept grant.

Abstract

This thesis describes the design and implementation of several novel, nanosecond pulsed, intracavity optical parametric oscillators for the generation of terahertz radiation. The application of the intracavity approach in the context of terahertz optical parametric oscillators has been demonstrated for the first time, and the pump wave energy required was thereby reduced by an order of magnitude. The terahertz wave was tunable from under 1THz up to 3THz with a free running linewidth of ~50GHz and pulse energies up to ~20nJ (pulses were a few nanoseconds in duration). The terahertz beam profile was of Gaussian shape and could be focussed down to 2.3 times the diffraction limited spot size (M^2 values of 2.3 and 6.7 in the components of the beam parallel and perpendicular to the silicon prism array output coupler respectively).

Developments of this intracavity source with regard to the linewidth are also reported. Implementation of etalons in the optical (laser and OPO) cavities was shown to be a promising technique that brings the terahertz linewidth down below 1GHz (close to the transform limit of nanosecond pulses) while retaining the tuning range and beam characteristics of the free running system. Close to Fourier transform limited pulses were obtained (<100MHz linewidth) via an injection seeding technique, although with significantly increased system complexity. A deleterious effect caused by the mode beating of a multimode host laser was also discovered, in that sidebands were induced on the seeded downconverted wave. This has wider implications in the field of intracavity OPOs.

Finally, quasi-phasematching techniques implementing periodically poled lithium niobate were investigated as a way to lower the downconversion threshold energy requirement (by collinear propagation of the optical waves), and also to extract the terahertz wave rapidly from the (highly absorbing in the terahertz region) lithium niobate crystal. The existence of two phasematching solutions arising from the bidirectionality of the grating vector was identified as a serious design constraint in the context of an OPO where either solution can build up from noise photons, and so prefers the solution with the lowest walkoff of the downconverted waves - possibly resulting in unextractable terahertz radiation. Quasi-phasematching with an orthogonal grating vector (with identical but opposite phasematching solutions) was

demonstrated and cascaded downconversion processes observed and characterised. These cascaded processes are permitted by the collinearality of the optical waves and may allow efficiency improvements through overcoming the quantum defect limit.

This research has resulted in four peer reviewed papers in respected journals, and the intracavity terahertz OPO has been licensed to a company who have commercialised the technology (M Squared Lasers, Glasgow).

Publications

Papers

1. T. Edwards, D. Walsh, M. Spurr, C. Rae, M. Dunn, and P. Browne, "Compact source of continuously and widely-tunable terahertz radiation," Opt. Express 14, 1582-1589 (2006).

2. D. J. M. Stothard, T. J. Edwards, D. Walsh, C. L. Thomson, C. F. Rae, M. H. Dunn, and P. G. Browne, "Line-narrowed, compact, and coherent source of widely tunable terahertz radiation," Applied Physics Letters 92, 141105 (2008).

3. D. Walsh, D. J. M. Stothard, T. J. Edwards, P. G. Browne, C. F. Rae, and M. H. Dunn, "Injection-seeded intracavity terahertz optical parametric oscillator," J. Opt. Soc. Am. B 26, 1196-1202 (2009).

4. D. A. Walsh, P. G. Browne, M. H. Dunn, and C. F. Rae, "Intracavity parametric generation of nanosecond terahertz radiation using quasi-phase-matching," Opt. Express 18, 13951-13963 (2010).

Presentations Given

1. T. J. Edwards, D. Walsh, D. Stothard, M. Spurr, C. Rae, M. Dunn, University of St Andrews UK; P. Browne, Macquarie University, Sydney, Australia “Compact, solid-state source of continuously tuneable terahertz radiation” 2nd EPS-QEOD Europhoton Conference Pisa, Italy 10-15 September 2006. Europhysics Conference Abstracts Volume 30J p15. ISBN 2-914771- 41-X

2. Walsh D.A., Thomson, C.L. and Dunn, M.H., “Terahertz Generation by Intracavity Optical Parametric Oscillators”, 2nd UK/Europe-China Workshop on Millimetre Waves and Terahertz Technologies, Oxford, Oct. 2009.

3. D. Walsh, T. Edwards, D. Stothard, C. Rae, M. Dunn, and P. Browne “Compact and novel intracavity THz OPOs: Quasi Phasematching”, Poster Presentation. New Trends in Terahertz Imaging (NTTI) Summer School, 9-13 July 2007.

4. D. Walsh, C. Rae, M. Dunn, and P. Browne “Terahertz Generation from a Quasi Phasematched Intracavity Optical Parametric Device”, Poster Presentation. New Trends in Terahertz Imaging (NTTI) Summer School, 29 June - 3 July 2009.

5. D. Walsh, T. Edwards, D. Stothard, C. Rae, M. Dunn, and P. Browne "Intracavity Terahertz OPOs: Linewidth Reduction via Injection Seeding", Poster Presentation. New Trends in Terahertz Imaging (NTTI) Summer School, 29 June - 3 July 2009.

6. D. Walsh, C. Rae, M. Dunn, "Pyroelectric Detectors for Terahertz Detection : Preliminary Results", Poster Presentation. TeraNova Terahertz Systems and Industrial Applications, Royal Society, London, 25 February 2009.

Additional Presentations (not given myself)

1. Dunn, M.H., Walsh, D.A., Stothard, D.J., Edwards, T.J., Rae. C.F.R., "Line-narrowed, compact and coherent source of widely tunable THz radiation" (Invited Keynote) IRMMW-THz2007, Cardiff, UK, Sept. 2007, p613

2. Edwards, TJ., Walsh, D., Spurr, MB., Browne, P., Rae, CF., Dunn, MH., "Compact and coherent source of widely tunable THz radiation", Proc. SPIE,6402, (64020C), pp 64020-64020, 2006.

Contents

Chapter 1. Introduction and Thesis Plan

1.1. The "Terahertz Gap"

The majority of the electromagnetic spectrum have been investigated extensively and practical applications have been found for almost all frequency ranges. However, there is part of the electromagnetic spectrum that has yet to be fully exploited. The range of frequencies covered by this region is not consistently defined in the literature, but is generally accepted to be from about 300GHz to around 10THz (1mm to 30μm wavelength), having some overlap with the definitions of the far infrared. The region, which has been named by many as the "Terahertz Gap", lies between the microwave and millimetre wave frequencies that are typically generated by conventional electronic oscillators and the infra-red frequencies that can be generated by standard optical methods (laser sources, OPOs, laser frequency mixing). This gap was actually one of technology, by which it is meant that practical and powerful sources of radiation in the region did not exist – the radiation itself was (and is) certainly present. The devices on either side of the gap work in very different ways, on the low frequency side using electronic oscillators and on the high frequency side by exploiting semiconductor band gaps and atomic energy transitions, and there has been great difficulty adapting either technology to the terahertz regime.

There is, at the time of writing, still much of the basic enabling science yet to be done in the terahertz region as well as investigating its applications, although great inroads are now being made. No other part of the electromagnetic spectrum exists that is not exploited in some way and so it seems almost unthinkable that frequencies in the Terahertz Gap will have no practical uses. Until there are more practical sources available, and research is well underway, the full potential of terahertz radiation will remain, to a great extent, unrealised.

1.2. Source Technologies

There has been a significant research drive, over the last fifteen years or so, to fill the terahertz technology gap with practical sources. Due to the interest in exploiting this region there are many review papers on source technologies [1-9]. A graphical

summary of potentially portable and continuously tunable source technologies from a recent review paper by Tonouchi et al is reproduced in Figure 1.

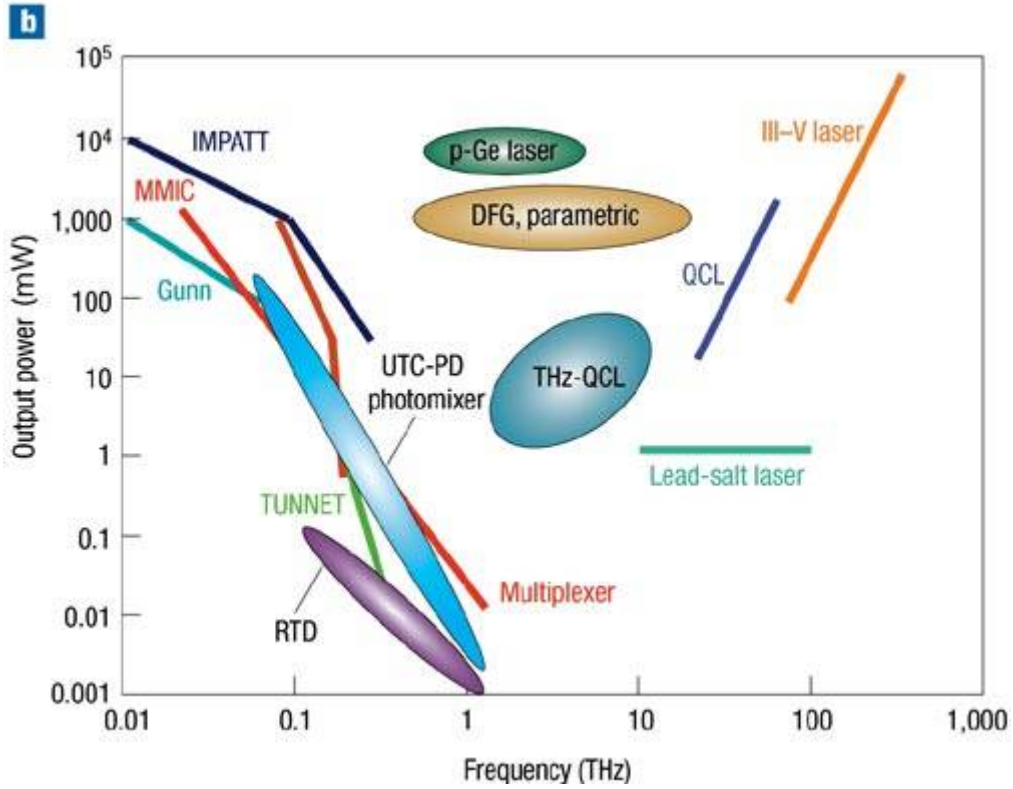

Figure 1 THz-emission power as a function of frequency. Solid lines are for the conventional THz sources; IMPATT diode stands for impact ionization avalanche transit-time diode, MMIC stands for microwave monolithic integrated circuit, TUNNET stands for tunnel injection transit time and the multiplexer is an SBD frequency multiplier. Ovals denote recent THz sources. The values of the last two are indicated by peak power; others are by c.w. power. Caption also from [8]

The most powerful and established sources are molecular gas lasers and free electron lasers (FELs). The molecular gas laser, like most other lasers, is not continuously tunable as it is restricted to frequencies predefined by the difference in frequencies between rotational modes of the molecular gas used. This makes it unsuitable for spectroscopic purposes. The FEL, however, is not limited in this way as the laser gain is provided by a modulated stream of accelerated electrons. These systems can also produce hundreds of Watts of terahertz radiation [10] and are unparalleled in this regard, however the FEL is a very large and expensive installation which makes it impractical for most research labs and applications.

The sources that are often regarded as having the most potential are quantum cascade lasers (QCL). Invented at Bell Labs in 1994 the QCL is a revolutionary device.

Instead of relying on fixed atomic transitions or transitions between the conduction and valence bands of a semiconductor, the QCL consists of multiple quantum wells - the characteristics of which can be designed to produce custom lasers operating at wavelengths not normally accessible. Whereas infrared QCLs have proved hugely successful, progress in the terahertz range is slow. THz QCLs still require cryogenic cooling and by their nature are not frequency tunable. Powers of tens of milliwatts and operating temperatures up to 164K have been reported[11], although these features were not obtained simultaneously.

Probably the most successful sources to date are those based on femtosecond pulsed laser, through optical rectification or photoconductive antennas. The output of these systems is a broadband pulse of radiation centered in the THz range. This pulse is then detected via electro-optic sampling techniques. The technique has an advantage in that the time-of-flight of the terahertz pulse can be measured, and using this data depth information can be retrieved. A good example of this is the work of Teraview in the nondestructive testing of pharmaceutical tablets[12]. There is a significant amount of work in the literature using these techniques, and commercial systems are available. The main drawbacks are the requirement for a femtosecond laser, and the necessity of applying Fourier techniques to recover spectral information, which can be sensitive to errors in the pulse sampling system alignment and multiple pulse reflections[13].

What we believe to be an up-and-coming technique is the terahertz optical parametric oscillator (OPO). These laser based systems exploit nonlinear optics to produce nanosecond pulses of terahertz radiation continuously tunable over the ~1 to ~3THz range with linewidths configurable to be as little as 100MHz or more than 100GHz[5]. They have advantages over photoconductive antenna based sources in that the spectral brightness can be superior, Fourier techniques are not required to retrieve spectral information, and they are based on simple neodymium lasers.

The nonlinear optics group in St Andrews has considerable experience in developing OPOs, in particular by implementing OPOs within laser cavities to greatly enhance their efficiency, versatility, and simplicity[14-16]. It was this experience that highlighted to the group that there was an opportunity to improve the terahertz OPO, and make it into an even more attractive option for the generation of radiation in the THz Gap.

1.3. Optical Parametric Oscillators

The optical parametric oscillator (OPO) is a device that exploits the second order nonlinear effect existing in many non-centrosymmetric materials to split photons of one energy into two new photons, the energies of which must sum to equal the original photon energy. The ratio of energies of the new "downconverted" photons can be controlled via phasematching techniques to produce a tunable output. This field has been widely developed to produce tunable sources, both pulsed and continuous wave, throughout the ultraviolet, visible and infrared regions and extending into the terahertz gap[17-26].

There are two primary considerations when designing an OPO. The first is finding a suitable material in which the photon splitting can take place as it will need to be transparent at all three photon frequencies as well as possessing a suitably high χ_2 nonlinear susceptibility. Secondly, the parametric process is proportional to the intensity of the input "pump" wave, and so a high power laser or a scheme to enhance the intensity, such as a resonant cavity, is required. OPOs are often pumped with Q-Switched lasers, as the peak intensity of these nanosecond pulses is many times higher than that available from a continuous wave laser.

The traditional setup of a parametric system is to have the nonlinear device and the pump laser as separate entities. Thresholds in such systems are reduced by resonating one or more of the downconverted waves, and perhaps also placing the nonlinear device in a resonant cavity for the pump wave ("pump enhanced"). The former technique produces what are known as singly or doubly resonant systems (the SRO and DRO respectively), DROs have a much lower threshold than SROs but are overly restricted in that the resonators of the downconverted waves must fit the allowed frequencies, producing an environmentally sensitive system that is difficult to set up and tune. SROs are much more manageable but have considerably higher thresholds. The application of a resonant cavity for the pump wave helps bring SRO thresholds back down to practical levels, however the pump resonator then needs to be actively locked and mode matched to the pump wave. Additional difficulties arise here when a Q-Switched laser is used, as most practical cavity locking schemes require a continuous wave laser to provide a constant locking signal (i.e. the cavity frequencies

supported can drift between laser pulses as there is no optical wave to which to reference).

1.4. Intracavity OPOs

The solution to many of the difficulties above can be found in the intracavity (or intersecting cavity) OPO where the nonlinear medium of this device is situated within the laser cavity itself. This obviates the need for cavity locking techniques and mode matching optics thereby producing simpler and much more robust systems. The method is also advantageous in that the losses associated with parasitic processes (Fresnel reflections, diffraction losses, laser output coupling efficiency etc) can be minimised, producing highly efficient devices. Extending this approach to terahertz OPOs is one of the significant advances reported in this Thesis, and indeed is the technique used in all of the terahertz OPO developments reported herein.

1.5. Thesis Plan

To begin with Chapter 2 discusses the historical development and operating principles of the THz OPO. The enhancement of the nonlinear coefficient by a polariton resonance in lithium niobate is discussed, and a method of calculating the threshold gain requirement of a THz OPO is put forward. Also calculations of the tuning range and phasematching bandwidths are given. The chapter ends with an analysis of a traditionally pumped (extracavity, SRO) terahertz OPO that is similar to the intracavity device developed in this research such that the effectiveness of the intracavity pumping technique can be judged.

Chapter 3 reports on the realization of the "intersecting cavity" THz OPO. The design of the system is described and its performance characterised and compared to the extracavity device analysed in Chapter 2. Examples of spectroscopy and imaging using the intersecting cavity THz OPO are also given, showing the utility of the source. This source has been published in Optics Express in 2006[27].

The next developments were the implementation of line narrowing techniques to the intersecting cavity system and this is reported in Chapter 4. The simple and effective method of positioning suitable etalons intracavity to the pump and idler waves resulted in a significantly narrowed terahertz output and this work has been published in Applied Physics Letters in 2008[28]. To reach the transform limited line width of

the few nanosecond terahertz pulses injection seeding of the system was implemented. The resulting device had a linewidth of <100MHz and interesting and an impactful discovery regarding the importance of single frequency pump waves was made. This was published in the Journal of the Optical Society of America B in 2009[29].

Chapter 5 is the final experimental chapter and describes the progress made in applying quasi-phasematching techniques to the intersecting cavity THz OPO. Significant advances in understanding the design considerations have been made and a working device is reported, although not with high efficiency at this time. Parts of this work were published in Optics Express in 2010[30].

The thesis then ends with Chapter 6, which contains the concluding remarks on the work reported and proposals for future investigations.

1.6. References

1. K. Kawase, J.-i. Shikata, and H. Ito, "Terahertz wave parametric source," Journal of Physics D: Applied Physics, R1 (2002).

2. J. M. Chamberlain, "Where optics meets electronics: recent progress in decreasing the terahertz gap," Philosophical Transactions of the Royal Society of London. Series A: Mathematical, Physical and Engineering Sciences **362**, 199-213 (2004).

3. P. H. Siegel, "Terahertz Technology in Biology and Medicine," IEEE Transactions on Microwave Theory and Techniques **52**, 2438 (2004).

4. P. W. Gwyn, "Filling the THz gap - high power sources and applications," Reports on Progress in Physics **69**, 301 (2006).

5. K. Kawase, Y. Ogawa, and C. Otani, "Terahertz-wave generation and real-life applications," in *Conference on Lasers and Electro-Optics/Pacific Rim 2007*(Optical Society of America, 2007), p. ThH3_1.

6. J. A. L'Huillier, G. Torosyan, M. Theuer, Y. Avetisyan, and R. Beigang, "Generation of THz radiation using bulk, periodically and aperiodically poled lithium niobate – Part 1: Theory," Applied Physics B: Lasers and Optics **86**, 185-196 (2007).

7. J. A. L'Huillier, G. Torosyan, M. Theuer, C. Rau, Y. Avetisyan, and R. Beigang, "Generation of THz radiation using bulk, periodically and aperiodically

poled lithium niobate – Part 2: Experiments," Applied Physics B: Lasers and Optics **86**, 197-208 (2007).

8. M. Tonouchi, "Cutting-edge terahertz technology," Nat Photon **1**, 97-105 (2007).

9. G. K. Kitaeva, "Terahertz generation by means of optical lasers," Laser Physics Letters **5**, 559-576 (2008).

10. N. G. Gavrilov, B. A. Knyazev, E. I. Kolobanov, V. V. Kotenkov, V. V. Kubarev, G. N. Kulipanov, A. N. Matveenko, L. E. Medvedev, S. V. Miginsky, L. A. Mironenko, A. D. Oreshkov, V. K. Ovchar, V. M. Popik, T. V. Salikova, M. A. Scheglov, S. S. Serednyakov, O. A. Shevchenko, A. N. Skrinsky, V. G. Tcheskidov, and N. A. Vinokurov, "Status of the Novosibirsk high-power terahertz FEL," Nuclear Instruments and Methods in Physics Research Section A: Accelerators, Spectrometers, Detectors and Associated Equipment **575**, 54-57 (2007).

11. B. Williams, S. Kumar, Q. Hu, and J. Reno, "Operation of terahertz quantum-cascade lasers at 164 K in pulsed mode and at 117 K in continuous-wave mode," Opt. Express **13**, 3331-3339 (2005).

12. A. Fitzgerald, B. Cole, and P. Taday, "Nondestructive analysis of tablet coating thicknesses using terahertz pulsed imaging," Journal of Pharmaceutical Sciences **94**, 177-183 (2005).

13. M. Naftaly, and R. Dudley, "Linearity calibration of amplitude and power measurements in terahertz systems and detectors," Opt. Lett. **34**, 674-676 (2009).

14. M. Ebrahimzadeh, G. A. Turnbull, T. J. Edwards, D. J. M. Stothard, I. D. Lindsay, and M. H. Dunn, "Intracavity continuous-wave singly resonant optical parametric oscillators," J. Opt. Soc. Am. B **16**, 1499-1511 (1999).

15. D. J. M. Stothard, P. Y. Fortin, A. Carleton, M. Ebrahimzadeh, and M. H. Dunn, "Comparison of continuous-wave optical parametric oscillators based on periodically poled $LiNbO_3$ and periodically poled $RbTiOAsO_4$ pumped internal to a high-power Nd:YVO4 laser," J. Opt. Soc. Am. B **20**, 2102-2108 (2003).

16. D. Stothard, C. F. Rae, and M. H. Dunn, "An Intracavity Optical Parametric Oscillator With Very High Repetition Rate and Broad Tunability Based Upon Room

Temperature Periodically Poled MgO:$LiNbO_3$ With Fanned Grating Design," Quantum Electronics, IEEE Journal of **45**, 256-263 (2009).

17. H. E. Puthoff, R. H. Pantell, B. G. Huth, and M. A. Chacon, "Near-Forward Raman Scattering in $LiNbO_3$," Journal of Applied Physics **39**, 2144-2146 (1968).

18. J. Gelbwachs, R. H. Pantell, H. E. Puthoff, and J. M. Yarborough, "A tunable stimulated Raman oscillator," Applied Physics Letters **14**, 258-262 (1969).

19. J. M. Yarborough, S. S. Sussman, H. E. Puthoff, R. H. Pantell, and B. C. Johnson, "Efficient, Tunable Optical Emission from $LiNbO_3$ without a Resonator," Applied Physics Letters **15**, 102-105 (1969).

20. S. S. Sussman, "Tunable Light Scattering from Transverse Optical Modes in Lithium Niobate," in *Physics*(Stanford University, 1970), p. 116.

21. B. C. Johnson, H. E. Puthoff, J. SooHoo, and S. S. Sussman, "Power and linewidth of tunable stimulated far-infrared emission in $LiNbO_3$," Applied Physics Letters **18**, 181-183 (1971).

22. J. F. Scott, "Light scattering from polaritons," Am. J. Phys. **39**, 1360-& (1971).

23. M. A. Piestrup, R. N. Fleming, and R. H. Pantell, "Continuously tunable submillimeter wave source," Applied Physics Letters **26**, 418-421 (1975).

24. M. A. Piestrup, R. A. Powell, G. B. Rothbart, C. K. Chen, and R. H. Pantell, "Cerenkov radiation as a light-source for 2000-620-Å spectral range," Applied Physics Letters **28**, 92-94 (1976).

25. K. Kawase, M. Sato, T. Taniuchi, and H. Ito, "Coherent tunable THz-wave generation from $LiNbO_3$ with monolithic grating coupler," Applied Physics Letters **68**, 2483-2485 (1996).

26. K. Kawase, J.-i. Shikata, H. Minamide, K. Imai, and H. Ito, "Arrayed silicon prism coupler for a terahertz-wave parametric oscillator," Appl. Opt. **40**, 1423-1426 (2001).

27. T. Edwards, D. Walsh, M. Spurr, C. Rae, M. Dunn, and P. Browne, "Compact source of continuously and widely-tunable terahertz radiation," Opt. Express **14**, 1582-1589 (2006).

28. D. J. M. Stothard, T. J. Edwards, D. Walsh, C. L. Thomson, C. F. Rae, M. H. Dunn, and P. G. Browne, "Line-narrowed, compact, and coherent source of widely tunable terahertz radiation," Applied Physics Letters **92**, 141105 (2008).

29. D. Walsh, D. J. M. Stothard, T. J. Edwards, P. G. Browne, C. F. Rae, and M. H. Dunn, "Injection-seeded intracavity terahertz optical parametric oscillator," J. Opt. Soc. Am. B **26**, 1196-1202 (2009).

30. D. A. Walsh, P. G. Browne, M. H. Dunn, and C. F. Rae, "Intracavity parametric generation of nanosecond terahertz radiation using quasi-phase-matching," Opt. Express **18**, 13951-13963 (2010).

Chapter 2. The Terahertz OPO

2.1. Introduction

In this chapter the history and characteristics of the lithium niobate based terahertz OPO will be discussed. An attempt has been made to avoid the inclusion of such things as derivations from first principles of the equations describing the operation of an OPO, as this is no doubt familiar to the reader and also readily available in the form of textbooks such as that of Shen [1]. Instead there are descriptions of how the parts of the device operate, and the chapter will end with an analysis of published results by others regarding an extracavity pumped terahertz OPO with respect to the optical pumping levels and terahertz radiation produced, which will provide a basis for comparison with the intracavity device to be described in the following chapter.

2.2. History

The technique of generating THz radiation by the lowest order A_1 polariton enhanced second order non-linear effect in lithium niobate was first demonstrated in 1969 by Gelbwachs et al [2]. Although it must be noted that in this early device the terahertz wave was not coupled out of the crystal and measured - only the infrared idler (stokes) wave was detected, but this does infer the presence of the THz wave. That same year Yarborough et al [3] reported a development of the device where the terahertz wave was both tunable and extracted. This device had no resonant idler cavity as such, but a lossy resonator was formed by the parallel polished ends of the crystal and tuning was accomplished by rotation of the crystal.

There were some further developments until the mid 1970s (including significant work by Piestrup et al [4, 5]) when research in the area seemed to peter out. Indeed it was not until 1996 that a new development was reported by Kawase et al.[6] working at the RIKEN institute of technology, as the “terahertz gap” started gaining interest. Much work has since gone into the development of the terahertz parametric source, including comparisons of parametric generators and oscillators, improved output coupling techniques that maximize the THz signal and directional stability, line narrowing by the use of injection seeding, smooth and agile tuning techniques, and investigations into the effects of crystal properties such as temperature and MgO doping (interesting due to its reduction of photorefractive damage). In addition to this

fundamental source work the usefulness of these sources in both imaging and spectroscopy has also demonstrated [7].

The research group headed by K. Kawase at the Riken institute, Japan, is the only group with significant activity in the development of terahertz parametric sources outside our own in St Andrews. Much of the work there has been developing the technique that worked most satisfactorily for them – that of injection seeded, extracavity pumped parametric generation. The key features of which are that a relatively powerful Q-switched pump laser is required, and that instead of having a resonating cavity for the idler, thereby allowing it to build up from noise during the pump pulse, there is no cavity, and instead a single frequency laser is shone through the crystal with the appropriate frequency and angle with respect to the pump for a phasematched terahertz generation process to occur. This allows for the production of narrow linewidth pulses (near transform limited), however the system is much more complicated than the oscillator approach as multiple single frequency lasers are required, as well as a means to systematically realign the seed laser if tuning is to be accomplished.

The rest of this chapter will now cover the various aspects important in the design and operation of a terahertz OPO in general, laying the foundations for the design and characterisation of the devices described in the following chapters.

2.3. Nonlinear Crystal: MgO:LiNbO$_3$

The basis of any frequency converter based on parametric generation is the medium in which the nonlinear optical effect takes place. In theory all media behave in a nonlinear fashion if the optical intensity is high enough, however the second order effect of parametric amplification is only present in materials that do not have a center of symmetry. Also, it is advantageous to use a medium with a high nonlinear coefficient in order to reduce the input energy required to bring the device above threshold. Materials that exhibit both of these properties are non-centrosymmetric crystals, and so it is these materials that form the basis of most practical parametric sources.

There are several requirements placed on the crystal chosen: it must be transparent at the pump, signal (terahertz in this case) and idler frequencies, it must have a sufficiently large nonlinear coefficient, and it must be possible to satisfy the condition

of phase matching the three waves. The majority of parametric generation to date has been based around lithium niobate ($LiNbO_3$) crystals, sometimes with MgO doping (a common dopant used to reduce photorefractive damage); studies extending from the initial observation of the effect by Yarborough et al in 1969 [2], through to more recent examples utilising improved output coupling techniques [8]. This is because of two properties of the material. Firstly, the d_{eff} is enhanced due to an interaction with the A1−symmetry soft phonon mode (a so called "polariton resonance" that couples to the electromagnetic waves) at ~248cm^{-1} (~7.4THz). It must be noted, however, that the existence of the polariton resonance at terahertz frequencies in MgO:$LiNbO_3$ is a double edged sword. Whilst its presence greatly enhances the nonlinear process, making the crystal a feasible choice, it also means that the generated terahertz radiation couples easily to the phonon modes of the crystal lattice and thus is readily absorbed. Absorption coefficients between 20cm^{-1} and 80cm^{-1} in the range 1.2THz to 2.4THz have been measured [9]. To minimize this problem the terahertz must exit the crystal with as short a path length as possible, meaning that conventional collinear phasematching (shown in Figure 7i) would not be practical as the terahertz wave would have to traverse most of the crystal length before escaping into free space (and indeed is not actually possible as shown later in section 2.5). Secondly, the dispersion in the material enforces a non-collinear phase matching geometry that although reducing the nonlinear gain due to walk-off of the three waves (see section 2.10.1), provides a simple tuning mechanism (see section 2.5) and more significantly allows the terahertz wave to be generated at a large angle to the pump wave – thereby exiting the crystals side facet. This, in conjunction with positioning the generation region next to the side of the crystal, means that the terahertz wave will traverse a much shorter path within the crystal and hence experience a much smaller absorption. The combination of features described above form an alternating virtuous/vicious circle (see Figure 2), and allow tunable terahertz generation in lithium niobate.

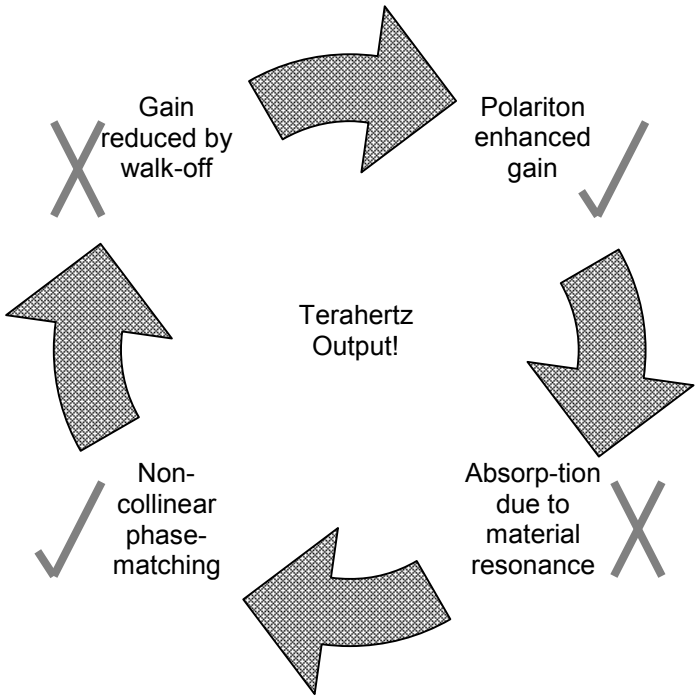

Figure 2 Circle of features in lithium niobate that allows useful, tuneable terahertz generation. Each disadvantage is counteracted by another advantageous feature.

In the next few sections these features will now be elaborated upon in order to describe how the terahertz OPO functions.

2.4. Polariton Enhanced Nonlinear Coefficient

As previously mentioned the Terahertz OPO generates terahertz waves by exploiting stimulated polariton scattering, and as such the device differs from conventional OPOs in that the second order nonlinear effect is enhanced by a material resonance. In the general case the physical interpretations of the nonlinear response mechanism is as follows: as an electromagnetic wave passes through a dielectric material the oscillating electric field induces a displacement in the cloud of electrons surrounding the atoms of the material, as these electrons oscillate they re-radiate at the same frequency yet with a slightly delayed phase with respect to the incident electromagnetic wave, interfering with it in such a way that the electromagnetic wave appears to have been delayed (this is the cause of the refractive index). These electrons can be thought of charges on springs (i.e. they are associated with particular atoms) and for small disturbances oscillate with simple harmonic motion, however at large disturbances the spring restoring force experienced by the electron is no longer linearly proportional to it's displacement and simple harmonic motion is no longer

exhibited – this response give rise to the nonlinear effects such as harmonic generation, sum frequency, difference frequency, parametric generation (second order effects), Kerr effect, phase conjugation (third order effects) etc… However, if the atoms themselves begin to oscillate due to the incident field then phonon vibrations can be induced. In the case where this results in a displacement of the ions of the lattice a time varying polarization is induced in the medium with an associated electromagnetic wave. This can significantly alter the optical response of the material.

The following theory and calculations (quoted in cgs units with SI unit conversions) are extracted from a paper by Shikata et al [10], and are included to show how the gain coefficient varies with the terahertz generation frequency. The approach is actually a distillation of the derivation of the exponential gain coefficients performed by Sussman in 1970 [11].

The low signal (unsaturated) exponential gain coefficient, g_0, is expressed in the standard way in terms of the second order nonlinear coefficient, χ_P by:

$$g_0(cgs) = \sqrt{\frac{\pi\omega\omega_i I_p}{2c^3 n_T n_i n_p}}\chi_P \rightarrow g_0(SI) = \frac{1}{8\pi}\sqrt{\frac{\omega\omega_i I_p}{2\varepsilon_0 c^3 n_T n_i n_p}}\chi_P \qquad (2.1)$$

(in cgs units to the left, and using SI units to the right) where I_p is the intensity of the pump wave, n_p, n_i and n_T are the refractive indices of the pump, idler and terahertz waves, and ω and ω_i are the frequencies of the terahertz and idler waves (note that this is a deviation from the usual convention where the frequencies are labelled pump, signal and idler in order of decreasing frequency. In this case it is the lowest frequency, terahertz, wave that is of interest, and so the second highest frequency is labelled the idler in an attempt to avoid confusion (this is also the convention followed by the Kawase et al)). This is of the same form as for the parametric gain [1] except that χ_P is enhanced by approximately a factor of five due to the polariton resonance [10]. The second order nonlinear susceptibility is then expressed by:

$$\chi_P = d_E + \frac{S_0\omega_0^2}{\omega_0^2 - \omega^2}\cdot d_Q \qquad (2.2)$$

where S_0 is the phonon oscillator strength, and ω_0 is the frequency of the phonon. d_E $(=16\pi d_{33})$ is the relevant 2nd order nonlinear coefficient and d_Q is the term for the 3rd order process, which is given by:

$$d_Q(cgs)=\sqrt{\frac{8\pi c^4 n_p\left(\frac{S_{33}}{L\Delta\Omega}\right)_0}{S_0\hbar\omega_0\omega_i^4 n_i\left(\bar{n}_0+1\right)}}\rightarrow d_Q(SI)=16\pi^2\sqrt{\frac{2\varepsilon_0 c^4 n_p\left(\frac{S_{33}}{L\Delta\Omega}\right)_0}{S_0\hbar\omega_0\omega_i^4 n_i\left(\bar{n}_0+1\right)}} \qquad (2.3)$$

(in cgs units to the left, and using SI units to the right) where c and $\hbar$ are the speed of light and Planck's constant, ω_i is the frequency of the idler wave, $\bar{n}_0=\left(e^{\frac{\hbar\omega_0}{kT}}-1\right)^{-1}$ is the Bose distribution function (where k is Boltzmann's constant and T is the crystal temperature) and the quantity $\left(S_{33}/L\Delta\Omega\right)_0$ is the spontaneous Raman scattering efficiency of the lowest A_1-symmetry phonon mode, S_{33} being the fraction of power scattered into a solid angle $\Delta\Omega$ near normal to the optical path length L (and is proportional to the scattering cross-section).

The exponential gain coefficients for the terahertz and idler waves (g_T and g_i) were then found by solving the coupled wave equations (factoring in the polariton induced absorption), although details of the derivation are not included by Shikata et al. [10], giving:

$$g_T=g_i\cos\phi=\frac{\alpha_T}{2}\left(\sqrt{1+16\cos\phi\left(\frac{g_0}{\alpha_T}\right)^2}-1\right) \qquad (2.4)$$

where ϕ is the phasematching (walk-off) angle of the terahertz wave (the angle at which the terahertz wave is generated with respect to the pump wave), α_T is the terahertz absorption coefficient, and g_0 is the low-loss gain limit. The absorption coefficient is given by:

$$\alpha_T=\frac{2\omega}{c}\mathrm{Im}\left(\varepsilon_r+\frac{S_0\omega_0^2}{\omega_0^2-\omega^2-i\omega\Gamma_0}\right)^{\frac{1}{2}} \qquad (2.5)$$

where ε_r is the relative permittivity of the crystal and Γ_0 is the half width of the phonon.

Using equation (2.4) the gain for the terahertz wave can be calculated for different generation frequencies and temperatures in lithium niobate (see Figure 3).

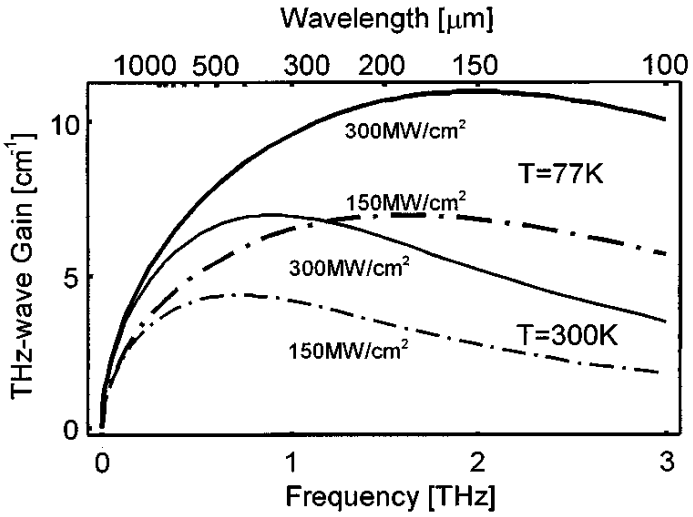

Figure 3 gain coefficients at room and liquid nitrogen temperatures calculated for the terahertz wave generated via polariton scattering from the lowest order A_1-symmetry mode in lithium niobate. The pump wavelength was set to be 1.064μm. [10]

The data in Figure 3 shows the significance of the absorption limitation on the terahertz OPO gain, as a significant improvement is observed on cryogenically cooling the crystal. This absorption is detrimental in two additional ways: by reducing the interaction length of the waves, and by direct absorption of the terahertz wave as it propagates through the crystal before being output coupled. Figure 4 shows the terahertz absorption coefficients, both calculated (using equation (2.5)) and directly measured, by Shikata et al [10].

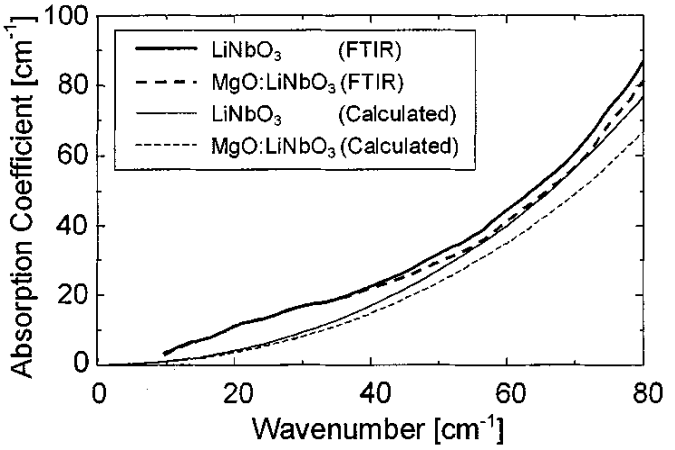

Figure 4 calculated and directly measured absorption coefficients of MgO doped and undoped lithium niobate. [10]

When looked at together Figure 3 and Figure 4 it can be seen why all sources based on parametric generation in lithium niobate have a tuning range from ~1THz to ~3THz. The high frequency end is largely limited by strong absorption, and the low frequency gain falls off rapidly below ~0.5THz (the lower frequency limit tends also to be limited by the geometry of the idler cavity intersecting the pump wave).

In the intracavity system described in the following chapter we therefore expected a tuning range somewhere in the region of 1THz to 3THz, and so the following sections modelling the tuning and output coupling of the terahertz wave concentrate on this region.

2.4.1. MgO Doping

The paper published by Shikate et al in 2000 [10] on the analysis of terahertz OPOs also investigates the use of MgO doped lithium niobate crystals. Doping levels of 5% and 9% beside an otherwise identical undoped crystal were implemented in a terahertz OPO, with the 5% doped crystal proving to be the more efficient generator – producing 5 times more terahertz radiation whilst retaining the same tuning curve (implying a largely unchanged refractive index/phasematching condition). To investigate the cause of the enhancement Shikate et al performed Raman spectroscopy of the doped and undoped crystals, finding an enhanced scattering in the doped crystal. This increases the contribution of d_Q, equation (2.3), to the nonlinear susceptibility and therefore also increases the gain. They go further to propose that the increase in conductivity resulting from the doping (and illustrated by the increased Raman scattering) induces optical losses, thereby explaining there being an optimum doping level.

The interest in using MgO doped crystals lay in their lower susceptibility to photorefractive damage than undoped lithium niobate. This damage manifests as a change in refractive index when exposed to an intense optical field, which would be a significant problem when pumping the crystal with high intensity fields necessary to bring an OPO above oscillation threshold, especially so if the crystal is placed within the cavity of a laser as the refractive index damage would significantly impair laser operation. Typically a doping level of 5% or 6% is sufficient to reduce the propensity to damage enough for use in intracavity pumped systems. For these reasons 5%

$MgO:LiNbO_3$ crystals were chosen for the intracavity terahertz OPOs developed in the following chapters.

2.5. Non-collinear Phasematching

In order for the parametric process to experience gain the condition of phasematching the three waves must of course be met. In other words the photons of the desired frequency and propagation direction generated throughout the gain region must add up together with the same phase, else they will cancel out to some degree thereby reducing efficiency. To put this in the form of an equation is to say:

$$\begin{aligned} \boldsymbol{k}_p &= \boldsymbol{k}_i + \boldsymbol{k}_{THz} \\ \frac{2\pi n_p}{\lambda_p}\hat{\boldsymbol{p}} &= \frac{2\pi n_i}{\lambda_i}\hat{\boldsymbol{i}} + \frac{2\pi n_{THz}}{\lambda_{THz}}\hat{\boldsymbol{t}} \end{aligned} \tag{2.6}$$

Where $\boldsymbol{k}$, n, and λ are the k-vector, refractive index, and wavelength of the pump, idler and terahertz waves as denoted by the suffixes p, i and λ respectively. $\hat{\boldsymbol{p}}$, $\hat{\boldsymbol{i}}$ and $\hat{\boldsymbol{t}}$ are unit vectors denoting the propagation directions of the pump, idler and terahertz waves respectively. So in order to calculate whether phasematching takes place we must have knowledge of the refractive indices at each wavelength in the nonlinear material. It is also a simple matter to determine which combinations of downconverted waves are allowed due to the conservation of energy i.e.

$$\frac{hc}{\lambda_p} = \frac{hc}{\lambda_i} + \frac{hc}{\lambda_{THz}} \tag{2.7}$$

where h is Planck's constant and c is the speed of light.

In the lithium niobate terahertz OPO the polarisations of all three waves are along the extraordinary crystal axis (usually denoted the z axis) and propagation is in the x-y plane. The refractive index of 5% MgO doped $LiNbO_3$ has been characterised in the region of the pump and idler waves by Zelmon et al [12] (NB there is an error in the published paper where the ordinary and extraordinary refractive indexes are swapped around), the result of which can be used to calculate the pump and idler k vector magnitudes. In the terahertz region the refractive index is much less well known, and no published Sellmeier equation could be found. In order to perform the phasematching calculations in the present work it was therefore necessary to produce one in-house. This was accomplished by fitting the arbitrary equation:

$$n_e(\lambda) = Ae^{-\frac{(\lambda-\lambda_0)}{t_0}} + C \tag{2.8}$$

to the data published in *Handbook of Optical Constants of Solids*, Palik 1985[13], where λ is the wavelength in microns. The values of the constants for the fitted equation are:

$$\begin{aligned} A &= 3.8123 \quad C = 5.07 \\ \lambda_0 &= -14.9 \quad t_0 = 65 \end{aligned} \tag{2.9}$$

The fit can be seen in Figure 5 along with the reported values.

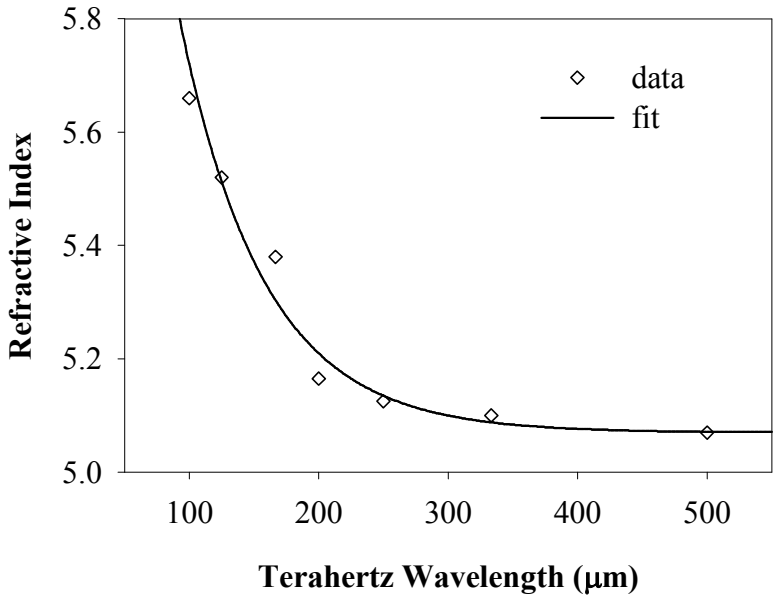

Figure 5 plot showing the fitted refractive index curve along with the experimental data points compiled in [13]. The fit covers the 100μm to 500μm spectral region, which encompasses the tuning range of 1THz to 3THz expected.

Using this knowledge of refractive indices the magnitudes of the k-vectors can be calculated for allowed idler-terahertz photon energy splits between 0.6THz and 3THz (100μm to 500μm). In the case where all three waves would be collinear, where walk-off losses are minimised, it can be readily shown that no phasematching solution exists in the 1THz to 3THz region(see Figure 6).

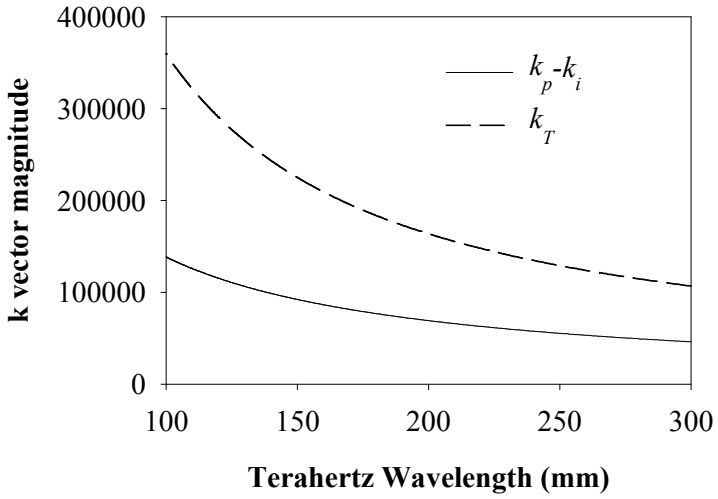

Figure 6 plot showing the values of the terahertz k vector alongside the difference between pump and idler k vectors (for the collinear case). Phasematching would be indicated by the lines crossing.

Phasematching collinearly would be advantageous in that the walk off losses are minimised thereby producing a system with high gain. However, in lithium niobate the strong absorption of the terahertz wave must be avoided by extracting it from the side of the crystal. We are able to design this condition, and meet the requirement of phasematching, by utilising the method of non-collinear phasematching. The essence of this technique is that the k vectors complete a triangle, rather than a straight line, as illustrated in Figure 7.

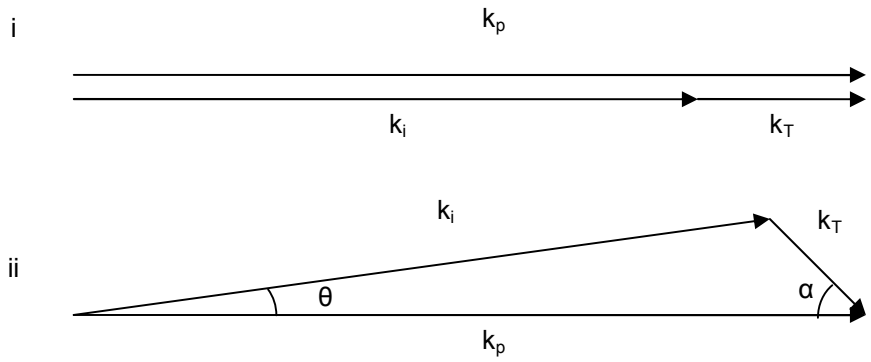

Figure 7 k vector diagrams illustrating phasematching solutions: i) the conventional collinear phasematching solution ii) the non-collinear phasematching condition existent in $LiNbO_3$ / $MgO:LiNbO_3$. Note the k vectors are not drawn to scale to enhance clarity; in reality the terahertz k vector is around 100 times shorter than the pump/idler k vectors.

An effect of using this non-collinear phasematching scheme is that the propagation directions of the idler/terahertz wave vary with frequency, which in this case is largely due to the dispersion of the terahertz refractive index and, to a lesser extent, by the relative change of the terahertz wave k vector (by a factor of 3) from 1THz to 3THz. The angular dispersions of the idler and terahertz k vectors (θ and α as shown in Figure 7) can be calculated using the cosine rule and are shown in Figure 8.

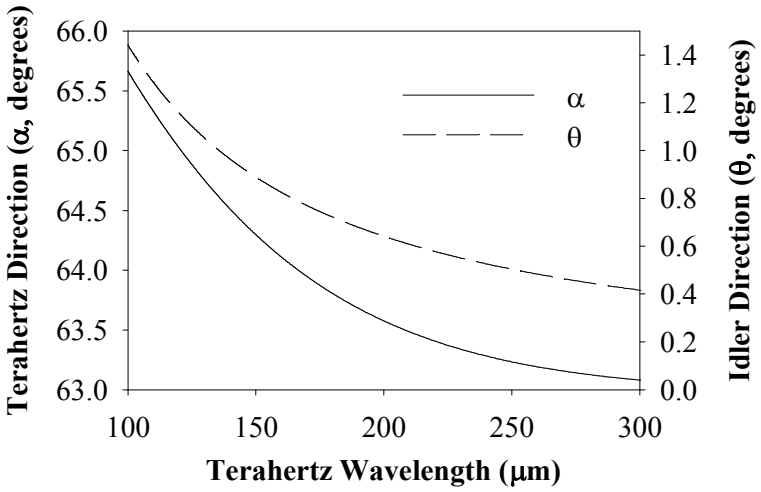

Figure 8 plot showing the dispersion of the k vector directions as defined in Figure 7. All angles are defined for the waves within the crystal.

2.6. Practical Schemes for Angle Tuning

In the context of the terahertz OPO, where the idler wave is resonated within an optical cavity, the feedback of the cavity is limited to a specific angle, the result of which is that only the idler that phasematches at the angle of said cavity will build up exponentially. Usually a simple two-mirror cavity is used where both of these mirrors are mounted on a shared "swing arm" that pivots around the central point of pump wave in the lithium niobate. This allows both mirrors to be moved simultaneously – providing a simple tuning mechanism. This will be utilised in the intracavity terahertz OPO as a simple, rapid tuning mechanism that allows useful extraction of the terahertz wave. During the course of developing the intracavity terahertz OPO it was realised that there is an issue with tuning the OPO in this way, as optimal idler cavity alignment was not consistent throughout the tuning range. To help describe the problem a schematic of the usual, two mirror, resonator design is shown in Figure 9.

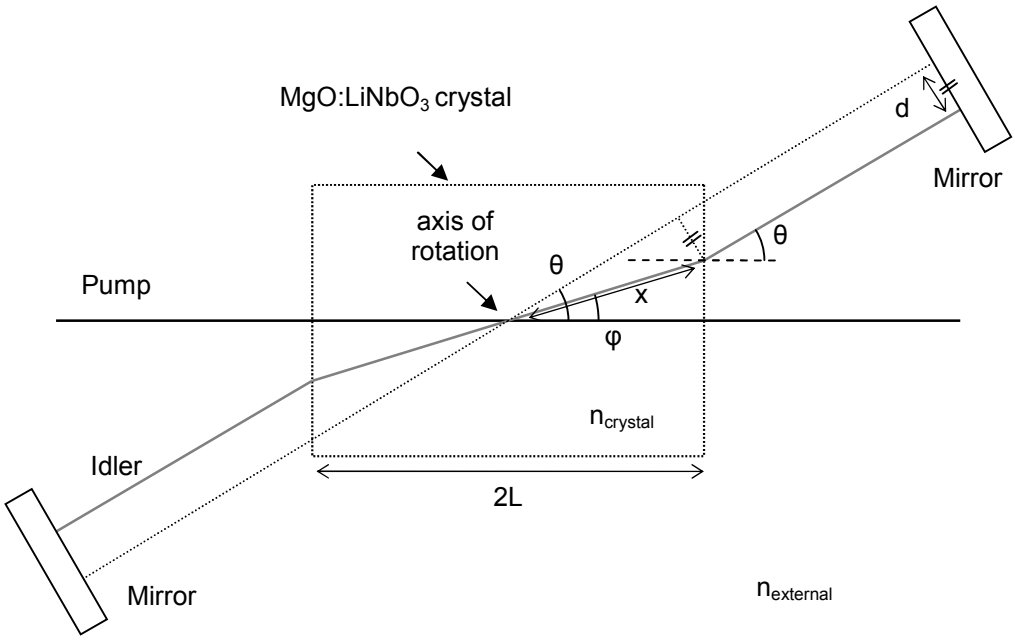

Figure 9 Schematic diagram (not to scale) showing the displacement of the idler mode on the cavity mirrors due to angle tuning.

It can be seen that due to refraction at the crystal faces there is an offset of the idler wave on the surface of the mirrors that is dependent on the cavity angle θ. An expression for this walk off can be derived as follows: first Snell's law is applied to the refraction of the idler wave at the crystal to air boundary,

$$n_{crystal}\sin(\varphi) = n_{external}\sin(\theta) \tag{2.10}$$

From simple geometry we have,

$$\cos(\varphi) = \frac{L}{x} \tag{2.11}$$

and,

$$\sin(\theta - \varphi) = \frac{d}{x} \tag{2.12}$$

Now rearranging (2.11) for x and substituting into (2.12) gives

$$d = \frac{L\sin(\theta - \varphi)}{\cos(\varphi)} \tag{2.13}$$

Using $n_{external} = 1$ for air, (2.10) can be substituted into (2.13) to give

$$d = \frac{L \sin\left(\theta - \sin^{-1}\left(\frac{\sin(\theta)}{n_{crystal}}\right)\right)}{\cos\left(\sin^{-1}\left(\frac{\sin(\theta)}{n_{crystal}}\right)\right)} \tag{2.14}$$

This can be simplified for small angles using the approximation $\sin(\theta) \approx \theta$ to

$$d = \frac{L\theta(n_{crystal} - 1)}{\sqrt{{n_{crystal}}^2 - \theta^2}} \tag{2.15}$$

And finally since θ is small (<<1),

$$d = L\theta \frac{(n_{crystal} - 1)}{n_{crystal}} \tag{2.16}$$

The displacement induced by a 50mm lithium niobate crystal (L = 25mm, n = 2.15) are shown in Figure 10. This analysis shows that the idler mode walks across the mirrors by almost 0.5mm over the whole tuning range – in a direction opposite to the mirror movement, which for a ~1mm diameter mode would mean that when optimised for low terahertz frequencies (i.e. where the mirror is as close to the laser mode as possible) no mirror overlap at all (i.e. no cavity) would remain at the higher angle, or that the mirrors would totally obscure the laser cavity at the low frequencies when set up for high terahertz frequencies.

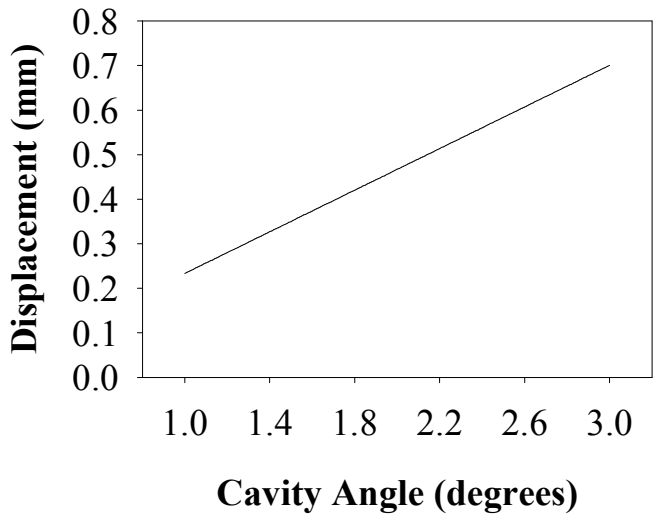

Figure 10 graph showing the calculated displacement of the idler mode on the cavity mirrors.

To avoid this difficulty, and thereby simplify the implementation of computer controlled automatic tuning, a novel idler cavity geometry (in the context of terahertz OPOs) was developed using two extra mirrors and an offset swing arm (see Figure 11). This system is characterised in Chapter 3 and has been adopted by MSquared Lasers of Glasgow as the tuning mechanism for their commercialised version of the intracavity terahertz OPO developed during this research. Tuning can also be achieved by individual angle tuning of each idler mirror by the same amount, but this is more complex as it requires the mirrors to be moved the exact same amount.

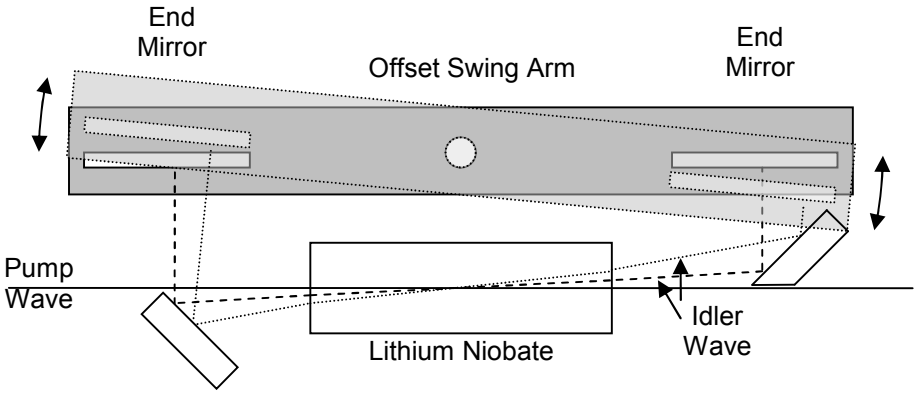

Figure 11 single parameter tuning mechanism showing two angle positions.

2.7. Collinear Phasematching Schemes

In addition to these designs, the availability of periodically poled lithium niobate opens up new opportunities for customising the phasematching condition. Here the crystal structure is periodically inverted in such a way as to stop the natural phase mismatch building up, allowing a "quasi phasematched" process to experience net gain. This can be included in the k-vector diagrams such as those in Figure 7 by the inclusion of a fourth vector representing the poling grating period. In particular such schemes allow the pump and idler wave propagation direction to be collinear, while still maintaining the non-collinear propagation of the THz radiation and hence its rapid exit from the crystal in order to minimise absorption. Quasi phasematching solutions have been demonstrated for the generation of terahertz radiation by the difference frequency generation between two lasers, but only recently has work been published by Molter et al that exploits this technique in an optical parametric oscillator[14]. This publication describes a complex injection seeded, pump enhanced system, and does not give a full account of the design considerations of the poled

crystal. Several poled crystals have been designed and tested for use in an intracavity terahertz OPO during the course of our own research, our work long preceding the publication by Molter et al. Our work yielded an optimal design differing from that published by Molter, and also provided a more complete description of the device in relation to several crucial characteristics. This work is written up in Chapter 6, and has resulted in both a paper publication [15] and a granted patent [16] – which was published prior to the work of Molter et al. A second and more recent patent has also been filed (May 2010). A large portion of the work was also presented in a poster at the New Trends in Terahertz Imaging (NTTI) summer school, in Paris in 2007.

2.8. Phasematching Bandwidth

A consequence of using a resonant idler cavity is that the resonator axis will select the phasematching solution that experiences net gain, and so have the effect of narrowing the output of a parametric oscillator compared to that of a parametric generator. In the low gain limit, as the phase mismatch $\boldsymbol{\Delta k}$ builds up, parametric gain decreases roughly as

$$\mathrm{sinc}^2\left(\frac{\boldsymbol{\Delta k} l}{2}\right) \tag{2.17}$$

where l is the interaction length of the three waves and

$$\boldsymbol{\Delta k} = \boldsymbol{k}_p - \boldsymbol{k}_i - \boldsymbol{k}_T \tag{2.18}$$

Due to this there is a range of frequencies that, although not subject to perfect phasematching, phasematch closely enough to experience overall gain. These frequencies lie within the phasematching bandwidth, which is defined as the range over which the overall gain, equation (2.17), is over $1/2$ its maximum, and is a reasonable estimate as to what the linewidth of the device will be.

If we take the idler wave direction as fixed by the resonator cavity then we have the situation illustrated in Figure 12, where we need to examine the phase mismatch that builds up by changing the idler frequency whilst maintaining its direction.

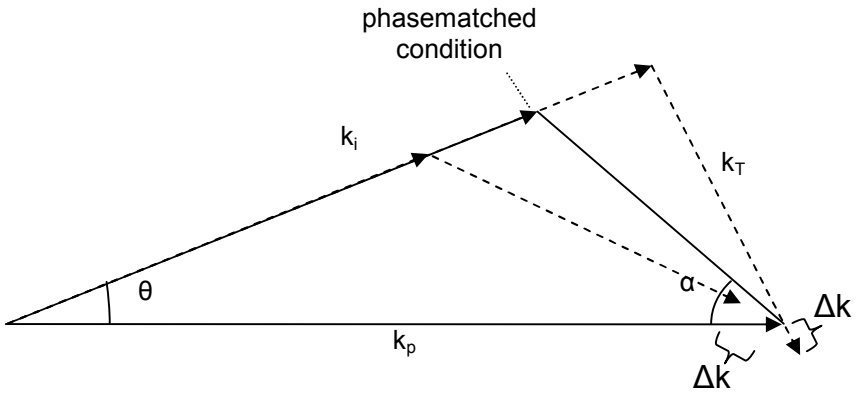

Figure 12 k vector diagram illustrating the origin of the phase mismatch that can build up in the non-collinear scheme when the idler angle is fixed by a resonant cavity.

This was analysed by writing a MathCAD worksheet that takes a given idler wave angle and then scans through the idler – terahertz frequency pairs allowable by the conservation of energy calculating the associated phase mismatch, given by

$$\Delta \boldsymbol{k} = \left|\boldsymbol{k}_p - \boldsymbol{k}_i\right| - \left|\boldsymbol{k}_T\right| \tag{2.19}$$

This was then used to determine the decrease in parametric gain according to equation (2.17). An example plot of the reduction in gain is shown in Figure 13 for an angle corresponding to the generation of approximately 1.5THz, showing a bandwidth of ~114GHz. [N.B. The interaction length (l) was estimated to be ~0.5mm using the reasoning outlined in section 2.10.1, equation (2.26) and assuming a beam width of 1mm and Terahertz walk off angle of ~65°.]

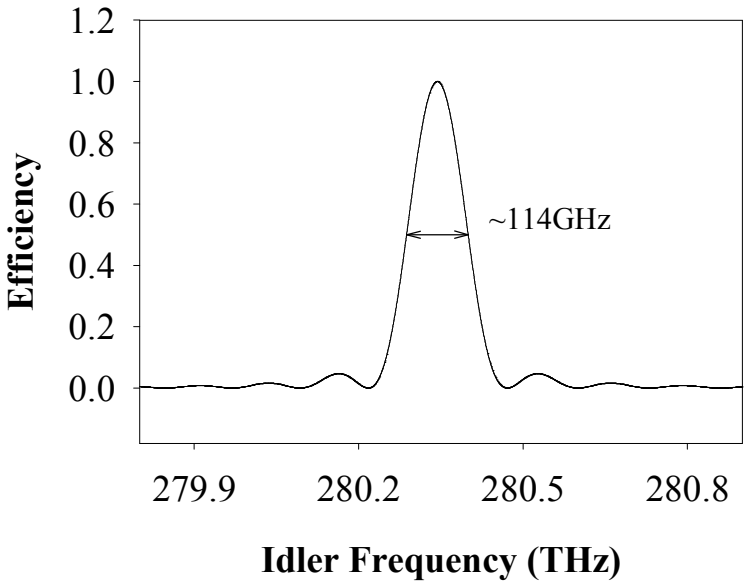

Figure 13 phasematching efficiency for an idler angle of 0.675° (~1.5THz). Calculated for a constant idler angle as would be defined by the idler resonant cavity.

To see how this bandwidth varies over the range of 1THz to 3THz, the range of angles shown in Figure 8 were input into the worksheet. The results are shown in Figure 14 and indicate a decrease in bandwidth at higher terahertz frequencies but the effect is not very large.

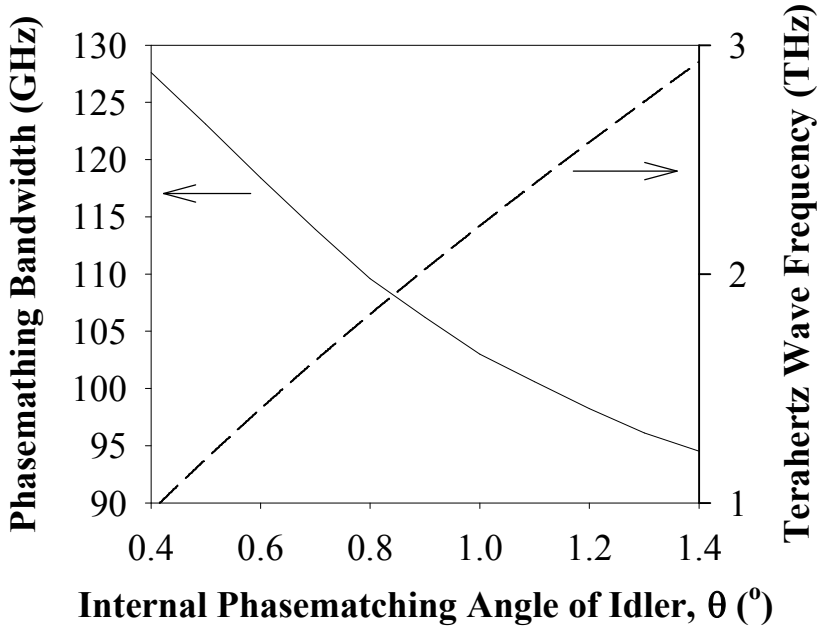

Figure 14 plot showing how the phasematching bandwidth varies with terahertz frequency assuming that the idler wave direction is fixed at each point by the resonant cavity.

2.9. Terahertz Output Coupling

Once the terahertz radiation reaches the crystal surface the proximity of the polariton resonance raises another issue – a high refractive index. Indeed, in the region between 1THz and 3THz MgO:$LiNbO_3$ exhibits a refractive index of around 5.2 (see Figure 5). This reduces the total internal reflection (TIR) angle to approximately 11° (to the normal) at the crystal to air interface. Due to the non-collinear phase matching used the terahertz radiation is being generated at an angle of roughly 25° to the normal of the crystal air interface (i.e. well beyond the TIR angle) meaning that none can escape. A standard antireflection layer is not suitable here, as this simply moves the total internal reflection to the antireflection layer to air interface (or using Snell's law: $n_{crystal}\sin(\theta_{crystal}) = n_{layer}\sin(\theta_{layer}) = n_{air}\sin(\theta_{air})$, which is equivalent to there being no intermediate layer at all). There are several methods reported in the literature to overcome this. The most simple is to cut the end of the crystal at an angle such that the terahertz is then incident close to the normal, as shown in Figure 15i (requiring that the cut be made at approximately 25° to the side face)., and is the technique used in the Piestrup device of 1975 [4], but still leaves a high Fresnel reflection at the crystal to air interface of around 46% (an antireflection coating could

now be implemented with a material of suitable refractive index, but it would of course vary in efficiency with tuning of the terahertz wave), and only the terahertz generated in close proximity to the cut can be extracted. Also, the terahertz radiation generated further from the end of the crystal has to traverse a greater distance (and hence suffers greater absorption) before escaping.

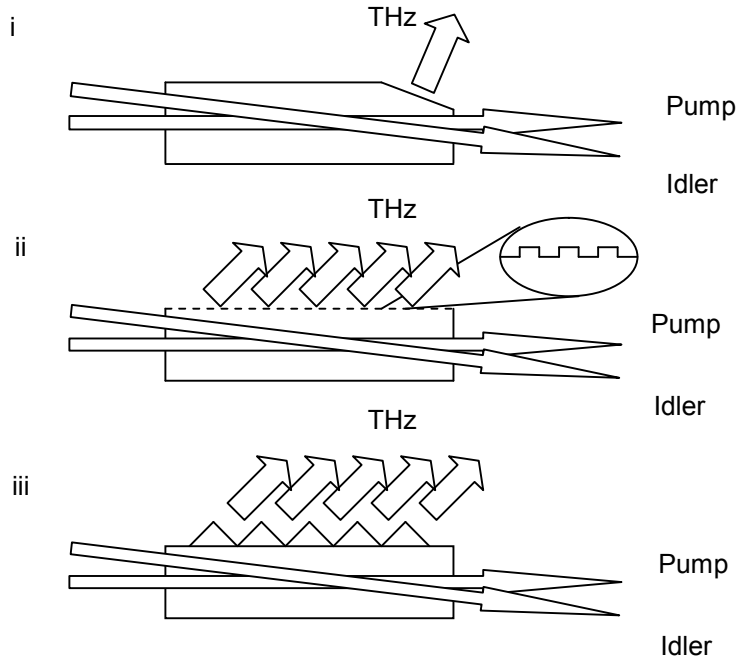

Figure 15 various terahertz output coupling schemes used in the literature.

In 1996 Kawase et al[6] reported improved output coupling (by over a factor of 250) by means of a "monolithic diffraction grating" (see Figure 15ii). The grating was formed by cutting grooves into the surface of the crystal itself using a precision dicing saw. This technique has the advantage that the terahertz can be extracted along the full length of the pump and idler overlap region, but the trade off is that the terahertz output angle varies enormously with tuning (the wavelength is varying from 100μm to 300μm). Hence detector and coupling optics would need to be realigned when the device was tuned, significantly complicating the implementation of the source.

The most useful output coupling technique (and the one utilised in the intracavity device) is by the use of high resistivity silicon prisms as shown in Figure 15iii. The intermediate refractive index of the silicon (n~3.4) increases the TIR angle to about 41° at the crystal to silicon interface and reduces the Fresnel reflection here to around 8.5% (given an incidence angle of around 25° to the normal). The prisms are

designed such that the terahertz arrives at near normal incidence to the silicon to air interface (the output face is set to be at ~40° to the crystal's side), greatly reducing the angular dispersion of the terahertz wave with tuning, albeit with a Fresnel reflection loss of roughly 30%. High resistivity (i.e. high purity) silicon is specified, as in low purity silicon more charge carriers can be released when illuminated by the scattered pump and/or idler waves (which will lie in the region of 1064nm to 1080nm), which causes the reflection of the terahertz wave. This technique was also pioneered by Kawase et al [17].

Calculations of the exit angles with frequency tuning were performed to compare the dispersion levels of the 3 options, the results of which are shown in Figure 16. For the purpose of the comparison the silicon prism array and corner cut techniques were optimised to give minimum dispersion (near orthogonal exit), and the grating coupler design was based on the grating used by Kawase et al. in [6] (which had a grating period of 125μm).

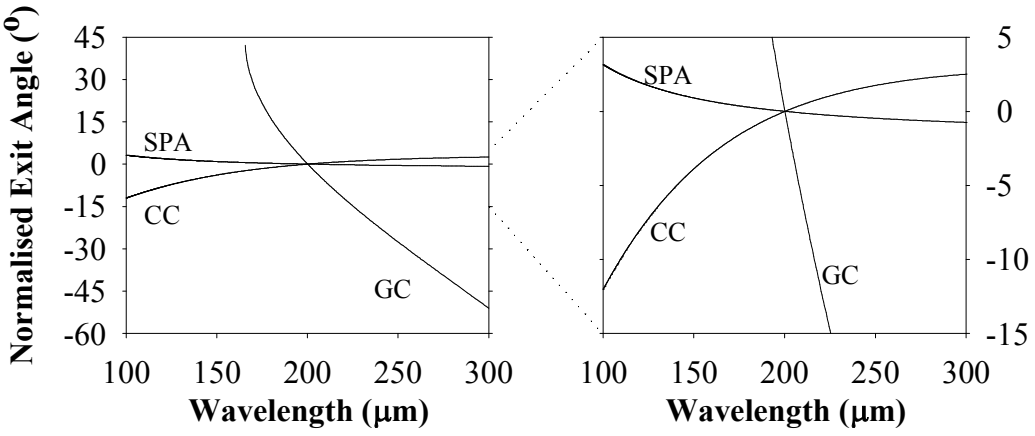

Figure 16 plots showing the calculated angular dispersion of the output coupled terahertz wave for corner cut (CC), grating coupler (GC) and silicon prism array (SPA) approaches. All plots are normalised to the exit angle of 200μm output.

It can readily be seen that the grating coupler is not a good choice for a tuneable system; the system modelled does not even output couple the whole tuning range, cutting off at ~165μm. Of the remaining two the silicon prism array offers the least angular dispersion, and with the reduced Fresnel losses is therefore the best option for output coupling.

2.10. Operation Threshold in the Terahertz OPO

Since the enhancement resulting from stimulated polariton scattering can be modeled as that of second order parametric generation, albeit with a modified nonlinear coefficient, we propose the following theoretical treatment to analyse the threshold gain requirements.

The process of parametric generation is a second order nonlinear optical effect (i.e. one that is proportional to the optical electric field raised to the second power), and describes the interaction of 3 electromagnetic waves: an input pump wave, and two lower frequency, downconverted waves in a nonlinear medium. The wavelengths of the downconverted waves are constrained by the conservation of energy such that:

$$\frac{hc}{\lambda_p} = \frac{hc}{\lambda_i} + \frac{hc}{\lambda_T} \tag{2.20}$$

where h is Planck's constant and c is the speed of light. λ is the free space wavelength of the wave denoted by the subscripts p, i and T for the pump (highest frequency and is present at the start), idler (next highest frequency) and terahertz waves (lowest frequency) respectively.

By the substitution of the complex electric fields of the three waves ($E_{p,i,T}$), along with the polarisation response of the medium into the one dimensional wave equation a set of three equations can be derived that describe the behaviour of the three waves (known as the "coupled wave equations") as they propagate along a direction z:

$$\begin{aligned} \frac{dE_T}{dz} &= i\kappa_T E_p E_i^* e^{i\Delta kz} \\ \frac{dE_i}{dz} &= i\kappa_i E_p E_T^* e^{i\Delta kz} \\ \frac{dE_p}{dz} &= i\kappa_p E_T E_i e^{i\Delta kz} \end{aligned} \tag{2.21}$$

Where Δk is the phase mismatch parameter and

$$\kappa_x = \frac{\omega_x \chi_{eff}^2}{2n_x c} \tag{2.22}$$

Where ω is the angular frequency n the refractive index at the wave denoted by the subscript, $\chi_{eff}^{(2)}$ is the effective second order nonlinear susceptibility tensor, and c is the speed of light.

Using these coupled equations, and a few assumptions, it is possible to derive the gain experienced by either one of the downconverted waves in a single pass of the nonlinear medium. The assumptions are that all three waves are plane waves (neither converging nor diverging), that perfect phasematching is achieved ($\Delta k = 0$), and that the pump wave is constant through the crystal (not being depleted). So, for a crystal length L the single pass, unsaturated, multiplicative power gain of the resonated idler wave, G, can be expressed:

$$G = \cosh^2(\Gamma L) \tag{2.23}$$

where Γ is calculated from the small signal gain:

$$\Gamma^2 = \frac{8\pi^2 d_{eff}^2 I_p}{c\varepsilon_0 n_p n_i n_T \lambda_i \lambda_T} \tag{2.24}$$

where n and λ are the refractive index and wavelength at the wave denoted by the subscripts, ε_0 is the permittivity of free space, I_p is the intensity of the pump wave, and d_{eff} is the effective nonlinear coefficient.

2.10.1. Interaction Length

The previous expression for the single pass gain is not adequate if for some reason the interaction length of the three waves is limited. This can happen if, for instance, there is significant absorption of one of the downconverted waves. Or indeed if the propagation direction of one of the downconverted waves causes a "walk-off" from the other waves, as may be required for phasematching to be satisfied. In this situation the length has to be broken down into smaller, identical, segments over which the three waves do interact, for which equation (2.23) can then be applied. The total single pass gain is then calculated by multiplying together the gain of each of the segments i.e.

$$\begin{aligned} G &= \cosh^2(\Gamma l)_1 \times \cosh^2(\Gamma l)_2 \times \ldots \times \cosh^2(\Gamma l)_N \\ &= \cosh^{(2N)}(\Gamma l) \end{aligned} \tag{2.25}$$

where l is the length of a segment, and $N = L/l$ is the number of segments that make up the length of the pump wave. This situation is shown in Figure 17 for the case of the walk-off of one of the waves.

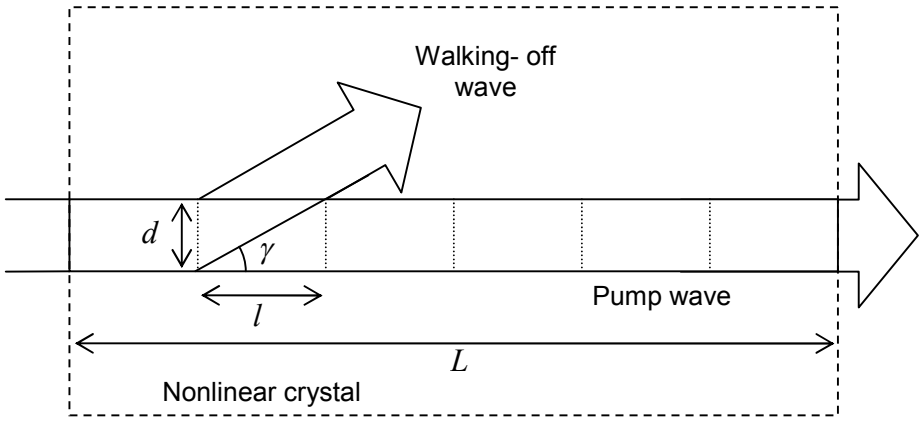

Figure 17 illustration of the reduction in interaction length due to one of the downconverted waves propagating at an angle to the other waves.

If γ is the walk-off angle and d is the pump beam diameter, then the interaction length can be expressed by:

$$l = \frac{d}{\tan(\gamma)} \tag{2.26}$$

for the case of walk-off. If the downconverted wave is being absorbed then instead the interaction length is defined by the absorption length as:

$$l = \alpha^{-1} \tag{2.27}$$

where α is the absorption coefficient.

2.11. An Extracavity Pumped System

For the purpose of this introductory chapter on terahertz generation by parametric methods a description of a device reported by Kawase et al. in 2001[17] now follows, with the important features highlighted and described. An analysis of the threshold pumping requirements of the device will also be included such that a comparison with the intracavity device developed during the course of the PhD research can be made. This source is analysed because it is the closest system design reported to our

intended intracavity terahertz OPO design – which will be described in the next chapter.

Kawase et al have also demonstrated extracavity pumped terahertz OPOs, where the infrared idler wave is resonant. The most powerful system they report using this method[17] produced up to 192pJ pulses of THz energy when pumped by a laser producing 34mJ, 25nS long pulses (assuming FWHM) at a repetition rate of 50Hz. Operation threshold was found to be at a pump energy of 18mJ. The tuning range extended from 100μm to 330μm for the terahertz wave. The device is illustrated in Figure 18.

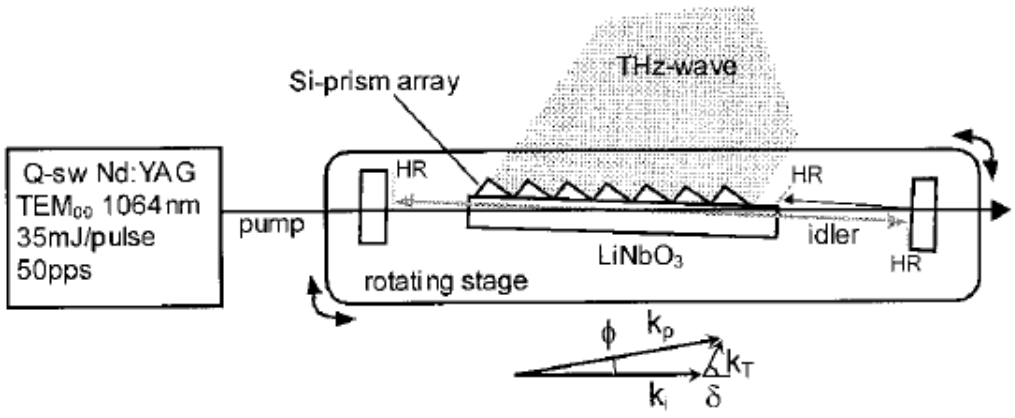

Figure 18 Schematic diagram of the pulsed terahertz OPO reported by Kawase et al[17] (the source of this diagram). The pump laser used was a commercial system. Tuning of the cavity was achieved by rotation of the whole OPO (i.e. the mirrors, crystal and silicon prisms are mounted on one plate which is rotated).

The pump laser was a Q-Switched Nd:YAG laser – a well understood "workhorse" laser that is readily available and reliable. The terahertz OPO itself is a relatively simple device, comprising a nonlinear crystal (lithium niobate, 5mm tall (crystal z axis) by 65mm long (x axis) by 6mm wide (y axis)) which is antireflection coated at the ends for the 1064.4nm pump light, an array of silicon prisms for output coupling of the terahertz radiation, and two high reflectivity mirrors (HR) that form the 15cm long resonant cavity for the idler wave (which tuned from 1067nm to 1075nm) that were only coated half way across to allow the pump beam through. The diameter of the pump beam was given as 1.5mm, however the measurement method was not stated (i.e. full width half maximum, e^{-1}, e^{-2}, knife edge, pinhole/CCD?). The terahertz beam was also characterised, and although close to the prisms (~10cm or

less) the output lobes of each prism could be made out, at larger distances (>40cm) the beam rapidly became Gaussian like.

2.11.1. Gain Estimation

From the analysis put forward by Brosnan and Byer [18] it is generally accepted that around 140dB of net gain is required for a pulsed OPO to reach threshold. That is to say that for M round trips of the cavity (within the temporal envelope of the pump pulse), each having a single pass gain represented by (2.25), the threshold is given by

$$\begin{aligned} 140dB &= \cosh^{2N}\left(\Gamma l\right)_1 \times \cosh^{2N}\left(\Gamma l\right)_2 \times \ldots \times \cosh^{2N}\left(\Gamma l\right)_M \\ 140dB &= \left(\cosh^{(2N)}\left(\Gamma l\right)\right)^M = 10^{14} \end{aligned} \tag{2.28}$$

which can be used to estimate the required gain in an OPO with limited interaction length of the waves. For the terahertz OPO described in section 2.10 we have to make several assumptions and estimates have to be made in order to calculate the estimated small signal gain. To begin with the build up time of the idler pulse is estimated to be 15nS and the round trip time of the idler cavity was estimated from the idler cavity length (l_{ic}) to be $t_c = \frac{2l_{ic}}{c} = \frac{2\times 0.15}{3\times 10^8}$ which is 1nS. This indicates that there is time for $M = 15$ round trips of the idler cavity. It is also assumed now that there are no parasitic losses for the idler wave, such as leakage through cavity mirrors or diffraction of the beam out of the resonant mode. Assuming a walk-off limited gain over the whole 65mm long crystal gives a value for $N = \frac{L}{l} = \frac{65mm}{1.5mm/\tan 65^\circ} \approx 93$.

Now from rearranging (2.28) and substituting these values in we have

$$\cosh\left(\Gamma \times 0.7mm\right) = \sqrt[2\times 15\times 93]{10^{14}} \tag{2.29}$$

which yields a required value for Γ of ~2.2cm^{-1}. Given that the pumping pulse is of 18mJ in 25nS at threshold, and the beam area is calculated (we assume a FWHM diameter of 1.5mm) to be 1.77×10^{-2}cm^2 gives an intensity of ~41MWcm^{-2}. Comparing these results to the calculations performed by Shikata et al (displayed in Figure 3) indicates that these values are consistent in as much as the value falls below the gain predicted for an intensity of 150MWcm^{-2} of around 3-4cm^{-1} and considering that there is uncertainty in the beam diameter. Additionally if the figure for the

intensity, along with an estimated d_{eff} of ~125pm/V after Shikata et al [10] and a wavelength of 200μm, we get a value for Γ of ~1.9cm^{-1}.

2.12. Summary

In this chapter we have introduced the history of the parametric approach for terahertz generation from optical waves, and the physical basis for the polariton enhanced gain presented. We have also described the components and techniques required to produce a useful system. Finally a method for the analysis of the gain (optical intensity) required to reach terahertz generation threshold has been described and applied to an extracavity device published by Kawse et al, which will serve as a point of comparison for the following chapters detailing the intracavity systems developed during the PhD research.

2.13. References

1. Y. R. Shen, *The principles of nonlinear optics* (Wiley-Interscience, New York, 1984).

2. J. Gelbwachs, R. H. Pantell, H. E. Puthoff, and J. M. Yarborough, "A Tunable Stimulated Raman Oscillator," Applied Physics Letters **14**, 258-262 (1969).

3. J. M. Yarborough, S. S. Sussman, H. E. Puthoff, R. H. Pantell, and B. C. Johnson, "Efficient, Tunable Optical Emission from $LiNbO_3$ without a Resonator," Applied Physics Letters **15**, 102-105 (1969).

4. M. A. Piestrup, R. N. Fleming, and R. H. Pantell, "Continuously tunable submillimeter wave source," Applied Physics Letters **26**, 418-421 (1975).

5. M. A. Piestrup, R. A. Powell, G. B. Rothbart, C. K. Chen, and R. H. Pantell, "Cerenkov Radiation As A Light-Source For 2000-620-A Spectral Range," Applied Physics Letters **28**, 92-94 (1976).

6. K. Kawase, M. Sato, T. Taniuchi, and H. Ito, "Coherent tunable THz-wave generation from $LiNbO_3$ with monolithic grating coupler," Applied Physics Letters **68**, 2483-2485 (1996).

7. K. Kawase, Y. Ogawa, Y. Watanabe, and H. Inoue, "Non-destructive terahertz imaging of illicit drugs using spectral fingerprints," Opt. Express **11**, 2549-2554 (2003).

8. K. Kawase, M. Sato, K. Nakamura, T. Taniuchi, and H. Ito, "Unidirectional radiation of widely tunable THz wave using a prism coupler under noncollinear phase matching condition," Applied Physics Letters **71**, 753-755 (1997).

9. K. Kawase, J.-i. Shikata, and H. Ito, "Terahertz wave parametric source," Journal of Physics D: Applied Physics, R1 (2002).

10. J. Shikata, K. Kawase, K. Karino, T. Taniuchi, and H. Ito, "Tunable terahertz-wave parametric oscillators using $LiNbO_3$ and $MgO:LiNbO_3$ crystals," Microwave Theory and Techniques, IEEE Transactions on **48**, 653-661 (2000).

11. S. S. Sussman, "Tunable Light Scattering from Transverse Optical Modes in Lithium Niobate," in *Physics*(Stanford University, 1970), p. 116.

12. D. E. Zelmon, D. L. Small, and D. Jundt, "Infrared corrected Sellmeier coefficients for congruently grown lithium niobate and 5 mol.% magnesium oxide doped lithium niobate," J. Opt. Soc. Am. B **14**, 3319-3322 (1997).

13. E. D. Palik, *Handbook of Optical Constants of Solids* (Academic Press Inc. London, 1985).

14. D. Molter, M. Theuer, and R. Beigang, "Nanosecond terahertz optical parametric oscillator with a novel quasi phase matching scheme in lithium niobate," Opt. Express **17**, 6623-6628 (2009).

15. D. A. Walsh, P. G. Browne, M. H. Dunn, and C. F. Rae, "Intracavity parametric generation of nanosecond terahertz radiation using quasi-phase-matching," Opt. Express **18**, 13951-13963 (2010).

16. C. F. Rae, M. H. Dunn, and J. A. C. Terry, "Parametric Terahertz Radiation Generation With Lateral Beam Coupling " (2005).

17. K. Kawase, J.-i. Shikata, H. Minamide, K. Imai, and H. Ito, "Arrayed silicon prism coupler for a terahertz-wave parametric oscillator," Appl. Opt. **40**, 1423-1426 (2001).

18. S. Brosnan, and R. Byer, "Optical parametric oscillator threshold and linewidth studies," Quantum Electronics, IEEE Journal of **15**, 415-431 (1979)

Chapter 3. The Intersecting Cavity Terahertz OPO

3.1. Introduction

In this chapter I shall describe the design, construction and characterisation of the very first "intersecting" cavity terahertz OPO (ICTOPO). The designation as an intersecting cavity, rather than intracavity, device owes to the more descriptive nature of the term. The majority of intracavity OPOs share a cavity mirror, and usually the resonators share a common axis within the nonlinear crystal. Due to the nature of the phasematching required in the case of the ICTOPO, none of the three downconverted waves share a common propagation direction resulting in cavities that overlap within the nonlinear crystal but share no resonator mirrors nor a common axis, hence the intersecting cavity designation. The work outlined in this chapter has led to a publication [1], several conference presentations [2, 3], and has also been presented at several international meetings (see publications section for full details). A number of patents have also resulted from this work, which have been licensed to MSquared Lasers – an SME in Glasgow, Scotland, who have commercialised, and sell internationally, the basic ICTOPO system written up in this chapter.

The assistance of Dr Tom Edwards and Dr David Stothard in this early work, both with performing the experiments and in understanding the science behind the device is acknowledged.

3.2. System Design and Characterisation

3.2.1. Overview

The experimental set-up of our intersecting cavity terahertz OPO is show in Figure 19, and was inspired by the extracavity device demonstrated by Kawase et al [4]. The similarity in design provides a reference point for directly comparing performance (intracavity intensities at threshold in particular). Referring to Figure 19 the Q-Switched laser cavity was formed by mirrors M1 (R>98% @ 1064nm, high transmission @ 808nm) which was coated directly on the Nd:YAG laser crystal and M2 (R=90% @ 1064nm) which was a standard dielectric laser mirror, and was ~37cm in length. The output coupler was chosen for the ease with which intracavity pulse intensity could be calculated, by multiplying by a factor of ten the laser pulse intensity

measured extracavity. Clearly, higher intracavity intensities and so lower thresholds would result from using a reflectivity of 100% for M2, and to output couple all the laser field (excluding that lost by parasitic mechanisms) into the downconverted waves, however the novelty is in the first demonstration of the intracavity approach itself rather than claiming that an optimal efficiency was achieved. Components QW (quarter wave plate), PC (Pockels cell), and POL (air spaced cube polariser) constitute a quarter-wave Q-Switch (QS) and set the polarisation of the laser to be orthogonal to the plane of the diagram. The laser gain medium, LG, was a cylindrical Nd:YAG crystal (1.3% doping, Northrop Grumman) 7mm long and 4mm in diameter, on the end of which mirror M1 has been deposited. Pump light at 808nm was provided by a temperature stabilised quasi-continuous wave laser diode module (LD) bought off the shelf from LIMO GmbH, and is delivered via an optical fibre with a core diameter of 800μm to a pair of aspheric lenses (AL), which image the end of the fibre into LG with a 1:1 ratio. This circular end pumping provides an efficient coupling of energy into the desired laser mode diameter of ~1mm – and is much more efficient than side excitation schemes or flash lamp pumping.

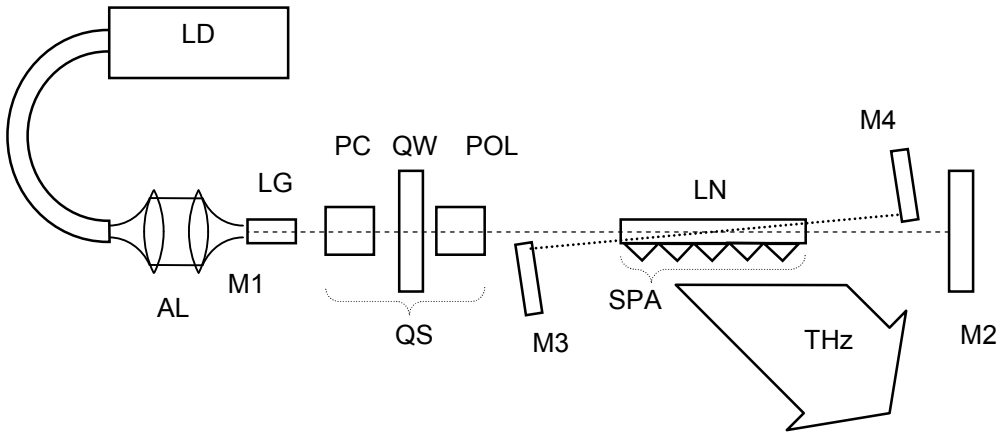

Figure 19 Design of the intersecting cavity terahertz OPO. The dashed and dotted lines represent the Q-Switched laser and idler waves respectively.

The nonlinear crystal (LN) has dimensions 5mm x 5mm x 50mm and has its crystallographic z axis parallel to the polarisation of the laser (i.e. also coming vertically out of the page). The x axis of the crystal is parallel to the laser axis and the 50mm long side of the lithium niobate. Each end is antireflection coated at 1064nm and the 5mm x 50mm side faces, through which the terahertz is extracted, have a good optical polish. Against one of these polished sides an array of 7 high resistivity

(>10kΩcm) silicon prisms is held in place by a specially designed mount to ensure good optical contact so that the terahertz radiation may be coupled out.

The resonator that forms the OPO idler cavity (in conventional OPO terminology the frequencies are labelled “pump”, “signal”, and “idler” in the order of decreasing frequency, but in this case the wave of interest is the lowest frequency so we call the generated infrared wave the “idler”, and the lowest frequency the “THz” wave) is formed by the plane mirrors M3 (high reflectance for idler) and M4 (R~98% for idler), and is 13cm in length. Due to the high difference in frequency of the pump and THz waves the idler wavelength is very close to that of the pump, enabling the use of standard Nd:YAG laser mirrors. Both of these mirrors are on individually adjustable mounts which are themselves mounted on a common swing arm that pivots around the centre of the nonlinear crystal. Rotating the angle of this “intersecting” cavity changes the angle that feedback is provided at, altering the phase matching such that the idler and signal (terahertz) are tuned.

3.2.2. Pump Laser Properties

Previous work on the extracavity systems have primarily used 1064nm wavelength pump sources with a mode diameter of 1mm, as such this configuration was replicated for the intracavity system. The benefit of a ~1μm pump laser is the availability of well established Neodymium based gain media, which have proved robust systems for practical application. These materials are discussed more in section 3.2.3. This beam diameter was retained as there is a trade off to be made, and a ~1mm beam diameter has been demonstrated as a good compromise in the work of Kawase et al (whether the measurement was, for example, $1/e^2$ or FWHM was not stated so here we assume $1/e^2$). A smaller diameter causes the interaction length of the three waves, determined by the walk-off associated with the THz-wave, to be reduced, reducing the round trip gain significantly. Conversely a larger diameter reduces the peak intensity for a given pulse energy, and hence would increase the pump energy required to reach threshold. Beam diameter also has an effect on tuning and extraction of the terahertz wave. A larger pump diameter would generate a larger idler beam diameter, and as there is an angle between these waves a large beam prevents the overlapping region (where the terahertz wave is generated) being near the crystal surface and so the terahertz wave experiences more (polariton resonance enhanced in lithium niobate) absorption before

being extracted. If the overlapping region is kept close to the surface then the idler wave will be clipped by the aperture of the crystal, reducing efficiency and tuning range to those frequencies corresponding to lower angles. Conversely a small beam will result in a reduced interaction length within the crystal as the pump and idler walk off each other, and as the energy in the pump wave is limited by crystal damage it cannot be increased to compensate.

3.2.3. Laser Crystal

Nd:YAG was the gain medium chosen for the pump laser. This is an efficient four level system lasing primarily at 1064.4nm. The material possesses a number of physical attributes making it very suitable for use in lasers. Its strength and hardness are high enough that no special fabrication procedures are needed to cut and polish crystals into the required size and shape, and the material has a high thermal conductivity, which is beneficial for the minimising of localised temperature gradients that lead to thermal lensing. High optical quality Nd:YAG crystals are readily available, with no natural birefringence present, and optical pumping can be achieved using readily available diode lasers operating at ~808nm. The use of Nd:YAG in Q-Switched lasers is common, as the materials fluorescence lifetime is relatively long (~230μs) allowing a large population inversion to build up.

The alternative gain materials, Nd:YLF and Nd:YVO_4, were rejected on several grounds: Nd:YLF, whilst showing less thermal lensing and having a longer fluorescence lifetime (480μs) making it initially more attractive for Q-Switched lasers than Nd:YAG, has a smaller (by 3 to 4 times) emission cross section, and exhibits natural birefringence along with a polarisation dependent output which makes correct alignment important to avoid losses. Additionally, (792nm) diode lasers suitable for optical pumping are less available than those for Nd:YAG. Nd:YVO_4 has a higher emission cross section (by 5 times) than Nd:YAG, and a broader absorption profile making it less sensitive to the frequency drift of a diode laser with temperature. The fluorescence lifetime is much shorter (~100μs) however, making it less practical for Q-Switching, and birefringence and polarisation of the laser output are present. The absorption of the pump (at around 809nm) also depends on polarisation, varying almost by a factor of four, which could lead to issues when coupling the pump to the

gain crystal via an optical fibre (non-polarisation maintaining) as the absorption length may not be consistent. [5]

3.2.4. Electro-Optic Q-Switching

The process of Q-switching requires an intracavity element in the laser that can rapidly alter the cavity quality ("Q") between a low Q state, where the laser will not operate, to a high Q state allowing laser oscillation. The mode of operation is as follows: initially the Q-switch is set to spoil the laser cavity whilst the laser gain medium is pumped to create a population inversion (far larger than the steady state inversion level of the laser), the pumping then ceases and the Q-switch opens. Now a large round trip gain is present in the cavity, so a laser field rapidly builds up from noise and depletes the stored population inversion. Once the inversion is depleted there is no more gain, and so the pulse then falls away in a few round trips, the decay time depending on round trip losses and the cavity length. Laser pulses produced in this manner are typically between 1 and 100ns in duration.

The cavity Q must be switched rapidly (in less than the build up time of the laser pulse) otherwise multiple lower energy pulses can be produced, and must be spoiled sufficiently to prevent significant "prelasing" which reduces the population inversion available to the Q-switched pulse. There are a number of methods available to Q-switch a laser cavity, some active which require triggering, and some passive which occur with no interference. Of these the electro-optic Q-switch is the most suitable for producing the high pulse energies required by the intracavity terahertz OPO. Diffracting light out of the cavity with an acousto-optic modulator (AOM), does not reduce the cavity Q enough to prevent prelasing during the intense pumping phase. Along with passive Q-switching methods (intracavity saturable absorbers), this method does not typically produce high energy pulses. Another advantage of the electro-optic Q-switch arises from its reliance on a polariser, forcing the polarisation of the laser into a predetermined state. This is important with regard to the terahertz OPO as the pump wave must be polarised along the z axis of the $MgO:LiNbO_3$.

The quarter-wave ($\lambda/4$) electro-optic Q-switch implemented comprises three components: a polariser, a quarter-wave plate, and a Pockels cell designed for a quarter wave retardation with the application of a an electric field, with the latter two components on the same side of the polariser within the laser resonator as illustrated

in Figure 20. The principal axes of the quarter-wave plate and Pockels cell are aligned at 45° to the polarisation set by the polariser, such that along one of the principal axes the laser light will see an optical path $\lambda/4 + N\lambda$, where N is an integer, longer than the other. In the low Q condition the Pockels cell is inactive, and any light initially polarised in the direction of the polariser will transit the Pockels cell with no change, but on passing through the quarter-wave plate becomes circularly polarised. After reflection at the end mirror the light then passes through the quarter-wave plate a second time becoming polarised orthogonally to it's original state and as such is rejected by the polariser. To switch to a high Q cavity a potential of a few kilovolts is applied across the Pockels cell inducing birefringence and forming a second quarter-wave plate. This either adds to or cancels out the effect of the first, depending on the relative orientations of the fast and slow axes, rotating the polarisation by either π or 0 radians which in both cases is then transmitted by the polariser. There are several other variations of the electro-optic Q-Switch but this quarter-wave design allows the use of a lower voltage across the Pockels cell than required for half-wave operation, and the addition of the quarter-wave plate allows the voltage to be applied only when the Q-Switch is opened for the pulse to build up.

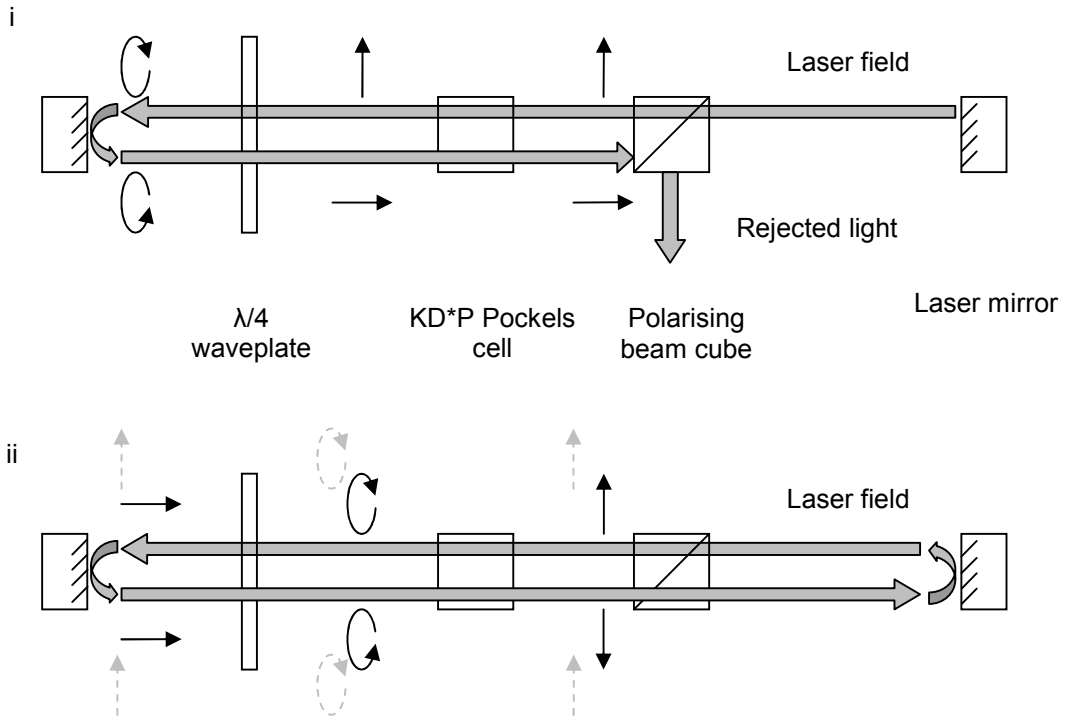

Figure 20 Illustration of the quarter wave Q-Switch layout and its effect on polarisation i) with Q-Switch closed, and ii) with Q-Switch opened allowing laser pulse build up. Black arrows represent the polarisation state of the laser light.

The components used in the intracavity terahertz OPO were a polarising beam cube (Northrop Grumman AP00003454/Type II), a multiorder waveplate (Thorlabs WPMH10M-1064), and an "Impact 8" KD*P Pockels cell with driver from Cleveland Crystals, inc. The orientation of the principal axes of the quarter-wave plate when situated in the laser cavity with the polariser could be determined by finding the angles of maximum laser power when running quasi continuous wave, the orientation required is then at 45° to one of these peak orientations. The Pockels cell was marked such that the required orientation was identifiable, and was provided with a calibration sheet specifying the quarter-wave voltage to be ~3.5kV. Q-Switched laser operation was found to be insensitive to the voltage applied within a range of a few hundred Volts – suggesting other cavity losses (such the 10% output coupling mirror used) dominated.

3.2.5. End pumping

The most efficient way to pump a laser gain material is to excite only the area that is going to be usefully coupled into the oscillating laser mode, so minimising pump energy requirements. This also avoids excess heating of the crystal from the thermal component in the decay of the population, reducing the thermal lensing and damage. Traditional methods of pumping a laser such as using flash lamps (where the flash lamp is positioned along one focus of a cylindrical resonator with elliptical cross section, and the laser gain material along the other) and side pumping schemes using diode bar lasers, involve exciting large regions where no energy is extracted by the laser mode. More recent advances have led to the availability of high power, high brightness, fibre coupled laser diodes that emit light from a small circular aperture with no astigmatism. If in conjunction with this the gain medium is coated with a suitable dielectric coating that reflects the laser and transmits the pump diode light, then this can act as one of the laser cavity mirrors whilst allowing pump light to be launched axially into the laser gain medium.

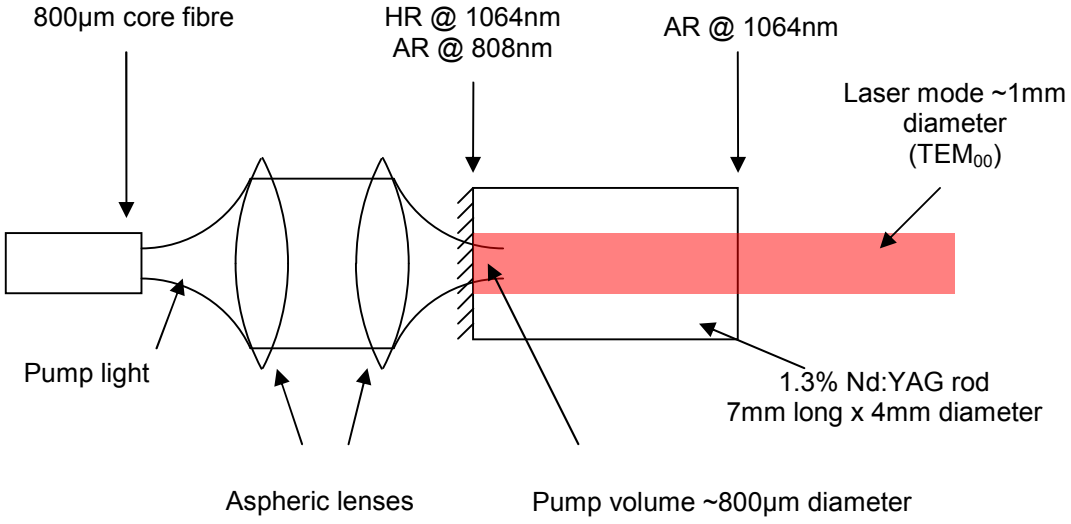

Figure 21 End pumping scheme used in the intracavity terahertz OPO. The highest efficiency is achieved by ensuring that the pump volume has a similar diameter to the mode volume.

The end pumping scheme used in the intracavity terahertz OPO is illustrated in Figure 21, where the pump diode light is imaged with a 1:1 ratio into the Nd:YAG crystal. Confining the pump volume to less than the TEM_{00} mode diameter also increases the

losses incurred by higher order modes, helping enforce single mode, TEM_{00} operation. [5-7]

3.2.6. Pump Characterisation

A quasi continuous wave LIMO fibre coupled diode laser was purchased for the purpose of end pumping the intracavity terahertz OPO. This laser was capable of producing up to 100W of continuous wave radiation in pulses up to 500μs duration in a 20% duty cycle (i.e. up to 400Hz) and was coupled into an 800μm core optical fibre. The pulse characteristics of this laser allow pumping the Nd:YAG for ~2 fluorescence lifetimes (τ ~ 250μs), allowing a significant build up of population inversion for later extraction via Q-Switching, whilst maintaining a lower average power than continuous pumping would require for the same result. Laser diodes are prone to temperature tuning effects, so to ensure optimal efficiency the laser diode was temperature stabilised via a thermo-electric cooler at 25°C, where minimum transmission through the Nd:YAG was observed, and hence maximum energy absorption.

The output of pump light from the fibre was characterised against increasing diode driving current so that the absolute pump energies were known. This is vital for accurate characterisation of the intracavity terahertz OPO. The energy-current characteristic is shown in Figure 22, and displays the anticipated linear dependence of energy on drive current when above laser threshold (~23A).

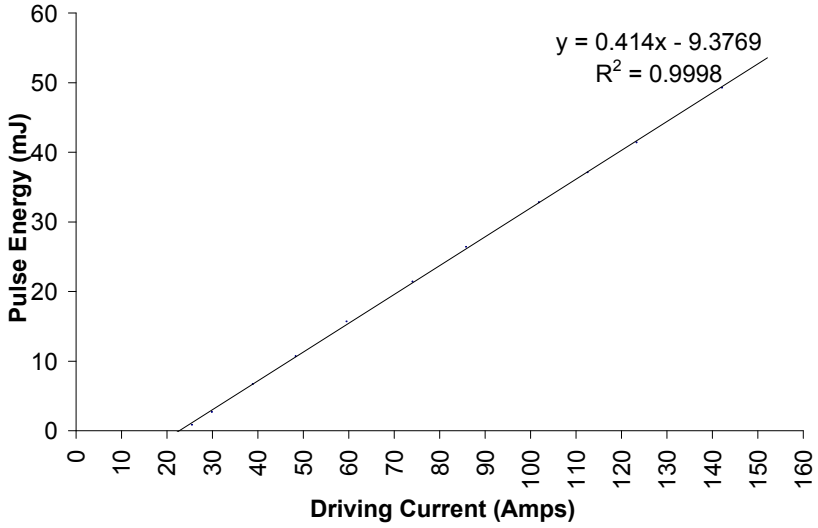

Figure 22 Pump Energy-Current characteristic of the laser diode output from the coupling fibre. Pulses were 500μs in duration.

The pump beam area was experimentally measured using the layout shown in Figure 23. An aperture was used to control the depth of field, and various neutral density filters and/or spectral filters were used to suitably attenuate the light falling on the CCD camera. Using this set up the 808nm pump beam was verified to be ~800µm in diameter and very circular, but showed some localised peaks in intensity (Figure 24).

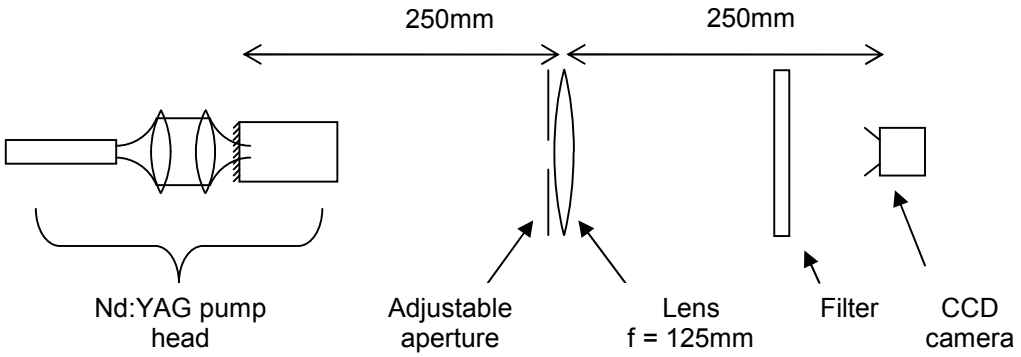

Figure 23 1:1 imaging layout used to investigate pump beam area.

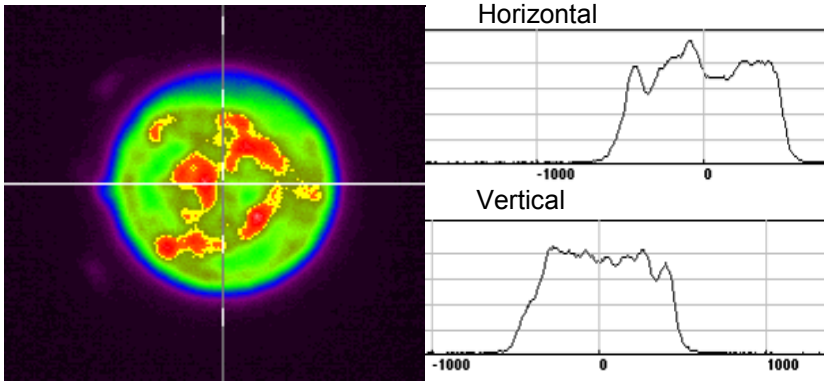

Figure 24 Illustrations of the pump beam profile within Nd:YAG crystal. The mode is highly circular and ~800µm in diameter, but shows localised "hot spots".

The pump volume was then measured by inserting an RG1000 absorption filter into the imaging system and can be seen in Figure 25.

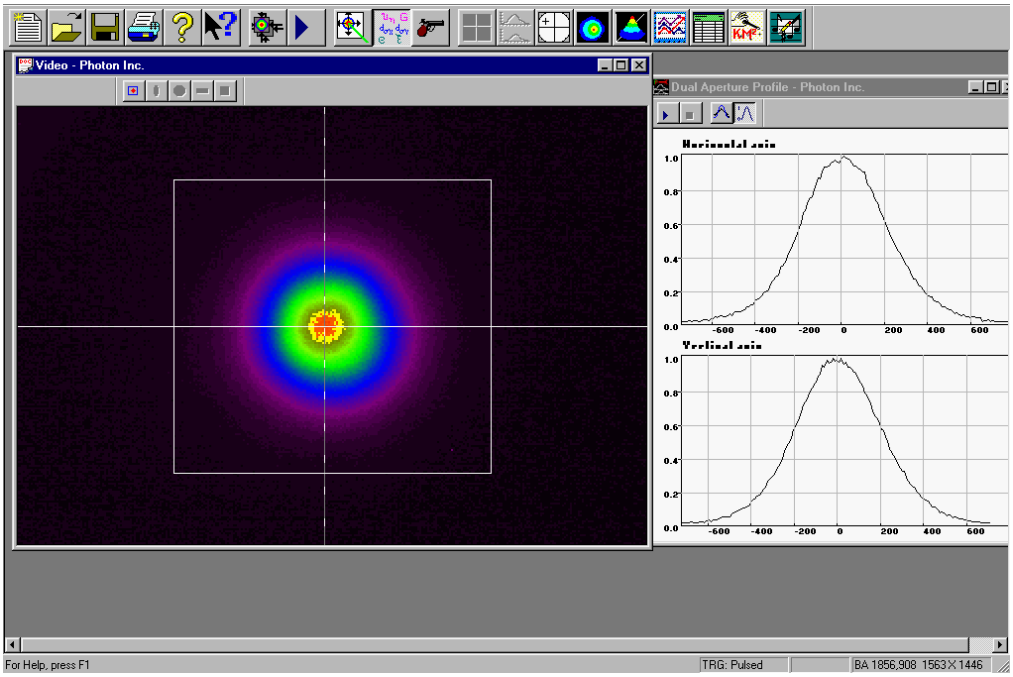

Figure 25 Pump volume profile (1064nm fluorescence) obtained by blocking residual 808nm light with an RG 1000 absorption filter. The hot spots in the pump beam are not transferred to the pump volume, which is Gaussian-like with a diameter of ~800µm.

The pump profile was also monitored whilst changing the diode driving current throughout its full range, and also at temperatures ±5° of the optimal 25° to investigate sensitivity to these factors. No measurable change was observed. If the diode lasing wavelength were slightly tuned away from the peak absorption the pump volume would extend along the axis of the laser mode and would not be measurable in this manner. However, this would distribute the energy and therefore thermal load over a larger volume, possibly forming a more stable laser cavity.

3.2.7. Laser Cavity Mode

As mentioned in section 3.2.2 the diameter of the pump mode was required to be ~1mm in the nonlinear crystal. This was accomplished by a combination of a 6m radius of curvature output coupler and the end pumping technique employed. Using the laser cavity modelling software "PSST!" reveals that the curvature of the output coupler alone is insufficient to create this beam width, supporting a larger mode of ~1.4mm $1/e^2$ diameter as seen in Figure 26.

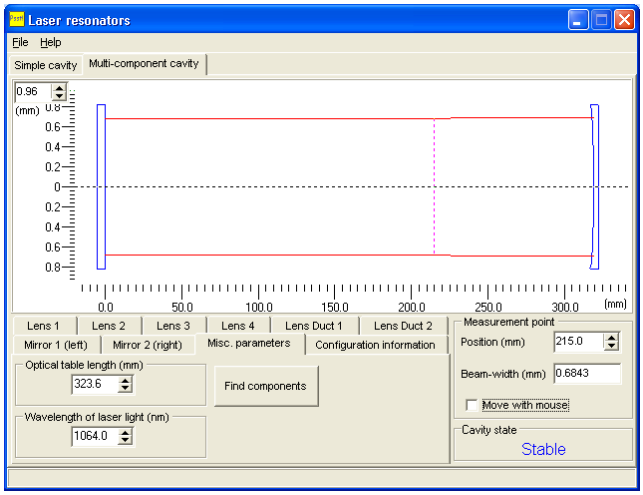

Figure 26 intracavity beam width of the laser calculated using PSST! Cavity length used here is taking into account the reduced optical lengths of the cavity elements (e.g. 50mm of lithium niobate, n~2.2, reduces in length to 50/2.2= 23mm).

However the end pumping scheme causes a combination of soft aperturing, gain guiding, and thermal lensing in the Nd:YAG gain medium that results in a laser mode that in practice has a diameter of ~1mm $1/e^2$, only slightly larger than the pump volume diameter. This was confirmed experimentally using a BeamPro CCD based beam profiling system. An example beam profile is shown in Figure 27, from which it can be seen that the laser mode was Gaussian-like and circularly symmetrical.

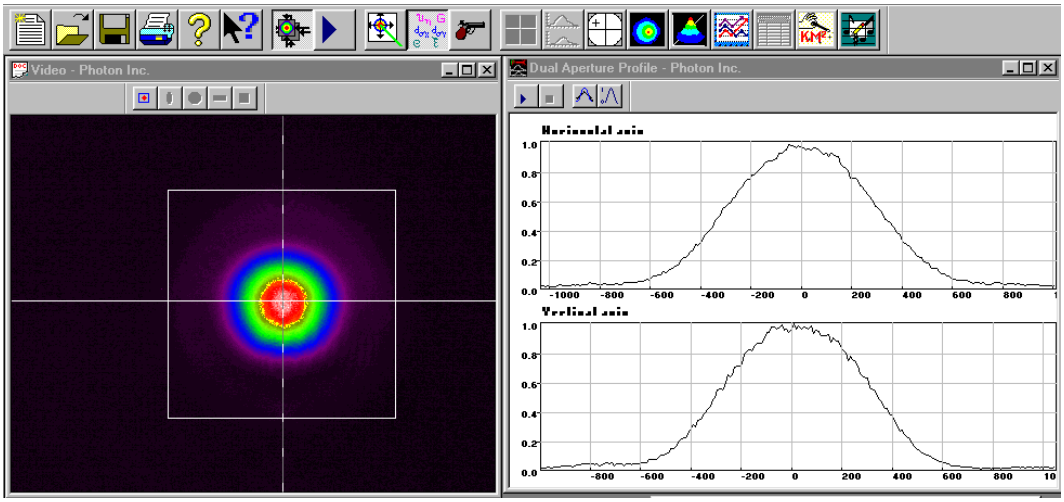

Figure 27 example beam profile captured a few centimetres from the laser output coupler.

A series of profiles were performed at increasing distances so that the beam divergence could be ascertained and the intracavity mode size deduced. This allowed confirmation of the full beam width to be ~1mm ($1/e^2$ diameter) within the laser at the

position of the nonlinear crystal (see Figure 28). The fit was performed using MathCAD and assuming the beam waist was positioned on the laser mirror coating of the Nd:YAG gain medium.

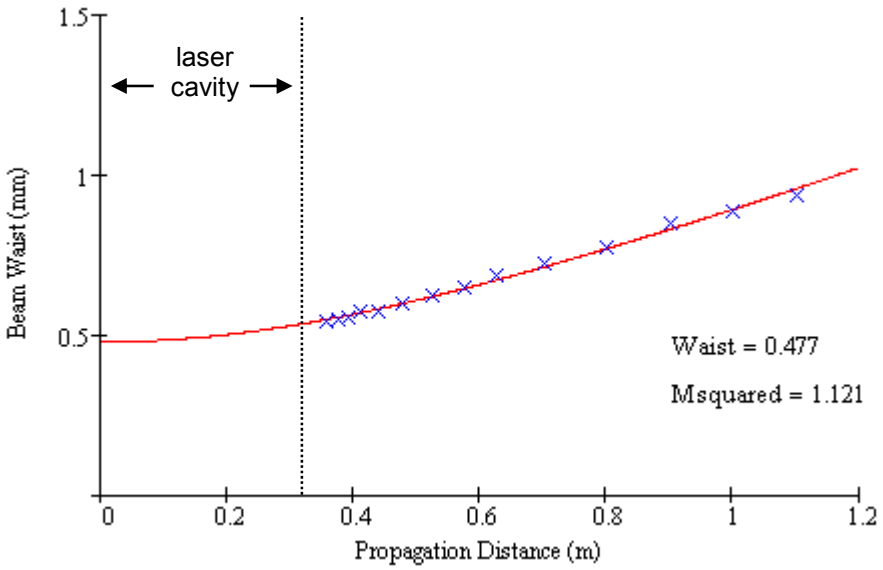

Figure 28 Plot showing a fit to horizontal beam profiles. Note that the beam waist is given as the radius at $1/e^2$. The fit assumes the beam waist to be in the Nd:YAG crystal. Distances from 0 to ~0.32m correspond to positions within the laser cavity, where it can be seen that the fit suggests a close to collimated beam.

3.2.8. Nonlinear crystal

The choice of 5% MgO doped lithium niobate is discussed in chapter 2. In the device described here a 50mm length crystal was purchased, which although shorter than the 65mm piece used by Kawasi et al in a similar device [4] actually provides a greater overall gain length to the idler wave. This is simply because in this case the pump wave is resonant in the laser cavity, and therefore gain is present in both directions of the idler through the crystal. Whilst this wastes half of the terahertz generated as each direction of the idler wave produces terahertz in a direction 180 to that which can be extracted by the silicon prisms and is promptly absorbed by the crystal. There is an advantage, however, in that this technique reduces the threshold pump energy requirements.

3.2.9. Idler Cavity

Due to the low frequency of terahertz waves relative to the ~1μm pump wave (~1:100) the idler frequency is very close in frequency to that of the pump. This means that laser mirrors and optics designed for Nd lasers do not differ much from their design parameters when used for the idler wave, allowing the use of off-the-shelf components for the idler resonator. These mirrors, however, do not tend to have the optical coatings applied right up to the edge (necessary due to the small angle between pump and idler waves), and so it was necessary to have a side polished down in-house until the coating was at the very edge (see Figure 29). Plane mirrors were utilised for the idler cavity as when tuning the OPO the idler walks across the mirror surface, as shown in Chapter 2, and a cavity with curved mirrors designed to provide a stable mode in a specific configuration would then become misaligned.

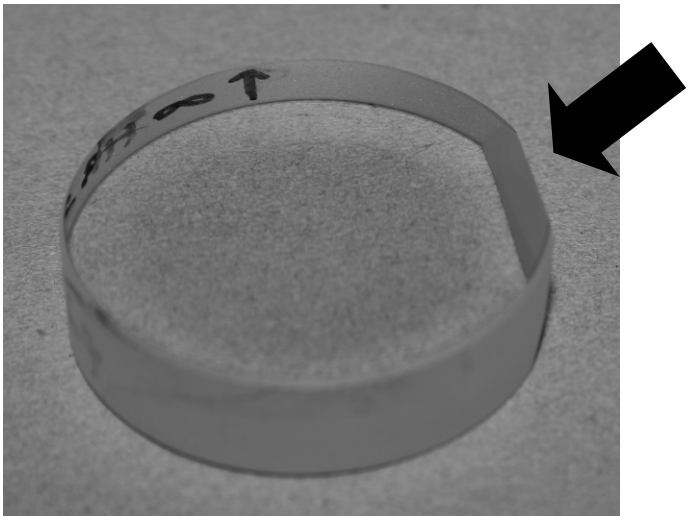

Figure 29 Photograph of an off-the-shelf high reflectivity @ 1064nm, plane mirror showing where edge has been polished down for use as an idler cavity mirror.

These mirrors were then mounted on adjustable stages at either end of a common "swing arm", which was in turn mounted on a stage providing rotation in the horizontal plane pivoting about the centre of the arm (providing the single parameter tuning mechanism of the system). This assembly was mounted on translation stages providing vertical adjustment as well as adjustment perpendicular to the laser axis in the horizontal plane to allow accurate positioning of the swing arm pivot point over the centre of the nonlinear crystal. A photograph of the set-up in the fully constructed laser is shown in Figure 30.

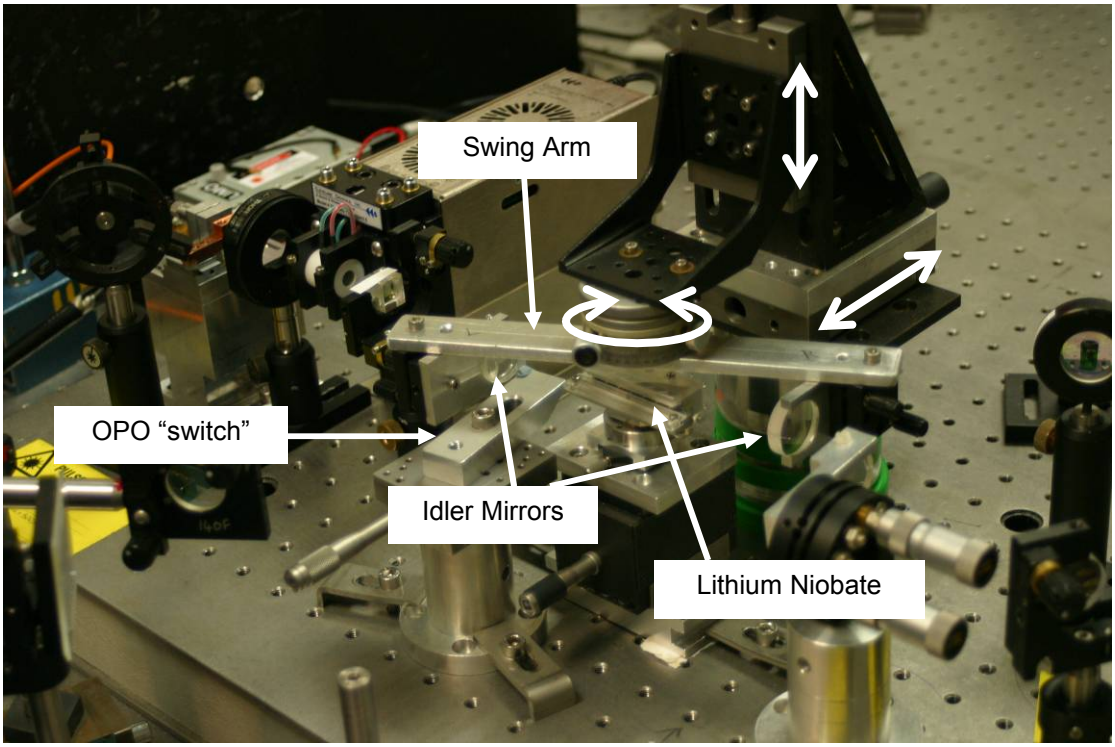

Figure 30 photograph showing the idler cavity design. The OPO "switch" was a piece of card mounted on a translation stage that could be inserted into the idler cavity to "deactivate" the downconversion process. This provided a way to characterise the downconversion performance of the intracavity terahertz OPO.

Positioning of the idler cavity was accomplished by first placing the mount such that the pivot of the swing arm was directly above the centre of the lithium niobate, and idler cavity mirrors were in approximately the right position to form a resonator (judged by eye). Then an iterative process of 1) rotating the idler cavity, with the laser aligned and running, until one of the idler mirrors clipped the intracavity field as judged by a drop in laser power, and then 2) translating the whole swing arm such that the clipping idler mirror was moved away from the laser mode, and then repeating from step 1) until a point where translating the swing arm no longer results in an increase in laser power is reached, was performed. In this position both mirrors were just on the verge of clipping the laser beam, and so in the correct position to intercept the idler wave generated by the downconversion process. The positions of the rotation and horizontal translation stage were then noted down, and the idler cavity rotated by 2° (idler cavity angles vary from ~1° to 3°, see chapter 2) such that the laser is now blocked by the idler mirrors. Now the idler mirrors (which were Nd:YAG laser mirrors) were aligned such that a laser cavity was formed between

each mirror and the mirror coating on the Nd:YAG crystal was formed (using the horizontal stage to switch which mirror was being aligned), thus ensuring that each mirror was parallel to the other, and in the same, horizontal, plane when angle tuned. The positions of the rotation and horizontal stages were then returned to the positions noted previously, and indications of downconversion looked for (e.g. by either looking at the temporal profile of the Q-switched laser pulses, using a viewer card to look for output at the 98% idler mirror, or attempting to block the idler cavity and looking for the increase the laser power that would indicate that downconversion had be stopped). On observation of downconversion a slight adjustment of the idler mirrors, looking to minimise laser output (being careful not to clip the laser cavity), was performed to ensure optimal alignment. A useful technique was to observe the pump temporal profile whilst making this adjustment, aiming for maximum depletion but maintaining a short build up time.

3.2.10. Silicon Prisms

The silicon prisms were designed according to the calculations performed in Chapter 2 where it was shown that the terahertz wave propagates through the silicon at an angle of ~60° to the laser axis (and crystal:silicon interface). For minimum dispersion the prisms were cut such that the terahertz wave exited the silicon at near normal incidence. The actual design used is shown in Figure 31.

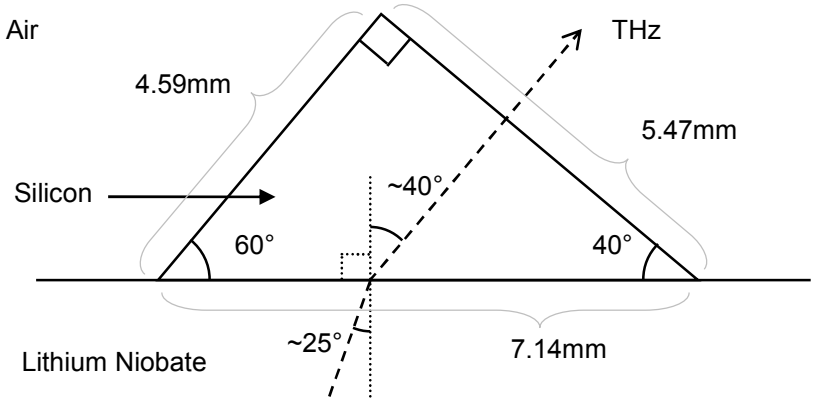

Figure 31 silicon prism output coupler design. The longest side (pressed against the prism) is 50mm/7 = 7.14mm.

3.2.11. Crystal Mount

A custom mount was designed for the dual purpose of providing adjustment of the position and attitude of the lithium niobate within the laser cavity, and to hold an array of silicon prisms firmly against the polished crystal side. A photograph of this mount is shown in Figure 32, and shows the plastic clamps pressing the prisms against the crystal surface. Between the clamps is clear aperture through which the terahertz wave could be output coupled.

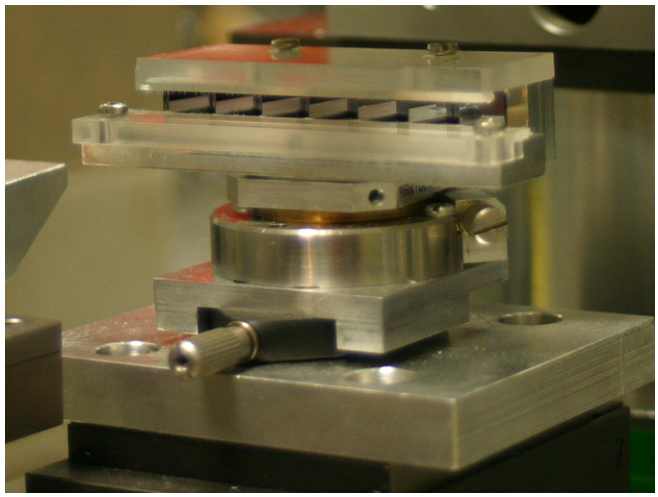

Figure 32 Photograph of crystal mount with silicon prism output coupling array.

3.2.12. Terahertz Collimation

The terahertz wave is generated within the overlap region of the pump and idler beams, and as such is exiting the device from a letterbox like aperture. In the dimension along the overlap region the beam width is relatively large compared to the terahertz wavelength and so the beam will not diverge quickly. However, perpendicularly to this the terahertz generation is limited by the diameters of the pump and idler beams, which are both ~1mm, resulting in a relatively fast divergence angle – this condition is much like that exhibited by diode lasers. The expected terahertz wavelengths are around 100 to 300µm, and so the approximate divergence angle from such an aperture can be from 6° to as much as 17°.

In order to collect and collimate the terahertz beam along an optical path for the purposes of spectroscopy and imaging work this astigmatism had to be compensated. To do this a cylindrical lens (plano-convex, r = 5cm) was designed and made in-house from high density polyethylene (n~1.5 across the THz range), to collimate the quickly

diverging axis when placed at a distance of 10cm from the crystal. After this collimating lens standard off-axis parabolic mirrors could then be used to manipulate the beam.

3.3. Results

The fully constructed system is shown from above in Figure 33. The system has a small footprint on the bench of only ~30cm x ~40cm (not including the laser diode driver etc…), and was constructed from optical components that are all readily available. The focus of this early research was to demonstrate the feasibility of the intersecting cavity approach, rather than to push for high repetition rates or pulse energies, and so the thermal management of the laser was not extensive and the system was restricted to low repetition rates.

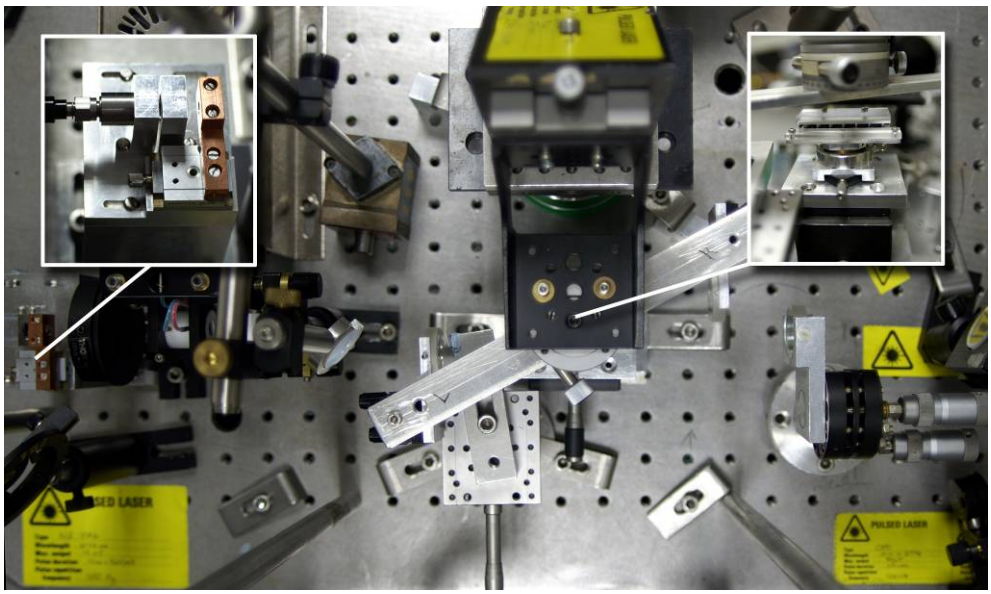

Figure 33 top view of the completed intersecting cavity terahertz OPO.

3.3.1. Operation Characteristics

To characterise the downconversion performance of the intersecting cavity OPO the energy characteristic of the Q-switched laser was measured with the OPO cavity present and blocked by the "switch" shown in Figure 30. The results, plotted in Figure 34, show that the laser output is heavily depleted by the operation of the OPO, showing the characteristic "clamping" of the laser power at OPO threshold levels. It can also be seen from this plot that the pump wave is depleted by ~50% when running significantly above threshold.

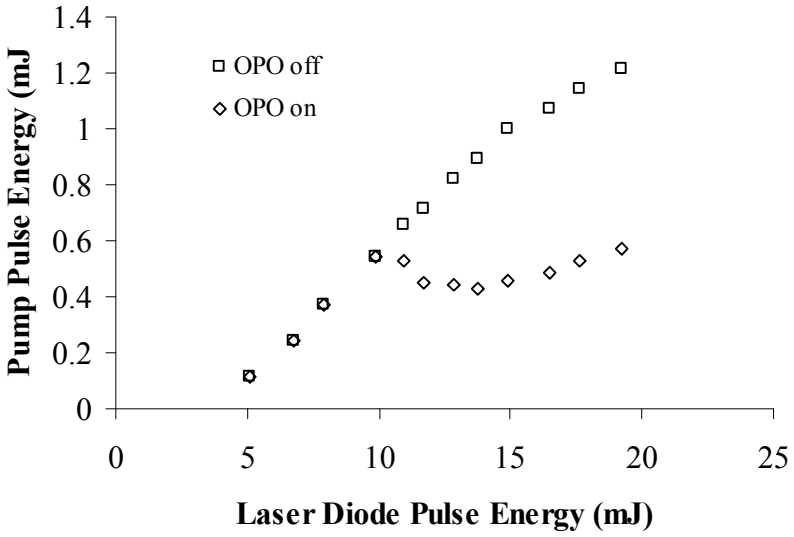

Figure 34 Typical energy characteristic of the Nd:YAG laser – in this case with the OPO tuned to output 1.6THz radiation, showing the clamping of the output pulse energy above OPO operation threshold. It can be seen that the OPO operates effectively, down converting ~50% of the pump light at twice OPO threshold. The laser can be operated at over twice lasing threshold implying that a large portion of the population inversion is being extracted by the Q-switch pulse.

3.3.2. A Note on Laser Efficiency

Figure 34 indicates that the slope efficiency of the laser is only around ~10%, showing that the laser is operating quite inefficiently. A large part of the inefficiency arises from the pump pulse duration: as pumping occurs for 500μs, around twice the population lifetime of 230μs, there is immediately an efficiency of just 41% (only 41% of the pump energy is still stored in the inversion). Then the quantum defect in pumping at 808nm and lasing at 1064nm has an efficiency of 76%. This combination results in there only being ~31% of the pump energy stored in the population inversion for extraction by the Q-switched laser pulse. However, there is still a large discrepancy in the energy extracted through the output coupler and that in the population inversion by a factor of ~3. It is likely that this energy is being lost to parasitic processes, such as surface reflections, laser mode clipping by the idler cavity mirrors, and perhaps thermally induced birefringence in the Nd:YAG crystal. In an attempt to quantify the cavity losses an analysis of the laser threshold with different output coupling percentages was performed with a similar laser set-up. As derived by Findlay and Clay [5, 8] the relation

$$-\ln R = 2KP_{TH} - L \tag{3.1}$$

holds, where R is the output coupler reflectivity, P_{TH} is the laser threshold, K is a conversion factor encompassing all the efficiencies of the laser system, and L is the parasitic cavity loss. Therefore a linear fit to a plot of $-\ln R$ vs. the laser threshold P_{TH} will reveal the value of L where $P_{TH} = 0$. This analysis is plotted in Figure 35.

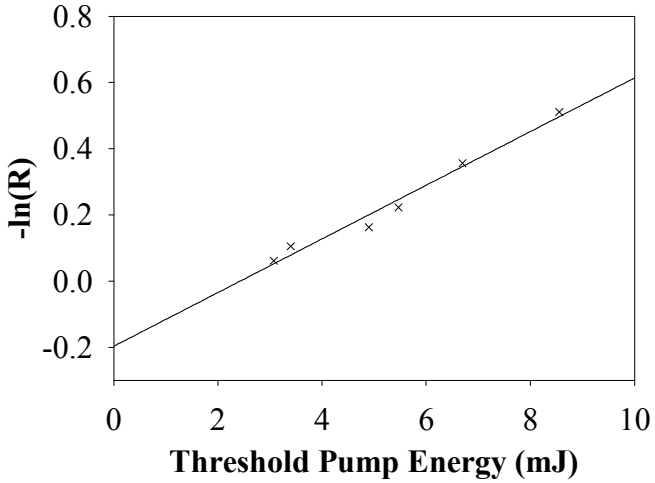

Figure 35 Findlay-Clay analysis of a similar laser cavity to that used for the intracavity terahertz OPO.

As can be seen from Figure 35 the straight line fit yielded a value for L of 0.2. This is a considerable loss and there is no doubt that this is an area for improvement, however it does not diminish the main outcome of this research (that is the demonstration of parametric generation of terahertz radiation pumped intracavity to a laser).

If the cavity losses are accepted to be ~20%, and the output coupling extracts 10%, then the total laser energy at 1064nm is approximately 3 times that measured exiting the output coupler. Comparing this with the ~31% storage of input pump diode energy brings the extraction efficiency above 90%.

3.3.3. Comparison to Extracavity Technique

Oscillation threshold was reached when the Nd:YAG was pumped with 10mJ (20W for 500μs) of primary pump light at 808nm, at which level the laser was outputting 0.6mJ pulses at 1064 nm (corresponding to a generation of 1.8mJ in total). When this is compared to the reported 18mJ of 1064.4nm pump (and subsequently much larger

primary pump energy) threshold of a similar extracavity device[4] the benefits of the intersecting cavity approach are clear, in this case reducing the laser pulse energy required by an order of magnitude.

When pumping at roughly twice OPO threshold with a pump diode pulse energy of ~19mJ the laser produced pulses of ~1.2mJ (3.6mJ in total) in the absence of OPO operation (achieved by physically blocking the OPO idler cavity), reducing to ~0.6mJ (1.8mJ in total) with the OPO down-converting. This indicates that, in total, 1.8mJ of idler and THz radiation is being generated. Unfortunately only a small fraction of this is converted into THz photons due to the large difference in frequency; the quantum defect is as low as 0.35% at 1THz and up to 1.1% at 3THz. Here the OPO was generating 1.6THz, indicating that 10.2μJ of terahertz radiation was being produced inside the crystal. However, when the terahertz pulse energy was measured using a calibrated composite silicon bolometer (QMC Instruments Ltd. model QSIB/2), an energy of ~20nJ was recorded. The primary cause of this ~1000 fold decrease in energy is the aforementioned absorption of terahertz frequencies in lithium niobate, in addition to the factor of two reduction due to terahertz being generated in the opposite direction (into the crystal) on the backward pass of the pump and idler waves. This value compares favourably with the terahertz pulse energy quoted for a similar device reported in [4] of 200pJ (requiring 30mJ of 1064nm energy), and is more than adequate for many spectroscopic and imaging applications.

3.3.4. Pulse Temporal Profiles

Figure 36 shows the temporal characteristics of the pump and idler pulses at twice threshold. Again it can be seen that the pump undergoes ~50% down-conversion. Importantly it can also be seen that the idler pulse builds up swiftly just after the peak of the pump pulse, which undergoes rapid cavity dumping. These features indicate close to optimal extraction of the energy stored in the Nd:YAG crystal is achieved, followed by cavity dumping of the oscillating pump field into THz and idler waves before it decays away by parasitic losses (in this case including the laser output coupling mirror). The profile of the idler also provides some indication of the THz pulse duration, it being generated mainly during the build up phase of the idler wave. This suggests the THz pulse is <10nS in duration, and with pulse energies around 10nJ have a peak power of >1W.

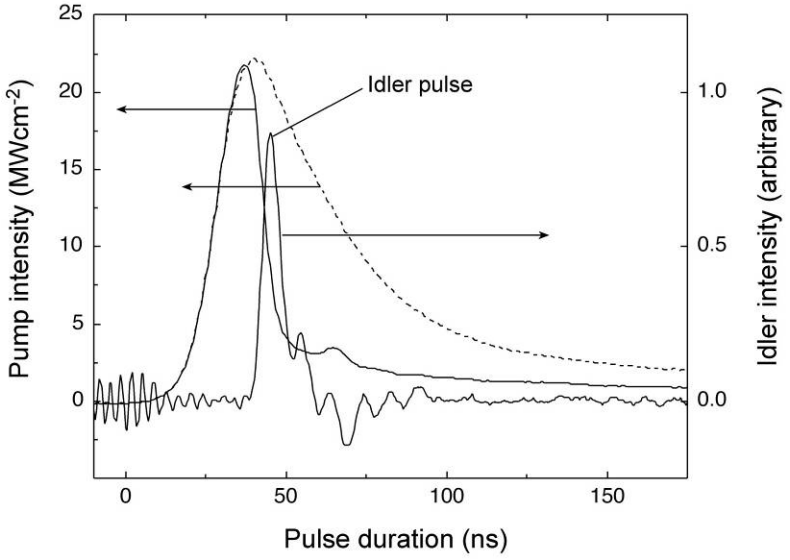

Figure 36 Temporal profiles of pump and idler waves. The cavity dumping of the pump wave is clearly illustrated. Dotted line represents the measured pump profile in the absence of OPO operation, again showing ~50% downconversion.

Considering that the two mirrors used for the idler cavity had high and 98% reflectivity coatings the decay of the idler wave at first appears to be too short. Figure 36 indicates it to be less than 10ns, whereas for a stable cavity with no parasitic losses the decay time can be calculated as:

$$t_c = \frac{T_{roundtrip}}{-\ln(R_1 R_2)} = \frac{0.4 \diagup 3\times10^8}{-\ln(0.98)} = 66\text{ns} \tag{3.2}$$

As this cavity is borderline unstable in design (due to the plane mirrors) it is necessary to consider the round trip losses due to diffraction of the intracavity beam using the method of Fox and Li [5, 9]. The Fresnel number (F) of the idler cavity is given by

$$F = \frac{a^2}{L\lambda} \tag{3.3}$$

Where a (~0.5mm) is the beam radius ($1/e^2$), L (~200mm) is the cavity length, and λ (~10^{-3}mm), resulting in a Fresnel number of 1.25. With this figure the round trip losses for a plane-parallel cavity are around 1dB, or ~20%. This corresponds to a cavity decay time of around ~6ns, which is consistent with the recorded temporal profile.

In a similar manner to the calculations performed in Chapter 2 section 2.9.1 gain requirements can be calculated for the intracavity case allowing a comparison to be

made with the extracavity case. Estimating the pump pulse duration to be ~50ns at threshold, and an idler cavity that is ~20cm optical length gives

$$M = \frac{50\times10^{-9}}{\left(\frac{2L_{opt}}{c}\right)} \sim \frac{50\times10^{-9}}{\left(\frac{0.4}{c}\right)} \sim 37.5 \tag{3.4}$$

as the number of round trips of the idler cavity during which parametric gain is present. Now considering the interaction of the three waves to be limited by the walk-off gives an interaction length of $l = \frac{1}{\tan 65^\circ} \sim 0.5\,\text{mm}$. In the intracavity regime the pump wave is resonant, and so gain is present in both passes of the idler wave through the lithium niobate, doubling the effective crystal length per round trip. Hence the number of gain sections is $N = \frac{100}{0.5} = 200$. Again assuming that 140dB of gain is required to bring a pulsed device to threshold from noise gives a required gain of:

$$\Gamma = \frac{\cosh^{-1}\left(\sqrt[2*M*N]{10^{14}}\right)}{l} \sim 1.3\text{cm}^{-1} \tag{3.5}$$

Which is rather less than that required for the extracavity case as calculated in chapter 2 (2.2cm^{-1}), which is to be expected as in this case gain occurs twice per round trip for the idler wave. This figure can be compared to the calculated gain for the present intracavity intensity. The intracavity peak power is calculated from the pulse energy extracted from the output coupler, the reflectivity of the output coupler, and the pulse duration as $P = \frac{0.6\times10^{-3}}{50\times10^{-9}} \times \frac{1}{1-0.9} = 120000\,\text{W}$. The peak intracavity pulse intensity is therefore 1.53x10^{11}Wm^{-2}, for a beam diameter of 1mm. If we again assume an enhanced d_{eff} of 125pmV^{-1} and use the equation

$$\Gamma^2 = \frac{8\pi^2 d_{eff}^2 I_p}{c\varepsilon_0 n_p n_i n_T \lambda_i \lambda_T} \tag{3.6}$$

this gives a calculated gain coefficient of ~1.2cm^{-1} – which is in agreement with the estimated gain required.

3.3.5. Tuning Characteristic

To date the THz output has been tuned from 900GHz up to 3.05THz with pulse energies in the 10nJ region for frequencies up to around 2.1THz, beyond which the power drops off rapidly as illustrated in Figure 37. At the low frequency end of the tuning range the gain is reduced due to the increasing separation of the THz wave frequency and the polariton resonance, but the more significant issue is the angle required between the idler and pump cavities. Frequencies lower than 1THz require an angle of less than 1°, and considering that the pump and idler waves are both ~1mm in diameter an idler cavity 13cm long is already clipping the intracavity laser field. One solution would be the lengthening of the idler cavity but this has two limitations: the idler cavity length is limited by the laser resonator cavity components, and excessive lengthening of the cavity will increase the build up time of the OPO, degrading its performance. Figure 37 shows the extension of the tuning range from 1.2THz down to 900MHz by the lengthening of the idler cavity by 25mm at each end. A potential solution is the use of a "supermirror"[10] with sharp cut off between the idler frequencies and the laser wavelength, such that the idler is reflected and laser transmitted. Such a mirror could be placed in the laser resonator with no ill effect, allowing tuning to lower frequencies whilst maintaining a short idler cavity. Unfortunately it has not so far proven possible to find a company capable of producing such a mirror for us to try; the aforementioned demonstration used a mirror produced in-house.

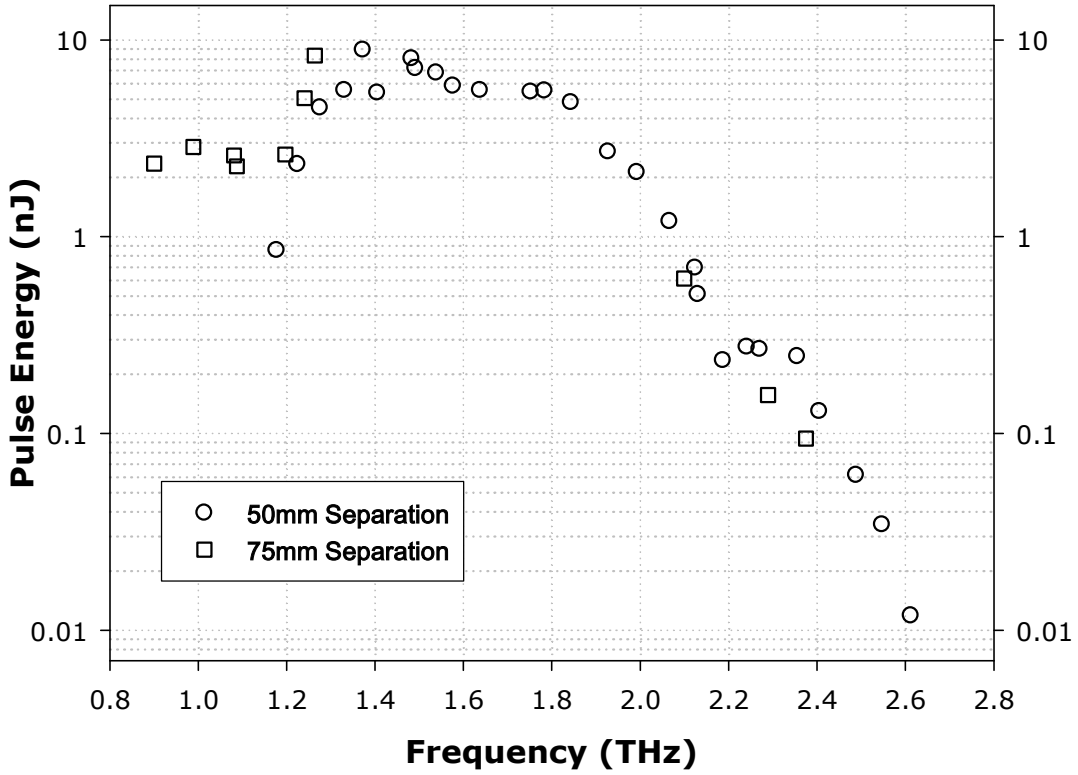

Figure 37 Terahertz power spectra recorded using a calibrated silicon bolometer. Data is shown for two idler cavity configurations, with idler mirrors either 50 or 75mm from the MgO:$LiNbO_3$ crystal, to illustrate the possible extension of the tuning range.

The generation of higher frequencies faces further problems: as the intersecting cavity angle increases the overlap of the pump and idler wave decreases, and the idler cavity begins to be clipped by the crystal aperture. In practice a balance must be found between moving the generation region away from the crystal face to avoid this clipping, and keeping it close enough to minimise the significant absorption loss, which is also increasing as the generate THz wave's frequency approaches that of the polariton resonance.

To verify the tuning of the terahertz radiation a set of measurements of the idler frequency vs. the idler wave angle were made. The angle of the idler wave was determined by measuring its separation from the pump wave at a distance of 50cm from the centre of the nonlinear crystal (i.e. outside the laser cavity) and using trigonometry (also compensating for the reduced optical length of the nonlinear crystal due to its refractive index). The relative angle change was also double checked by directly reading the position of the rotation staged used to adjust the swing

arm. This gave the external angle of the idler wave and so the internal generation angles calculated in Chapter 2 need to be converted to external angles via Snells law. The result of this experiment is shown in Figure 38, and shows the good agreement between the calculated curve and the experimental data.

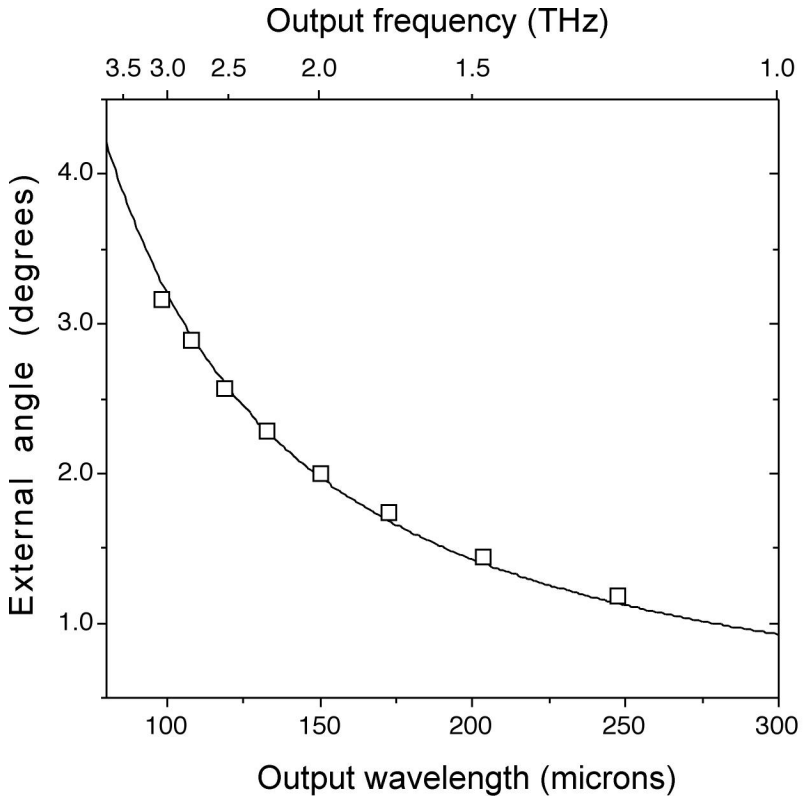

Figure 38 Tuning of ICTOPO with idler cavity angle. Squares represent experimental data points, and the solid line represents the theoretical tuning curve based on Sellmeier equations for pump/idler from Zelmon et al [11] and compiled THz indexes [12].

3.3.6. Linewidth and Threshold

The linewidth of the terahertz radiation is restricted due the conservation of energy by both the linewidths of the pump wave and that of the idler wave. Therefore by measurements of these linewidths the approximate linewidth of the terahertz wave can then be inferred; an example of the idler wave measurement is shown in Figure 39. This is useful as no terahertz wavemeters are currently available.

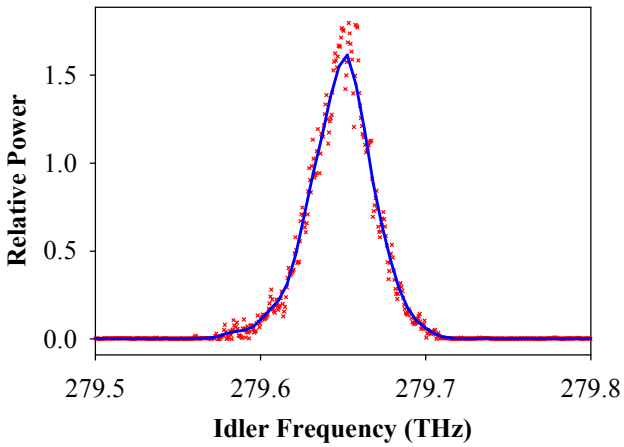

Figure 39 Example idler spectral content corresponding to the generation of 2.2THz, recorded via an optical spectrum analyser. The blue line is the smoothed raw data (red crosses).

A series of measurements of the idler wave across the tuning range of the terahertz OPO were made using an optical spectrum analyser, the results of this are shown in Figure 40.

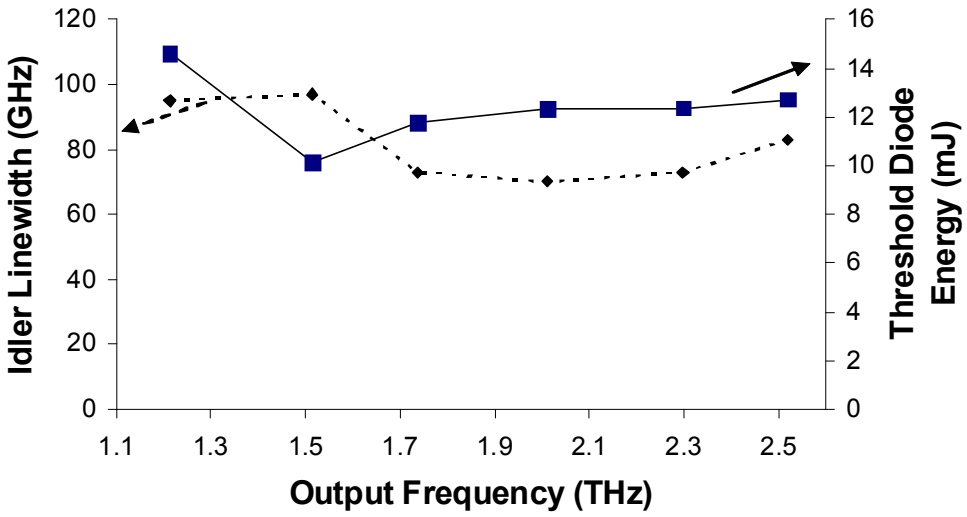

Figure 40 Measurements of the FWHM linewidth of the idler wave across the tuning range of the terahertz OPO alongside downconversion threshold levels.

Alongside the idler bandwidth, measurements of the downconversion threshold were made and are also shown in Figure 40. The linewidth of the laser itself was measured to be ~15GHz using an Angstrom Wavemeter WL-7, indicating that the linewidth of the idler wave was the dominant contributing factor. It can be seen that the threshold energy requirement dips around 1.5THz, corresponding the peak of the gain curve

shown in Chapter 2. Additionally the idler linewidths are comparable to the phasematching bandwidth calculations also presented in Chapter 2. The linewidth measurements were all performed with the same primary pump energy, meaning that the OPO was higher above threshold when the threshold measure was lower. When the OPO is higher above threshold the idler wave builds up more rapidly, experiencing fewer round trips of the idler cavity. This generally has the effect of broadening the idler linewidth, as on each pass of the gain the idler wave is narrowed by the phasematching bandwidth profile. This behaviour can be seen in Figure 40, where the linewidth at 1.5THz is higher than at any of the other frequencies measured.

3.4. Terahertz Absorption

Much of the terahertz wave generated is absorbed by the lithium niobate before it escapes into the silicon prism array and then free space. It was possible to verify the large absorption coefficients predicted by the theory outlined in the previous chapter by varying the transmission path of the terahertz radiation within the lithium niobate. The terahertz pulse energies from an optimally aligned set up were measured at a set frequency as a reference. Then the terahertz generation region was moved incrementally away from the silicon prisms by translation of the lithium niobate crystal (a suitable translation stage is shown in Figure 32) whilst monitoring the detected pulse energy. The detected pulse energy should follow the Beer-Lambert law, and so decay exponentially with increasing depth. The results of this experiment, which was performed at ~227μm, are shown in Figure 41.

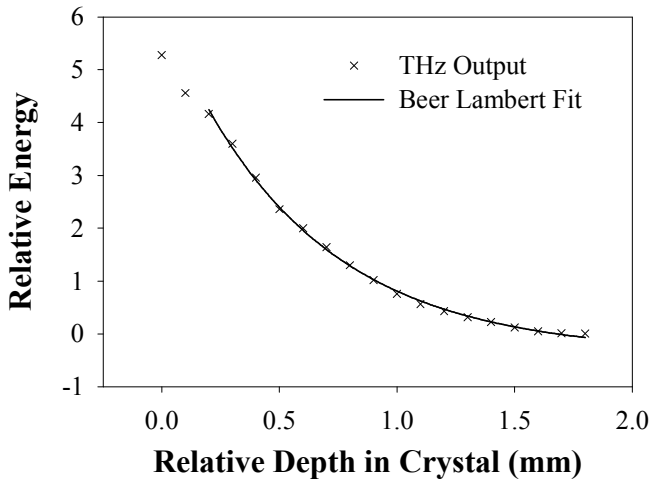

Figure 41 Plot showing extracted terahertz pulse energy vs relative depth of generation region within the nonlinear crystal. The first two data points are disregarded as some power is lost due to clipping of the beams by the edges of the crystal.

The first two data points do not fit well with the rest, the fit to the data suffers when they are included and it can be seen that the remaining points, if the first two are ignored, all lie on the same exponential decay line. The reason for this is that when the system is aligned for optimal terahertz pulse energy extraction there is a trade off between optimal alignment of the intracavity terahertz OPO and the close proximity of the generation region to the silicon prisms, as clipping of the idler and pump waves by the lithium niobate crystal ends can occur if the generation region is too close. This is regularly observed in setting up the system and is why the first two data points are ignored – the decrease in power due to absorption is somewhat compensated by the improved operation of the OPO.

The fit of the data plotted in Figure 41 to the Beer-Lambert law gives and absorption coefficient of 17.1±0.5cm^{-1}, which is close to the value in [13] of around 20cm^{-1}.

3.5. Terahertz Detection

Initially all measurements of the terahertz wave were performed with a composite silicon bolometer purchased from QMC Instruments Ltd. The bolometer was a model QSIB/2 and was provided with calibration data to enable accurate terahertz pulse energy measurements to be taken. The detector element is maintained at ~4.2K during operation, requiring cryogenic cooling with liquid helium and liquid nitrogen. This makes it significantly more inconvenient to use and maintain than the source

technology itself, however it was used in order to perform absolute energy measurements, and it was also the most sensitive detector available giving the highest dynamic range. Detection has also been demonstrated using pyroelectric detectors and Golay cells, which although providing a lower dynamic range are still quite effective at detecting the terahertz pulses from this source. Further development to improve the implementation of pyroelectric detectors is currently underway.

The entrance aperture of the bolometer has a high density polyethylene window, behind which are two low-pass filters (cut off at 3THz), one held at liquid nitrogen temperature, and one at liquid helium temperature. There is also a 10mm aperture, f=3.5, Winston cone (a cone of parabolic cross section that is a non-imaging concentrator of radiation) integrated into the entrance aperture to couple as much of the incident radiation on the detection element as possible. A mode matching horn would not be appropriate here as the tuning range of the source is wider than the narrow range that could be mode matched. An example of the bolometer output for a terahertz pulse is shown in Figure 42.

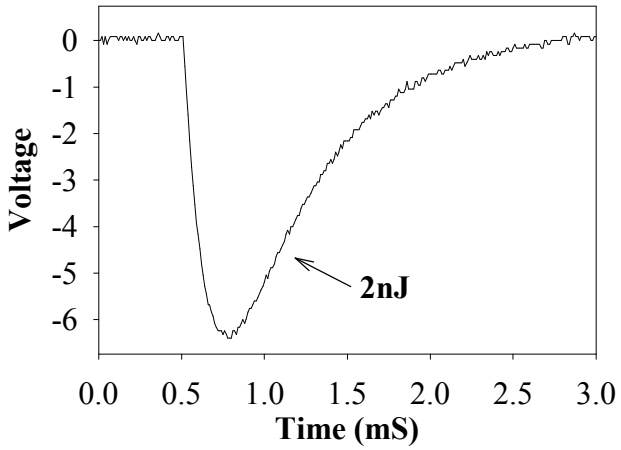

Figure 42 bolometer output after the integrated amplifier stage set to 100x gain. The pulse energy is the area integrated under the curve multiplied by the voltage responsivity.

The calibration provided required integrating over the pulse envelope, converting the instantaneous voltage to Watts using a responsivity of 26.49kV/Watt. The minimum energy measureable in this manner was <1pJ on a single pulse basis, resulting in a dynamic range of better than $1{:}10^4$ without the application of pulse averaging or lock-in amplifier techniques.

3.5.1. Pulse Stability

Observation of the pulses produced by the bolometer revealed significant amplitude jitter. To investigate the degree of the problem the energies of 200 consecutive pulses (with the OPO running at approximately twice threshold) were measured and are plotted in Figure 43.

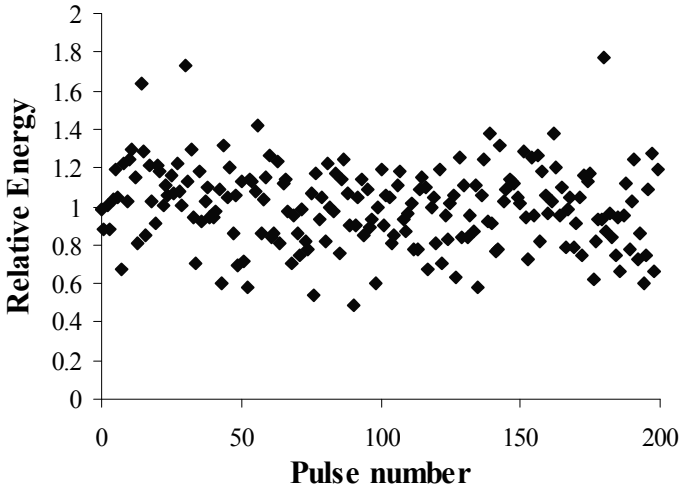

Figure 43 Plot showing the normalised energies of 200 consecutive terahertz pulses. Significant amplitude jitter is present; the standard deviation of the pulse energies was 21%.

As can be seen there is a large spread in pulse energies, the ratio between the smallest to largest being a factor of 3. Whilst this behaviour is undesirable it is manageable through simple multipulse averaging techniques which reduce the error in the measurement by a factor of $N^{-1/2}$ where N is the number pulses averaged over. This was the approach taken for the majority of this research, with averages being taken of typically 16, 32 or 64 (selected due to available oscilloscope settings) pulses – a trade off being made between accuracy and capture time. A superior technique would be to sample a small part of the wave with a second detector, in order to normalise the pulse energies on a shot by shot basis. This was not possible in the early experiments due to the availability of only one terahertz detector, however work is now in progress to develop a spectroscopy system using this approach that will implement recently acquired pyroelectric detectors and/or Golay cells for detection.

Another way that the terahertz pulse energy might be normalised was investigated: the Manley Rowe relations show that the energy downconverted into terahertz photons is directly proportional to that converted in to idler photons, and so monitoring the idler

pulse energy might give an indication of the terahertz pulse energy. To investigate this possibility the idler leaking through the 98% reflectivity mirror of the idler cavity was focussed onto a fast photodiode and recorded simultaneously with the terahertz energy as recorded by the bolometer. Due to the large discrepancy in pulse durations (milliseconds from the bolometer and nanoseconds from the photodiode) two oscilloscopes were used, both being triggered by a single pulse source that also initiated the terahertz OPO. 50 synchronous measurements were made and are plotted in Figure 44.

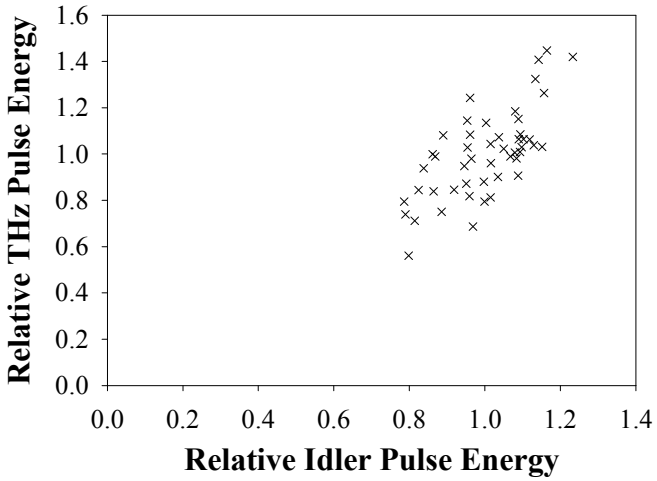

Figure 44 Plot showing the relationship between idler energy leaked through a cavity mirror and terahertz pulse energy for 50 synchronous measurements.

If the technique were to be useful then the points would show a strong correlation and little scatter. It can be seen that this was not the case: there is a degree of correlation but it is insufficient for the accurate prediction of the terahertz pulse energy without again applying averaging techniques. This is perhaps due to the THz wave being generated into two opposite directions, the percentage split between which varies from pulse to pulse.

3.5.2. Long Term System Stability

When performing the characterisation experiments the terahertz power remained, when taking multiple pulse averages, quite stable. Indeed the interferometry and raster scanned imaging experiments took up to ~30mins (depending on the degree of averaging used and the resolution required). However, it was observed that over the course of a working day the system power would fall off considerably, and could be

brought back with a slight adjustment of the laser output coupling mirror alignment. For this reason it was believed for a long time that the power fall off was due to a mechanical problem in the set up; perhaps the mirror mounts were slack allowing them to creep, or perhaps the changing temperature in the lab was causing misalignment due to expansion effects.

Additional systems were constructed for the investigation of line narrowing techniques (which are described in chapter 4), and these systems also exhibited this behaviour. Interestingly the behaviour also seemed to vary in frequency with different lithium niobate crystals in the same laser (original crystals were replaced with identical, 5%MgO doped, ones due to optically induced coating damage). These features highlighted that this problem was quite likely to be caused by the crystals themselves. A quick verification of this was performed by logging the laser power over a day with no crystal in the cavity, which showed no loss in power at all.

To try and get a better understanding of the problem the power in the idler wave was logged over a period of ~14 hours, with no adjustments being made to the laser during the experiment. The behaviour of the idler power is shown in Figure 45.

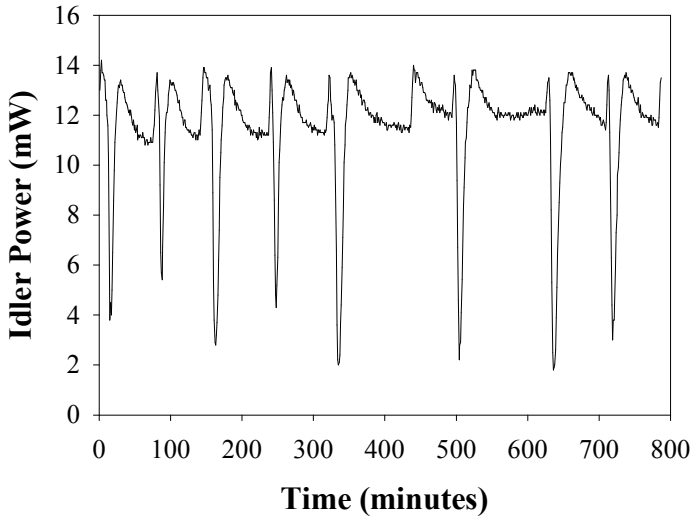

Figure 45 Long term logging of the power generated in the idler wave. Periodic fluctuations can be seen.

The operation of the OPO has a cyclic pattern, with the downconversion slowly decreasing over a period of an hour or so followed by a relatively rapid dip, after which the OPO recovers and start the cycle again. Further investigation was performed by monitoring the laser on a CCD beam profiler as it passed through a dip

in operation. The beam profiler was used to log the position of the beam on the CCD and its horizontal and vertical beam widths (see Figure 46).

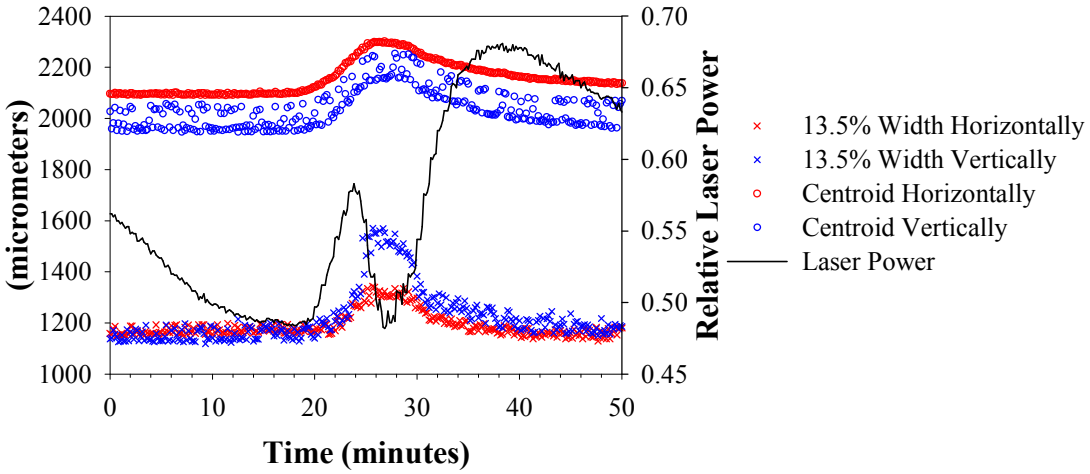

Figure 46 Laser characteristics plotted as a dip in OPO output occurs. The dip at ~23mins corresponds a dramatic short term drop in idler power as seen in Figure 45.

It was discovered that not only does the laser power suffer modulation, the beam is temporarily diverted and its width increased. Two potential causes of this effect were investigated: thermally induced lensing, and a thermally induced change in the optical length of the crystal where the crystal z axis is not aligned parallel to the polarisation of the laser (which would cause varying losses at the intracavity polariser due to the varying degree of polarisation rotation of the intracavity laser field). The latter theory was disproved by placing the crystal between two polarisers such that the orientation of the optic (z) axis could be verified to be parallel to both the side and end faces, which it indeed was. Thermal lensing was discounted due to the lengthy periods of stability. Also, these techniques would not explain the long period of stability followed by a rapid loss and then recovery of laser power.

After discussion of the problem with crystal manufacturers it was decided to acquire crystals that had gold coatings applied to the top and bottom (z axis faces) and to electrically connect the coatings together when in use. This proved very successful in stopping the cyclic behaviour making the system stable. We theorise that the behaviour is caused by an internal electric field that builds up as the charged atoms in the material migrate upon absorption of optical energy, so inducing a change in refractive index via the electro optic effect. This behaviour is to be expected, however it was not foreseen – probably because much of the work in the group has

utilised periodically poled lithium niobate, which is used with the laser polarisation parallel to the z axis of the crystal. This material in this orientation does not exhibit a problem as the periodic reversal of domains greatly reduces the effect[14].

3.5.3. Polarisation

As mentioned in earlier sections the pump wave is polarised vertically in the system - parallel to the extraordinary axis of the lithium niobate crystal. The polarisations of the downconverted waves are also parallel to this, giving a vertically polarised terahertz wave exiting the crystal. In order to characterise the terahertz wave polarisation, and to provide a means of attenuating the pulse energy, a polariser was purchased from QMC Instruments. This polariser consisted of a wire grid that was set in high density polyethylene for the protection of the fine wire used. The experimental set up is shown in Figure 47; the polariser was positioned in a collimated section of the terahertz wave and held in a rotation mount that had markings every degree.

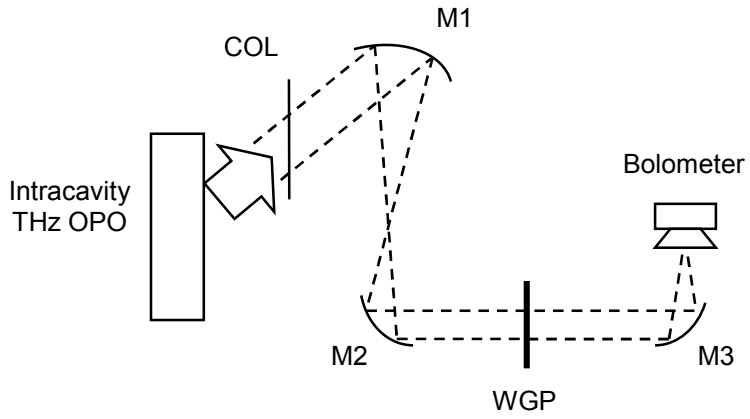

Figure 47 Experimental layout for characterising the terahertz polarisation. Mirrors M1, M2 and M3 (M2 and M3 are identical) are all gold coated off-axis parabolics purchased from Janostech, with effective focal lengths of 101.6mm and 50.8mm, and deflections of 60° and 90° respectively. WGP denotes the position of the wire grid polariser, and COL denotes the cylindrical lens used for initial collimation.

A set of pulse energy measurements at 1.5THz were then performed varying the angle of the polariser. 64 pulses were averaged on an oscilloscope to reduce the standard error in the energy measurement to ±~2.5%. The results are plotted in Figure 48 and compared to Malus' law.

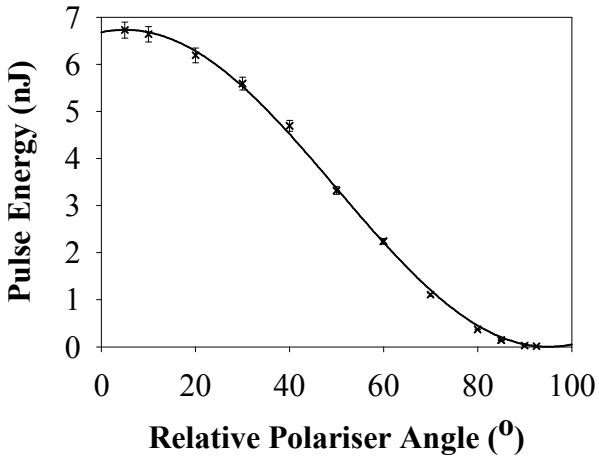

Figure 48 Plot showing the transmission of the metallic grid polariser with varying angle. The crosses denote the transmitted pulse energy measured using the bolometer, the solid line is a fit to a squared cosine curve (Malus' law) and shows good agreement.

The terahertz wave shows a high degree of polarisation and the wire grid polariser behaved as predicted by Malus' law. The maximum pulse energy transmitted was 6.7nJ, and the energy at maximum extinction was 4.5pJ, giving an extinction ratio of ~1500:1.

3.5.4. Spatial Profiles

It was expected that the source would produce a terahertz beam with a close to Gaussian profile, as was observed in the work of Kawase et al [4]. To provide initial collimation a cylindrical lens was designed to collimate the rapidly diverging vertical component of the beam at a distance of ~10cm from the silicon prism array output coupler. The bolometer used for terahertz energy measurements was a single element detector, and so beam profiling was performed using the knife-edge and scanned aperture techniques. The experimental set up for characterisation of the beam is shown in Figure 49.

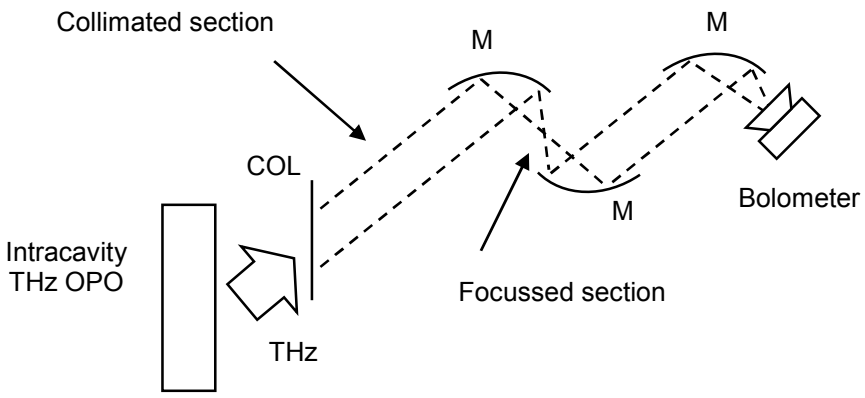

Figure 49 Experimental layout used for measuring the terahertz beam profile. The terahertz wave is collimated at approximately 10cm from the silicon prism output coupling using a high density polyethylene cylindrical lens (f=10cm) produced in house.

A two axis stage driven by computer controlled stepper motors was used to automatically scan a razor blade horizontally, and then vertically, through the collimated section of the beam at several positions whilst logging the averaged terahertz pulse energy. This data can then be smoothed and numerically differentiated with respect to the position of the knife edge to reveal the profile of the beam. An example of the horizontal beam profile measured using this technique is shown in Figure 50.

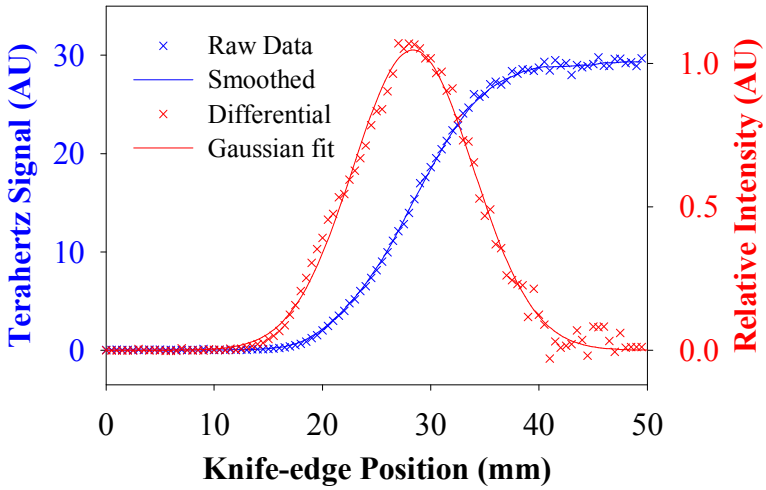

Figure 50 Plots showing how the raw terahertz pulse energy measurements were transformed into beam profiles. Data processing and Gaussian profile fitting were performed using the SigmaPlot 8 software package.

This analysis was performed at ten positions, each separated by 1cm, both horizontally and vertically along the collimated section of the beam to verify the degree of collimation achieved. After careful optimisation by repeated beam profiling and adjustment of the cylindrical lens the final results are shown in Figure 51.

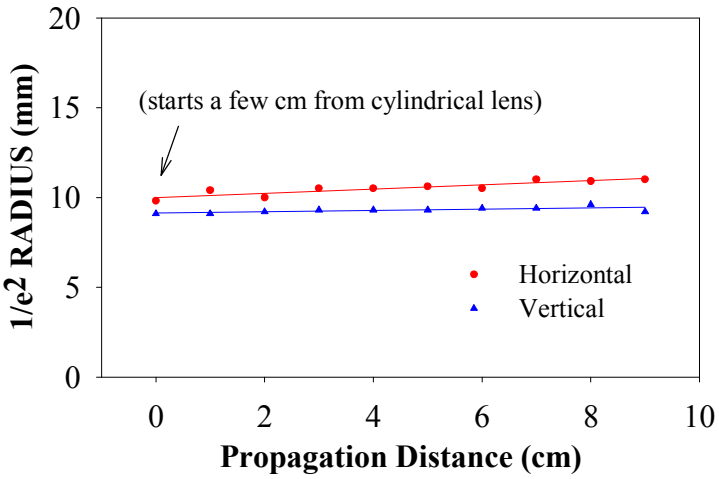

Figure 51 Plot showing beam waist of the propagating terahertz beam. A high degree of collimation is evident.

This plot shows that it is possible to achieve a high degree of collimation of the source in both axes by careful alignment of the cylindrical lens alone.

This collimated beam was then focussed through a waist using an f=50.8mm off axis parabolic mirror (90° deflection). The same knife-edge technique was used here, taking readings every 1mm along the propagation axis of the beam, to find the minimum spot size achieved. The results of this experiment are shown in Figure 52.

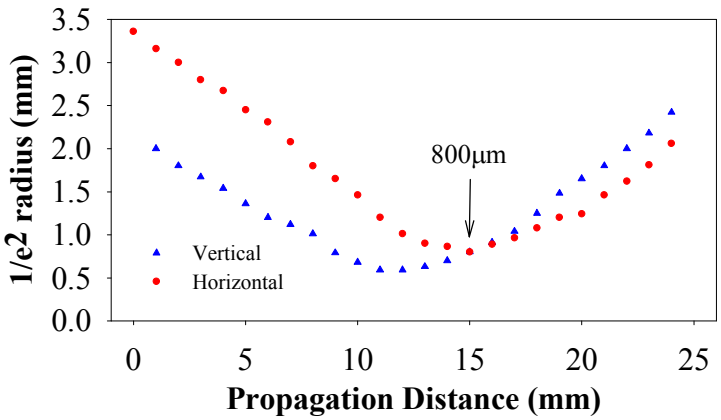

Figure 52 Horizontal and vertical beam dimensions through the waist produced by an f=50.8mm off axis parabolic mirror. Propagation distance is measured with respect to the arbitrary staring position of the measurements.

The beam is showing a slight astigmatism possibly due to slight misalignment of the parabolic mirror, however an approximately circular waist of ~800µm was achieved. Assuming an input beam radius of 10mm, propagation distance of 50.8mm (the focal length), and given that the terahertz wavelength was 220µm, the beam radius propagation equation:

$$w(z) = w_0 \sqrt{1 + \left(\frac{\lambda z}{\pi w_0^2} \right)^2} \tag{3.7}$$

which can be rearranged to give a quadratic expression for w_0^2:

$$0 = \left(w_0^2 \right)^2 - w_0^2 w(z)^2 + \frac{\lambda^2 z^2}{\pi^2} \tag{3.8}$$

can be used to find the minimum waist for an ideal Gaussian beam. This gives w_0 to be ~360µm, or ~10mm (the solutions focussed or collimated beam sections respectively). Taking the first solution suggests a waist 2.3 times the ideal diffraction limited spot was achieved.

The M^2 values for the horizontal and vertical components of the THz beam were calculated to be 6.7 and 2.3 respectively. Reasons for the lower quality beam in the horizontal dimension include the phase and propagation angle deviations across the THz wave front introduced by the silicon prism array output coupler.

Further measurements using a scanned 100µm aperture were performed at the beam waist to further characterise the spot, as it is possible that the knife-edge technique can miss fine structure in the beam profile. The resulting scan is shown in Figure 53

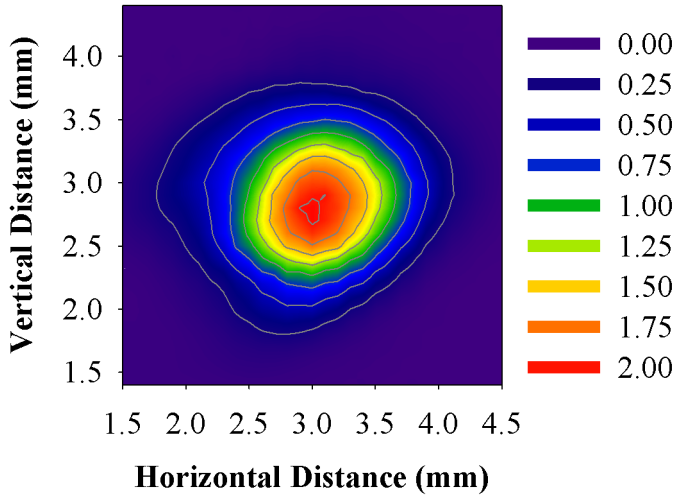

Figure 53 Beam profile at waist taken using the raster scanned aperture technique. A 100µm aperture was used at 100µm steps.

As can be seen the aperture scan did not reveal any fine structure in the beam profile, verifying its highly symmetric Gaussian nature.

3.6. Applications of the ICTOPO

3.6.1. Spectroscopy via Manual Frequency Tuning

Most common terahertz spectroscopy techniques (FTIR and THz TDS) rely on Fourier techniques to recover spectral information from broadband transmissions. In this setup, such techniques are unnecessary due to the narrow linewidth and tunability of the source. Simply measuring the transmission as the device is tuned yields swift spectroscopic information which is unaltered by windowing and sampling effects that can alter data obtained via computerised fast Fourier transforms.

To demonstrate the devices application to spectroscopy a simple transmission spectrometer was set up, the layout of which is shown in Figure 54.

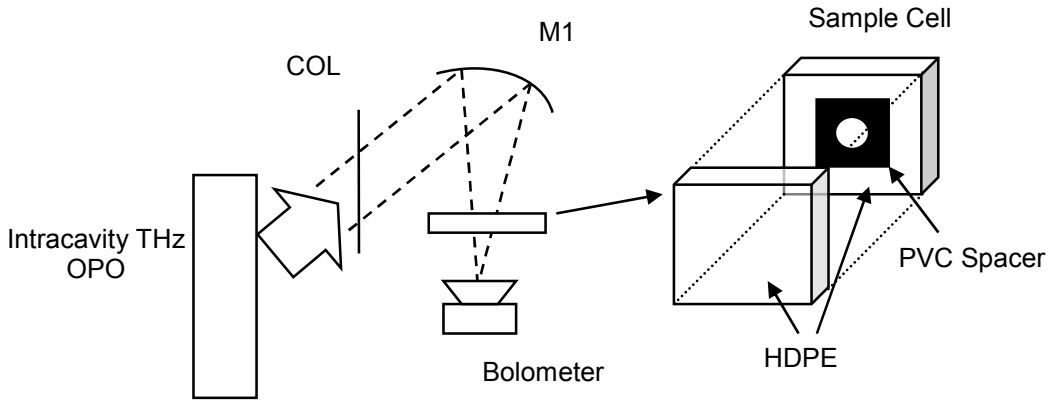

Figure 54 Transmission spectroscopy experimental set up. After collimation with the cylindrical lens (COL) the terahertz beam was focussed through sample and into the bolometer using a gold coated, f=101.6mm off axis parabolic mirror (M1). The samples were loaded into the hole in a polyvinyl chloride spacer (100µm deep, 1cm diameter hole) and pressed between two HDPE flats (2mm thick).

The experimental procedure was simple. The terahertz wavelength was first calculated by measuring the difference between the pump and idler waves being produced. Then the pulse energy transmitted through the sample cell was measured using the bolometer, applying 64 times averaging. The sample cell was then immediately swapped with an empty reference cell and transmitted energy recorded again, in order to remove any residual absorption spectrum or interferometric effect of the cell itself. The samples used were all solids that are generally found in powder form, and were all ground in a pestle and mortar to a fine dust before loading into the cell.

The samples were supplied to us under the EPSRC "Think Crime" programme as substances that were linked to criminal activities. In particular samples of Noscapine (often found in heroine), Phenacetin (an analgesic that is sometimes "cut" into cocaine, and is banned in Western countries as it has been linked to the development of cancers), and L-Glutamic acid (a flavour enhancer that is similar in structure to cocaine and occasionally cut with it) were analysed, and the resulting absorption profiles are plotted in Figure 55.

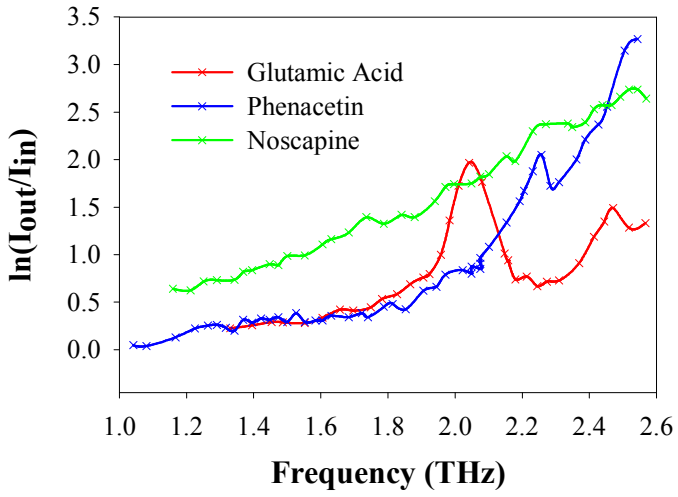

Figure 55 Plot showing the absorption profiles of the 3 samples analysed.

No distinct absorption peak was observed for Noscapine, and only a weak feature at ~2.2THz was detected in Phenacetin, however a significant absorption feature was observed in Glutamic acid at ~2THz, which is in agreement with spectral features reported in the literature [15]. Even though not all samples exhibited distinct spectral features, terahertz spectroscopy may still be informative in these cases if analysed with regard to the rate of change of absorption with frequency, for instance, or perhaps by applying principal component analysis techniques[16].

3.6.2. Raster Scanning

As a simple demonstration of how the system could be using for imaging tasks an organic sample (salami) was chosen to be scanned with the terahertz beam. Salami was chosen as it has obvious fat/tissue features resolvable with the terahertz spot size produced. A thin (~1mm) slice was mounted on vertically and horizontally scanning motorised stage and positioned at the focus point of the terahertz beam shown in Figure 49. Again the wavelength was 220µm and the spot size approximately 1.6mm (full width at e^{-2}). As the sample was rastered through the beam focus the transmitted pulse energies were recorded, building up a terahertz transmission profile (see Figure 56).

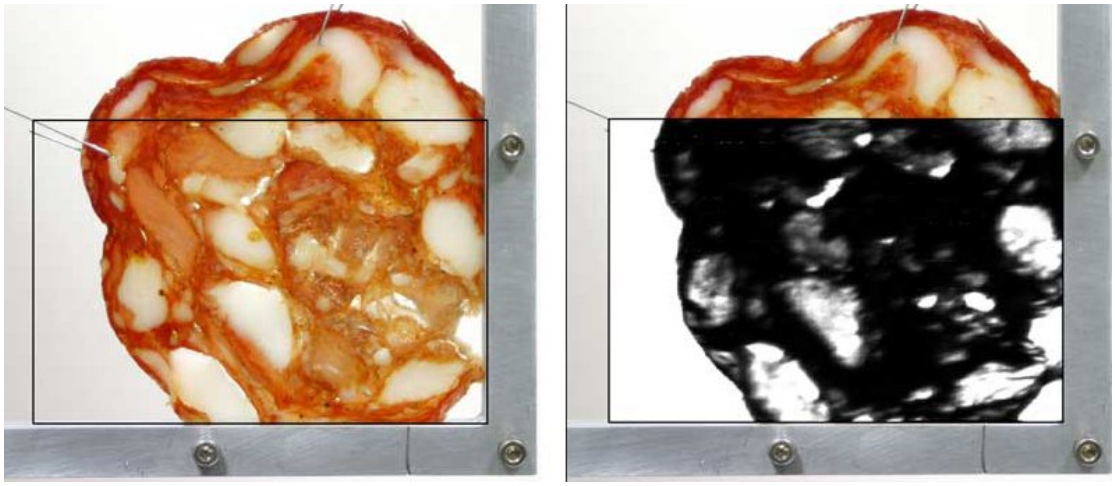

Figure 56 Terahertz transmission (white=full transmission, black=no transmission) profile (85mm by 60mm) of a sample of salami shown with a photograph of the corresponding area in the visible spectrum (backscattered light). The resolution of the scan (250µm) is sufficient to see the features visible in the optical spectrum and extra detail not visible to the eye is revealed in the fatty sections (most probably areas of high water concentration – a well known strong absorber).

The image produced serves to demonstrate the potential of the source for imaging applications, indicating that pulse averaging provides a very successful way of removing the pulse to pulse amplitude jitter. The use of a reference detector would decrease the scan time by a factor of the number of pulse averages needed to obtain a steady reading, in this case a factor of 32.

3.7. Ongoing Work

3.7.1. Computer Controlled Spectrometer

The tuning mechanism of the intracavity terahertz OPO is undergoing development in order to extend the continuous tuning range of the device. To this end the system outlined in the previous chapter, where two "dog leg" mirrors are introduced in the idler cavity to avoid the idler beam walk-off issue, is being implemented. The current set up is shown in Figure 57.

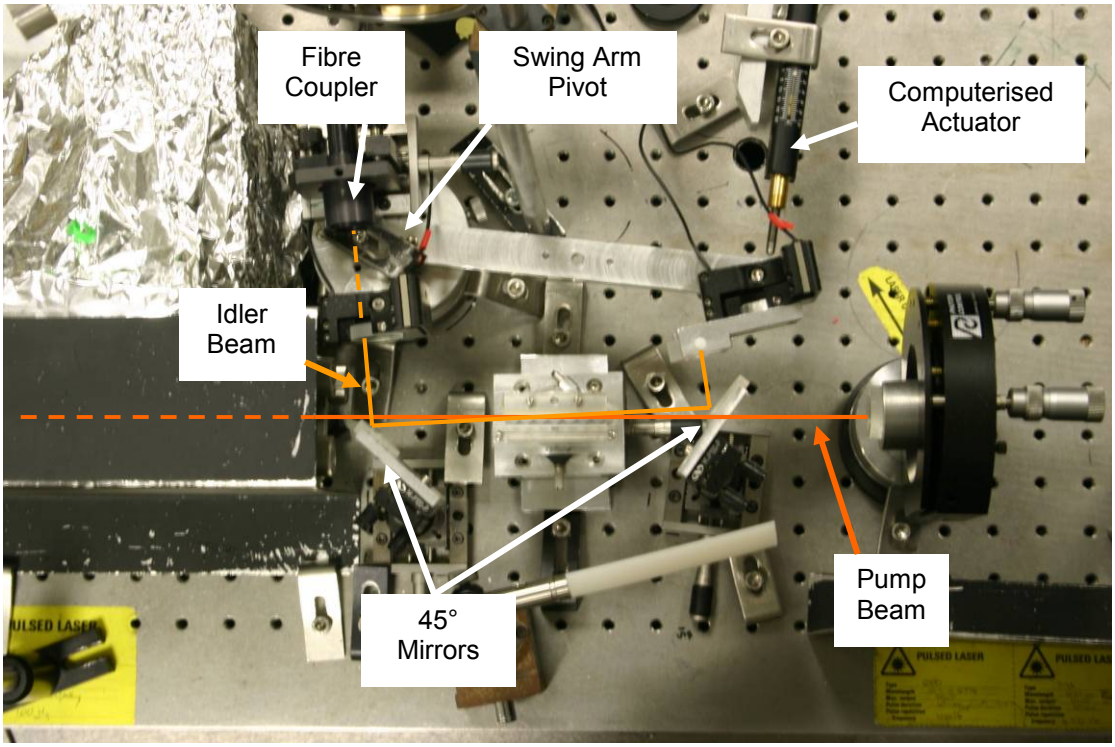

Figure 57 Top view of system under development for enhanced continuous tuning range.

Using this system it is now possible to easily scan through the tuning range of the intracavity terahertz OPO using only a computer controlled linear actuator. Currently the terahertz frequency is inferred by synchronously and automatically logging the idler wave during a scan with an Angstrom WL-7 wavemeter (the leaked idler wave is sampled by the fibre coupler labelled in the photograph), however the implementation of an actuator that can be moved to an absolute position will enable the absolute terahertz wavelength to be calibrated against this, negating the need for the wavemeter other than for initial set up. Some preliminary scans are shown in Figure 58.

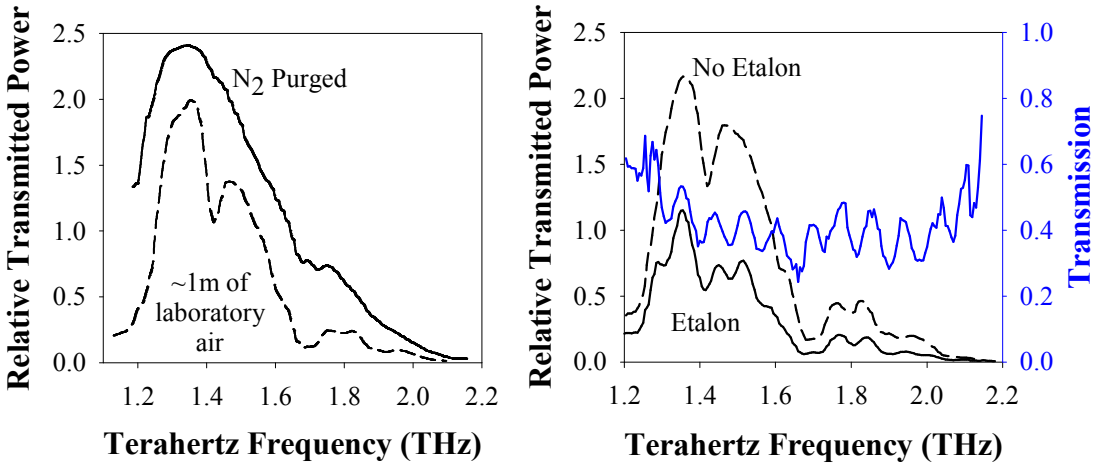

Figure 58 Preliminary spectra captured using the modified idler cavity. On the left is a simple before and after power spectrum through an enclosure built to allow nitrogen purging of the terahertz transmission line, strong water vapour absorption is clearly seen. On the right is the transmission spectrum of a 540µm thick silicon etalon, showing modulation at the free spectral range (measured from the spectrum ν = 84±3GHz, calculation using n = 3.2 and 540µm thickness gives ν = 82GHz).

This technique will allow autonomous and repeatable operation of the device, more data points to be captured with longer integration times for accuracy in a shorter time. It is now being developed into a complete spectrometer system implementing newly acquired, room temperature, pyroelectric detectors, a reference terahertz pulse measurement to counter the pulse amplitude jitter, and a nitrogen purged transmission line to minimise the absorption by water vapour.

3.7.2. An Easy-To-Use Terahertz Interferometer

During the course of the research a summer student (Ian Bledowski) was given the task of making a direct measurement of the terahertz wavelength. There are several difficulties in performing these measurements in the terahertz region; beam splitters and semi reflecting mirrors are rare and usually of fragile (and often lossy) metal mesh construction, and the alignment of a Michelson interferometer is hindered by the inability to observe the beam other than with bulky detectors (there is no equivalent of infrared viewer cards available for use in the terahertz range, for instance). To solve this problem a Michelson interferometer employing a "split mirror" design was produced in-house. Instead of attempting to find a 50% reflectivity/transmission beam splitter, this design spatially splits the beam across two intersecting fingered

mirrors (see Figure 59), providing the optimal 50% splitting (which is frequency independent), has no polarisation dependence and significantly reduces the complexity of lining up the system.

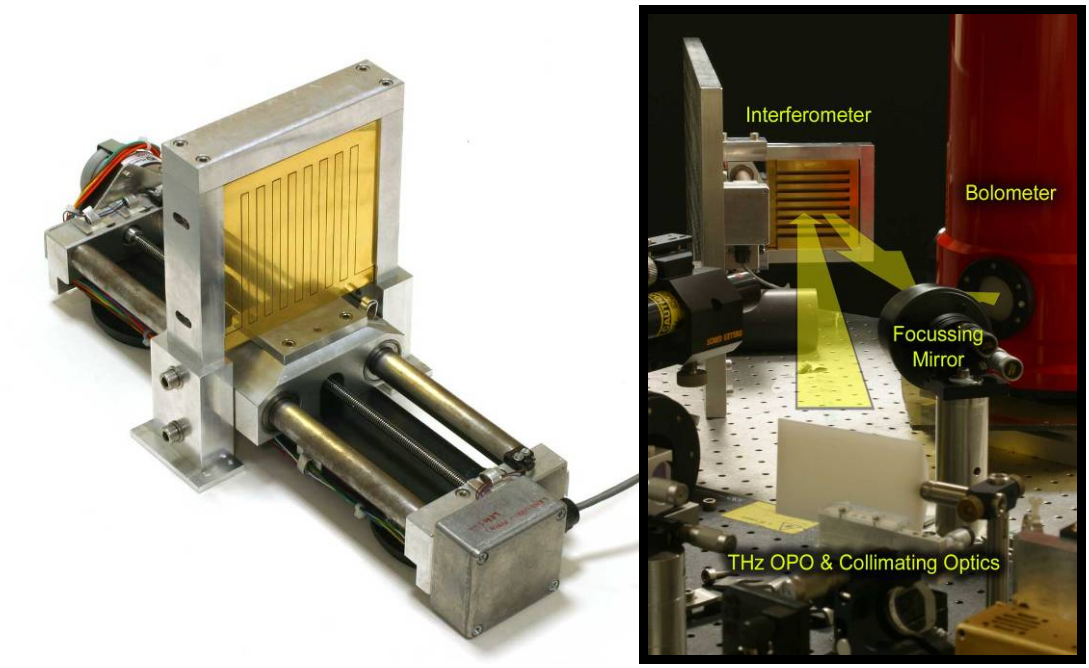

Figure 59 Photographs of the "split mirror" interferometer. In the left image it can be seen how the mirrors intersect one another, and that one of them is attached to a stepper motor driven translation stage. On the right is a photograph of the interferometer in action, with the mirrors slightly displaced. (photographs courtesy of Dr David Stothard)

In use optimal alignment is found when the centre of the terahertz beam hits the gap between two fingers (else a small dc offset is introduced), the angle of reflection is minimised (to minimise the spatial walk off of the two beams), and the reflection plane is parallel to the "fingers" of the mirror as seen in Figure 59 (so that the front most mirror does not "shadow" the rearmost one). The stepper motor drives the translation stage through a 50:1 gearbox, reducing the 48 steps per revolution of the motor to 2400 steps per revolution of the lead screw of the stage. The pitch of the lead screw was 1.27mm per revolution, resulting in a step size for a single pulse of 529nm to 3s.f. which is well below the 100μm to 300μm tuning range of the terahertz OPO. It should also be noted that a correction must be made to account for the angle of incidence of the terahertz beam on the split mirrors decreasing the effective path difference, hence making the wavelength measured seem longer by a factor of $\cos\theta$, where θ is the angle between the incident beam and the normal to the mirror surface.

To test the interferometer the intracavity terahertz OPO was tuned to ~1.8THz and the interferogram captured using the experimental layout shown in Figure 59.

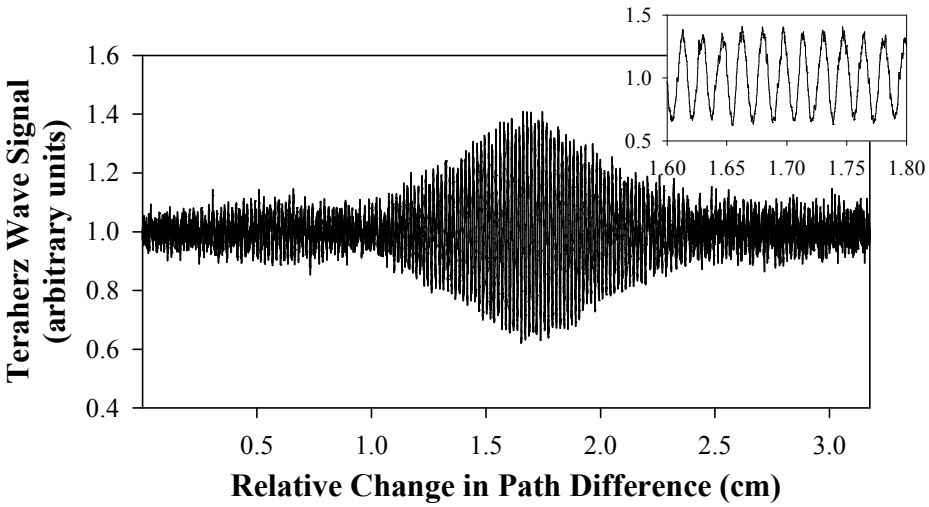

Figure 60 Interferogram of the terahertz output at ~1.8THz. The interferogram has been corrected for laser power drift using a moving average. That the interferogram does not approach extinction in the centre of the pattern (zero absolute path length difference) indicates that the terahertz beam was not spread optimally between the mirrors.

The wavelength of the terahertz output can be directly deduced from the inter fringe spacing (see inset of Figure 60), allowing a very swift measurement to be made. However it is possible to obtain more information by applying a computer based fast Fourier transform technique (FFT) to the interferogram, which can then reveal the full spectral content of the beam. As an example the fast Fourier transform of the interferogram in Figure 60 was taken using Microcal Origin, and is shown in Figure 61.

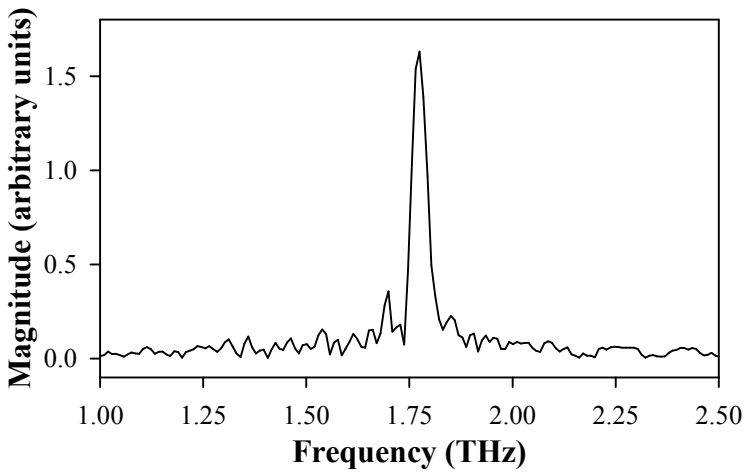

Figure 61 Spectrum of the terahertz beam using the FFT function of Microcal Origin. A Hanning window was applied to suppress the side lobes induced by the finite number of samples taken.

Directly measuring the wavelength (over ten fringes) from the interferogram and then using the FFT yield terahertz frequencies of 1.79±0.03THz and 1.775±0.005THz respectively (after correcting for the small angle of incidence). The FFT technique is more precise as it is using more information, however the resolution is limited by the total sampling length which comes at the cost of longer experimental runs. Additionally the bandwidth was found to be ~40GHz FWHM using the FFT technique.

Although this work was successful it is still much more practical on a day to day basis to infer the terahertz wavelength by measuring the wavelength of the pump and idler waves using either a suitable optical spectrum analyser or wavemeter.

3.8. Conclusions

In this chapter the experimentally realised ICTOPO has been described and characterised. The comparison with a similar extracavity device shows the advantage of the intracavity approach in the order of magnitude reduction in 1064nm pump wave energy required to bring the TOPO above threshold, although the order of magnitude improvement in THz energy output is hard to explain. One possibility is that higher quality (resistivity) silicon prisms were used in the ICTOPO for output coupling of the THz wave resulting in a lower absorption.

The pulse stability issues of the source have been discussed; the pulse to pulse amplitude jitter was characterised and the solutions of multi pulse averaging or preferably using a second, energy referencing, detector proposed. The longer term dynamics were also investigated revealing a problem with the material, a solution was found in coating the top and bottom surfaces of the lithium niobate (those perpendicular to the extraordinary crystal axis) with a conducting material and electrically connecting them together to subdue the optically induced refractive index changes.

The terahertz beam profile was shown to be Gaussian like and of good quality, the benefits of which are in the increased propagation lengths and small focal spot sizes. These features are advantageous for imaging systems and aid the beam handling and collection of the terahertz wave in an experiment. Some examples of spectroscopy and imaging have also been shown emphasising the utility of the system.

The system has also been licensed to MSquared Lasers of Glasgow who have commercialised the device (Firefly THz), and are selling the product internationally.

3.9. References

1. T. Edwards, D. Walsh, M. Spurr, C. Rae, M. Dunn, and P. Browne, "Compact source of continuously and widely-tunable terahertz radiation," Opt. Express **14**, 1582-1589 (2006).

2. T. J. Edwards, D. Walsh, M. B. Spurr, P. G. Browne, C. F. Rae, and M. H. Dunn, "Compact and coherent source of widely tunable THz radiation," L. Colin, and P. O. Gari, eds. (SPIE, 2006), p. 64020C.

3. T. J. Edwards, D. Walsh, M. B. Spurr, P. G. Browne, C. F. Rae, and M. H. Dunn, "Compact solid-state source of continuously tunable terahertz radiation.," in *2nd EPS-QEOD Europhoton Conference*(Pisa, 2006).

4. K. Kawase, J.-i. Shikata, H. Minamide, K. Imai, and H. Ito, "Arrayed silicon prism coupler for a terahertz-wave parametric oscillator," Appl. Opt. **40**, 1423-1426 (2001).

5. W. Koechner, *Solid State Laser Engineering,* 5th edition, (Springer Series in Optical Sciences, 1999).

6. T. Y. Fan, and R. L. Byer, "Diode laser-pumped solid-state lasers," Quantum Electronics, IEEE Journal of **24**, 895-912 (1988).

7. P. Laporta, and M. Brussard, "Design criteria for mode size optimization in diode-pumped solid-state lasers," Quantum Electronics, IEEE Journal of **27**, 2319-2326 (1991).

8. D. Findlay, and R. A. Clay, "The measurement of internal losses in 4-level lasers," Physics Letters **20**, 277-278 (1966).

9. A. G. Fox, and T. Li, "Resonant modes in a maser interferometer," Bell Syst. Tech. J **40** (1961).

10. M. Hiroaki, I. Tomofumi, and I. Hiromasa, "Frequency-agile terahertz-wave parametric oscillator in a ring-cavity configuration," Review of Scientific Instruments **80**, 123104 (2009).

11. D. E. Zelmon, D. L. Small, and D. Jundt, "Infrared corrected Sellmeier coefficients for congruently grown lithium niobate and 5 mol.% magnesium oxide doped lithium niobate," J. Opt. Soc. Am. B **14**, 3319-3322 (1997).

12. E. D. Palik, *Handbook of Optical Constants of Solids* (Academic Press Inc. London, 1985).

13. J. Shikata, K. Kawase, K. Karino, T. Taniuchi, and H. Ito, "Tunable terahertz-wave parametric oscillators using $LiNbO_3$ and $MgO:LiNbO_3$ crystals," Microwave Theory and Techniques, IEEE Transactions on **48**, 653-661 (2000).

14. M. Taya, M. C. Bashaw, and M. M. Fejer, "Photorefractive effects in periodically poled ferroelectrics," Opt. Lett. **21**, 857-859 (1996).

15. Z. Yan, D. Hou, P. Huang, B. Cao, G. Zhang, and Z. Zhou, "Terahertz spectroscopic investigation of L-glutamic acid and L-tyrosine," Measurement Science and Technology **19**, 015602 (2008).

16. K. Kawase, Y. Ogawa, Y. Watanabe, and H. Inoue, "Non-destructive terahertz imaging of illicit drugs using spectral fingerprints," Opt. Express **11**, 2549-2554 (2003).

Chapter 4. Linewidth Improvements

The linewidth of the terahertz generated by the basic intracavity source described in the previous chapter was around 50GHz, comparable to that of other nanosecond pulse OPOs [1]. This is adequate for a wide variety of spectroscopic measurements of solids and liquids, as spectral lines these substances exhibit are significantly broadened. There are, however, applications that require narrower linewidths: the spectroscopy of low pressure gases being an example. The intracavity OPO approach lends itself well to line narrowing strategies which are more traditionally implemented in the parent pump laser, due to the conservation of energy between pumping and down-converted signal and idler photons involved in the parametric process. The control of the linewidths of the two resonant optical waves by necessity controls the linewidth of the terahertz wave. This is because the highest terahertz frequency generated cannot exceed the largest difference between pump and idler frequencies (highest pump with lowest idler), and the lowest cannot be lower than the least difference (lowest pump with highest idler). As such, limiting the linewidth of the pump and idler fields leads to a concomitant reduction in the terahertz linewidth. As the pump and idler fields are simply optical fields resonant within their respective Fabry-Perot cavities, a host of established line narrowing techniques can be brought to bear in order to realize a narrow linewidth THz ICOPO.

In this chapter we shall deal with two approaches to line narrowing: firstly, the insertion of etalons into the laser and idler cavities is described, followed by the technique of injection seeding, where a single frequency laser beam is injected in to the idler cavity. As we shall see, both techniques have a substantial impact on the linewidth obtained in the THz field. The former approach was particularly successful, in the context of substantial linewidth reduction, and robust device performance with very little cost in terms of added complexity, and led to a paper on the system has been published in a Applied Physics Letters [2]. In contrast the ultimately superior linewidth exhibited by the injection seeded system was somewhat compromised by significantly enhanced system complexity. For this investigation, a second THz ICOPO system, nearly identical to that outlined in chapter 3, was built in order that the continuing development and refinement of the original system, and its application to spectroscopy and imaging could occur in parallel with the developments described in this chapter. The successful implementation of injection seeding proved highly

problematic, but that difficulty was eventually realised to be due to unforeseen laser pulse dynamics that will be discussed later in this chapter. This work has also led to publication, in this case in JOSA B[3].

Various aspects of the work described in this chapter were conducted in collaboration with a number of colleagues, namely Drs Tom Edwards, David Stothard and Pete Browne and Miss Caroline Thompson, whom I acknowledge and to whom I express my gratitude.

4.1. Etalon Line Narrowing

As the linewidth of the THz field is a convolution of the pump and idler fields, the first step towards narrowing the terahertz linewidth is to consider the linewidth of the pump laser itself. The spectral characteristics of a basic laser are determined by several factors: the bandwidth of the gain medium, the length of the laser cavity, the duration of lasing action, and the presence of spatial hole-burning of the optical gain within the laser gain medium. The gain bandwidth of Nd:YAG (the laser crystal used throughout this study) is around 6 Angstroms (~160GHz) (homogeneously broadened line shape) and has a Lorentzian profile. On top of this lies a series of frequencies determined by the longitudinal modes supported by the laser cavity (from Fabry-Perot theory) and the overlap of these spectral profiles determines the gain presented to the optical field. It is at this point that the duration of the laser output becomes important, as the longer the laser is running the more the frequency with the highest gain (the cavity mode near the peak of the gain profile) will come to dominate. For a Q-Switched laser, as used for the intracavity THz OPOs, the laser pulse is merely nanoseconds long, producing wider bandwidth pulses than the same laser cavity running continuous wave. The duration of the pulse is also important in determining the absolute minimum bandwidth of the source – the (Fourier) transform limited bandwidth. The laser within which the terahertz OPO was pumped had a free running linewidth of 15 to 20GHz (varying from pulse to pulse).

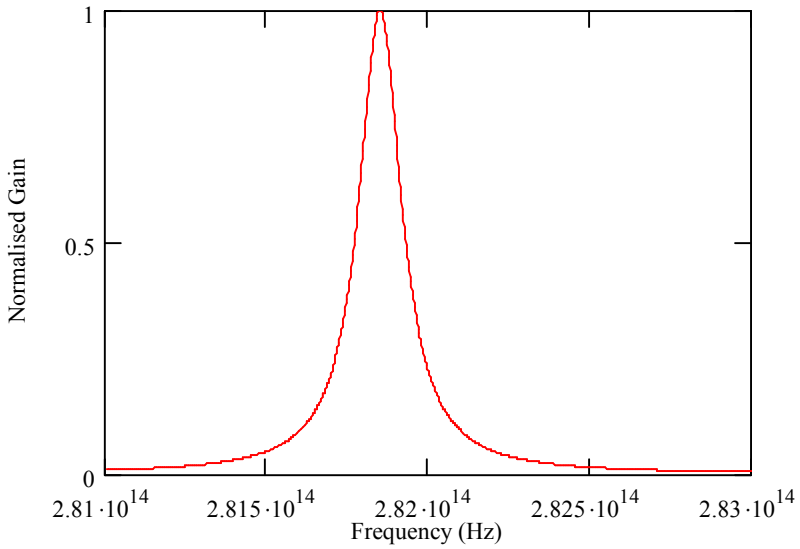

Figure 62 Lorentzian line shape of the Nd:YAG gain profile. The frequency comb of modes supported by the ~40cm long cavity has adjacent modes separated by c/2nl ~ 3.8×10^8, and so cannot be shown clearly on this graph.

Not all of the optical modes within the cavity experience gain due to spatial hole burning effects within the laser gain medium. Here, a dominant mode builds up from noise within the cavity, leaving insufficient gain to support adjacent cavity modes. Only cavity modes several free spectral ranges from the dominant mode, and hence whose standing-wave antinodes are spatially separated from the hole-burned gain regions left by the dominant mode, experience sufficient gain to resonate within the laser cavity. These spatially hole-burned modes can be spectrally pushed further from the dominant line (and are, hence, easier to suppress through intracavity frequency-selective elements) by placing the laser gain medium at the end of the laser cavity, as is implemented in this system.

4.1.1. Intracavity Etalons

One of the simplest techniques used to narrow a laser's output is to insert an etalon into its resonator. The etalon is a simplest form of a Fabry-Perot cavity where the two mirrors (usually multilayer dielectric coatings) are formed by opposing surfaces of a plane parallel polished transparent substrate. The transmission profile is simple to calculate[4], and so a reflectivity and thickness can be chosen such that only a narrow slice of frequencies near the centre of the gain bandwidth experiences net roundtrip gain within the laser cavity. The absolute frequency can be tuned by changing the

optical thickness of the etalon, which can be achieved by varying the angle of the etalon with respect to the laser axis (a fact exploited later in the idler cavity) or by changing the temperature of the etalon. This latter approach eliminates problems associated with walk off but leads to greater system complexity and frequency tuning cannot be typically implemented with the same speed as angle tuned systems. The characteristics of the etalon used, and its angle, will determine both the spectral output of the laser and its absolute frequency: the higher the reflectance of the etalon mirrors (higher finesse) the narrower the transmission, however this comes at the price of greater losses experienced by the laser, caused by any reflectivity mis-match between the two surfaces of the etalon and increased intra-etalon walkoff, and so a compromise must be made. In addition, higher finesse etalons lead to substantially enhanced fields within their cavity and so both the substrate and optical coatings must be able to accommodate these very high circulating fields without suffering damage. An important point to note is that the laser mode is narrowed on each pass of the etalon; longer optical pulses therefore result in more round-trips through the etalon, enhancing its effect and leading to a narrower linewidth output.

The design of the optical cavities employed by both the pump and idler waves result in circulating mode geometries which are particularly well suited to the accommodation of etalons. This is due to their near collimation and broad mode diameter. Both of these factors reduce the effects of walk off losses as the etalon is angle tuned. These deleterious effects are reduced further by the high free spectral range (and hence, mechanically thin) etalons we use in this study.

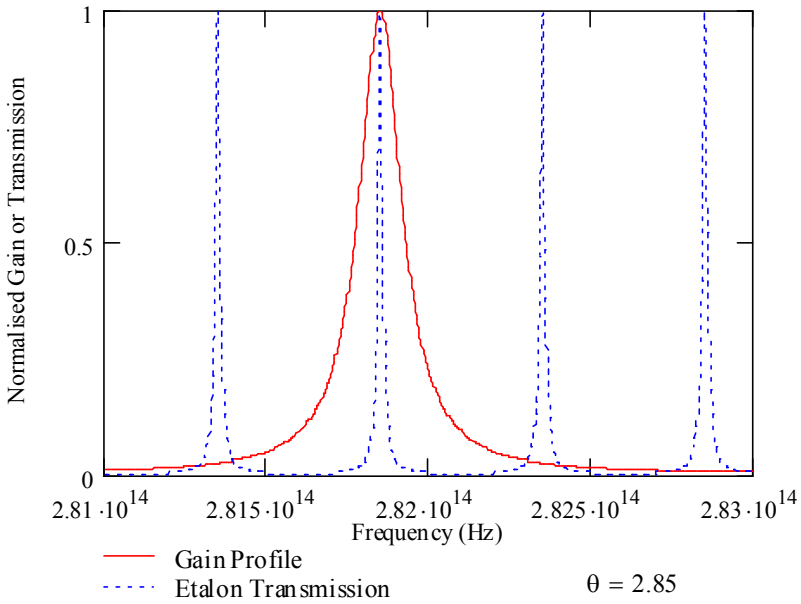

Figure 63 Line shape of the ~1064nm Nd:YAG laser line gain with a superimposed etalon transmission curve. The etalon modeled is 300µm thick and has a reflectivity of 90%, and is oriented at 2.85° from "flash" (orthogonal to laser beam).

4.1.2. Idler Cavity

The parametric gain has an associated phase matching bandwidth, much like the gain bandwidth associated with a laser transition. Narrowing of the pump wave alone will result in narrowing of the downconverted terahertz wave, however there will still be a range of frequencies over which the downconversion process will phasematch. With no idler resonator present, such as in an terahertz optical parametric generator[5], the whole tuning range experiences single pass gain with no one frequency dominating; as such the output of these devices tends to be very broad (>1THz), unless frequency selection is performed, for instance by injection seeding. In the terahertz parametric oscillator feedback is provided in the form of a resonant cavity that feeds back the idler wave produced at a specific angle. This exponentially increases the gain experienced by the idler wave at this angle, thereby providing a degree of frequency selection. For a fixed idler wave angle, as defined by the plane-parallel idler cavity used in this case, limits the phasematching bandwidth (as calculated in Chapter 2) to be around 100GHz. As the idler field builds up from parametric fluorescence, distributed over this spectral range, substantial shot-to-shot frequency jitter is experienced and when averaged over many pulses the idler linewidth assumes a

profile similar to that of the phase-matched bandwidth. Even if the pump wave were of a single frequency, without further effort to reduce the range of idler wavelengths that experience enough gain to reach threshold the linewidth of downconversion will therefore still be significant. The solution is to also include an etalon in the idler cavity in addition to that placed within the parent pump laser cavity. This then results in control of the idler field and THz production from two fields of narrow linewidth; the linewidth of the THz field assuming that of the narrowed pump and idler fields.

If the etalon properties are appropriately selected (i.e. the free spectral range is large enough) then precise tuning of the line-narrowed idler wave, and hence the terahertz output, over the phasematching bandwidth can be effected by tuning of the idler etalon angle alone. This was demonstrated in the system developed in the course of this work, which is described in the following pages. Tuning over a larger range would require synchronous tuning of the idler cavity and etalon angles, with some mechanism for compensating for the increasing losses induced by the etalon at large angles (perhaps an air spaced, piezo tuned etalon), and is the subject of ongoing research within the group.

We conclude this section with a brief discussion on why narrowing of the terahertz wave is not performed directly i.e. by placing an etalon or other wavelength element directly in the terahertz wave or injection seeding it. The terahertz wave is not resonant in the intersecting cavity terahertz OPO, and as such placing an etalon in the terahertz wave will merely have the effect of filtering the output of the OPO. The narrowing thus achieved will be of a much lesser degree as only a single pass of the etalon would be achieved, and the resulting usable power would be reduced. Also, injection seeding with single frequency terahertz radiation is not possible for two reasons: there are no practical sources of tunable single frequency radiation that cover all the tuning range, and the high absorption of terahertz radiation by the nonlinear crystal would prevent the seed being coupled in.

4.1.3. Experimental System

The experimental system was a development of the basic system described in the previous chapters. All components remained largely unaltered save for the spacing of components which were slightly modified to provide clear spaces for the etalons. The system is shown diagrammatically in Figure 64. The etalon used to narrow the laser

linewidth, E1, was positioned near the output coupler of the laser. To include an etalon in the idler wave the cavity axis had to be spatially separated further from the pump wave or else the etalon would impinge on both waves. This was accomplished by including a high reflectivity, 90° reflection angle, mirror (M5) where mirror M3 was originally, and moving M3 to retro reflect the idler a few centimetres orthogonally from the laser axis. Angular adjustment of E2 about the vertical axis was realised by mounting the etalon on a precision galvanometer. This allowed the transmission peak of the etalon to be tuned in to match the phasematching solution corresponding to the idler cavity angle, and then also to allow the fine tuning of the idler wave within the phasematching bandwidth of the idler cavity. The galvanometer driver was controllable by computer, allowing the automatic scanning of the terahertz frequency (etalon E2 angle) over the phasematching bandwidth of the OPO.

The etalons were chosen, from the limited range that were available to us, on the basis of free spectral range (large enough to ensure only one resonant mode) and surface reflectivity (too low a finesse would not narrow sufficiently, and too high would cause unacceptably high round-trip losses). The etalons were chosen from a set of 10%, 40% and 80% surface reflectivities in both 300µm and 600µm thicknesses.

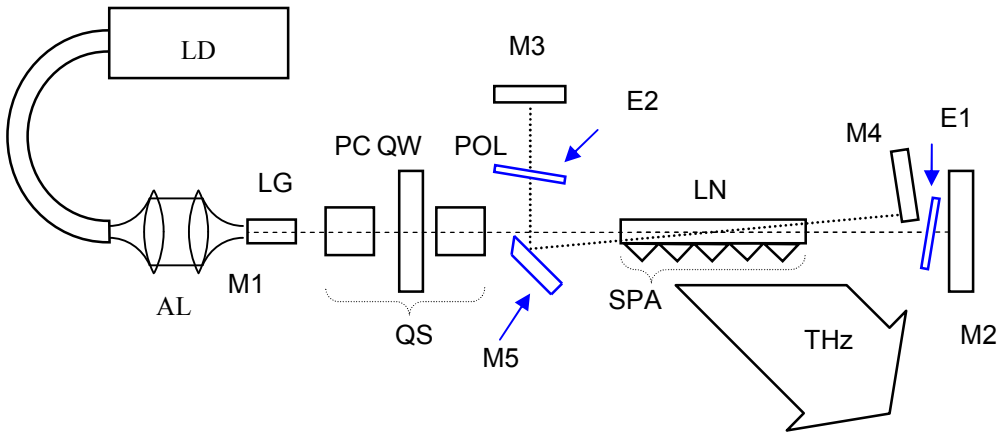

Figure 64 Etalon line narrowed system layout. The system is almost identical to the non-narrowed system outlined in chapter 3 with the modifications highlighted in blue.

Optimal performance was achieved with etalons E1 and E2 both being 600µm thick (free spectral range ~166GHz), and with reflective coatings of 40% and 80% respectively (finesse values of approximately 3 and 14, respectively). The effect of etalon E1 on the per-pulse energy obtained from the free-running Nd:YAG laser (i.e.

with parametric down-conversion suppressed) was negligible and easily recoverable by increasing the primary diode pump power. The low impact of the etalon on pump laser performance was the behaviour to be expected given the already substantial pump cavity round-trip loss. Placing etalon E2 had a similar effect on the idler wave, requiring greater pump laser energies to bring the OPO above threshold, although at no point in the tuning range of the OPO did the insertion of the etalons increase pumping requirements by more than 17%. As the extracted THz energy was limited by damage to the nonlinear crystal coatings by the resonant idler and, more importantly pump fields, the OPO could not be brought as far above threshold, limiting the downconversion efficiency compared to the free running system. For example the system with both etalons reached 1.2x OPO threshold and exhibited ~32% downconversion (as measured by monitoring the laser pulse energy with a power meter through the output coupler of the laser cavity), and at a similar primary pumping energy the free running system with only etalon E1 reached 1.4x oscillation threshold and exhibited ~42% downconversion.

4.1.4. Narrowing of Pump and Idler Waves

The free running linewidth of the laser, in the absence of etalon E1, was measured to be ~20GHz, which narrowed to <1GHz when etalon E1 was included, as measured by a Fizeau-wedge wavemeter (Angstrom WS-7). Insertion of the etalon E1 in itself effected a reduction in linewidth of the idler wave, bringing it down to ~15GHz on a single pulse basis. When the second etalon, E2, was placed in the idler cavity then this further reduced the linewidth down to <1GHz on a single pulse basis, although there was shot to shot frequency jitter which, as will be shown in the next section, resulted in a broader than expected terahertz linewidth of ~5GHz. Such a linewidth is compatible with the resolution of individual atmospheric pressure-broadened spectral lines exhibited by gases and vapours.

4.1.5. Spectroscopy: Part 1

To investigate the impact of the line narrowing upon the ICOPO in the context of its application to very high resolution spectroscopic measurements, spectroscopy of water vapour at a reduced pressure was performed. We chose water vapour as the candidate for this study due to its abundance in air and because its spectral features are extremely well characterised. Conducting the measurement at reduced pressure reduces the absorption linewidth and so the measurement becomes instrument limited by the linewidth of the OPO. Whilst we can deduce the linewidth of the THz field from that of the resonant pump and idler, this experiment therefore affords us a mechanism by which the linewidth of the THz field can be ascertained directly.

To minimise the interference of atmospheric water vapour on recorded spectra we constructed an air-tight enclosure around the terahertz beam path that could be purged with dry nitrogen gas from a cylinder. The laser itself was not enclosed to allow adjustments to optimise the laser and set the OPO's tuning range, so the purging enclosure was extended with expanded polystyrene encompassing the collimating cylindrical lens and finishing only a couple of centimetres from the silicon prism array output coupling, as shown in Figure 65.

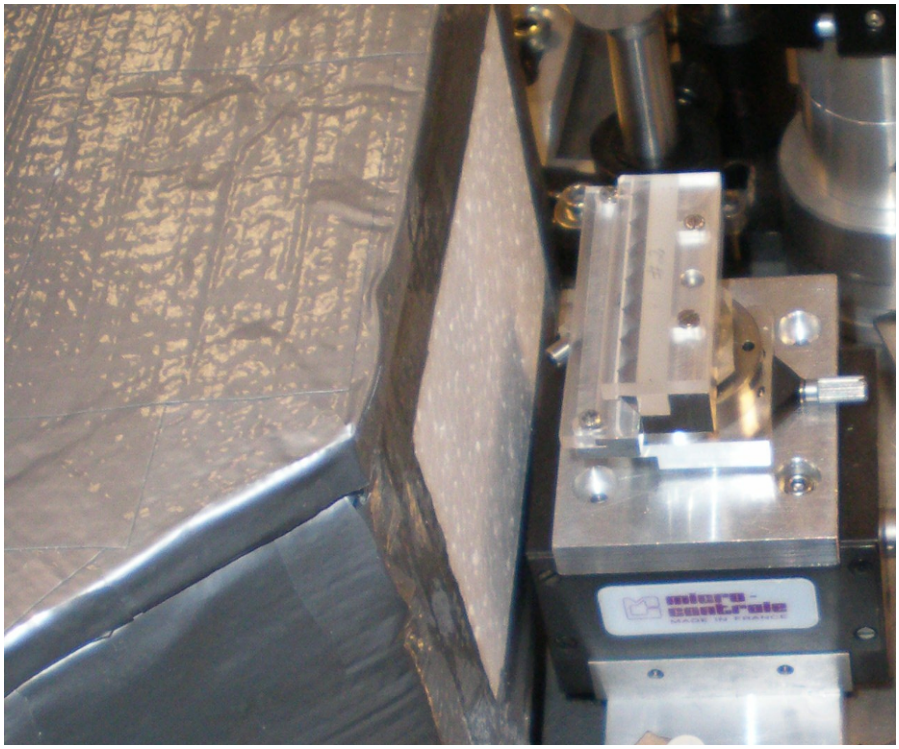

Figure 65 Photograph showing the short beam path that was through laboratory air before entering the nitrogen purged enclosure.

The spectroscopy system lay out is shown in Figure 66. The beam was first collimated by a HDPE cylindrical lens (COL), which compensated for the fast vertical divergence. It was then reflected off two off-axis parabolic mirrors (OAPM1&2, f = 101.6mm & 50.8mm respectively) which formed a compressing telescope resulting in a narrower collimated beam that could easily pass through the 25mm diameter by 30cm long absorption cell without clipping. The beam was then finally focused into the bolometer with a final parabolic mirror (f = 50.8mm) for detection. A boxcar integrator was used to average the pulse energies of 32 pulses to reduce the noise in the measurement, which was then recorded by computer along with the galvanometer position. In this way the transmission of the sample cell could be autonomously recorded as a function of wavelength as the etalon angle and detected signal were controlled and recorded by the computer.

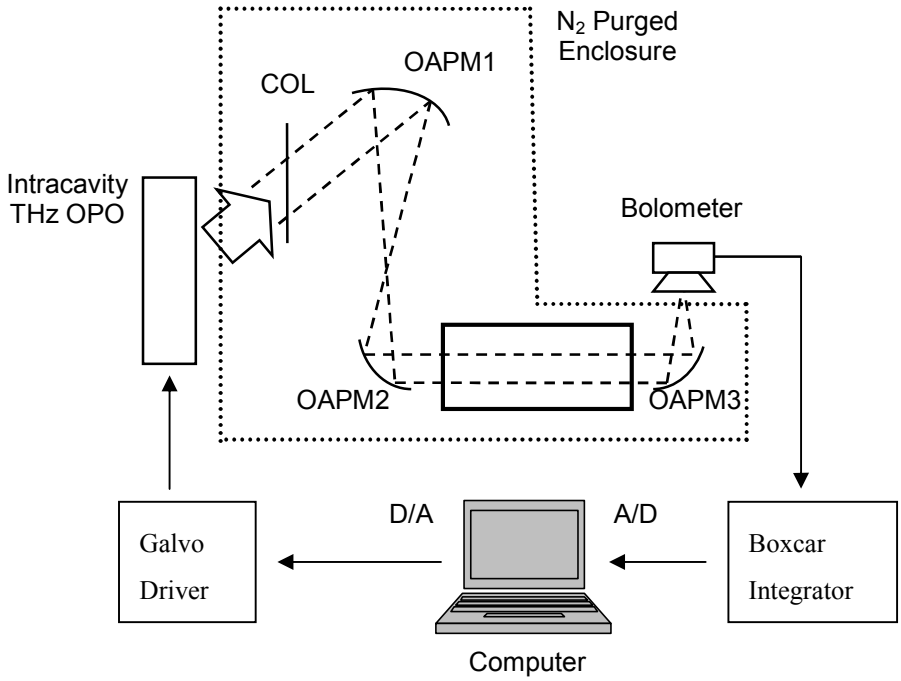

Figure 66 Schematic of spectroscopy system, the enclosure (the dotted line) was made from clear acrylic sheets and expanded polystyrene supported on a metal frame. Polythene film was lain down on the optical bench to cover the mounting holes, and components were fixed in place by screwing through the film.

To set the frequency range of the narrowed OPO the etalon E2 was raised out of the idler cavity temporarily, such that the centre wavelength of the free running idler linewidth envelope could be adjusted. This was achieved by setting the idler cavity angle such that the idler frequency generated corresponded to the centre of the tuning range over which the spectroscopy was to be performed, and then repositioning the etalon in the idler cavity orthogonally to the optical axis, i.e. "on flash".

The galvanometer driver changed the angle of the etalon E2 by an amount directly proportional to the input voltage supplied by the computer. However, the transmission frequency of the etalon changes with angle approximately as the cosine of the angle of incidence of the input wave. To calibrate the frequency with respect to the voltage supplied the narrowed idler frequency and the corresponding angle at which it occurred were measured at several galvanometer drive voltage points. The idler frequency was measured using a wavemeter (Angstrom WS-7) and the etalon angle (θ) was calculated by observing the offset (x) of the first rejected spot on a screen positioned a distance (d) from E2, as shown in Figure 67.

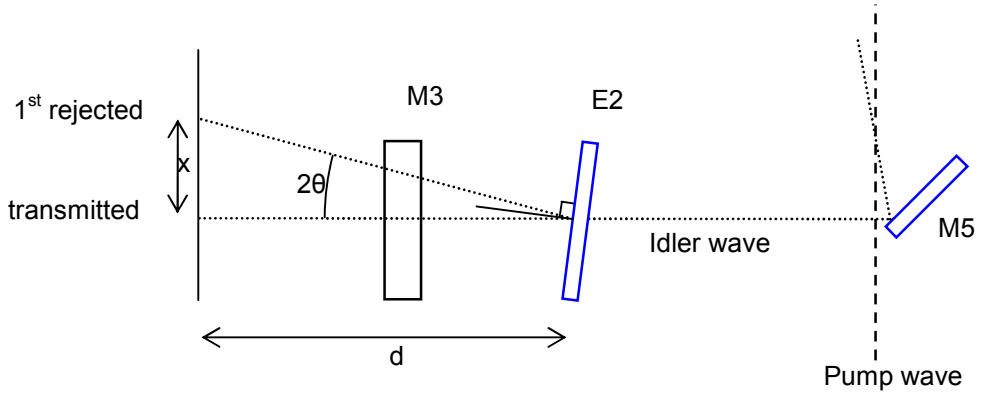

Figure 67 Outline of the method used to calibrate the applied voltage (galvanometer angle) to the idler frequency.

The pressure broadening of water vapour absorption lines at ~1bar gives rise to an absorption linewidth of around 5GHz FWHM. In order to more accurately deduce the source linewidth this was reduced by performing the spectroscopy at a pressure of 180mbar, at which the 40.283410cm^{-1} (1.207666THz) and 40.988310cm^{-1} (1.228799THz) lines have a width of ~1GHz FWHM (using data from the HITRAN 2008 database [6]).

4.1.6. Results

The trace shown in Figure 68 shows the transmission of saturated air at 180mbar and 18°C (corresponding to a water vapour partial pressure of 22mbar). The dotted line represents the transmitted signal, and shows the Gaussian like tuning range of the terahertz OPO when only tuning etalon E2, as well as the two absorption dips corresponding to the water vapour absorption lines. The other plots shown in the diagram are calculated, assuming Beer-Lambert absorption, and using line strengths and pressure broadened widths from the HITRAN database convolved with a Gaussian of various linewidths representing the source (3, 5 or 7GHz FWHM), and also multiplied by a Gaussian (fitted by eye) to represent the tuning bandwidth of the terahertz OPO. It is clear that the observed data agrees closely with modelling based on an assumed 5GHz source linewidth.

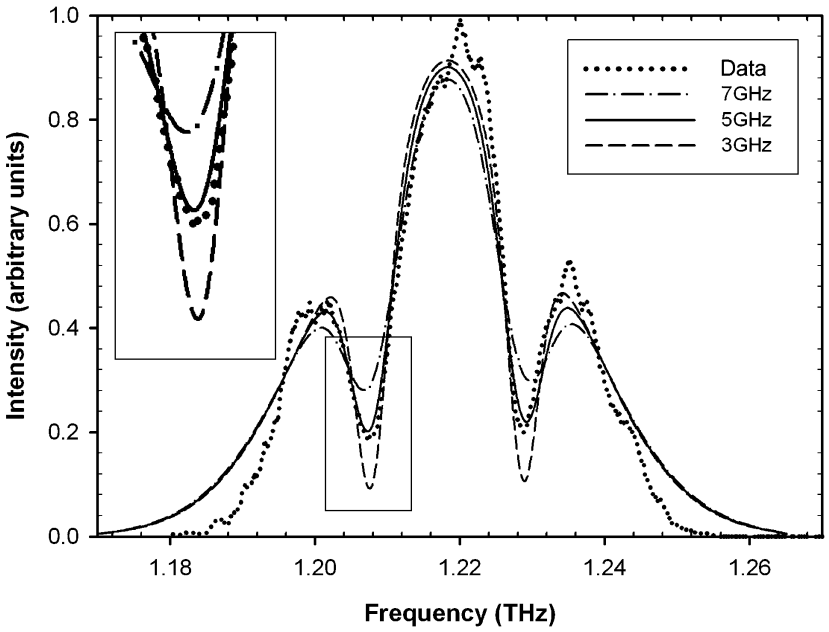

Figure 68 Transmission of a water vapour cell at 180mbar at (22mbar water vapour pressure). The dotted curve represents the signal detected by the bolometer, whilst the other three curves were modelled using MathCAD and data from the HITRAN database for several assumed source linewidths.

4.1.7. Spectroscopy: Part 2

As mentioned in the previous section the measurement of the idler with a wavemeter capable of single pulse measurements (Angstrom WS-7) revealed that there was significant pulse to pulse frequency jitter. Due to the multipulse averaging employed to overcome the terahertz pulse energy jitter this results in an effective broadening of the THz linewidth. In an attempt to overcome this effect to further improve resolution, without adding further complication to the optical setup, instrumental improvements were made to the way in which the data was recorded and analysed. The wavelength of each pulse was logged with the corresponding terahertz pulse energy, and then the terahertz pulse energies would be averaged over set frequency bins, rather than sequentially. Although this system needed a wavemeter capable of single pulse measurements, it was simpler to implement as the angle to frequency calibration routine for etalon E2 was avoided.

The experimental layout was again that shown in Figure 66, but for the characterisation of this technique a study of the 1.4969THz carbon monoxide absorption line was performed rather than a study of water vapour. The advantage to

this is that the quantity of carbon monoxide present in the sample cell is independent of the temperature of the system, whereas the partial pressure of water vapour would change. It is also preferred as atmospheric water vapour absorption in the laboratory can then be avoided so as to not interfere with the accuracy of the result. Carbon monoxide exhibits a series of absorption lines in the 1 to 3THz region attributed to rotational modes of the molecule. Figure 69 shows the comb of equally spaced carbon monoxide lines overlaid by the water vapour absorption spectrum – both produced using an in-house MathCAD worksheet written to use data from the most recent HITRAN 2008 database [6]. It is clear that water vapour exhibits many absorption features in the terahertz region, and that many of these overlap with carbon monoxide lines. There is however a gap around the 1.4969THz carbon monoxide absorption line, which also lies around the peak energy output of the intracavity terahertz OPO, and so this line was selected for study.

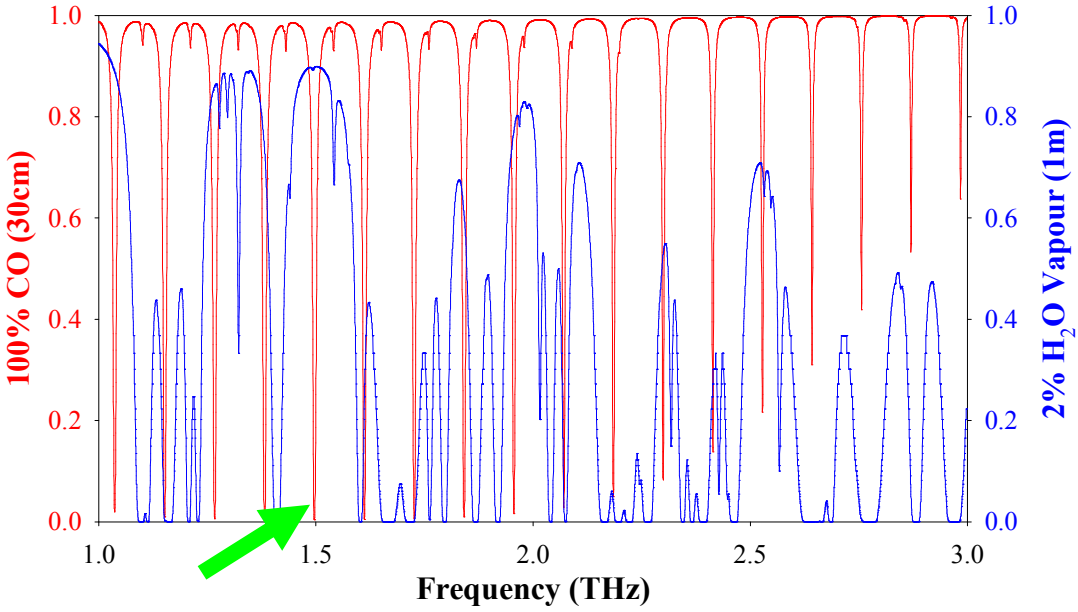

Figure 69 Transmission profiles of carbon monoxide and water vapour at ~atmospheric pressure (1000mbar). It can be seen that water vapour, although only modelled at a partial pressure of 2% atmospheric, dominates the absorption. There is a carbon monoxide line at ~1.5THz that is relatively clear of the water vapour background.

As before the centre frequency of the free running (no idler etalon) OPO was set to the frequency of interest before inserting etalon E2 in the "on flash" condition. The calibration step was then skipped and the etalon angle scanned by an automatic voltage ramp input to the galvanometer driver. Concurrently with this, single pulse

measurements of the transmitted THz pulse energy and the idler frequency were recorded by computer with measurements being triggered by the Q-Switch driver trigger. This technique ensured that energy and frequency measurements were synchronous and not over sampled (multiple measurements of the same pulse energy which would affect the averaged result). The frequency of the pump laser was recorded with the wavemeter before and after each run, and the data only used if the frequencies were the same. This was because of slight frequency drifting in the pump and occasional hops between etalon modes, most likely caused by fluctuations in the ambient conditions in the lab (the temperature in particular).

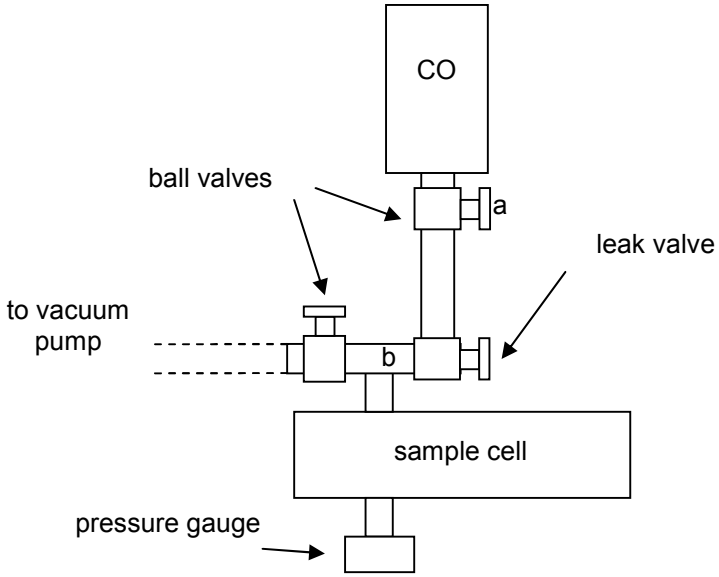

Figure 70 Schematic diagram of sample cell filling set-up.

The sample cell was prepared by first evacuating the system up to valve "a", as shown in Figure 70, down to $< 10^{-5}$mbar using an Edwards PicoDry turbopump. Valve "b" was then closed off and separated from the vacuum pump and the leak valve was also shut. Valve "a" was then opened and carbon monoxide slowly leaked into the sample cell up to the desired pressure, at which point the leak valve was closed and the carbon monoxide cylinder separated from the cell. The cell was then placed in the beam path within the nitrogen purging enclosure. Spectroscopy runs were then performed alternately with the cell, or with two HDPE windows identical to those in the cell, in the beam path to remove any absorption/interference effects induced by the cell windows to obtain a baseline measurement.

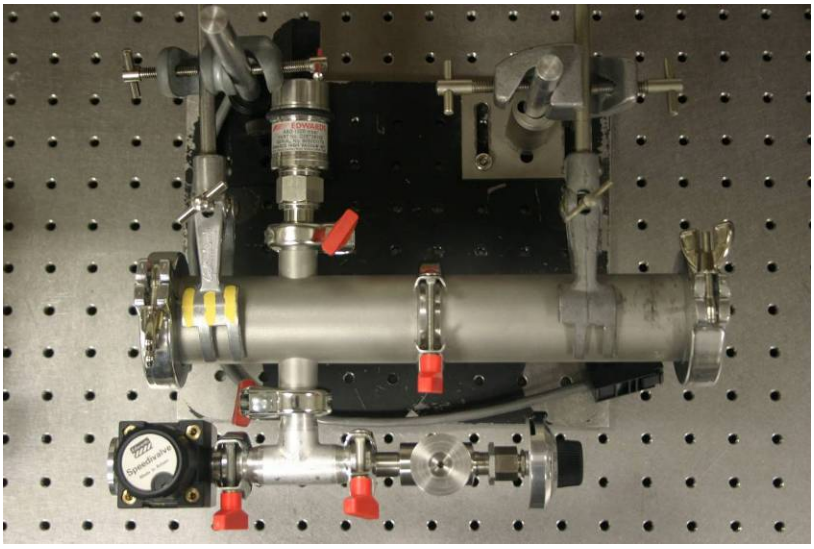

Figure 71 Gas cell used for carbon monoxide spectroscopy. In the center is the metal piping used for the cell consisting of a straight section of inner diameter 1.5" and another section with side ports. The upper port in the photograph is connected to an Edwards ASG1000 gauge for the measurement of the carbon monoxide pressure. The lower port connects to two valves: to the left is a connection to a vacuum pump, and to the right is a leak valve for allowing carbon monoxide into the cell. The cell windows are ~5mm thick HDPE, piping is stainless steel throughout.

4.1.8. Results

A sample spectrum of carbon monoxide is shown in Figure 72, including the background baseline measurement which here also indicates the tuning range of the OPO (around 30GHz in this case). The absorption dip in the transmission spectrum is clearly visible, however there is still some amplitude noise in the signals even after the averaging is performed (for the graph a moving average of width 1GHz was used to clarify the absorption feature for reproduction in this thesis. This corresponds to around 40 samples being averaged due to the scanning speed of the etalon).

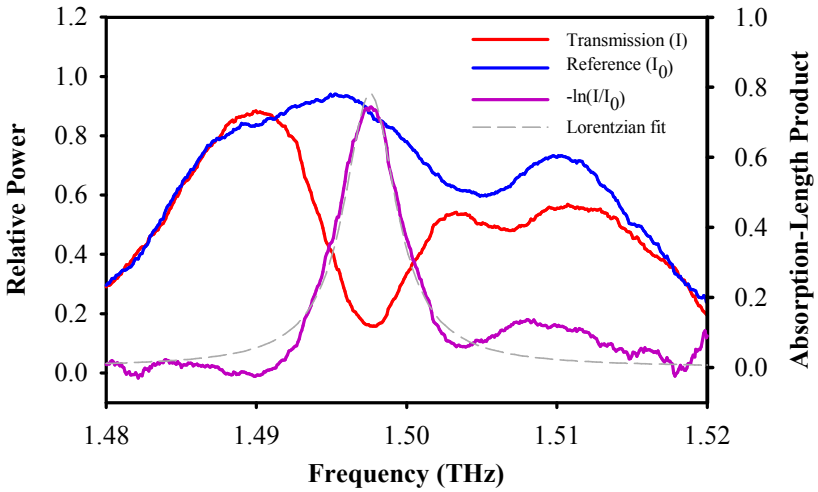

Figure 72 Example of reference and spectroscopic scans taken at ~650mbar. A moving average has been applied to smooth the data (~2GHz wide) for clarity.

In order to extract linewidth and absorption coefficients from the data the reference signal was first split into frequency bins 250MHz wide and the average signal calculated over each bin. This was then multiplied by a Beer-Lambert absorption with Lorentzian line shape (due to pressure broadening, see (4.1)) whose coefficients were numerically fitted to the (identically binned) transmission spectrum by eye.

$$\text{Transmission} = \text{Reference} \times e^{-\left(\frac{\Delta\nu^2}{\Delta\nu^2+(\nu-\nu_0)^2}\alpha L\right)} \tag{4.1}$$

The results of this analysis are shown in Figure 73 and Figure 74. The natural linewidth of this transition is only a few megahertz, so the "y intercept" of the best fit to the $\Delta\nu$ of the absorption line is a good approximation of the effective source linewidth, which in this case is ~500MHz.

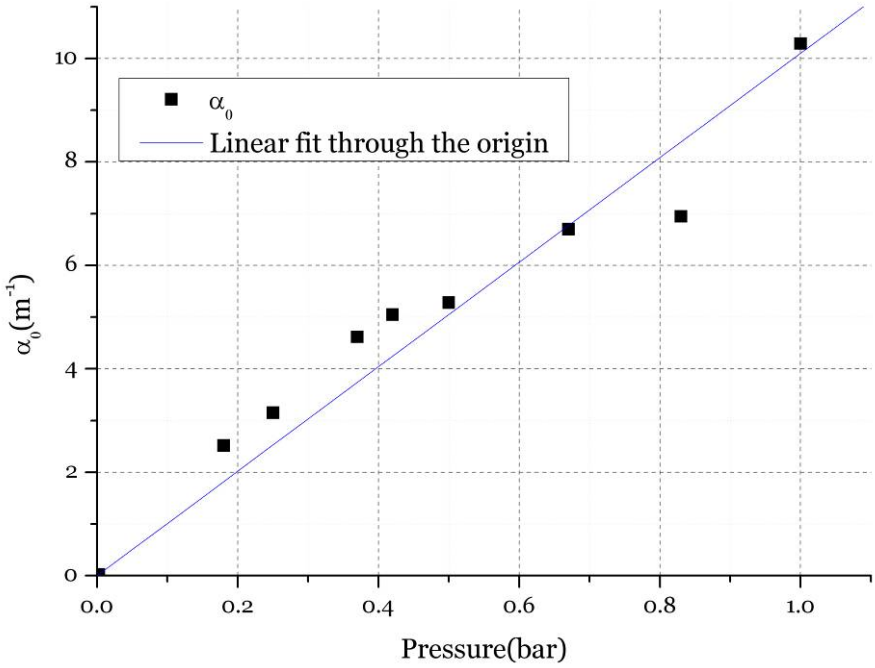

Figure 73 Plot of the fitted absorption coefficient of the 1.4969THz carbon monoxide rotational transition line.

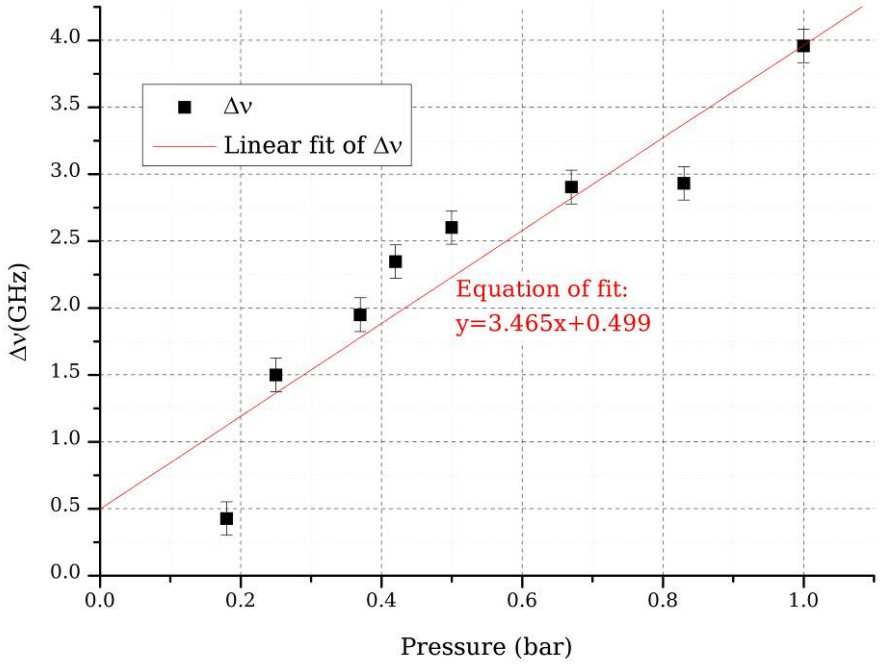

Figure 74 Plot of the linewidth of the 1.4969THz carbon monoxide rotational transition line as a function of pressure. The fitted line indicates a pressure self-broadening coefficient of 3.5±0.5GHz/bar and an instrumental linewidth of 0.5GHz.

4.1.9. Discussion

To our knowledge this was the first application of etalons in a terahertz OPO idler cavity. The techniques described in the first part of this chapter were both simple to implement and effected a significant reduction in source linewidth (10 to 100 times improvement) as summarised in Table 1. The per pulse monitoring showed that the etalon within the idler cavity did not provide sufficient selectivity to ensure optimal stability of the idler frequency. This was not surprising as the etalon was not specifically designed for the purpose, but rather chosen from a limited selection that were available at the time this experiment was conducted. Further analysis and experimentation is needed to determine the optimal etalons for both the pump and idler waves and then a linewidth similar to or even narrower than that provided by per pulse monitoring may be achieved. This will require the compromise between selectivity, tuning range, and walk-off losses to be systematically investigated and tested.

This technique could be further refined through the implementation of an adjustable air spaced etalon. Such a system would allow for the simultaneous tuning of the idler phase-matching condition through idler cavity angle variation whilst adjusting the pass band of the etalon, enabling spectroscopy to be rapidly performed over the full tuning range of the OPO. Using a solid etalon (tuned by angle) precludes such a wide tuning range due to unacceptable high walk-off loss at the extremes of etalon angle.. An air spaced etalon would allow a small angle between idler and etalon to be maintained as the tuning can be performed by altering the mirror spacing.

Table 1 Summary of averaged FWHM linewidths.

Etalons implemented	pump (GHz)	idler (GHz)	THz (GHz)
None	20	~50	~50
Pump only	<1	~15	~15
Pump & Idler	<1	~5	~5
Pump & Idler (Single shot)	<0.5	<0.5	~0.5

4.2. Injection Seeding

The insertion of etalons in the system provides means for a substantial reduction in line narrowed output for a small penalty in terms of added system complexity. However the linewidth attained is still greater than the transform limit of the 1 to 10ns pulse widths, which assuming a Gaussian pulse shape ($\Delta\nu.\Delta t = 0.44$) is 44 – 440MHz. To reach this limit injection seeding of the idler wave with single frequency laser light was implemented. This forced the idler wave to take on the frequency and linewidth of the single-frequency seed light, and when the pump wave was also single frequency a single frequency terahertz wave was produced. This approach has been applied to extracavity pumped terahertz parametric systems, producing ~transform-limited linewidths of <100MHz FWHM[7].

The development of this seeded intracavity system has uncovered important and unanticipated detrimental effects on the spectral quality of the seeded down converted wave arising from the spectral quality of the pump wave - effects which may have implications beyond terahertz generation to any intracavity parametric system. In this section we describe the development of an intracavity terahertz OPO that was seeded by a tunable external cavity diode laser, and discuss the detrimental characteristics discovered during its construction.

4.2.1. The Principles of Injection Seeding

The difficulty in constructing a single frequency terahertz OPO (and indeed any pulsed OPO) arises from the short temporal duration of the pulses in nanosecond Q-Switched devices. This limits the degree of line narrowing that can be performed via multiple passing of the frequency selective components. The optical wave builds from noise photons and so there is a chance that a frequency close to that desired will build up first, which imposes a pulse to pulse frequency jitter and also allows multiple frequencies lying in the center of the gain to build in a single pulse. This can be mitigated, to some extent, by the use of components of higher selectivity (e.g. higher finesse etalons), but this results in a reduced round trip net gain which, in turn, leads to increased laser/OPO threshold.

These difficulties are not a concern in continuous wave lasers/OPOs where the temporal duration of the wave is essentially infinite, or at least very significantly

longer than the nanoseconds to microseconds of Q-Switched optical waves. This allows a huge number of passes of frequency selective components to take place.

The principle of injection seeding is to couple the very narrow linewidth optical wave from a continuous wave laser/OPO into the cavity of a pulsed system such that the optical pulse builds from already present, single frequency optical field instead of from spontaneous / parametric fluorescence. Successful injection seeding can be achieved even at very modest seed powers; even 1mW is ample as this power is still many orders of magnitude greater than that of, and therefore dominates over, the fluorescence from which the optical pulse builds.

Successful injection seeding does however require that the incident seeding mode is spatially matched into the fundamental resonant mode supported by the laser / idler cavity, and that that the seeded cavity is held on optical resonance with the incident field. The former is achieved through careful characterization of the seeding and seeded beam divergence, after which mode matching is accomplished through the placement of one or more lenses. The latter is attained through the use of cavity stabilization techniques. The requirement that the seeded cavity must be held at the peak resonance of the incident field precludes the use of simple stabilization techniques such as side-of-fringe; instead more advanced techniques such as the Pound-Drever-Hall [8] or Dither & Lock schemes must be implemented. In the experiment outlined in the following section we use the former of these techniques due to its inherent stability compared to that of the latter, and also due to the extensive expertise available due to the development of instrumentation previously carried out within the group for work on pump-enhanced, continuous-wave OPOs [9]

4.2.2. The Seed Laser

The seed laser was chosen on the basis of having several key features. First of all the linewidth had to be <50MHz, such that the transform limit of the terahertz pulses could be reached. Secondly a source that could be [ideally, smoothly] tuned over the whole range of the idler wave was preferred, so that it would not reduce the terahertz frequencies that could be generated by the terahertz OPO. In addition to the second point, the ability to tune the source whilst running single frequency was desired as this would also allow for the single frequency tuning of the terahertz wave giving a practical mechanism for performing spectroscopy. All of these requirements are met

by external cavity diode lasers (ECDLs) [10-12]. The ECDL comprises a semiconductor laser diode gain medium (which has a large gain bandwidth), a lens to collimate the output from the diode, and a blazed diffraction grating in the Littrow configuration providing feedback into the diode and allowing output coupling (usually through what would be the zero order diffraction angle if the grating was not blazed). The layout of the ECDL used is shown in Figure 75.

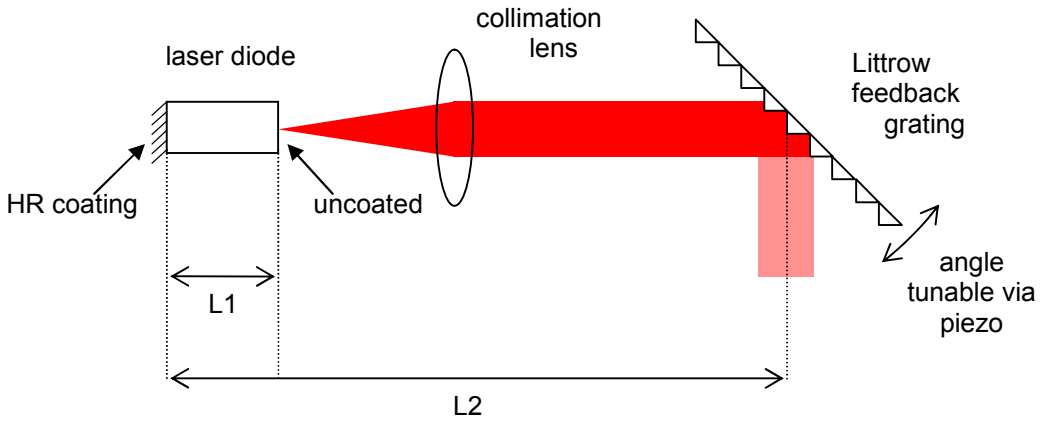

Figure 75 Schematic diagram of a typical, Littrow configured, ECDL.

The operating frequency in an ECDL comes about from the overlap of several frequency selective components: firstly there is the broad gain bandwidth of the semiconductor gain medium, then there is the feedback provided by the Littrow mounted grating which is used to coarsely and broadly tune the desired frequencies via its angle, and then there is the comb of frequencies supported by the total [Fabry-Perot] laser cavity (L2 in Figure 75), and the comb of frequencies supported by the low finesse coupled cavity formed by the HR coating on the back face of the gain medium and the Fresnel reflection from the front surface. The relative size of these effects is shown in Figure 76. In some cases the gain medium is antireflection coated to remove the additional complexity of the coupled cavity effect.

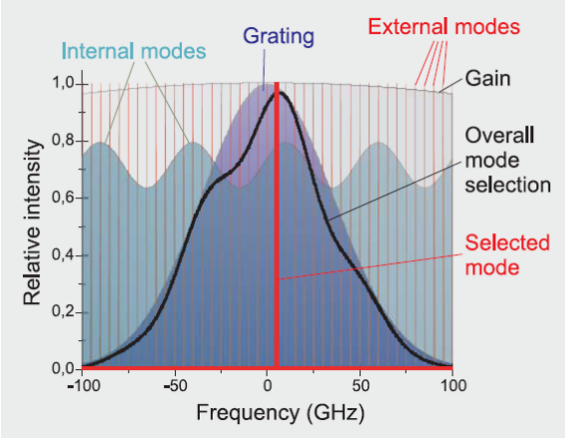

Figure 76 Illustration of the overlapping line narrowing effects of the various components of the ECDL. Reproduced from Toptica diode lasers brochure 2009. Retrieved June 2010 from "http://www.toptica.com/uploads/media/toptica_BR_tunable_diode_lasers_2009_01.pdf".

Continuous tuning of these lasers can be obtained over large frequency ranges (>100GHz), but is non-trivial to achieve. There are multiple effects that must be synchronised if tuning is to be broad and mode hop free. Primary selection is achieved by varying the angle of the feedback grating, which is easily achieved using a piezo electric actuator. However, this also has the effect of changing the cavity length and so altering comb of modes supported by the external cavity. In addition to this the optical length of the laser diode will be unchanged, and so the selectivity of this component may inhibit smooth tuning. Fortunately these problems have largely been resolved by ensuring the correct positioning and pivot point of the grating such that the cavity length is scanned correctly with grating angle [11], and by ramping the diode current, which induces a refractive index change in the semiconductor gain medium such that its optical length is also scanned with the grating angle tuning.

The laser chosen was a Toptica Photonics DL100 fitted with a diode centred at 1072nm and rated for up to 180mW optical output (up to ~70mW of which could be coupled out of the ECDL), see the photograph in Figure 77. This is a commercial system with mechanisms in place to allow the smooth single frequency tuning of the lasers output when correctly configured. This required careful setting of the initial operating temperature, drive current, piezo motor grating scan range, and the corresponding relative change in the drive current. With careful optimisation single mode tuning ranges of around 10GHz were readily achieved.

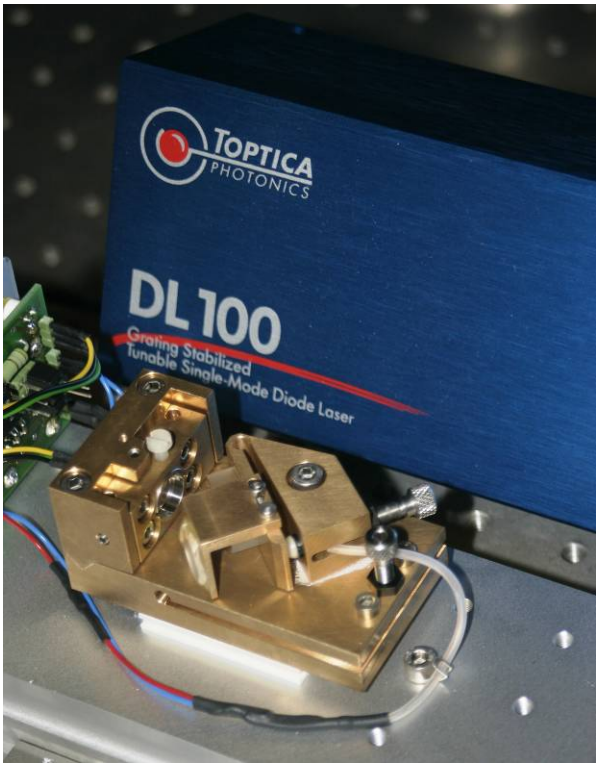

Figure 77 Photograph of the ECDL used as the single frequency seed.

This system also has a correcting mirror that is scanned with the grating angle, such that the pointing direction of the laser beam does not waiver when tuning of the grating angle is performed, as in [12]. Ultimately, the smooth tuning range of the THz output is limited by the range over which the idler cavity can be slaved to the incident seeding field. This is a function of the expansion range of the actuator used to hold the cavity on resonance, in this case a piezo tube stack. This component had an expansion range of ~5μm which, given a idler cavity length of 30cm, indicates a THz tuning range of 4.7GHz.

4.2.3. Experimental Layout

The experimental apparatus is outlined in Figure 78. The heart of the device is highlighted in the bottom center of the figure, and is based on the intracavity THz OPO reported described in previous sections. The main differences are in the length of the nonlinear crystal, laser cavity length, and the intracavity etalons used.

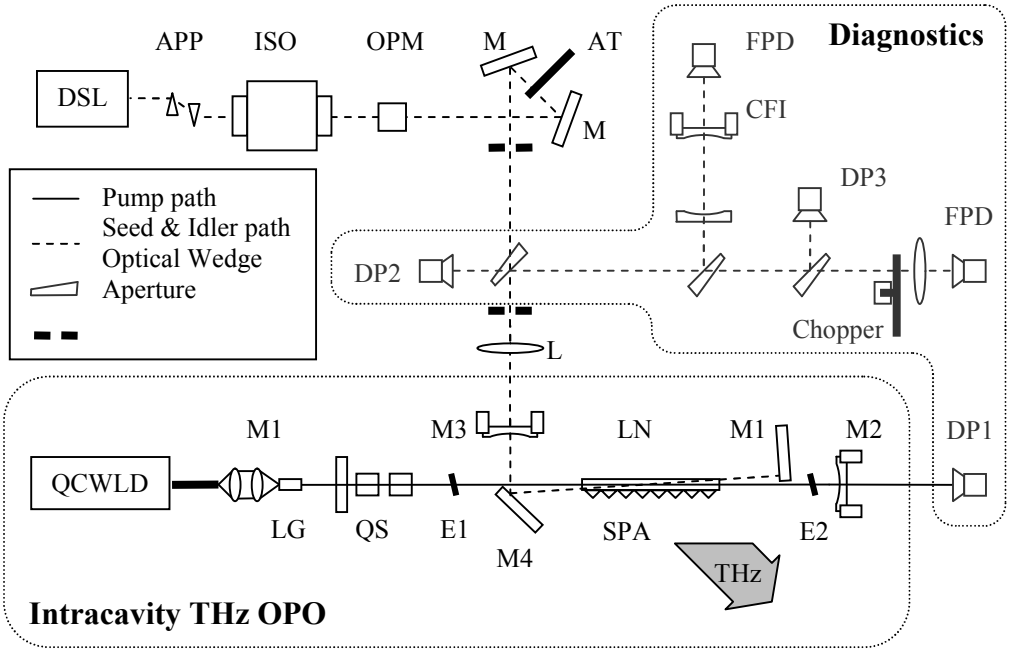

Figure 78 Schematic layout of the seeding experiment components on the optical bench.

The laser consisted of: (i) a Nd:YAG laser gain (LG) crystal of which one end was high-reflectivity (HR) coated in order to act as a mirror, M1, for the pump wave cavity; (ii) mirror M2 (5M radius of curvature), which acted as the high reflector at the other end of the pump wave cavity; and (iii) Q-switching (QS) components—these being the quarter wave plate, Pockels cell, and beam cube polarizer described previously. The cavity mirror M2 had a reflectivity of 98%, rather than being a high reflector, so as to allow monitoring of the pump wave during Q-switching, the output coupling of the pump wave was still predominantly through the downconversion process itself. For optimal efficiency the Nd:YAG was again end pumped (pump volume and laser mode are ~800μm in diameter) via a fibre-coupled laser diode array at ~808nm. There were two intracavity etalons in the pump wave cavity - E1 (40% reflectance and 600μm thick) and E2 (uncoated, ~4% reflectance and 3mm thick), which were selected to produce single longitudinal mode operation of the pump laser in conjunction with a prelasing technique for minimal loss (the importance of this will be explained in a later section of this chapter).

Also situated within the pump laser cavity is a 70mm MgO doped $LiNbO_3$ crystal (LN). Completing the intracavity OPO are the cavity mirrors of the (intersecting) idler wave cavity, these being: M3 (HR to edge, plane), M4 (HR to edge at 45°, plane) and M5 (R=60%, plane), the latter being mounted on a piezo-electric stage to

facilitate tuning of the idler cavity mode. All dielectric mirrors, as well as etalons, were specified for operation at 1064.4nm. An array of high-resistivity silicon prisms (SPA) lay along the edge of the lithium niobate crystal to couple out the terahertz wave. The complete laser and OPO cavity are shown in Figure 79.

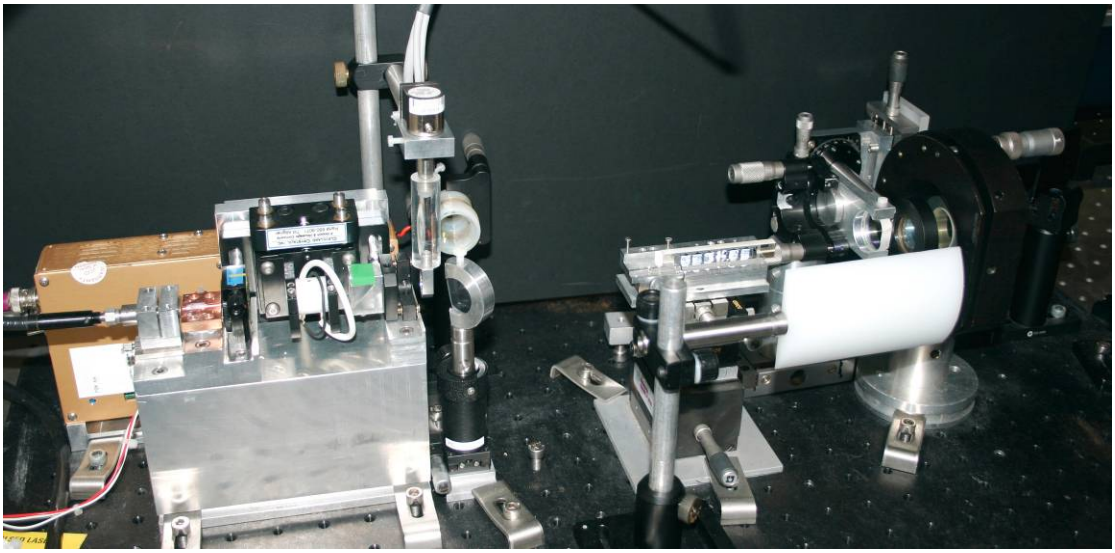

Figure 79 The seeded intracavity terahertz OPO. The seed laser and diagnostics are behind the piece of black card used as a backdrop for the photograph.

The OPO idler was seeded by the ECDL described in the previous section, and is shown in the upper left of the diagram. The output of this laser was passed through an anamorphic prism pair (APP) for ellipticity correction and a 60dB optical isolator (ISO) before passing through a 75MHz optical phase modulator (OPM), beam steering mirrors (M), a variable filter wheel (AT), and a mode matching lens (L) that coupled the seed laser in to the idler cavity.

The optical phase modulator was part of a Pound-Drever-Hall cavity-locking scheme that was implemented in order to maintain resonance of the seed light with an axial mode of the idler cavity – the need for which is explained in a later section. The electronics associated with this technique are not shown in the diagram for the benefit of clarity. An optical wedge was situated in the beam path to provide pick-offs for the monitoring of the seed and idler waves as well as directing the seed light rejected back from the idler cavity onto a fast photodiode (FPD), which was also part of the Pound-Drever-Hall locking system.

To confirm successful seeding a direct measurement of the idler spectrum was required, but idler pulses from the OPO and reflected seed light shared the same

optical path, making it ineffective to use either a wavemeter or a conventional scanned interferometer. To overcome this problem a wavelength diagnostic system that was only sensitive to the nanosecond pulsed light had to be conceived. The solution found was to use a slowly scanned confocal interferometer (CFI Tech Optics 2GHz FSR model) in conjunction with a fast responding photodiode (FPD) that could resolve the idler pulse envelope. A signal generator was used to provide a voltage ramp (period ~30s) to both a high voltage amplifier that drove the piezo tuning of the confocal interferometer, and the horizontal axis of a Tektronics TDS360 oscilloscope in x-y mode (as opposed to y-t mode). The transmitted beam was focused onto a 1ns rise time photodiode that was connected to the ac-coupled y axis of the oscilloscope. Oscilloscope measurements (25ns/div time base) were triggered by the Q-Switch driver, and as the x scan was effectively stationary during the OPO pulse the result was that the oscilloscope plotted a vertical line on the screen corresponding to the amplitude of the pulse detected, at a horizontal position set by the ramp voltage. The spectral content could then be calibrated by comparing features to the free spectral range of the interferometer (2GHz). Finally, there were three diagnostic points (DP1–3) where the insertion of a power meter, photodiode, or optical fibre (for coupling to a wave meter) was possible for measuring the seed laser, pump laser, or OPO output properties.

The following characterisation of the system was performed with an idler wave corresponding to ~1.5THz.

4.2.4. Idler Cavity Configuration

The literature [5, 7, 13-16] regarding the injection seeding of extracavity pumped terahertz OPOs suggests that the optical parametric generator (OPG) is the preferred device configuration (no idler resonator), as it is a simpler system and was found to produce greater terahertz pulse energies. However, our initial experiments attempting to injection seed an intracavity OPG were unsuccessful in producing an observable effect on the downconversion process. It was therefore necessary to investigate the idler cavities that would be suitable for injection seeding.─To determine the optimal cavity configuration for the THz generator, a series of idler pulse energy measurements were performed for: (i) a single-pass generator with no idler cavity mirrors (removal of both M1 and M3), (ii) a double pass generator where the single-

pass idler is fed back into the nonlinear crystal with a high reflector at M1 (removal of M3 alone), and (iii) an optical parametric oscillator in a configuration either with (a) a high reflector as M1 and an uncoated optical flat as mirror M3 (R~4%), or with (b) a high reflector as M1 and an output coupler (R=60%) as M3. The resulting downconverted idler pulse energies are compared in Figure 80.

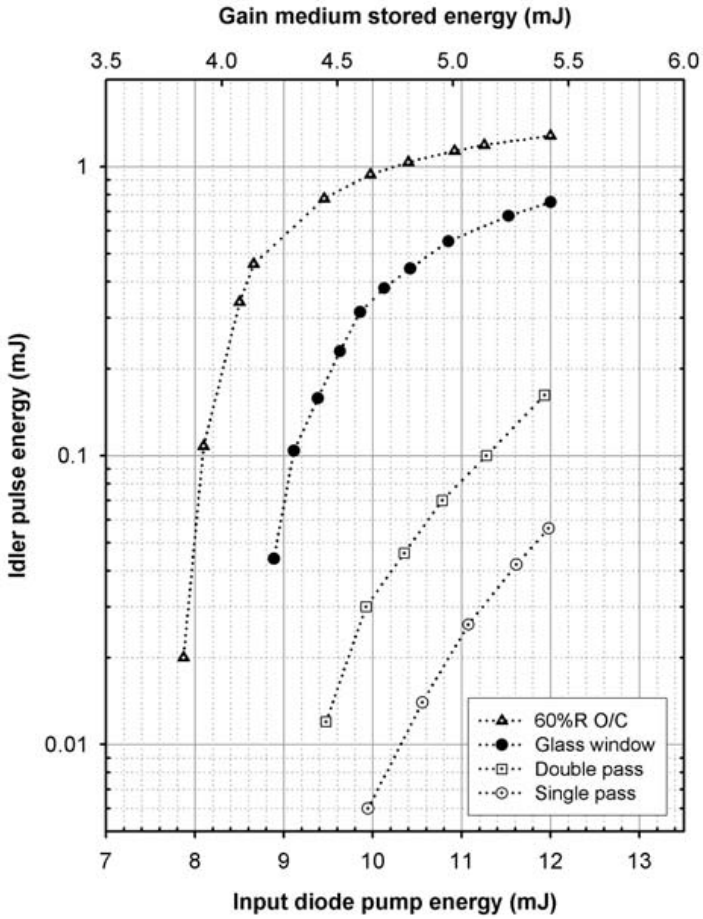

Figure 80 Idler pulse energy characteristics with different generator/oscillator configurations.

It can clearly be seen that even a modest cavity yields over an order of magnitude greater down converted energy. Indeed, implementation of the R=60% output coupler resulted in idler energies of ~1.2mJ and corresponded to the near-optimal condition of ~50% pump wave depletion when pumped a little less than twice the OPO threshold, as shown in Figure 81. Due to this a higher reflectivity mirror on the idler cavity was unnecessary and even undesirable, as it could overly constrain the system for injection seeding and reduce the idler signal available for diagnostic/monitoring purposes. Even seeding the idler wave with the maximum power available to us (~60mW) in configurations (i) and (ii) above failed to improve downconversion and hence the

generated THz levels were still very low. We theorise that discrepancy between our findings and those of Kawase et al [5, 7] may be in the total length of lithium niobate used. In the Kawase system two crystals were used with a combined length of 130mm and generation initiated in the first crystal, whereas here only 70mm was used, which presents a lower single pass gain coefficient to the idler wave.

With the idler cavity present it was possible to very accurately align the seed wave, as it could be collinearised with the idler beam using pinholes and the wavelength tuned to the measured idler frequency. For these reasons an oscillator configuration with R=60% was chosen as the device for injection seeding.

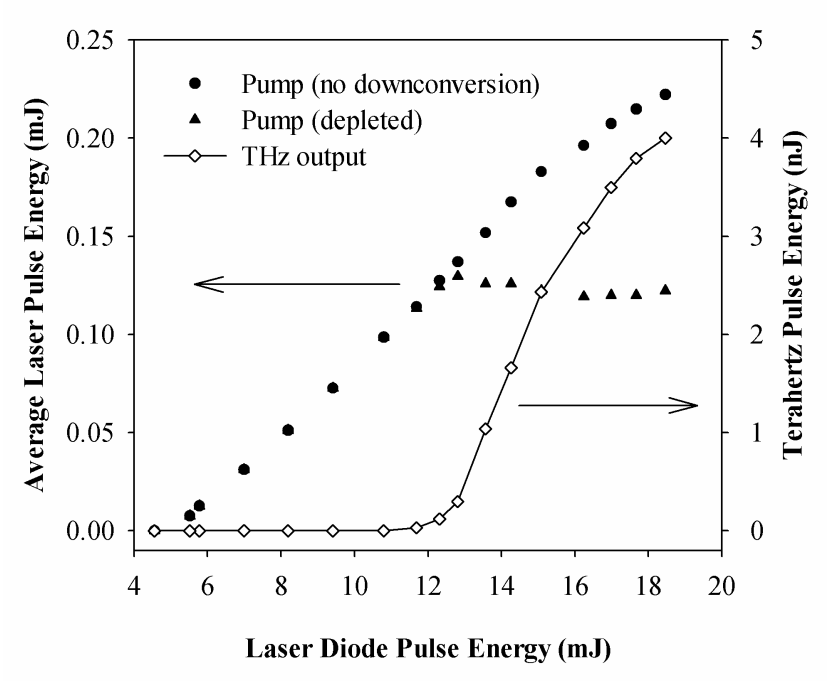

Figure 81 Energy characteristic of the laser (with an intracavity etalon for linewidth control) with and without parametric downconversion (achieved by physically blocking the idler cavity). The characteristic clamping of the laser power by downconversion above operation threshold is clearly visible. The maximum average terahertz pulse energy was measured to be 4nJ at the highest input energy, and energies are extrapolated back to threshold using the downconversion proportion. This data was recorded in the absence of seeding.

4.2.5. Idler Cavity Locking

Single frequency downconversion was achieved in the absence of cavity locking but the energy of the pulses generated was found to modulate as the seed was tuned on and off resonance with the idler cavity (shown later in the spectroscopy section,

Figure 89). Indeed cavity locking may not have been necessary at all if a second bolometer had been available to monitor the terahertz pulse energies produced.

The Pound-Drever-Hall technique is not the only locking technique (nor the simplest) that could have been implemented: a "side of fringe" method would also have worked, however the Pound-Drever-Hall technique has an advantage in that it can lock to the peak of the resonance.

As the error signal is proportional to the photodiode signal it was important to maximise the amount of rejected seed collected. This caused a problem as the nanosecond, millijoule level idler pulses, which deliberately share the same optical path, would then damage the photodiode. The solution to this was found to be to place a chopper wheel in the seed/idler path that would synchronously block the idler pulse which would otherwise be incident upon the photodiode. With the Pound-Drever-Hall technique when the optical signal is blocked the error signal drops to zero, and so the cavity remained on resonance for a period after the rejected seed was blocked. To ensure the chopper wheel and TOPO pulses remain in phase the trigger for the (808nm) quasi cw laser diode driver and electro optic Q-Switch were derived from the chopper wheel frequency. Traces of the optical and error signals are shown in Figure 82.

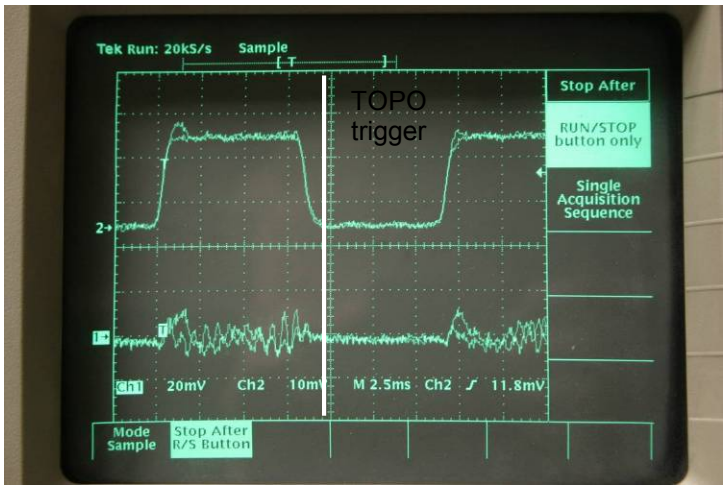

Figure 82 Photograph showing the chopped photodiode (upper trace) and error (lower trace) signals. Locking is regained quickly once the photodiode signal returns. In this case the error signal appears to be on the verge of oscillating, indicating that the feedback loop coefficients are too high.

Optimally, the feedback loop should be blocked for as short a time as possible with, say, a 10:1 duty cycle or more to ensure locking. However a 1:1 chopping cycle in conjunction with the moderate finesse of the idler cavity (due to the use of a 40% transmission output coupling mirror) ensured satisfactory operation in practice, as may be seen in the right of Figure 89 where the previously observed modulation has now been eliminated.

4.2.6. Obtaining a Single Mode Idler Pulse

It was anticipated that injection seeding of the idler wave cavity would result in single frequency idler wave generation, whether or not a single-mode pump wave was present. The frequency spectrum of the pump wave being taken up by the signal wave (i.e. the THz wave in the present case). Such behaviour has previously been demonstrated in conventionally pumped (i.e.. external to the laser) OPOs [17]. However, in the present case injection seeding did not initially result in a single frequency idler wave; even though idler pulses were affected with an earlier onset (a few nanoseconds) and greater intensity (an improvement of downconversion of ~3% was measured), the spectral content observed through the interferometer did not collapse into a single mode. Instead a forest of peaks separated by ~280MHz and extending further than the free spectral range of the interferometer (2GHz) was observed (see Figure 83(c) and (d)).

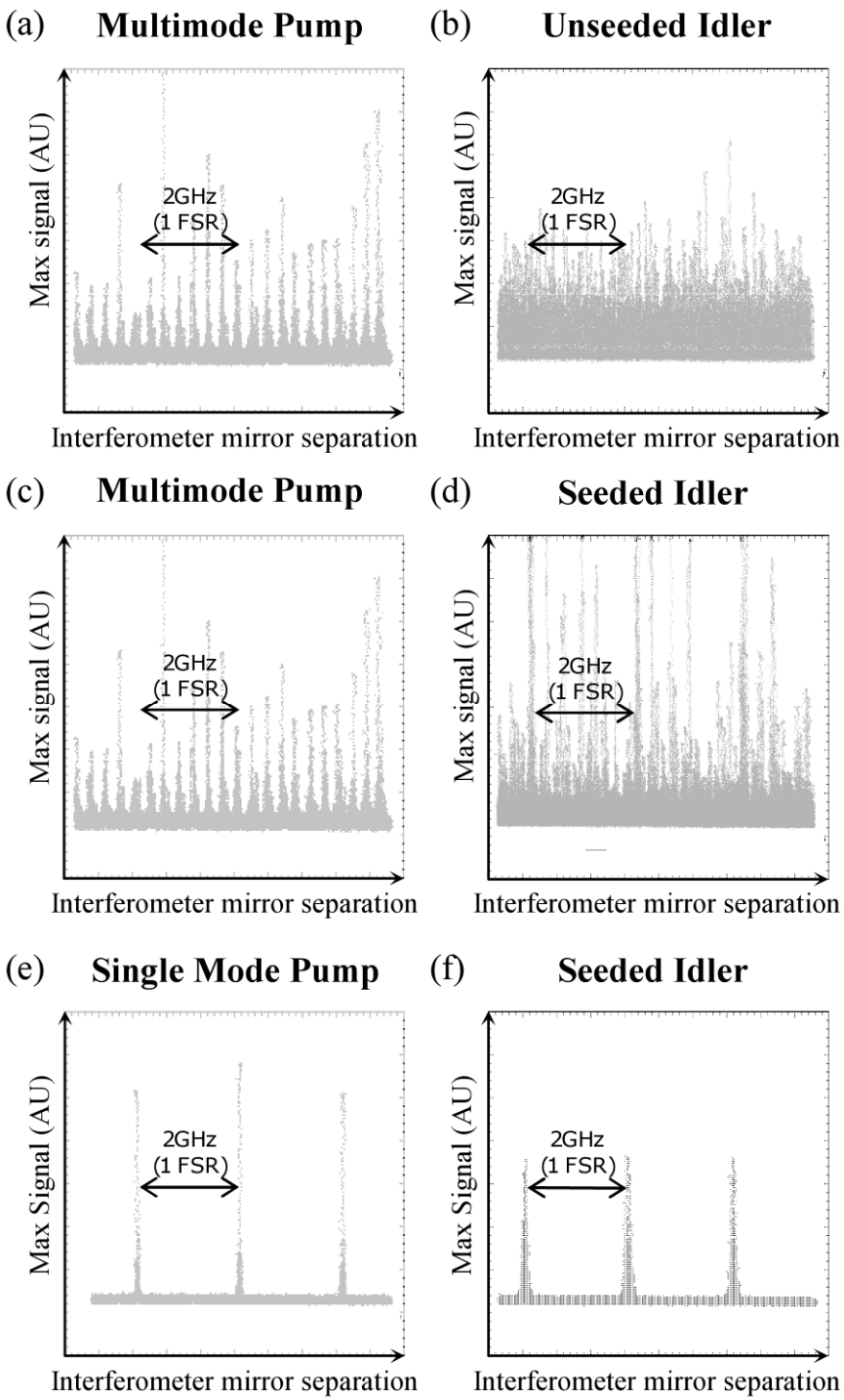

Figure 83 A series of confocal interferometer scans of pump and idler waves showing the spectral development from the unseeded device where the idler spectrum is wider than the free spectral range of the interferometer (a) and (b), through injection seeding the source when operating with a multimode pump where sidebands on the idler are evident and match the mode spacing in the pump (c) and (d), and down to single longitudinal mode operation of the pump and idler (and therefore terahertz) waves where the generated terahertz radiation must also be single frequency (e) and (f). The sidebands induced on the idler are clearly visible in (d), and it can be seen that the frequency separation matches those of the multimode pump in (c).

This frequency separation did not match the free spectral range of the idler cavity (500MHz), showing that it was not due to the beating of multiple idler cavity modes. However, the free spectral range of the pump laser cavity was ~280MHz, and the multimode nature of the pump radiation was confirmed upon measurement with the confocal interferometer. Observing the temporal behaviour of the pump laser pulses also showed deep modulation of the pulse envelope at this frequency, brought about via mode beating (see Figure 84).

The following physical mechanism is proposed for the multimode behaviour of the injection seeded idler wave: mode beating in the pump wave causes a temporally varying nonlinear gain in the lithium niobate crystal, which then imposes amplitude modulation on the growing idler wave thereby introducing sidebands. These sidebands would similarly be present in the terahertz output. We conclude that single-frequency operation of the pump laser is required, not only for the obvious reason that this is required in order to obtain single frequency operation in the non-resonant THz wave, but also to eliminate the sidebands induced on the injection-seeded idler wave. In the present case single frequency oscillation of the pump wave was attained via a prelasing technique described in the next section. Measurement with the confocal interferometer now confirmed operation of the pump laser on a single longitudinal mode with an associated linewidth of 70±10MHz (as measured using the confocal interferometer). The effect on the idler was that it, too, collapsed into single-mode operation with a linewidth of 130±10MHz (see Figure 83 (e) and (f)). Now that both pump and idler waves are single frequency (single longitudinal mode), it may be inferred that the THz radiation generated will also be single frequency to the same order as the pump and idler waves, as required. The terahertz spectroscopy described later in this chapter confirmed that this was indeed the case.

4.2.7. Prelasing

As the line narrowing effect of the etalons increases with an increasing number of passes of the optical beam it would be advantageous to run the laser CW or long pulse, however, the high peak powers delivered by Q-Switching are required to bring the device above operation threshold. Fortunately there exists a slightly modified electro-optical Q-Switching technique with which a compromise can be obtained [18]. The principle is that the Q-Switch is partially open before the main Q-Switch is

triggered. This initially highly lossy cavity allows a weak laser field (albeit many orders of magnitude larger than the noise power level) to build up over timescales much longer than the Q-Switched pulse build up and duration, and so experience a much greater line narrowing effect. Then when the Q-Switch opens fully the laser pulse grows from this narrow "prelasing" field taking on its spectral characteristics, rather than building from random noise photons.

The laser system employed for this device uses an electro-optic Q-Switch where the cavity Q is held low by a polariser combined with a quarter wave plate (the operation of a Pockels cell cancels out the quarter wave plate for high Q operation), and the system described was realized by slightly adjusting the quarter wave plate slightly off the maximum extinction condition until mode beating was removed from the laser pulse. The onset of a shorter laser pulse build up time was also a good indication that prelasing was taking place. Both of these effects are illustrated in Figure 84. The Pockels cell switching voltage could be adjusted to compensate for the slightly different birefringence compensation required to go to high Q, although this was found to be unnecessary.

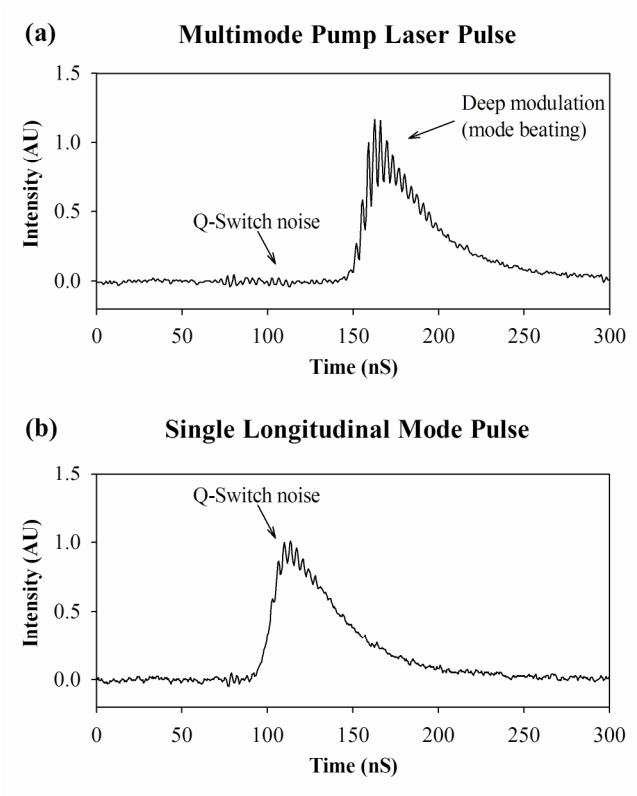

Figure 84 A comparison of multi- and single longitudinal mode pump pulse temporal profiles. (a) Deep modulation of the pump pulse is observed due to mode beating of multiple longitudinal modes of the laser cavity. (b) This modulation is removed when single-mode operation is induced via prelasing and a swifter build up time is also evident. The residual noise on the signal is caused by the Q-Switching electronics.

An Angstrom WS-7 wavemeter was then used to characterise the pump wave frequency and linewidth. Without prelasing the bandwidth was measured to be ~1.7GHz (ranging from 1.3 to 2GHz on a pulse to pulse basis), narrowing to <100MHz (below the resolution limit of the wavemeter) with prelasing. A new problem was observed when logging the pump frequency modulation over several seconds - a ~500MHz modulation in the laser frequency was present with a period of ~13s. This was found to be caused by the temperature control of the Nd:YAG crystal, as is highlighted by Figure 85, which shows the impact of disabling it.

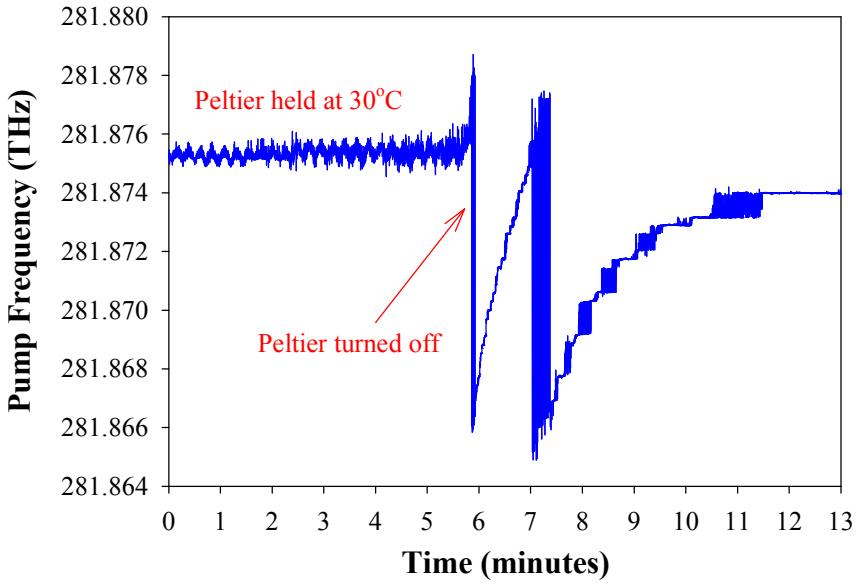

Figure 85 Response of laser frequency to temperature control. In the left of the plot the laser frequency can be seen to oscillate due to the feedback loop of the temperature controller. At around 6 minutes the temperature controller was turned off resulting in large fluctuations. Finally the system approached a steady state.

The fluctuation in actual temperature was measured to be less than a tenth of one degree (which was the limit of the precision of the temperature probe readout). It was possible to induce reasonably stable single mode operation for minutes at a time (see Figure 86) by allowing the system to run for a few minutes to reach equilibrium, and then slightly tweaking the laser cavity length via the piezo control on mirror M2 to stop cavity-mode hopping.

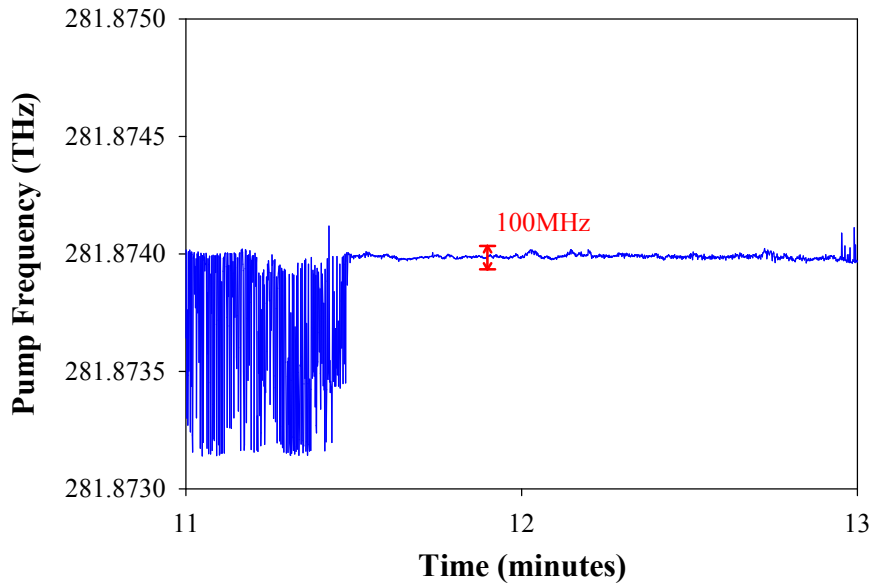

Figure 86 Stable single mode operation of the laser. Fluctuations at a level of <20MHz remained.

4.2.8. Downconversion Efficiency

Seeding the idler wave had a beneficial effect on downconversion efficiency of the TOPO. The system exhibited 50% pump depletion in the absence injection seeding – already an improvement on reported depletions for extra-cavity terahertz OPGs[13]. After injection seeding with 60mW the situation improved further with 68% downconversion observed (idler cavity on resonance with seed, 60% with cavity off resonance). Temporal profiles of the pump pulse exhibiting these efficient depletions are shown in Figure 87.

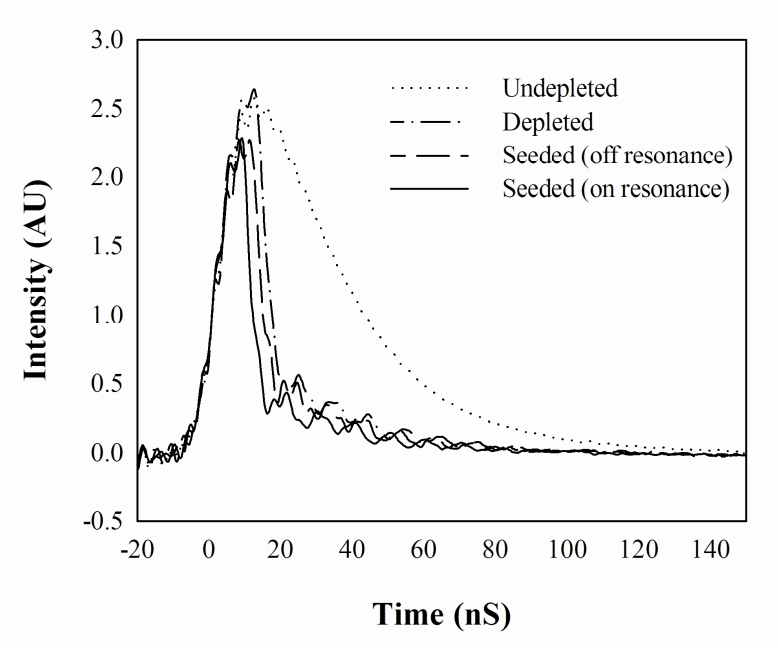

Figure 87 Temporal profiles of the pump pulse under different operating conditions. The difference in area under the curve from undepleted (OPO cavity blocked) to depleted (OPO operational but no seeding) is 50%. The profiles also exhibit a close to optimal temporal profile, with the circulating energy close to its peak before being cavity dumped into the idler and terahertz waves. Also shown are the effects of seeding with idler cavity off and on resonance, increasing the downconversion even further to 60% and 68%, respectively.

4.2.9. Seed Power Required

As previously mentioned the drive current of the seed laser influences the refractive index of the semiconductor gain medium, and so influenced the frequency of the seed laser, having the effect of limiting our choice of drive current and therefore seed laser power. A variable attenuator wheel was therefore included in the system to allow for the investigation of the effect of seed power on idler linewidth. Single mode idler pulses were observed with as little as 0.16mW of seed light (see Figure 88); however, a few tens of milliwatts were typically used to enhance the signal available to the Pound–Drever–Hall locking system.

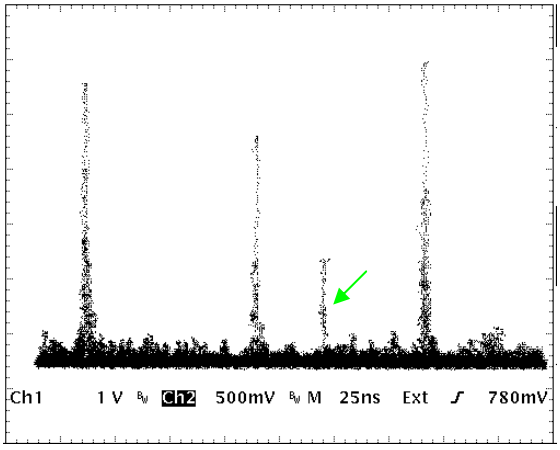

Figure 88 Confocal interferometer scan of the idler pulses produced with only 160μW of seed. The green arrow highlights a spurious transmission peak caused by a non single frequency idler pulse. This indicates that the idler wave was on the verge of consistent injection seeding.

4.2.10. Gain at threshold

Using the theory set out in Chapter 2 the threshold pumping condition can be analysed. The peak intracavity intensity of the pump pulse at threshold was ~24MWcm^{-2} (calculated from the beam diameter of 0.9mm, pulse energy of 0.13mJ, 2% output coupling, and pulse width of ~40nS), and knowing the complementary wavelengths of idler and terahertz waves to be 1070.7nm and 200μm then equation (2.24):

$$\Gamma^2 = \frac{8\pi^2 d_{eff}^2 I_p}{c\varepsilon_0 n_p n_i n_T \lambda_i \lambda_T} \tag{4.2}$$

Estimates that $\Gamma = 1.5\text{cm}^{-1}$

The gain required for the system to reach threshold can also be calculated using equation (2.28):

$$\left(\cosh^{(2N)}\left(\Gamma l_{eff}\right)\right)^M = 10^{14} \tag{4.3}$$

Where M the number of round trips is

$$\frac{t_{pulsewidth}}{t_{roundtrip}} = \frac{40\times10^{-9}\,\text{ns}}{2\times10^{-9}\,\text{ns}} = 20\,,$$

l_{eaf} the effective interaction length is

$$\frac{beamwidth}{\tan(\theta_{walkoff})} = \frac{0.9mm}{\tan 65^{\circ}} = 0.42mm$$

giving N to be

$$\frac{l_{crystal} \times 2}{l_{eff}} = \frac{70mm \times 2}{0.42mm} = 333$$

gain segments (two passes per round trip). This gives a figure for the required gain of $\Gamma = 1.7\text{cm}^{-1}$ which is close to that predicted.

4.2.11. Tuning and Spectroscopy

At a fixed intersection angle between the pump and idler cavity axes effective seeding over several gigahertz around the line centre was found to be possible, without the need for the cavity or crystal angle tuning but ensuring that the idler cavity was held on resonance with the seed wave, with no loss in terahertz output power. The effect of locking the idler cavity is shown clearly in Figure 89 with modulation at 500MHz (the idler cavity free spectral range). The DL100 ECDL driver could be set to apply an automatic saw-tooth frequency modulation to the seed wave (automatically adjusting the feedback grating angle and drive current synchronously), which provided a way to automatically tune the terahertz output and so perform spectroscopy. A scan of ~1.3GHz is shown in Figure 90, and shows that the terahertz power changed little over this range. Tuning over a range greater than this might be accomplished by implementing a scheme similar to that reported in [13].

Using this automatic tuning a series of spectra of carbon monoxide gas at reduced pressures were recorded in order to obtain an estimate of the terahertz linewidth directly. The methodology was identical to that outlined in section 4.1.7, except that instead of logging individual idler pulses with the wavemeter, a portion of the ramping seed wave was monitored. Therefore, rather than recording single pulse energies and then applying a binning function a boxcar integrator was used to average the energies over 32 pulses. Typical scans are shown in Figure 89 and Figure 90.

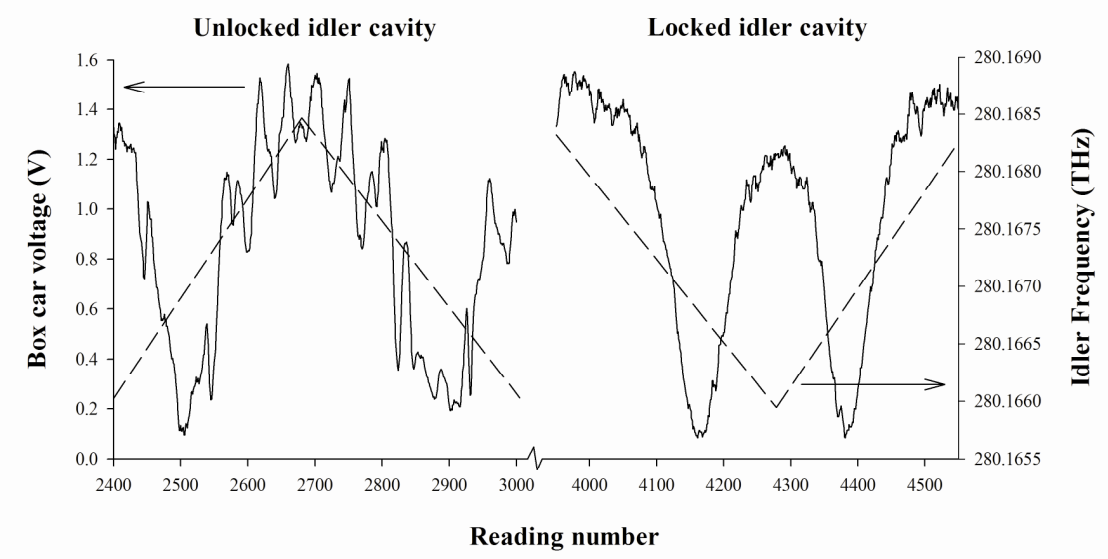

Figure 89 Graph illustrating the effect of locking the idler cavity to the seed frequency while tuning over the 1.4969THz absorption line at 80mbar. The dashed line shows the seed frequency as measured by wavemeter and the solid line the THz energy recorded by composite silicon bolometer. Note there are also discontinuities caused by mode hops of the pump laser in the unlocked data.

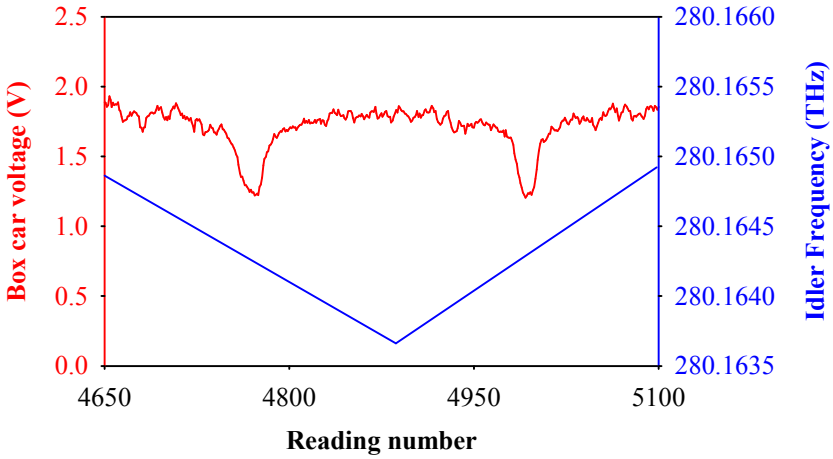

Figure 90 Plot showing the terahertz signal transmitted through a 30cm cell containing carbon monoxide at 5mbar as the seed wave is tuned. The absorption line shown is the 1.4969THz rotational transition. The consistency of the terahertz power can be seen.

Figure 91 shows the absorption profile of the transition recorded at 5mbar pressure, plotted on a logarithmic scale to allow extraction of the linewidth. The ratio of I/I_0 was found by fitting a horizontal baseline to the data in Figure 90. At this lowest attempted pressure of 5mbar (the lowest pressure our instrumentation will reliably allow us to reach) the absorption width falls to only 108 ± 10MHz. Since this result is

the convolution of the known absorption linewidth of the gas (~9MHz FWHM) with the source linewidth, an estimate of the source linewidth can be made. Assuming the source to have a Gaussian profile and the gas absorption a Lorentzian profile, the empirical expression found by Olivero and Longbotham [19] relating the FWHM linewidths of these to that of their convolution can be applied, resulting in a source linewidth estimate of ~98MHz. This is at the lower end of the 44 to 440MHz range of limits for 10 to 1ns pulses (respectively), but as no detector was available that could resolve the pulses temporally the achievement of a transform limited linewidth can only be estimated.

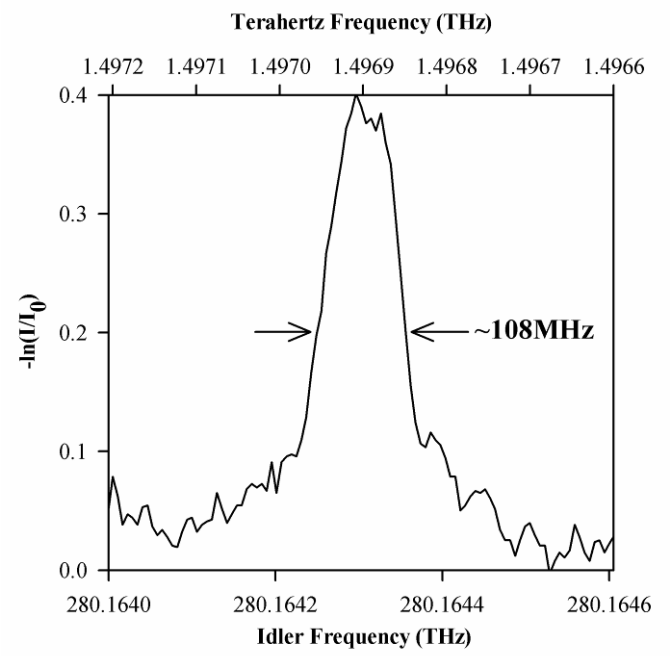

Figure 91 Plot showing the experimental scan of the 1.4969THz carbon monoxide absorption line recorded at 5mBar. The terahertz frequency scale is referenced to the absorption line frequency of 1.4969THz, the relative frequency being directly obtained from the idler frequency.

4.2.12. Discussion

We have demonstrated a terahertz source with a close-to transform limited linewidth that is continuously tunable over several gigahertz anywhere from 1 to 3THz. This was achieved while retaining the improvements in downconversion efficiency and extracted power associated with the intracavity technique, hence resulting in a very high precision spectroscopic tool. The continuous tuning range could also be readily extended to hundreds of GHz by using a widely tunable seed diode laser in combination with controlled alteration of the intersection angle between the optical

axes of the pump wave and idler wave cavities. Successful linewidth control was observed with only 160μW of seed power, which is an additional improvement on extracavity methods where seed lasers of up to 250mW are necessary to produce significant downconversion efficiency [5]. The parametric oscillator design was also found to be superior to that of a parametric generator, differing from the findings for extracavity devices. Indeed, generator schemes were not found to produce significant downconversion, even when seeded. This may be attributable to the roughly 100 times higher seed powers used for extracavity seeding, and that in an intracavity system the nonlinear crystal aperture must not clip the laser or idler cavity modes else a significant reduction in power is experienced, which may not be as evident in the externally pumped devices. The latter also means that the functioning device automatically prevents infrared light from impinging on the silicon prism array used for output coupling, thereby limiting the production of free carriers in the silicon, which strongly attenuate at THz frequencies, thereby significantly reducing power output. This may explain the order of magnitude greater THz pulse energies extracted from intracavity devices compared to external cavity devices.

The importance of the spectral quality of the pump laser was also highlighted in this experiment. Strong mode beating of the pump laser induced sidebands on the seeded idler wave as well as in the THz output. In the context of narrow linewidth extracavity OPOs, it is often the case that only one of the downconverted frequencies is of interest, and in these circumstances devices have been reported that forgo the use of a single-frequency pump laser by seeding the frequency of interest, with the other downconverted wave taking up the multimode "slack." For anyone intending to build such a device, particularly intracavity in nature, our work has clearly demonstrated that this shortcut may not be successful.

4.3. Conclusions

In this chapter two methods of narrowing the terahertz wave output of the intracavity terahertz OPO have been described. The etalon technique was both very successful and quite simple to implement requiring minimal redesign of the system. The single pulse measurements of the idler wave produced in this system were recorded to have very narrow linewidths, indicating that further investigation should be performed to optimise the characteristics of the intracavity etalons used. This may, in conjunction

with prelasing/injection seeding of the pump laser, also yield close to transform limited pulses. This work is being carried out, at the time of writing, by a new PhD student in the research group.

The injection seeding also proved successful in producing narrow linewidth pulses, approaching the transform limit of what was possible, albeit with a significant increase in complexity. The impact of laser mode beating on the spectral content of the seeded downconverted wave was a significant new discovery, having implications in all seeded, intracavity pulsed OPOs.

4.4. References

1. S. Brosnan, and R. Byer, "Optical parametric oscillator threshold and linewidth studies," Quantum Electronics, IEEE Journal of **15**, 415-431 (1979).

2. D. J. M. Stothard, T. J. Edwards, D. Walsh, C. L. Thomson, C. F. Rae, M. H. Dunn, and P. G. Browne, "Line-narrowed, compact, and coherent source of widely tunable terahertz radiation," Applied Physics Letters **92**, 141105 (2008).

3. D. Walsh, D. J. M. Stothard, T. J. Edwards, P. G. Browne, C. F. Rae, and M. H. Dunn, "Injection-seeded intracavity terahertz optical parametric oscillator," J. Opt. Soc. Am. B **26**, 1196-1202 (2009).

4. W. Demtröder, *Laser Spectroscopy: Basic Concepts and Instrumentation* (Springer, Berlin, 2003).

5. K. Kawase, J.-i. Shikata, K. Imai, and H. Ito, "Transform-limited, narrow-linewidth, terahertz-wave parametric generator," Applied Physics Letters **78**, 2819-2821 (2001).

6. L. S. Rothman, I. E. Gordon, A. Barbe, D. C. Benner, P. F. Bernath, M. Birk, V. Boudon, L. R. Brown, A. Campargue, J. P. Champion, K. Chance, L. H. Coudert, V. Dana, V. M. Devi, S. Fally, J. M. Flaud, R. R. Gamache, A. Goldman, D. Jacquemart, I. Kleiner, N. Lacome, W. J. Lafferty, J. Y. Mandin, S. T. Massie, S. N. Mikhailenko, C. E. Miller, N. Moazzen-Ahmadi, O. V. Naumenko, A. V. Nikitin, J. Orphal, V. I. Perevalov, A. Perrin, A. Predoi-Cross, C. P. Rinsland, M. Rotger, M. Simecková, M. A. H. Smith, K. Sung, S. A. Tashkun, J. Tennyson, R. A. Toth, A. C. Vandaele, and J. Vander Auwera, "The HITRAN 2008 molecular spectroscopic

database," Journal of Quantitative Spectroscopy and Radiative Transfer **110**, 533-572 (2009).

7. K. Kawase, H. Minamide, K. Imai, J.-i. Shikata, and H. Ito, "Injection-seeded terahertz-wave parametric generator with wide tunability," Applied Physics Letters **80**, 195-197 (2002).

8. R. W. P. Drever, J. L. Hall, F. V. Kowalski, J. Hough, G. M. Ford, A. J. Munley, and H. Ward, "Laser phase and frequency stabilization using an optical resonator," Applied Physics B: Lasers and Optics **31**, 97-105 (1983).

9. I. Lindsay, D. Stothard, C. Rae, and M. Dunn, "Continuous-wave, pump-enhanced optical parametric oscillator based on periodically-poled $RbTiOAsO_4$," Opt. Express **11**, 134-140 (2003).

10. M. Fleming, and A. Mooradian, "Spectral characteristics of external-cavity controlled semiconductor lasers," Quantum Electronics, IEEE Journal of **17**, 44-59 (1981).

11. K. Liu, and M. G. Littman, "Novel geometry for single-mode scanning of tunable lasers," Opt. Lett. **6**, 117-118 (1981).

12. C. J. Hawthorn, K. P. Weber, and R. E. Scholten, "Littrow configuration tunable external cavity diode laser with fixed direction output beam," Review of Scientific Instruments **72**, 4477-4479 (2001).

13. K. Imai, K. Kawase, H. Minamide, and H. Ito, "Achromatically injection-seeded terahertz-wave parametric generator," Opt. Lett. **27**, 2173-2175 (2002).

14. K. Imai, K. Kawase, J.-i. Shikata, H. Minamide, and H. Ito, "Injection-seeded terahertz-wave parametric oscillator," Applied Physics Letters **78**, 1026-1028 (2001).

15. K. Kawase, J.-i. Shikata, and H. Ito, "Terahertz wave parametric source," Journal of Physics D: Applied Physics, R1 (2002).

16. R. Guo, K. Akiyama, H. Minamide, and H. Ito, "Frequency-agile terahertz-wave spectrometer for high-resolution gas sensing," Applied Physics Letters **90**, 121127-121123 (2007).

17. Y. He, and B. J. Orr, "Tunable Single-Mode Operation of a Pulsed Optical Parametric Oscillator Pumped by a Multimode Laser," Appl. Opt. **40**, 4836-4848 (2001).

18. D. C. Hanna, B. Luther-Davies, H. N. Rutt, and R. C. Smith, "A two-step Q-switching technique for producing high power in a single longitudinal mode," Optical and Quantum Electronics **3**, 163-169 (1971).

19. J. J. Olivero, and R. L. Longbothum, "Empirical fits to the Voigt line width: A brief review," Journal of Quantitative Spectroscopy and Radiative Transfer **17**, 233-236 (1977).

Chapter 5. Quasi Phasematching and the Intracavity Terahertz OPO

5.1. Introduction

In this chapter the application of quasi phasematching techniques to intracavity terahertz OPOs is reported and discussed. The research was originally funded under an (Engineering and Physical Sciences Research Council) EPSRC grant "Generation of Terahertz Radiation by optical Parametric Oscillators" Ref: EP/C509919/1 and it was during this period that the initial experiments were based on designs where the terahertz wave was phasematched to propagate orthogonally to the pump. The problem of the grating bidirectionality, and therefore dual solutions, was recognised and the concept of using an orthogonally poled crystal that generated terahertz waves that could be output coupled using silicon prisms was reported to the EPSRC in the final project report in March 2007. The concept had also been presented at the New Trends in Terahertz Imaging (NTTI) summer school, Paris in the summer of 2007 (and again in summer 2009). Note that this is over 2 years prior to the publication of Molter et al (13th April 2009)[1] that reports a "Nanosecond terahertz optical parametric oscillator with a novel quasi phase matching scheme in lithium niobate" using an orthogonally poled grating vector, and so the work here was indeed original and pioneering. This is also backed up by a granted patent application covering quasi phasematching schemes dating back to 2005[2]. Publication of our work was delayed due to experimental difficulties in bringing the device above threshold without reaching intensity levels that induced crystal damage. Successful terahertz measurement was achieved, however, in May of 2009 with a redesign of the laser cavity (although significant pump depletion was still out of reach). Additionally the orthogonal grating design was realised to not actually be optimal for generating terahertz waves in this manner, the reasons for which are discussed later in this chapter. The work presented here has been published in Optics Express [3].

5.2. Issues with Non-Collinear Phasematching

All the systems discussed so far have utilised conventional phasematching techniques that rely on the refractive index of the material and propagation direction of the beams to keep the generation process in phase. This is a versatile advantageous solution in

the context of terahertz OPOs based on lithium niobate as it allows both easy extraction of the terahertz radiation from the edge of the nonlinear crystal avoiding strong absorption and a simple and effective tuning mechanism. At the ends of the tuning range of these systems though you are faced with two problems. At the low frequency end the idler cavity mirrors must be moved further and further from the nonlinear crystal to avoid the problem of them clipping the pump laser beam and hence inhibiting it's operation, unfortunately this has the effect of increasing the round trip time of the idler cavity (increasing the build up time of the idler and reducing the efficiency of the OPO) and there are also practical limits to the size of the idler cavity as the mirrors would soon run into cavity elements of the pump laser itself. At higher frequencies there is a different problem; as the angle between the pump and idler beams increases the idler beam soon begins to clip the near edge of the lithium niobate. To avoid this the crystal must be translated such that the beams no longer clip the edge, which results in the movement of the interaction region (where the terahertz is generated) further from the edge of the crystal. As previously mentioned the nonlinear process in lithium niobate at terahertz frequencies is enhanced by a polariton resonance, however, this polariton resonance effects a significant absorption, and becomes a problem when the generated terahertz has to propagate through the crystal to be extracted. Another issue at this end of the tuning range is that the higher angle between the beams reduces the overlap (generation) area and so may bring up the threshold and reduce power output. Fortunately there is a way these two problems might be circumvented and that is by using a quasi phasematching technique to collinearise the waves. This is the subject of this chapter.

5.3. Quasi Phasematching

When traditional phasematching techniques are used and you move away from the correctly phasematched condition the efficiency of generation falls away rapidly as a function of $\mathrm{sinc}^2(\Delta k\, l/2)$ (where Δk is the phase mismatch and l the crystal length). This is because as waves propagate through the crystal new radiation is added that cycles in and out of phase with the already present radiation, and hence cycles through constructive and destructive interference regions. The interaction is constructive until the generation process goes π out of phase, if at this point we could reset the phase difference to nothing we would then get another increase in field intensity, rather than

deconstructive interference. Looking at the coupled wave equations as defined in Chapter 2

$$\begin{aligned}\frac{dE_T}{dz} &= i\frac{\omega_T \chi_{eff}^2}{2n_T c}E_p E_i^* e^{i\Delta kz} \\ \frac{dE_i}{dz} &= i\frac{\omega_i \chi_{eff}^2}{2n_i c}E_p E_T^* e^{i\Delta kz} \\ \frac{dE_p}{dz} &= i\frac{\omega_p \chi_{eff}^2}{2n_p c}E_T E_i e^{i\Delta kz}\end{aligned} \tag{5.1}$$

we can see this is represented by adding π to the phase after each coherence length, which is equivalent to multiplying by -1 ($e^{i(\Delta kz+\pi)} = e^{i\Delta kz}e^{i\pi} = -1\times e^{i\Delta kz}$) and can be achieved by changing the sign of the nonlinear coefficient. This might be achieved by slicing the crystal up into slabs inverting every other section, but in the ferroelectric crystal lithium niobate this can be achieved by applying a periodic large electric field to permanently reverse the crystal structure. This periodically poled lithium niobate has been widely exploited in the field of optical parametric oscillators[4-7] and in nonlinear optics more generally.

In the case of terahertz generation this allows the design of custom phasematching conditions where pump and idler are collinear, whilst the terahertz wave is still produced at an angle that rapidly escapes the side of the crystal - necessary for efficient terahertz extraction. There have been several demonstrations of this type of phasematching in terahertz production via difference frequency generation using two laser sources, including both CW and pulsed techniques[8-11]. These systems, however, are inconvenient in that two sources are required, one of which must be tunable for a tunable terahertz source, and which must be properly overlapped in the nonlinear medium. Furthermore, if resonant cavities are desired to reduce thresholds and boost efficiencies then this leads to great difficulty, as in the CW case the cavity must be held on resonance for both frequencies simultaneously (the optical frequencies of the two lasers are so close that suitable dichroic mirrors are not readily available), or in the pulsed case the pulse repetition rate of both sources must be matched. Recently an extracavity, pump enhanced injection seeded OPO has been reported using this phasematching technique[1]. This system was also rather complex, consisting of an injection seeded Q-Switched Nd laser, a second tunable seed laser for the idler wave, and an enhancement cavity with active frequency

locking. This paper describes a degenerate quasi phasematching design which allowed the terahertz to be extracted, but fails to explain that indeed a close to degenerate design must be used in order to overcome a fundamental restriction of this technique in the context of a Terahertz OPO. A description of this restriction and a potential further improvement to the technique will now follow.

5.4. Orthogonal Generation Design

The phasematching condition can be represented in terms of k vectors as follows:

$$\mathbf{k}_p - \mathbf{k}_i - \mathbf{k}_T - \mathbf{\Lambda} = \mathbf{\Delta k} \tag{5.2}$$

Where $\mathbf{k}_p, \mathbf{k}_i$ and $\mathbf{k}_T$ are the pump, idler and terahertz wave vectors respectively and $\mathbf{\Lambda}$ is the additional grating vector component. When phasematching is satisfied the phase mismatch, $\mathbf{\Delta k}$, is zero. Initially it was thought that due to the large terahertz absorption losses it would be beneficial to have the terahertz wave traverse as little of the crystal as possible, which is accomplished by having the wave produced orthogonally to the pump. The design required for collinear propagation of pump and idler waves is illustrated in Figure 92.

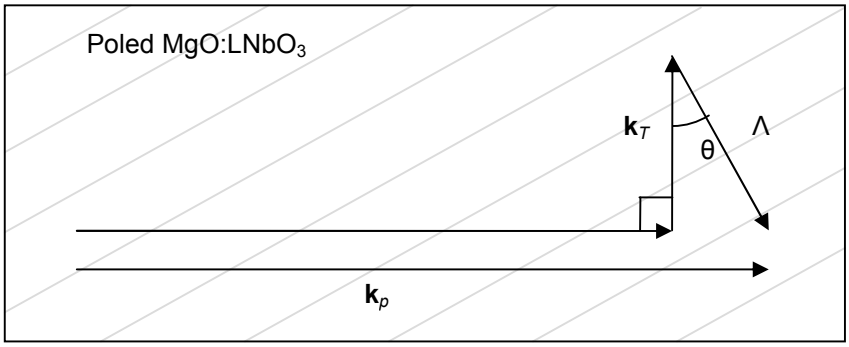

Figure 92 diagram illustrating the phasematching condition required for orthogonal terahertz generation. Wave vectors are not drawn to scale for clarity.

To calculate the crystal poling period and angle required to satisfy the design in Figure 92 knowledge of a few parameters is required. Firstly the desired terahertz frequency must be chosen, which then allows the calculation of the idler wave from the conservation of energy. Then the magnitude of the k vectors can be found using the refractive indices from:

$$|\mathbf{k}_x| = \frac{2\pi n_x}{\lambda_x} \tag{5.3}$$

Where $\mathbf{k}_x$, n_x and λ_x are the k vector, refractive index and wavelength at the frequency denoted by x (pump, idler or terahertz). It is then a simple matter to calculate the magnitude and angle of the grating vector, $\mathbf{\Lambda}$. Using Pythagoras we have:

$$|\mathbf{\Lambda}| = \frac{2\pi}{G} = \sqrt{|\mathbf{k}_p - \mathbf{k}_i|^2 + |\mathbf{k}_T|^2} \tag{5.4}$$

Where G is the grating period. Then using trigonometry we obtain:

$$\theta = \tan^{-1}\left(\frac{|\mathbf{k}_p - \mathbf{k}_i|}{|\mathbf{k}_T|}\right) \tag{5.5}$$

For the poling angle, θ.

There is a significant problem with the design arrived at in this way however, in that the grating vector does not have any inherent direction; as a k vector it can contribute in either direction as illustrated in Figure 93.

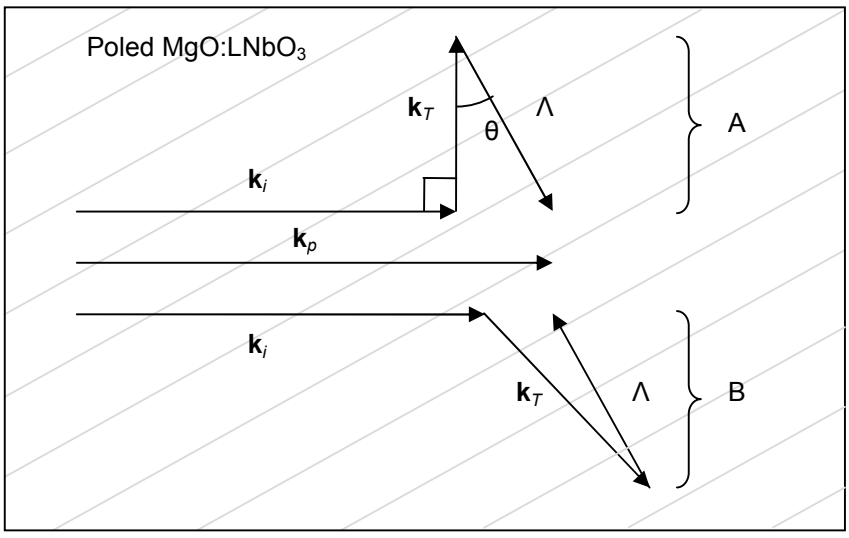

Figure 93 diagram depicting the two possible phasematching solutions, A and B, due to the inherent bidirectionality of the grating vector. K vectors are not to scale for clarity – in reality $\mathbf{k}_T$ and $\mathbf{\Lambda}$ are around 100 times smaller in magnitude than $\mathbf{k}_p$ or $\mathbf{k}_i$.

It can be seen in Figure 93 that there exists a second solution to that desired, and in this solution the terahertz wave is no longer orthogonal to the pump and idler waves. This results in a greater overlap of the three waves, leading to a higher gain for this solution. The implication is that a grating designed to give orthogonal terahertz output in a nanosecond terahertz OPO will not generally work on the orthogonal solution, as the higher gain solution will build up from noise first. Another major issue with this design is that the solution with more overlap may have difficulty escaping the MgO:$LiNbO_3$ due to total internal reflection at the crystal to air interface ($\theta_{crit} \approx 11^\circ$), or indeed the crystal to silicon interface ($\theta_{crit} \approx 41^\circ$) if an output coupling prism technique was attempted.

5.5. Solutions with Extractable Terahertz

In order to design a crystal with extractable terahertz radiation whilst maintaining collinear propagation of pump and idler waves a more comprehensive analysis of the phasematching solutions was required. A MathCAD worksheet that calculated the phasematching solutions for a given grating vector was developed for this purpose. The technique for finding solutions used here was different to that described above, in that the phase mismatch for every allowed combination of pump, idler and terahertz waves was calculated over the range of 0.6 to 3THz given a specified grating vector in order to show multiple solutions where they might exist. Essentially for a given pump and idler wavelength the left hand side of equation (5.6) was evaluated for both directions of the grating vector, and compared to the magnitude of the THz k-vector calculated using the right hand side of equation (5.6) where (λ_T) is the terahertz wavelength derived from the pump and idler wavelengths. Also the refractive index of MgO:$LiNbO_3$ as a function THz wavelength (n_T) must be known, for which the Sellmeiers described in Chapter 2 were used (our empirical fit to reported THz refractive indices and the Sellmeier of Zelmon et al for the infra red[12]).

$$\left|\mathbf{k}_p - \mathbf{k}_i \mp \mathbf{\Lambda}\right| = \frac{2\pi n_T}{\lambda_T} \tag{5.6}$$

Using these values the phase mismatch of a given grating was calculated for frequency combinations allowed by the conservation of energy. An example plot of the calculated k vector magnitudes is shown in Figure 94, where the "–grating" or

"+grating" designations refer to condition A or B respectively as defined in Figure 93. With this fit solutions can only be calculated within the range of 100µm to 500µm as no refractive index data outside this range was used. In particular this is true on the low wavelength side as the polariton resonance frequency is rapidly approaching here, which causes a significant change in refractive index.

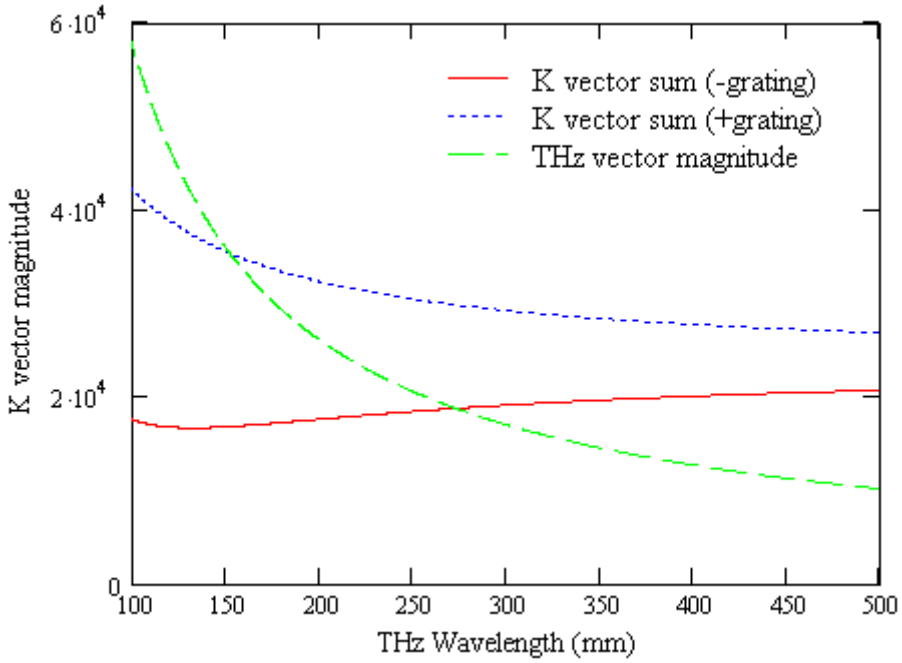

Figure 94 Plot showing the calculated k vector magnitudes for the terahertz wave and the two possible magnitudes of the sum of the other three k vectors for a grating angle of 45 degrees and period of 42.4 microns. Where the green (dashed) line crosses the red (solid) or blue (dotted) is where phasematching occurs.

In the situation shown in Figure 94 where a grating of 42.4µm period at 45° to the pump wave is examined showing that there are two solutions, producing 152µm and 273µm wavelength terahertz radiation. The angles are then simple to calculate and are 28° and 63° to the pump wave respectively.

An investigation of the effect of the grating vector angle was performed (see Figure 95) provided an interesting insight: when the angle subtended between the grating vector and the pump (/idler) vector is increased there can be a region where one or both possible solutions can be coupled out of the crystal using a technique similar to that used in the non-collinear design (that of applying an array of silicon prisms), because both solutions are within the total internal reflection angle for the interface between lithium niobate and silicon.

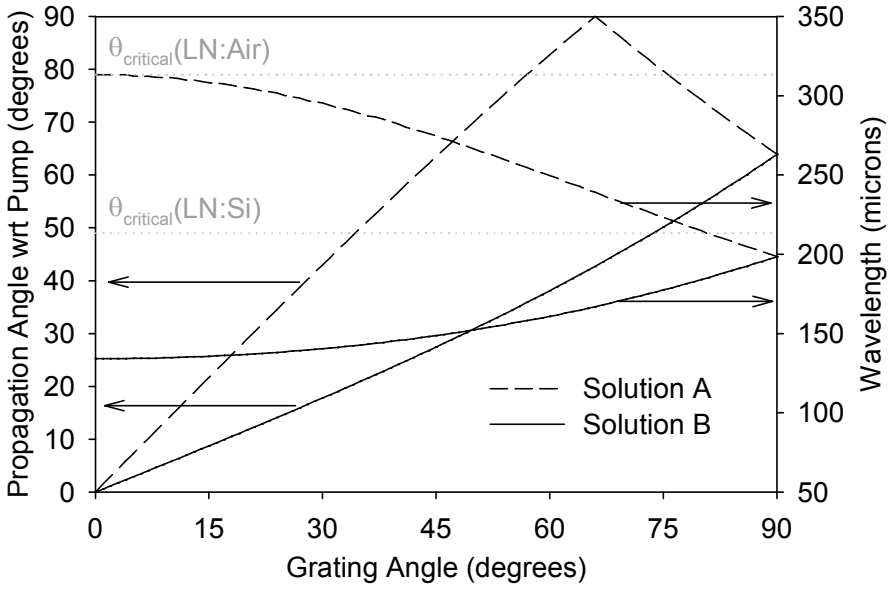

Figure 95 Plot showing the THz generation angle and wavelength for a 42.4 micron period grating at all possible grating angles. Above ~74° both solutions can be coupled into a silicon prism pressed against the surface. The critical angle is plotted as a constant (assuming a refractive index of ~5.2 in lithium niobate and 3.4 in silicon) but does in fact change very slightly with terahertz wavelength. For clarity this is omitted as it is only a small difference of only a couple of degrees.

In fact, it can be seen that if the grating vector is orthogonal to the pump vector the solutions become degenerate, ensuring that the terahertz OPO can not operate on the "wrong" solution. This is illustrated in Figure 96.

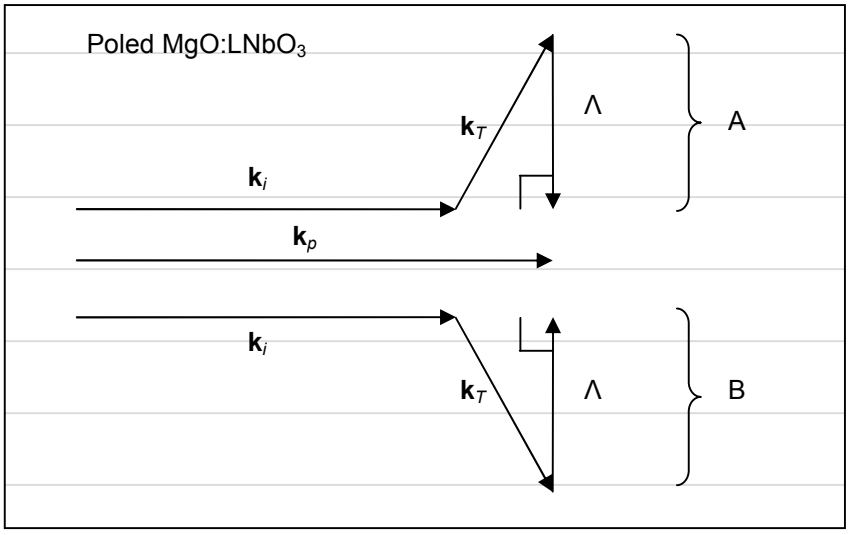

Figure 96 Diagram showing degenerate phasematching solution achieved with an orthogonal grating. Although two solutions still exist, they are mirrored about the pump axis and equivalent in terms of infrared idler and terahertz frequencies.

It should be noted however that this will result in terahertz generation into four directions (vs. two directions in the non collinear technique), reducing the terahertz radiation that might be extracted in one direction.

Realising that the orthogonal grating does not allow any uncertainty in the generated terahertz wave it is interesting to see if the geometry can be designed to produce terahertz radiation in over the same range as the non-collinear phasematched device (~100μm to ~300μm). Solutions were calculated for an orthogonal grating over the region of 0μm to 100μm periods, the results of which are shown in Figure 97.

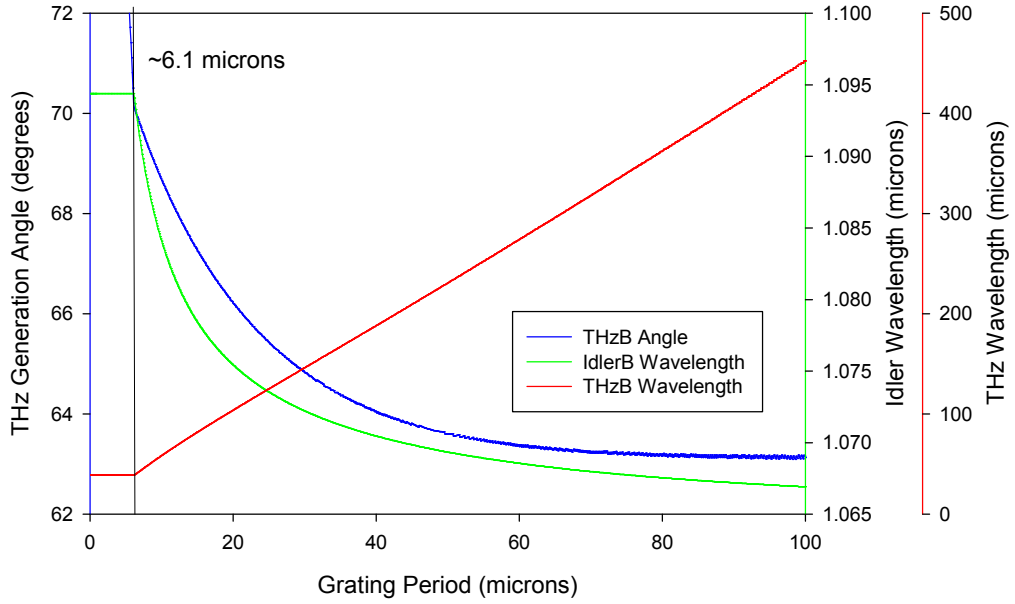

Figure 97 plot of the phasematching solutions against orthogonal grating period. Only one solution is graphed as the two solutions are equivalent. Below a period of around 6µm no solutions were found within the range of interest. It is interesting to note that the terahertz wavelength is almost linear with grating period and the generation angle does not change by more than a few degrees.

Looking at the calculated phasematched solutions suggests that the technique is capable of producing frequencies over the whole range of the non-collinear device, indeed frequencies that cannot be extracted from the non-collinear device may be accessible in this way.

5.6. Experimental Investigation

The initial experiments were conducted using crystals with gratings designed for orthogonal exit of the terahertz wave, as it was only due to the undesired operation of these crystals that the full implications of the grating vector bidirectionality was realised. Here I will present the original experiments, indicating the idler frequencies observed, and then describe more recent experiments using orthogonal grating vector designs.

5.6.1. Orthogonal Exit Designs

The first attempt at designing a custom phasematching condition was based, erroneously, on the idea of rapidly extracting the terahertz wave from the absorbing

crystal via orthogonal terahertz wave generation. The grating period was designed using the techniques above to generate 1.5THz radiation, at 90° to the pump wave, from a grating of period 35.7μm and direction of 67° to the pump wave (1070nm idler wave). The complimentary solution, taking the grating vector direction to be inverted, phasematched for 2THz at an angle of ~45° to the pump wave (1072.1nm). Due to a manufacturing error a crystal with the poling domain walls, rather than grating vector, at 67° to the pump wave was supplied and used initially, until it was understood what had happened and the correct crystal was delivered. The calculated phasematching solutions for this crystal were ~1.2THz at ~33° and 2.4THz at 14° (idlers of 1068.9nm and 1073.7nm respectively), neither solution being extractable. The crystal with the orthogonal exit design will be referred to as "crystal A", and the non-extractable solution crystal as "crystal B".

The production of periodically poled MgO:$LiNbO_3$ crystals, although yielding crystals of high optical quality and accurate poling periods, is still limited with respect to the thickness along which the poling takes place. The thickest dimension readily available from suppliers is still around 1mm, which unfortunately is not the ~3 or 4 times larger than the diameter of the intracavity laser beam of the basic laser design used previously as is required for minimal clipping losses. As a consequence it was decided to stick with the same design for the pump head and Q-Switch used in the non collinear systems and to incorporate an intracavity cylindrical telescope that reduced the vertical width of the beam. There was a trade off in the magnification factor here, as the experience gained using the non-collinear system suggested that the intracavity intensity required for OPO operation was not far below the damage threshold exhibited by the crystal coatings, so some clipping loss was tolerated in the hope that the crystal's propensity to damage was reduced. A factor of 2 was chosen as the starting point, and cylindrical lenses chosen from stock items to produce a telescope close to this ratio. The layout of this laser system is shown in Figure 98, and the intracavity mode was analysed using the in-house cavity modelling software "PSST!", an example of which is shown in Figure 99.

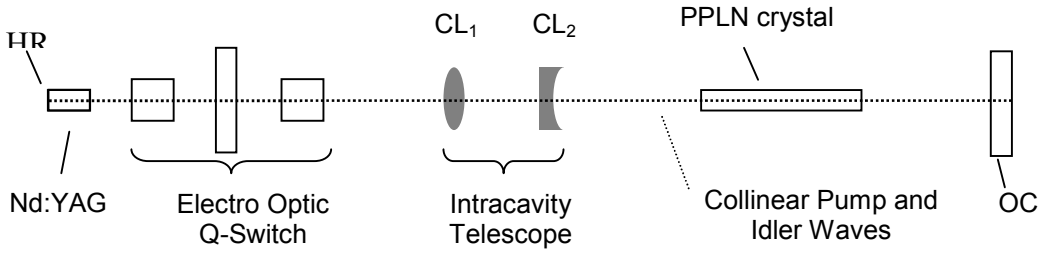

Figure 98 schematic diagram of the collinear intracavity OPO with cylindrical telescope arrangement.

The basic layout of the laser was the same as that used for the non-collinear experiments (i.e. the same laser diode model, Nd:YAG crystal, and electro optic Q-switching set up were used), the output coupler (OC) was of 90% reflectivity to more readily allow measurement of the intracavity waves (in these pulsed systems the build up time of the pulse is the dominant effect on threshold and so such a reflectivity should not have a great effect) and had a curvature of 6m. As in devices described in the previous chapters, the slight curvature of the output coupler, in conjunction with weak thermal lensing and soft aperturing by the pumped mode within the Nd:YAG crystal, produced a ~1mm diameter beam in the absence of the intracavity lens (i.e. in the horizontal plane). The optical cavity length was ~260mm, and the cylindrical lenses CL_1 and CL_2 were of focal lengths 61mm and -30.6mm respectively and set ~32mm apart as required to give a stable laser mode (see Figure 99 and Figure 100). Both lenses were antireflection coated for 1064nm. The nonlinear crystal was a 50mm x 5mm x 1mm (length x width x height) piece of periodically poled lithium niobate (PPLN) that was doped MgO at a level of 5%. As the idler wave and pump wave share the same resonant (laser) cavity the quarter wave plate used in the electro optic Q-Switch was of zero order design – if a high order waveplate was used instead the pump laser would function normally, however the phase delay would change more rapidly as the wavelength is detuned from the design wavelength, potentially causing significant losses for the idler wave.

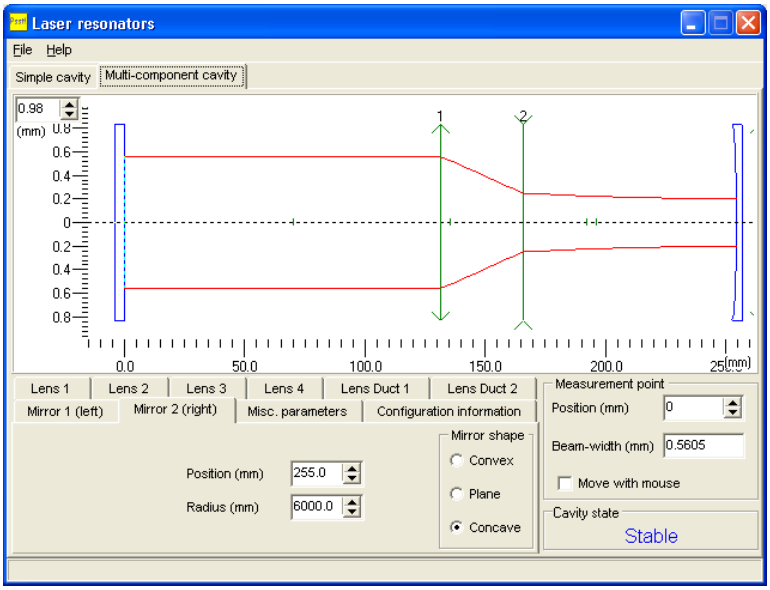

Figure 99 Simulation of the laser mode supported buy the cavity described in Figure 98. Optical components have been reduced to their effective optical lengths for simplicity. The simulation is part of the PSST! Software suit and uses the cavity matrix method to find the stable mode.

The sensitivity of the intracavity laser mode to the separation of the telescope mirrors was investigated by setting up a MathCAD worksheet that calculated the round trip cavity matrix at either end of the 50mm long PPLN crystal and solved for a stable laser mode. This was then iterated through for varying telescope lens separations. The calculated beam waists are plotted in Figure 100, which shows the relative insensitivity to precise lens positions.

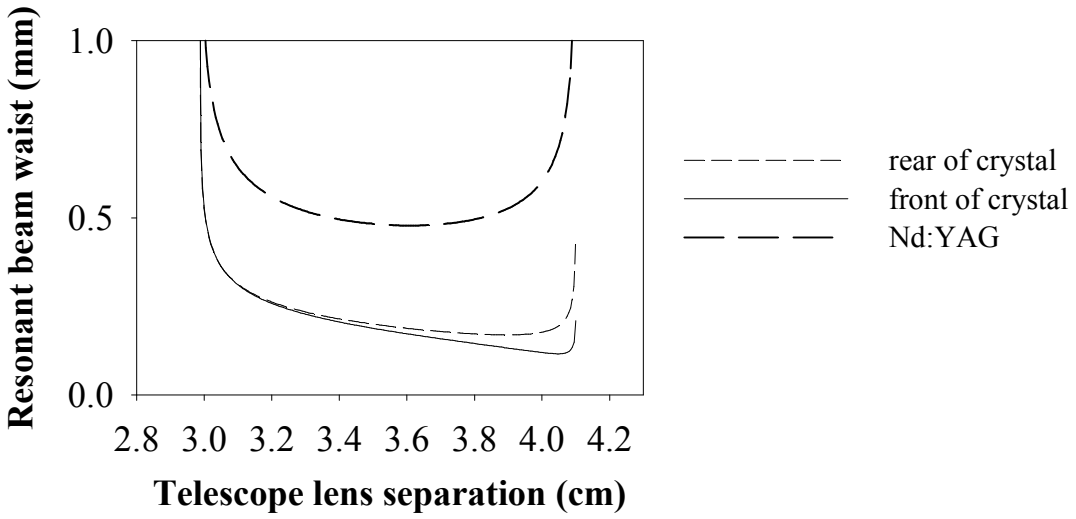

Figure 100 plot showing the resonant mode waist in the vertical plane (the plane of the action of the intracavity telescope) at either end of the poled crystal, and also at the Nd:YAG crystal. The waist at the front (near output coupler) and rear (near intracavity telescope) of the PPLN is relatively insensitive to telescope lens separation, as is the waist within the Nd:YAG.

The system was built to the above design by first setting up the laser with no intracavity lens nor PPLN crystal, and subsequently inserting the intracavity telescope such that the laser is again optimised, and then the PPLN crystal. At each stage adjustment of the cavity elements other than those being added was avoided as much as possible to maintain a constant beam axis and avoid departure from the intracavity mode designed. The telescope arrangement was mounted on a single stage with height, pitch and yaw adjustment, so that the telescope could be pre-aligned using a HeNe laser to be approximately the 2:1 ratio required and then positioned within the laser without adjusting the telescope lenses. Some adjustment of the output coupler was found necessary to compensate for the insertion of the PPLN crystal, probably due to a slight wedge in the crystal cut. An advantage of this system is that no special alignment method was required for the idler cavity in this design as the laser cavity serves this duty – operation of the laser indicates that the idler wave cavity is aligned. The realised system is shown in Figure 101.

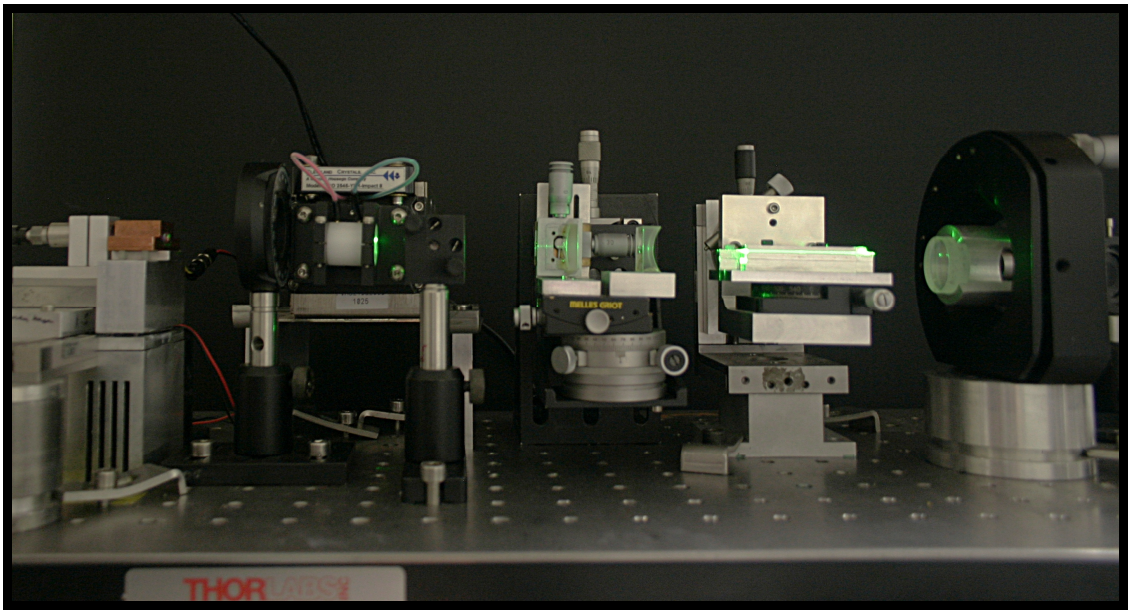

Figure 101 photograph of the running (green light due to parasitic doubling of the laser) quasi-phasematched intracavity terahertz OPO.

A series of beam profile measurements were then taken to verify that the intracavity mode was approximately that required. An example profile of the beam is shown in Figure 102 , where the ellipticity of the beam can be seen.

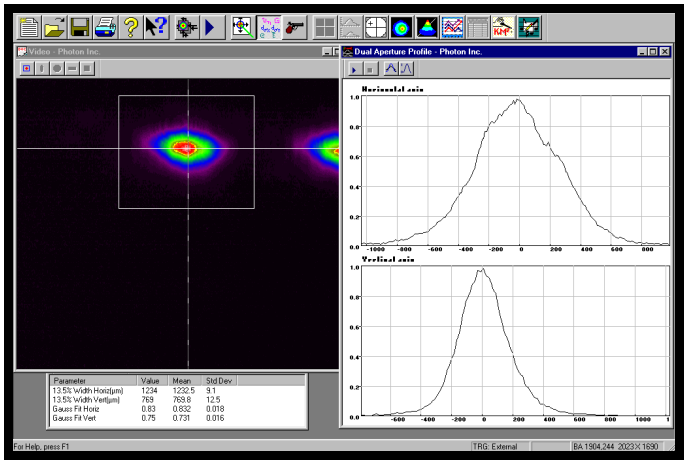

Figure 102 screen capture showing beam profile ~11cm from the output coupler as measured using a BeamPRO profiler camera and software. The second image to the right is due to back surface reflection of the glass slide used to sample the beam.

It was observed during the beam profiling that a small adjustment to either the telescope, PPLN or output coupler was all that was necessary to significantly alter the spatial mode from an elliptical shape. This alteration was always in the vertical plane and tended to produce TEM01 or TEM02 modes. It is possible that this sensitivity

could, in part, be responsible for the crystal damage issues observed when increasing the pumping levels; an increasing degree of thermal lensing in the Nd:YAG may have induced a mode change that caused hot spots to develop on the PPLN surface thereby seeding damage. An example of this mode alteration is shown in Figure 103.

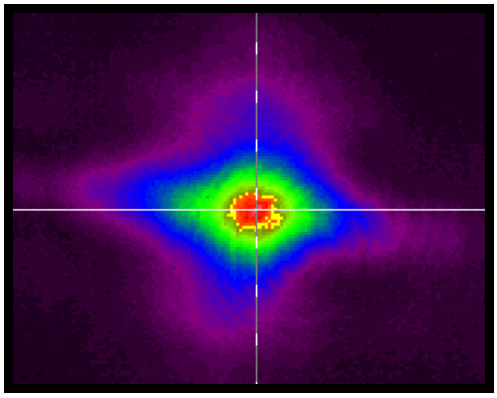

Figure 103 example beam profile with slightly out of alignment laser cavity. The beam has become star shaped, and developed a central hot spot.

The series of profiling measurements was then fitted to the standard Gaussian beam width propagation equation

$$\omega(z) = \omega_0 \sqrt{1 + M^2 \left(\frac{z\lambda}{\pi \omega_0^2} \right)^2} \tag{5.7}$$

where z is the propagation distance, ω_0 is the radius at the beam waist, λ is the wavelength of the light in question, and M^2 is the "m squared factor" – a measure of how much more the beam is diverging compared to an ideal Gaussian beam. In order to perform a fit to equation (5.7) it is necessary to assume that the beam waist lies on the output coupler, which is a reasonable assumption in the vertical plane where the mode is largely confined by the intracavity telescope, rather than the very long 6m radius of the output coupler.

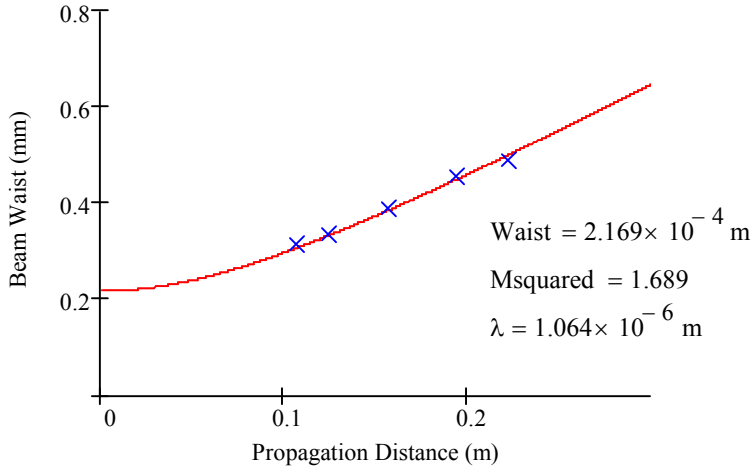

Figure 104 fit performed in MathCAD to vertical beam profiling measurements. Beam width seems to be in agreement with that designed for.

Unfortunately due to the sizes of the beam profiling camera and the mirror mount of the laser, is was not possible to take measurements any closer than ~11cm from the output coupler, which would have greatly enhanced the accuracy of the fit. Looking at the fit (Figure 104) it would seem that due to this a larger range of possible solutions could plausibly exist. However, it is clear that the waist must be within the laser or on the output coupler, meaning that at the location of the crystal (a few centimetres in from the output coupler) the beam width was around the 0.2mm to 0.25mm required.

The idler frequencies generated by both crystal geometries were measured by coupling both pump and collinear idler waves into an optical spectrum analyzer (OSA), and using the peak hold function over multiple scans. This was necessary to build up a trace as the OSA sampling was not synchronisable with the laser pulse, and the amplitude jitter of the downconversion was large. Idlers were measured for crystals A and B to be 1072.8nm and 1074.7nm (2.2THz and 2.7THz respectively), in rough agreement with the higher overlapping solutions (that cannot be extracted) predicted from the phasematching model of 1072.1nm and 1073.7nm – the discrepancy is put down to the uncertainty in the terahertz refractive index. An example trace is shown in Figure 105. Crystal A suffered significant optical surface damage before many diagnostics were performed, other than measuring the frequency of the downconverted wave, so this section will focus on crystal B. Damage to the crystals was more significant problem using the poled crystals as they only have 1mm

of vertical aperture, meaning that in a 5mm wide crystal there are only ~5 chances before the crystal is rendered useless (only 2 if terahertz extraction from the edge is required).

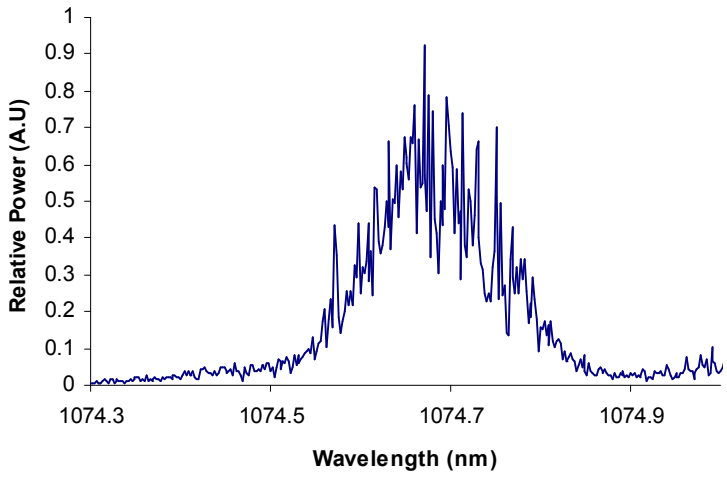

Figure 105 Example optical spectrum analyzer (OSA) trace showing the idler at 1074.7nm. The OSA was triggered at each data point from the Q-Switch trigger and the peak values from multiple runs are displayed here. The amplitude jitter of the downconversion is still evident.

Investigation of the downconversion efficiency is more difficult in this case where both pump and idler beams propagate collinearly. It was necessary to use a diffraction grating to first separate the beams spatially, after which signs of downconversion could be looked for. Upon doing this it was apparent that no significant depletion was observable in the pump temporal profile, but there were in fact some flashes of downconversion that were intermittent in nature – suggesting that the OPO was not yet above threshold.

Many attempts were made to bring the device significantly above oscillation threshold and obtain the >50% depletions observed in the non-collinear systems, such as extensive attempts at alignment optimization and increasing the laser pulse energy up to the point at which coating damage occurred, unfortunately with no success. Crystal damage was a recurring problem, occurring at laser pulse energies much lower than expected, and limited the extent of experimental investigation that could be performed as viable crystal aperture was expended. A photograph of one end of a PPLN crystal that suffered multiple damage spots is shown in Figure 106. One factor increasing oscillation threshold may have been that the extra length of the idler cavity (the laser

cavity) compared to the previous non-collinear systems increases the build up time of this wave and raised the threshold above that of the damage threshold. There were also additional losses for the idler pulse induced by the extra components within the laser cavity – even though losses were minimized via antireflection coatings and use of a zero order waveplate in the Q-Switch.

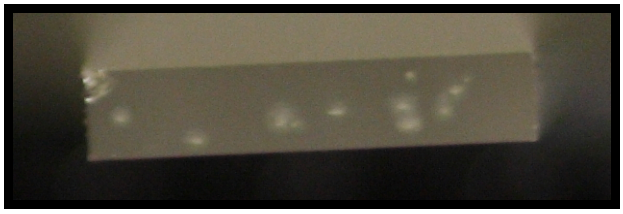

Figure 106 photograph showing the optically induced damage at one end of the PPLN crystal.

The laser energy characteristic of this design is shown in Figure 107, indicating when downconversion was observed in the form of occasional flashes. The intracavity intensity here was calculated to be ~19MW/cm^2.

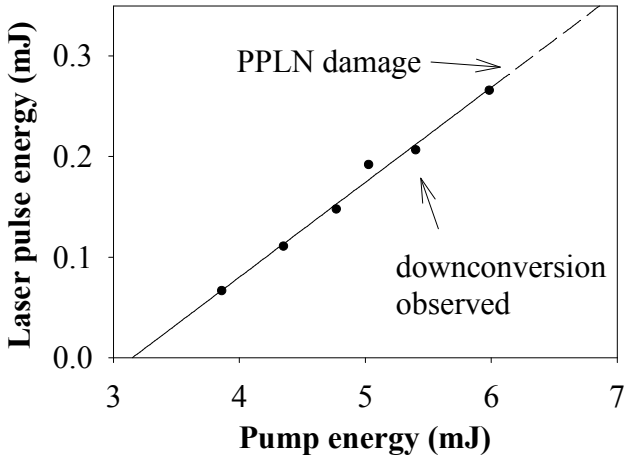

Figure 107 laser power characteristic. The low slope efficiency suggests a lossy laser resonator.

When observing the beams separated by the diffraction grating using a sensitive infrared viewer it was noticed that along with the pump and idler spots there was also a second idler spot. This second spot was much less intense as observed through the viewer, and occurred less frequently than the idler spot, but never appeared in the absence of the primary idler spot. It was also displaced by the diffraction grating in the same direction as the primary idler beam indicating that it had a longer wavelength, which was measured to be around 1085nm using an optical spectrum analyser (OSA, Hewlett-Packard 86140A). With the beams spatially separated it was

also possible to measure the temporal profiles of each beam, and the traces captured are shown in Figure 108. The significant features of this graph are that the pump profile does not show the cavity dumping observed in the non-collinear arrangement, and that both of the idler waves build up simultaneously.

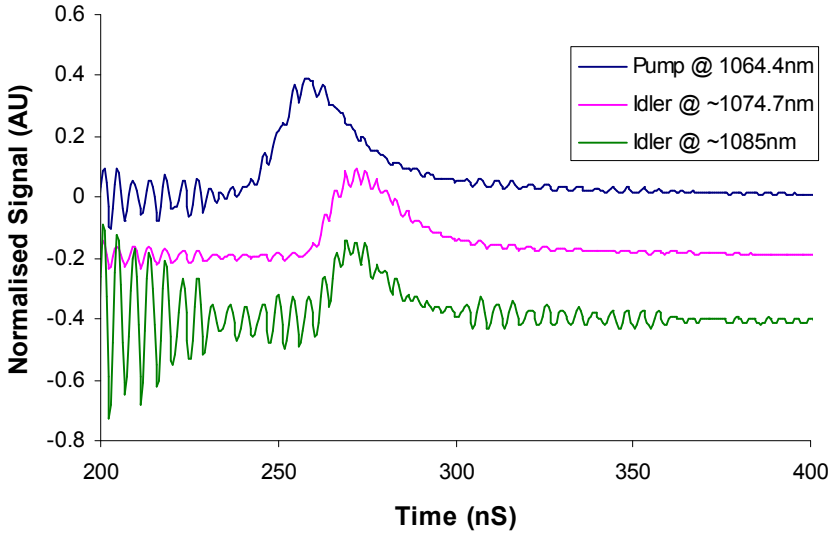

Figure 108 temporal profiles of the pump and idler waves observed from crystal B. The two idler waves were measured on two identical photodiodes simultaneously on the same oscilloscope with equal lengths of cabling. The pump pulse was measured in the same set up by changing the angle of the grating used to separate the beams. Ringing on all signals is due to noise from the Q-Switching electronics.

There could be two physical explanations for this: a higher order of the grating was produced a different phasematching solution (see Figure 109), or the idler wave was becoming the pump for a new downconversion process.

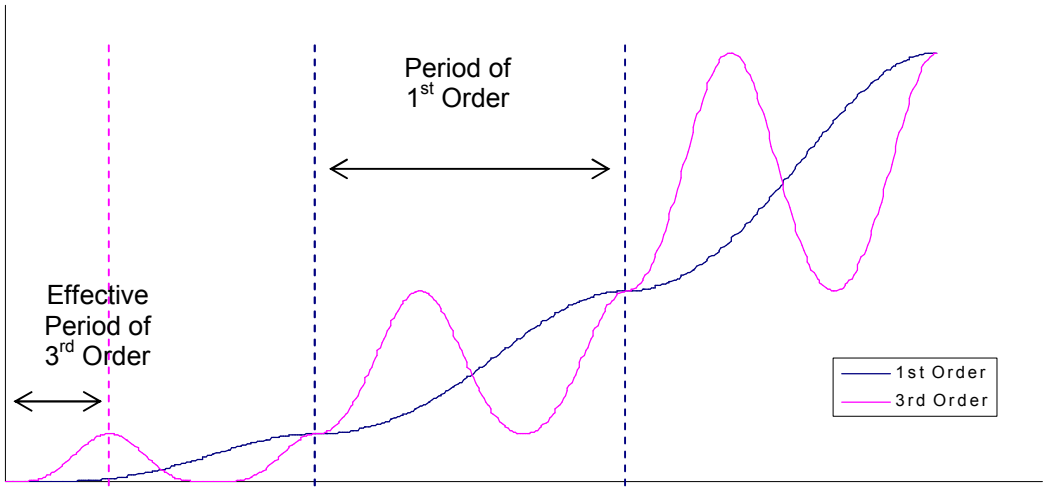

Figure 109 illustration of optical build up in a poled material. Without poling the downconverted wave would go in and out of phase with the newly generated photons causing it to oscillate. If the domain of the material is inverted where the phase slippage is π out of phase the destructive effect is swapped with a constructive one, producing an overall gain through the crystal. This figure also shows that the same is true if the domain is flipped every 3π. This does however reduce the effective crystal length by a factor of 3. This is true for any odd multiple of π.

To determine which of the theories fit best the phasematching solution for each proposition was calculated using the MathCAD model described earlier in this chapter. The results for both gratings for each theory are shown in Table 2, from which it is clearly seen that the cascaded process is a better fit.

Pump (nm)	Grating Order	Predicted Idler (nm)	Measured Idler (nm)
1064.4	1	1073.7	1074.7
1074.7	1	1084.2	~1085
1064.4	3	1097.4	~1085

Table 2 measured and calculated solutions to the phasematching condition for a variety of pump wavelengths and poling grating orders.

Additional supporting evidence is that the second, longer wavelength, emission was never observed without the presence of the first downconverted wave. Measurement of the temporal profiles of the pulses also shows simultaneous build up of the two

downconverted waves (see Figure 108), suggesting that it is not cascaded parametric downconversion. If it were then it would be expected that the secondary idler wave would not yet be above threshold, and would also have a characteristic build up period. This indicates a generation process that does not have a threshold – that of the difference frequency generation between the primary idler wave and the terahertz wave.

As significant pump depletion was not taking place it is difficult to determine the oscillation threshold, therefore the gain was analysed at the point where flashes of downconversion were observed. Applying the calculated intensity to equation (2.24) from Chapter 2 gives a figure for the low loss gain (Γ) of 1.6cm^{-1}, whereas using equation (2.28):

$$\left(\cosh^{(2N)}\left(\Gamma l\right)\right)^{M} = 10^{14}$$
$$\Gamma = \frac{\cosh^{-1}\left(\sqrt[2MN]{10^{14}}\right)}{l} \tag{5.8}$$

and applying the following estimated values: idler round trip time = 1.7nS, idler build up time = 15nS (round trips = M = 8.8), interaction length = 0.011mm (THz generation angle ~14°, so interaction length dominated by the large absorption at 2.7THz of ~90cm^{-1}), number of gain segments per round trip N = 9000 (for gain in both directions through the PPLN), gives a required Γ for oscillation of 18cm^{-1}.

5.6.2. Orthogonal Poling Design

To overcome the total internal reflection of the generated terahertz wave, and so successfully detect the terahertz wave, it was decided to implement an orthogonally poled crystal design. As previously shown the phasematching solutions of this design are degenerate in the terahertz/idler frequencies produced, and the THz generation angle is such that the generated terahertz wave can be extracted using the silicon prism output coupling technique described in previous chapters. The crystal design selected was poled with a period of 42.4μm, which the model predicts to phasematch at a wavelength of 200μm (1.5THz) at an angle of 65°. In this case, with orthogonal poling, only crystals that were up to 30mm in length could be ordered due to constraints in the poling technique used by the crystal producers. As such a crystal 30mm long by 5mm wide and 1mm high was ordered.

The alignment of the intracavity cylindrical telescope had proved quite difficult to achieve, and resulted in a laser that was observed to readily run on higher order transverse modes in the vertical plane (TEM01, 02 etc…), seemingly corresponding with damage being caused to the crystal surface. For this reason the cavity was redesigned with a single intracavity lens (focal length 200mm) producing a waist on the output mirror (this time of 97% reflectivity, to enhance feedback for idlers), and a collimated section in the Nd:YAG end. Total cavity length was approximately 35cm, with the lens 21cm from the output coupler. Operation on a TEM00, circular mode was enforced by the insertion of an aperture into the laser cavity next to the intracavity lens, increasing the loss experienced by higher order modes. Aperture size was determined by decreasing the diameter until power loss of the laser was observed and then slightly backing off.

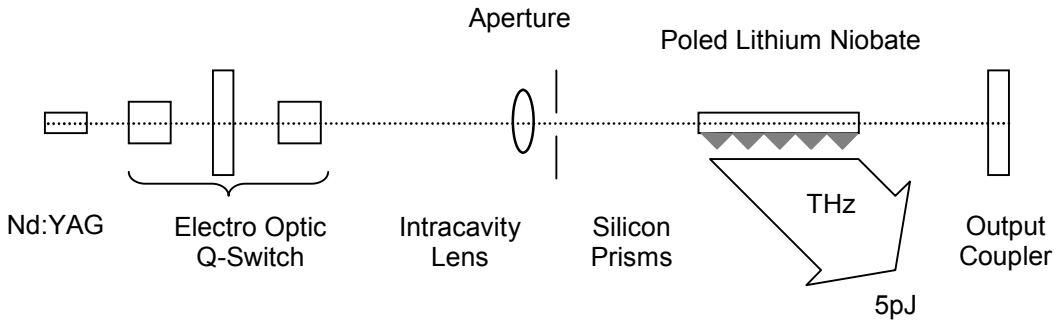

Figure 110 diagram illustrating the layout of the "orthogonal" intracavity terahertz OPO.

Again the intracavity mode was calculated using PSST! In this case a beam waist was chosen to be around 0.2mm (0.4mm diameter) within the poled crystal, so that there would be greater clearance of the beam in the 1mm vertical aperture of the PPLN crystal.

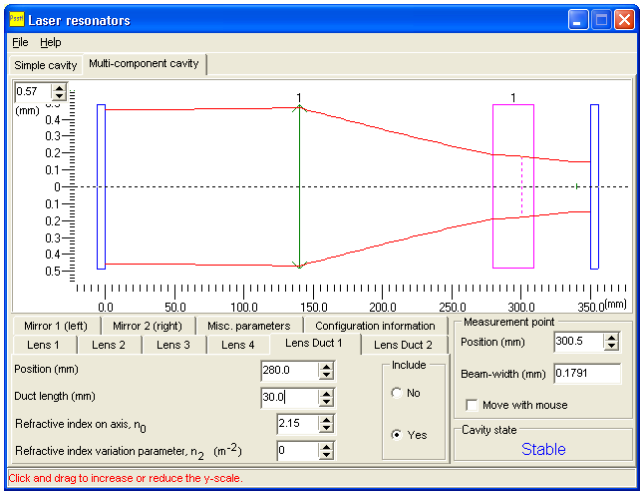

Figure 111 intracavity laser mode supported by the new design. The calculation was performed using the laser cavity modelling component of the PSST! software suite.

The system was built using a similar technique to that for the cylindrical telescope, with the laser cavity first being aligned with no PPLN, lens nor aperture. Each element was then added (PPLN last) and optimised using only its own position and orientation within the laser. The finished build is shown in Figure 112.

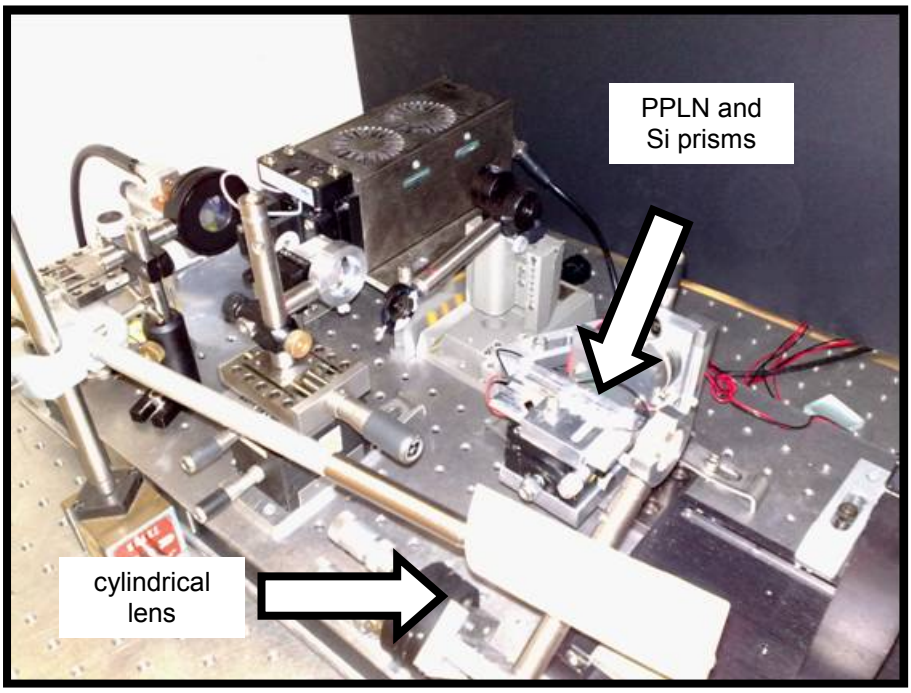

Figure 112 the realised system on the bench. Note the silicon prisms and cylindrical lens used to extract and collimate the terahertz wave.

In order to confirm the spot size within the laser crystal a beam profiler was used to take measurements of the extracavity laser field. As the output coupler in this design

was a plane mirror, the beam waist must have been situated on it, and therefore the beam propagation was symmetric about this point.

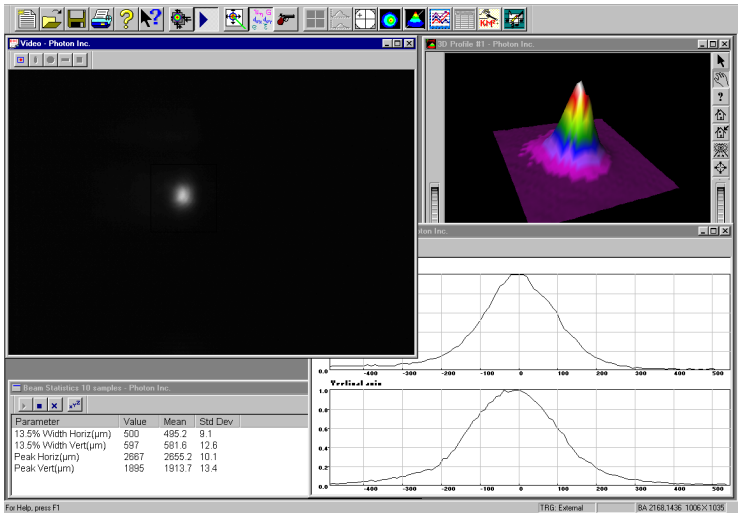

Figure 113 example beam profile measurement. The beam profile is much cleaner and symmetrically Gaussian than that from the intracavity telescope system.

The shortest distance from the laser output coupler that beam profile measurements could be made was reduced in this system to around 40mm, again limited by the CCD array of the BeamPro profiler being recessed into its case to accommodate the integral variable attenuator. The results of the profiling are shown in Figure 114, and show that the beam waist did not exceed 250µm inside the crystal.

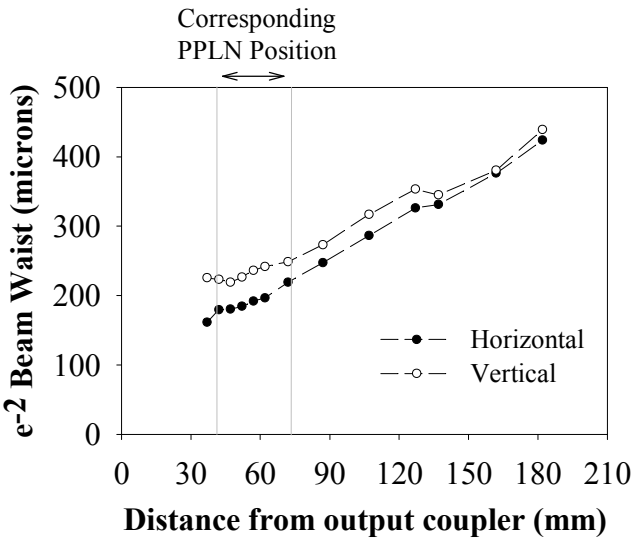

Figure 114 plot of beam waist measurements against increasing distance from the laser output coupler. It was not possible to position the CCD of the beam profiler any closer than achieved here due to mechanical limitations and the requirement for attenuation of the beam by ND filters.

In order to determine whether an idler was generated the same diffraction grating was employed as previously to separate the beams, but once again it proved impossible to obtain downconversion levels sufficient to deplete the pump pulse to a measurable degree, which can be seen from the laser power characteristic shown later in Figure 117.

After careful optimisation (highest laser power, shortest pulse rise time, and brightest idler spots) observation of the spots produced by separating the beams with the grating revealed more idler spots than the two seen previously. A flashing spot was observed diffracted to the opposite side of the pump spot to that of the idlers, indicating that a higher frequency was also being generated. To verify the spectral output of the device the beams were measured simultaneously on the OSA. As the OSA cannot record all frequencies simultaneously (it utilises a scanning grating and single element detector) it was set to the "peak-hold" function in order to record the signal over multiple sweeps (for around 10 minutes with around 20 seconds per sweep). The results of the scans are shown in Figure 115, and show that four down-converted frequencies were present, as well as one up-converted wave. It is evident that the frequency separation of each adjacent pair of frequencies is a constant value.

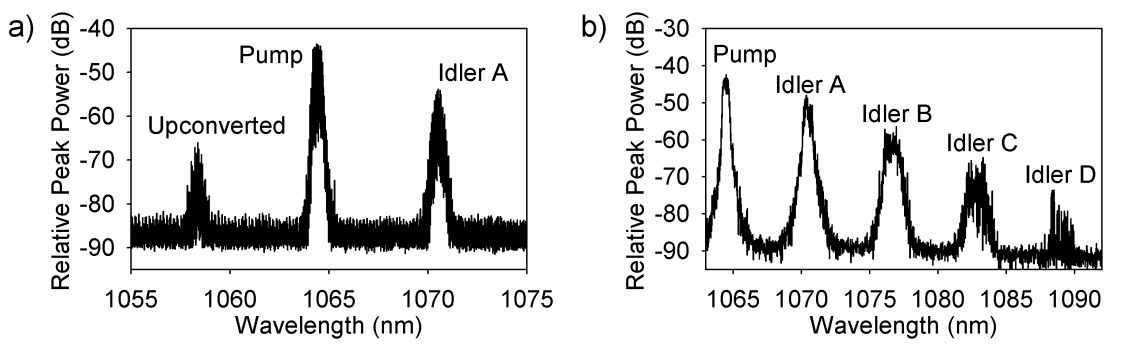

Figure 115 OSA traces showing: a) that an up-converted wave is also present with the same frequency separation as that of the idler waves. This indicates that sum frequency generation of the pump and terahertz wave is also occurring. And b) a cascade of downconverted frequencies. Each idler is separated from the previous by the same step in frequency – that of the terahertz wave.

A measurement of the frequency gaps between downconverted waves will give the corresponding terahertz frequency that was generated. This was achieved by taking approximate frequency measurements of each downconverted wave, as well as the pump and plotting them in order of descending frequency, see Figure 116. The gradient of the linear fit through these points, assuming that this is a cascaded downconversion process, will be the frequency of the terahertz wave.

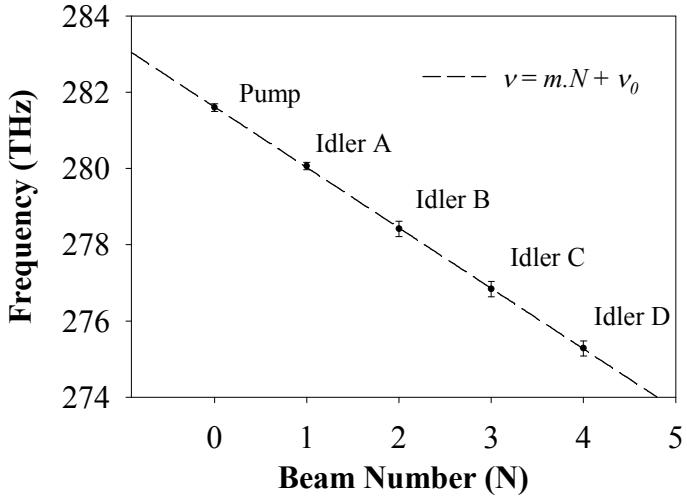

Figure 116 plot of detected frequencies in descending order.

The coefficients of the fitted line are $\nu_0 = 281.6 \pm 0.02$, and $m = -1.584 \pm 0.012$, giving the terahertz wavelength to be 189.4μm ± 1.4μm to 4s.f. The fact that the frequencies can be fit to a straight line so well points to a cascaded process. This is due to the large refractive index dispersion in the terahertz range (see chapter 2); if each idler

wave was being generated from the pump wave then the generated terahertz frequencies would be rapidly approaching the polariton resonance at ~7.6THz and so experiencing a quickly increasing refractive index. This would significantly alter the phasematching condition, and not allow for the regular frequency separations observed. An analysis of the phasematching solutions using the method described in Section 5.5 is shown in Table 3, and demonstrates how the cascaded processes fit much more closely to what is observed than generation via utilising higher orders of the grating.

Cascaded Processes				Higher Grating Order Processes				Measured
Pump(nm)	THz(μm)	θ	Idler(nm)	order	THz(μm)	θ	Idler(nm)	Idler(nm)
1064.4	200	65	1070.1	1	200	65	1070.1	1070.5
1070.5	200	65	1076.1	3	79	68	1079	1076.8
1076.8	200	65	1082	5	51	70	1086.9	1082.9
1082.9	200	65	1088.8	7	39	71	1094.6	1089

Table 3 comparison of solutions calculated for both cascaded and higher grating order processes to the measured downconverted waves.

In this system there was enough headroom before the onset of damage to perform measurements of the pulse energy characteristics of the idler waves, which should show if there was any clamping of the pump wave and whether the downconversion had a threshold. The idler waves were separated by only a few millimetres at a distance of ~15cm from the diffraction grating, enabling a 1mm wide slit to be used to separating one idler wave from the others. This idler was then focussed down onto a fast (1nS rise time) InGaAs photodiode and the output pulse envelope captured on an oscilloscope. A set of calibrated neutral density filters were used to prevent saturation of the photodiode. After averaging over 64 pulses the area under the composite pulse was calculated and referenced to that of the pump wave – the energy of the pump wave being known as it was large enough to be measured on a thermopile directly. The frequency being measured was easily selected by alteration of the diffraction grating angle by up to 1° in total. The results are shown, along with the power characteristic of the laser, in Figure 117. Only the first two idler waves were recorded

in this way as the consequent idler pulses were so intermittent in nature as to be indistinguishable from the noise level.

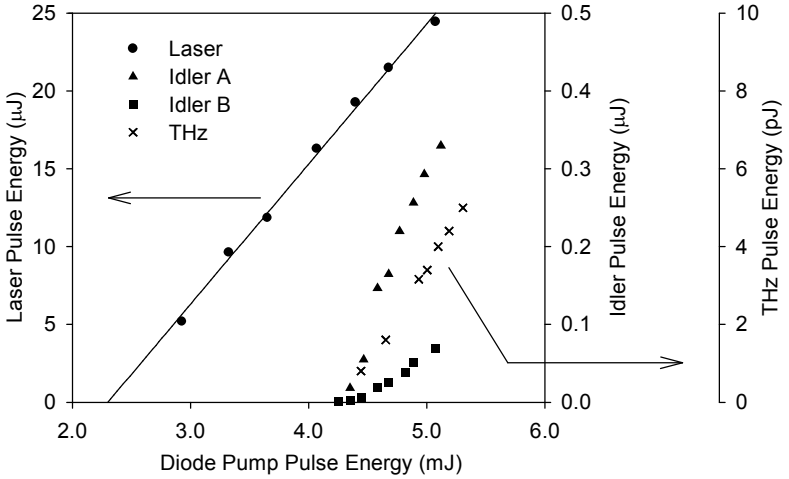

Figure 117 Graph showing the power characteristics of the orthogonally poled system. No measurable downconversion/clamping of the pump laser is observed, but the idlers show distinct threshold behaviour – both measured idlers and terahertz wave having the same threshold. The measured terahertz wave also shares this behaviour and threshold level.

Figure 117 also shows the measured terahertz pulse energy characteristic. The terahertz wave was focussed by an off-axis parabolic mirror of ~76mm effective focal length onto the composite silicon bolometer (same model used in previous chapters) approximately 15cm after being collimated by the cylindrical lens. Calculation of the pulse energy was performed using the technique described in Chapter 3. This graph shows that the two idlers measured, and the terahertz output, had approximately the same threshold, but that the laser pulse energy was not clamped to the level at idler threshold, which would be expected from such an intracavity OPO when above oscillation threshold. The plot also highlights the common threshold of the downconverted waves suggesting an instantaneous process of cascaded downconversion (such as difference frequency generation, DFG), rather than one with an associated build up time (such as parametric oscillation). Interestingly the power characteristic of Idler B seems to increase quadratically with pump energy. This makes sense in terms of the DFG between say, Idler A and the THz wave, as the generated wave would be proportional to the product of the input wave energies - which are both growing linearly with pump energy.

A set of 100 pulses for each wave was also captured using this set up and are shown in Figure 118. It is quite clear that the idler pulses amplitude jitter is quite large, increasingly so as wavelength increases, but the leading edges of the pulses do not suffer a large timing jitter – certainly no larger than the timing jitter on the pump pulses themselves. It can also be seen that each downconverted wave has approximately the same build up time with respect to the pump pulse, with perhaps a slight delay of on a few nanoseconds to the previous wave. It is also evident that there is no depletion of the pump pulse, indicating that the device has a low downconversion efficiency.

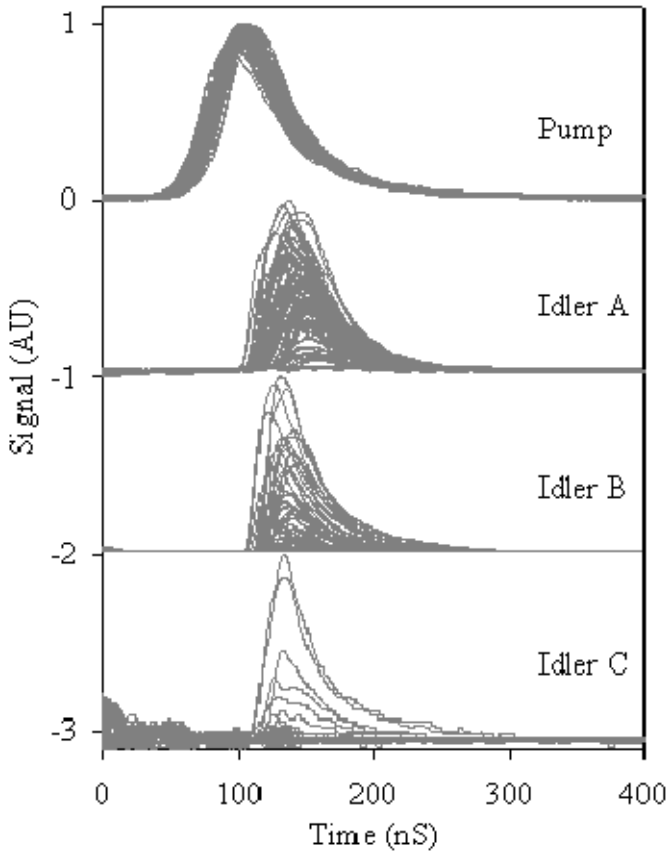

Figure 118 sample temporal profiles of the pump wave and the first 3 downconverted waves captured on the oscilloscope using a fast photodiode (~1ns rise time). The fourth downconverted and the up-converted waves were barely present and so difficult to observe in this manner.

The fact there is almost no time delay between consecutive downconverted pulses indicates that the generation process must be one where there is no pumping threshold to overcome. The only explanation that fits all the measurements is that a parametrically generated idler wave then interacts with the terahertz wave now

present via difference frequency generation to produce another, lower frequency, idler wave.

Once again, as no pump depletion was taking place it is difficult to directly analyse the technique with regard to threshold oscillation, but applying the calculated intensity to equation (2.24) from Chapter 2 in this case gives a figure for the low loss gain (Γ) of 0.92cm^{-1}, whereas using equation (2.28) and applying the following estimated values: idler round trip time = 2.7ns, idler build up time = 50nS (round trips = M = 19), interaction length ~0.2mm (THz generation angle ~65°, so interaction length dominated by this), number of gain segments per round trip N = 300 (for gain in both directions through the PPLN), gives a required Γ for oscillation of 3.8cm^{-1}.

It should be noted that a deleterious effect was observed during the course of this work with an orthogonal grating vector. The pump wave was being diffracted out of the laser cavity by the crystal poling due to a phase discontinuity growing as the beam propagated along the domain inversion walls[13]. This clearly also has an impact on the idler wave in that the round trip losses would be increased and so steps to minimise this effect need to be introduced. A crystal design to avoid this problem is proposed in section 5.7.

5.6.3. Direct Terahertz Wavelength Measurement

The terahertz wave had already been shown to have a generation direction close to 65° within the crystal, as this was necessary for the output coupling of the wave using the silicon prisms technique so that the pulse energies could be measured. It was now decided to perform a direct measurement of the terahertz wavelength using a scanning Fabry-Perot interferometer to confirm the generation frequency. The Fabry-Perot implemented metal mesh mirrors that were designed for use in a millimetre wave device and so were quite lossy and uncharacterised in the THz region. For this reason the results are only used to determine the wavelength and not the linewidth of the THz wave. The experimental layout is shown in Figure 119.

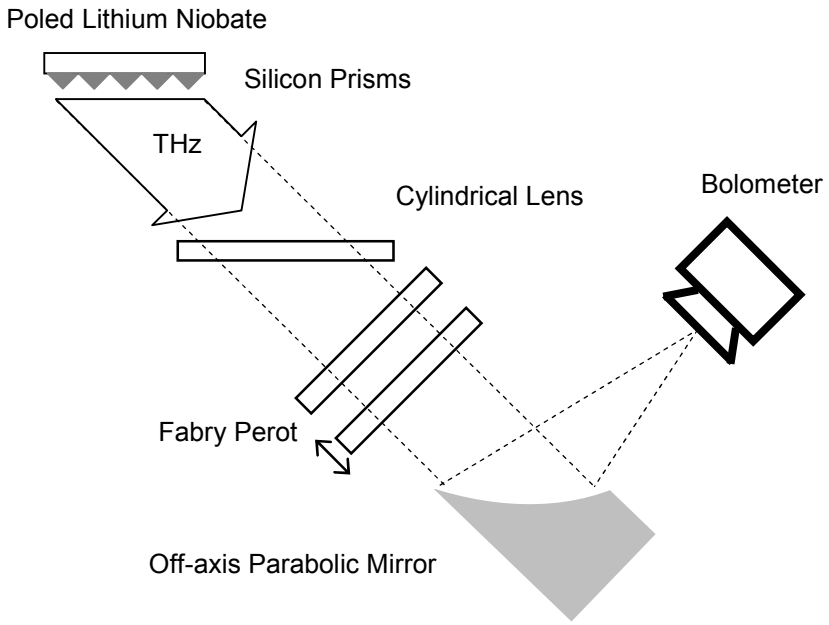

Figure 119 layout of the experiment used to measure the terahertz wavelength directly.

The mirror position was controlled via a custom program written in Labview, which also captured the bolometer signals by communicating with an oscilloscope. The software automatically moved the mirror in steps of 2.08μm (25 steps of 83.3nm), captured the terahertz pulse traces, and stored the integrated area of the pulse with mirror position. Several experimental runs had to be performed so that the Fabry-Perot mirrors could be adjusted to produce a clear interferogram, however crystal damage prevented an extensive alignment procedure being performed. Although the Fabry-Perot mirrors were optimised with respect to each other the angle of incidence of the terahertz wave on the interferometer could have been up to 10° off, as initial alignment was performed by eye and no there was no opportunity for improvement. The raw data from this experiment is shown in Figure 120. Due to the amplitude jitter 32 pulses were averaged over at each data point.

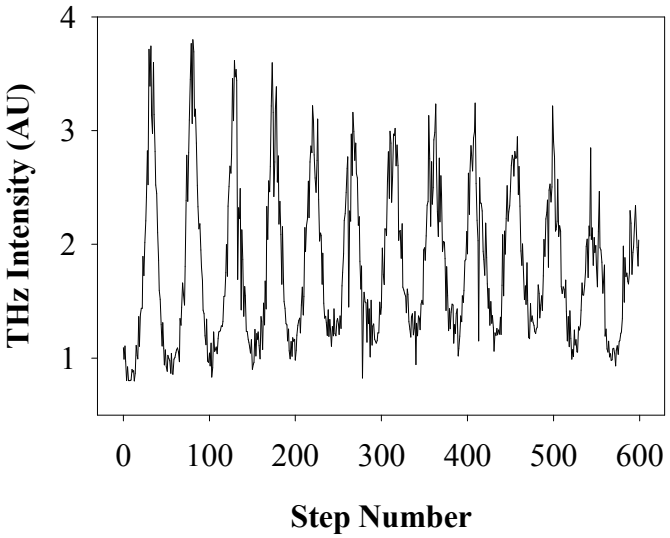

Figure 120 scanned Fabry-Perot transmission of the terahertz wave.

The positions of successive transmission peaks in Figure 120 were taken by eye and plotted against fringe number as shown in Figure 121. A straight line fit through these points gives a gradient of 96.81μm ± 0.5483μm, corresponding to a wavelength of 193.6μm ± 1.1μm. As the alignment could have been up to 10 off axis, could result in an measurement that was a factor of $\frac{1}{\cos(10°)} = 1.015$ times longer than was actually incident on the interferometer. So the actual range of values is from 189.6μm to 194.7μm, or 192.2μm ± 2.6μm to 4s.f., which agrees with the value measured from the spacing of idler waves on the OSA, and is close to that predicted (the error in prediction is put down to uncertainty in the terahertz refractive index).

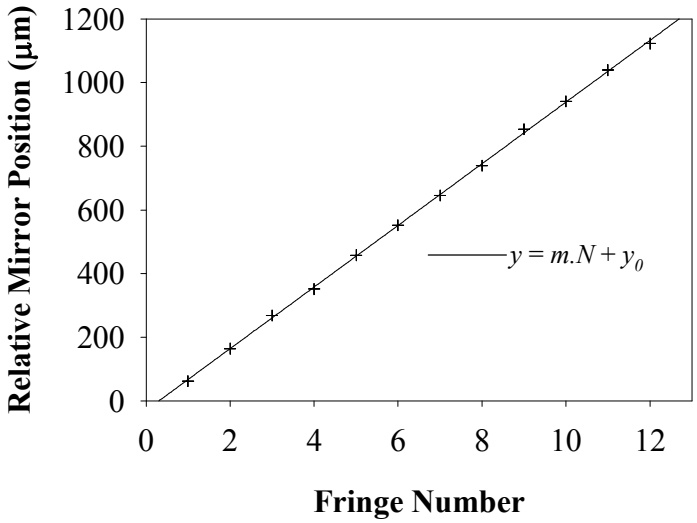

Figure 121 plot showing how the mirror position changes at consecutive transmission peaks.

5.7. Proposed Developments

The performance of the devices described in this chapter seems to be limited by insufficient idler gain within the duration of the pump pulse to allow it to grow very large. There are two routes to improving this: increasing the intensity (which is not possible due to damage of the nonlinear medium), or decreasing the idler cavity length and thereby providing more round trips of the gain during the pump pulse. To accomplish the latter a common method is to insert a frequency selective mirror into the laser cavity that transmits the laser wavelength and reflects the idler (/signal) wave, creating two separate cavities that overlap within the nonlinear crystal and share an end mirror. This is normally quite achievable as the resonated waves tend to be quite far apart in wavelength, however in the intracavity terahertz OPO these wavelengths are very close together. From correspondence with laser mirror producers it seems that the sharp cut off in reflectivity is possible, but the resulting multilayer coating is prone to damage at lower fluences that required for operation intracavity to a Q-Switched laser.

Etalons are often used as frequency selecting components within laser cavities. Indeed the use of them to line narrow in intracavity terahertz OPO is discussed in Chapter 4. If the device were above threshold, i.e. the gain was sufficient for the laser cavity to serve as the idler resonator, then an etalon could be designed to switch the solution that dominates with the crystals designed to generate orthogonally

propagating THz, allowing the radiation to be extracted. This would be accomplished by designing the free spectral range of the etalon to match the frequency spacing between pump and idler waves that phasematch with the orthogonal process, hence rejecting the other solution out of the cavity. As there is not enough gain to accomplish this a different approach is suggested: using the etalon in the "flash" condition where it is orthogonal to the beam, rather than at some slight angle. The result of this is that instead of rejecting the reflected wave out of the cavity it is now fed back into the cavity. By designing the free spectral range to pass both the pump wave and the idler to be rejected, the desired idler wave now experiences a sub-cavity much shorter than the laser cavity, increasing the number of round trips possible during the laser pulse and so providing much more gain. To avoid coupled cavity effects it may be required to insert another etalon designed to pass only the pump. The layout of this design is shown in Figure 122.

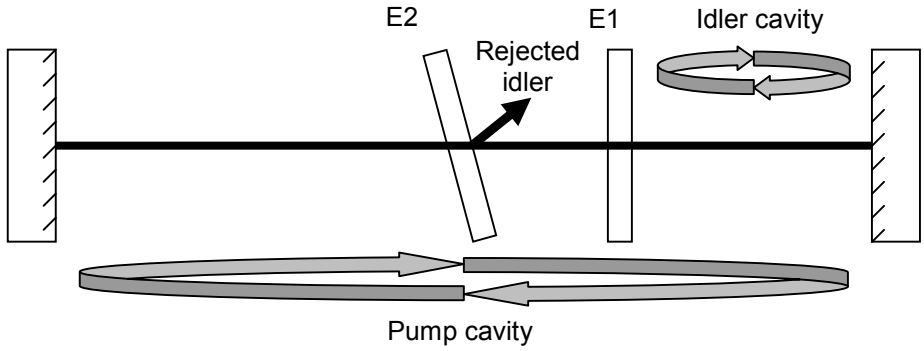

Figure 122 Proposed cavity design incorporating one etalon E1 as an intracavity frequency selective mirror, and a second etalon E2 to reject the leaked idler wave from the laser resonator preventing coupled cavity effects.

There is an extra difficulty in the etalon design however, in that not only does the free spectral range have to be correct, but the absolute frequencies of the pass bands must coincide with the frequencies of the laser and idler. The usual way this is achieved is by adding a slight tilt to the etalon, which has the effect decreasing the path difference. If the angle is fixed to the flash condition then tuning has to be accomplished by physically changing the etalon thickness, perhaps by temperature tuning a solid etalon, or by piezo tuning an air-spaced etalon. This technique could

also be applied to the orthogonally poled crystals, but with greater ease as only the laser frequency needs to passed by the etalon.

5.8. Double Solution and Diffraction Avoidance

During the course of the experiments it was realised that some of the laser beam was being diffracted out of the resonator horizontally by the orthogonally poled crystal. This is most probably due to the slight variation in refractive index at the domain inversion walls (a HeNe laser at 633nm was diffracted through the crystal to confirm the effect, and a diffraction pattern fitting that predicted by the poling period was observed) which builds a phase delay in the wave front of the laser beam as it travels along it. This effect has been observed and reported in the literature[13], but is generally not a problem as the domain walls are usually orthogonal, or at some high angle to, the pump wave in "normal" phasematching configurations. This effect is not only detrimental to the laser in the intracavity OPO, but also introduces losses for the idler waves. To avoid this problem we can see from Figure 95 that it is possible to have a grating vector that is close to the orthogonal angle, for which both solutions are still extractible using the silicon prism technique. It is proposed that the optimal poling design be chosen slightly off orthogonal, such that the angle of the grating vector (θ) presents a homogeneous phase delay across the laser beam by ensuring the domain walls overlap at least once. This is clarified in Figure 123 where d is the domain width (half the grating period), L is the length of the crystal and w is the horizontal distance the domain wall has shifted.

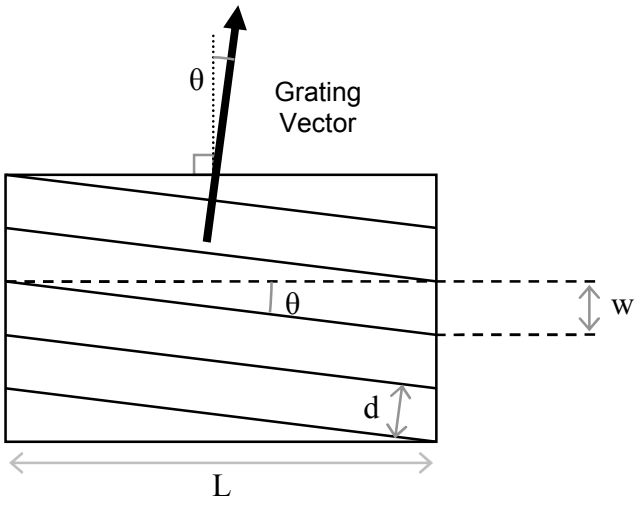

Figure 123 proposed poling design to allow extraction of the terahertz wave and avoid diffraction losses.

The grating period should be designed such that the relation

$$L\tan(\theta) > \frac{d}{\cos(\theta)} \tag{5.9}$$

is satisfied.

5.9. Conclusions

We have demonstrated the possibility of using a quasi-phasematching scheme to collinearise the pump and idler waves in an intracavity system. Terahertz frequency output was observed and measured although at a very low level in comparison to the intersecting cavity approach. The problem is believed to be that the increased round trip time and parasitic losses experienced by the idler wave overcome any advantage in parametric gain experienced by the collinearisation. A couple of ideas implementing frequency selective components within the cavity have been suggested and attempted, but damage constraints limited the success of the approach.

5.10. References

1. D. Molter, M. Theuer, and R. Beigang, "Nanosecond terahertz optical parametric oscillator with a novel quasi phase matching scheme in lithium niobate," Opt. Express **17**, 6623-6628 (2009).

2. C. F. Rae, M. H. Dunn, and J. A. C. Terry, "Parametric Terahertz Radiation Generation With Lateral Beam Coupling" patent number WO/2006/010916, (2005).

3. D. A. Walsh, P. G. Browne, M. H. Dunn, and C. F. Rae, "Intracavity parametric generation of nanosecond terahertz radiation using quasi-phase-matching," Opt. Express **18**, 13951-13963 (2010).

4. W. R. Bosenberg, A. Drobshoff, J. I. Alexander, L. E. Myers, and R. L. Byer, "93% pump depletion, 3.5-W continuous-wave, singly resonant optical parametric oscillator," Opt. Lett. **21**, 1336-1338 (1996).

5. P. E. Powers, T. J. Kulp, and S. E. Bisson, "Continuous tuning of a continuous-wave periodically poled lithium niobate optical parametric oscillator by use of a fan-out grating design," Opt. Lett. **23**, 159-161 (1998).

6. D. J. M. Stothard, M. Ebrahimzadeh, and M. H. Dunn, "Low-pump-threshold continuous-wave singly resonant optical parametric oscillator," Opt. Lett. **23**, 1895-1897 (1998).

7. L. E. Myers, R. C. Eckardt, M. M. Fejer, R. L. Byer, W. R. Bosenberg, and J. W. Pierce, "Quasi-phase-matched optical parametric oscillators in bulk periodically poled $LiNbO_3$," J. Opt. Soc. Am. B **12**, 2102-2116 (1995).

8. M. Cronin-Golomb, "Cascaded nonlinear difference-frequency generation of enhanced terahertzwave production," Opt. Lett. **29**, 2046-2048 (2004).

9. K. Kawase, M. Mizuno, S. Sohma, H. Takahashi, T. Taniuchi, Y. Urata, S. Wada, H. Tashiro, and H. Ito, "Difference-frequency terahertz-wave generation from 4-dimethylamino-N-methyl-4-stilbazolium-tosylate by use of an electronically tuned Ti:sapphire laser," Opt. Lett. **24**, 1065-1067 (1999).

10. Y. Sasaki, A. Yuri, K. Kawase, and H. Ito, "Terahertz-wave surface-emitted difference frequency generation in slant-stripe-type periodically poled $LiNbO_3$ crystal," Applied Physics Letters **81**, 3323-3325 (2002).

11. K. L. Vodopyanov, "Optical THz-wave generation with periodically-inverted GaAs," Laser & Photonics Review **2**, 11-25 (2008).

12. D. E. Zelmon, D. L. Small, and D. Jundt, "Infrared corrected Sellmeier coefficients for congruently grown lithium niobate and 5 mol.% magnesium oxide doped lithium niobate," J. Opt. Soc. Am. B **14**, 3319-3322 (1997).

13. M. Muller, E. Soergel, K. Buse, C. Langrock, and M. M. Fejer, "Investigation of periodically poled lithium niobate crystals by light diffraction," Journal of Applied Physics **97**, 044102 (2005).

Chapter 6. Conclusions and Future Work

This thesis has described the design, implementation and characterisation of novel intracavity terahertz optical parametric oscillators that make the parametric technique an attractive option for investigating the "THz Gap". Indeed the original system outlined in Chapter 3 has been protected by several patents, which have been licensed to the company MSquared Lasers of Glasgow who have commercialised the system, and are now selling units internationally.

The advantage of the intracavity cavity design in reducing the pump energy requirements for the THz OPO has been proven, explicitly so in Chapter 3 where the laser pulse energy that was required to reach threshold was an order of magnitude lower than a similar extracavity THz SRO. The temporal profile of the laser pulse in this system shows the near optimal condition of the cavity dumping of the laser field into the downconverted waves at the peak of the pulse. This condition allows for maximal extraction of the population inversion stored in the laser crystal (when running several times above laser threshold) providing efficient operation. This condition is not guaranteed however, and it seems somewhat fortuitous that this was systematically observed in various OPOs when running at twice OPO threshold, as it is dependent on both the laser build up time as well as that of the idler. Modelling of the laser and idler pulse dynamics should be undertaken to find the dependence of this characteristic on the idler cavity properties (with respect to cavity length and mirror reflectivities) for a given laser design.

The pulse amplitude jitter of THz wave was found to be significant and correlation with the idler pulse energy was poorer than expected. This can be worked around by implementing reference detectors, but it is still an undesirable attribute. The proposal made in Chapter 3 that the THz pulse energy is being unevenly split between the two opposite generation directions (corresponding to the two opposite passes of the pump and idler waves) needs to be investigated, perhaps by the use of a thin (in the plane of the phasematching process) MgO:$LiNbO_3$ crystal such that the THz pulses can be extracted from both sides and recorded simultaneously. If this is the problem then solutions may lie in using unidirectional ring cavities for the pump and/or idler waves. Another solution may be in shortening the standing wave idler cavity and using lower

reflectivity mirrors to increase the number of round trips taken while maintaining a constant idler wave build up time.

The terahertz beam profile was shown to be Gaussian like and of good quality in the vertical component of the beam in particular exhibiting an M^2 factor of 2.3. The Horizontal beam quality was not as good, having an M^2 factor of 6.7, but this could be improved by moving to a single prism output coupling method rather than an array that distorts the terahertz wave front. The benefits of this generally good beam quality are in the increased propagation lengths and smaller focal spot sizes achievable. These features are advantageous for imaging systems and aid the beam handling and collection of the terahertz wave over longer distances, and assist in making the intracavity cavity THz OPO an attractive source.

The disappointing attribute of generating THz wave parametrically in MgO:$LiNbO_3$ crystals is the low energy of THz pulse that is extracted. In this research maximum pulse energies of 10 to 20nJ were regularly obtained, which is a significant improvement over extracavity pumped systems in the literature and capable of saturating the bolometer used for measurements, giving dynamic ranges in excess of 10,000:1. However it is not as easily detected using cheap and robust pyroelectric detectors (dynamic ranges of ~100:1 were obtained with various pyroelectric elements). The disappointment arises from the fact that, internally to the crystal, pulses of several microjoules are being generated, and it is material absorption that limits the output power. There are a number of ways this absorption may be reduced: the implementation of a quasi-phasematching scheme that generates a faster exiting THz wave (although this has been found in this research to be non trivial), the optimum pump beam profile should be investigated to find if an advantage can be gained this way (for instance the implementation of a tall, thin profile that can edge up to the crystal interface more closely – although this would reduce the THz walkoff length), or perhaps most the promising route is to look at implementing new nonlinear materials such as orientation-patterned gallium arsenide (OP GaAs) – which has already been demonstrated in optical rectification and difference frequency generation techniques.

The techniques used for narrowing the THz wave output by restricting the pump and idler linewidths proved successful and what are estimated to be transform limited linewidths were obtained with injection seeding. This came at the cost of greatly

increased system complexity compared to utilising intracavity etalons. A thorough analysis of the optimal etalon choices should be made to attempt to approach the transform limit by this method, and to enable the system (if possible) to be tuned continuously with this narrow linewidth across the whole 1 to 3THz tuning range. Once this has been accomplished the construction of a THz spectrometer would then allow a critical comparison of this method with that of THz-TDS and FTIR techniques.

The implementation of quasi phasematching techniques in this research ran in to several difficulties. Of most importance was the realisation that poled crystals designed for the orthogonal generation of THz radiation, to enable its rapid exit and therefore minimum absorption, could have a second solution due to the bidirectionality of the grating vector. In the crystals modelled and implemented this second solution was found to be the solution to reach threshold first, and was not propagating at an extractible angle. The investigation of quasi phasematching schemes is continuing in the group, with the aims of designing crystals that will allow collinear propagation of pump and idler waves (to increase the nonlinear gain region and also allow cascaded downconversion processes to be phasematched) whilst producing extractable THz radiation, and also to extend the tuning range of the non-collinear phasematching scheme to higher and lower frequencies. The investigation of the interplay between laser and idler wave build up times would provide insights into how the collinear pump and idler (where the laser cavity is also the idler cavity) system might be successfully realised. Future systems will be able to avoid the reduced intracavity beam waists of the devices reported herein, and so alleviate the crystal damage problems encountered, by taking advantage of advances in crystal poling techniques that now allow 3mm thick PPLN to be produced. A deeper understanding of the refractive index of MgO:$LiNbO_3$ in the terahertz range would be of great benefit to this work, by improving the accuracy of the phasematching calculations.

It was realised early in the research presented herein that the advantages in having a room temperature, robust and simple source technology are somewhat obviated if a cryogenically cooled detection system was required. To this end the development of novel electro-optic detection scheme is being developed that exploits the high peak power in the THz pulses. The concept is to induce a change in refractive index via the

electro-optic effect in a material such as ZnTe, which would then be observed via the change in the polarisation state of a probe laser. This technique could theoretically resolve the temporal profiles of the terahertz pulses. An additional detector technology has proven utile – the Golay cell. Golay cells are not as robust or inexpensive as pyroelectric elements, but the one under test (a Tydex GC1-P) sits between the pyroelectric detectors and the composite silicon bolometer, typically providing a dynamic range in excess of 1000:1.

Overall the research presented in this thesis has broken new ground in the parametric generation of THz waves, yielding 5 patents and 4 research papers (as well as several conference presentations). The work has had impact in the field in that a system was developed which, through licensing and knowledge transfer activity with MSquared lasers, is now enabling more research groups to delve into the THz Gap.